

# UNCLASSIFIED

AD NUMBER
AD877768
NEW LIMITATION CHANGE
TO Approved for public release, distribution unlimited
FROM Distribution authorized to U.S. Gov't. agencies and their contractors; Administrative/Operational Use; NOV 1970. Other requests shall be referred to Air Force Aero Propulsion Lab., Wright-Patterson AFB, OH 45433.
AUTHORITY
AFAPL ltr 29 Apr 1971

THIS PAGE IS UNCLASSIFIED

AD 877768

AFAPL-TR-70-27

20

# ELASTROHYDRODYNAMIC LUBRICATION

## PRELIMINARY DESIGN MANUAL

J. M. McGrew

A. Gu

H. S. Cheng

S. F. Murray

Mechanical Technology Incorporated

TECHNICAL REPORT AFAPL-TR-70-27

November 1970

This document is subject to special export controls and each transmittal to foreign governments or foreign national may be made only with prior approval of the Air Force Aero Propulsion Laboratory (APFL), Wright-Patterson Air Force Base, Ohio 45433.

Air Force Aero Propulsion Laboratory  
Air Force Systems Command  
Wright-Patterson Air Force Base, Ohio

DDC  
RECEIVED  
DEC 21 1970  
RECEIVED  
C 352

AD No. \_\_\_\_\_  
DDC FILE COPY

# NOTICE

When Government drawings, specifications, or other data are used for any purpose other than in connection with a definitely related Government procurement operation, the United States Government thereby incurs no responsibility nor any obligation whatsoever; and the fact that the government may have formulated, furnished, or in any way supplied the said drawings, specifications, or other data, is not to be regarded by implication or otherwise as in any manner licensing the holder or any other person or corporation, or conveying any rights or permission to manufacture, use, or sell any patented invention that may in any way be related thereto.

This document is subject to special export controls and each transmittal to foreign governments of foreign nationals may be made only with prior approval of the Air Force Aero Propulsion Laboratory (APFL), Wright-Patterson Air Force Base, Ohio 45433.

ACCESSION FOR	
CFBTI	WHITE SECTION <input type="checkbox"/>
DDC	BUFF SECTION <input checked="" type="checkbox"/>
UNANNOUNCED	<input type="checkbox"/>
JUSTIFICATION	
BY	
DISTRIBUTION/AVAILABILITY CODES	
DIST.	ASAIL. <input type="checkbox"/> SPECIAL
2	

Copies of this report should not be returned unless return is required by security considerations, contractual obligations, or notice on a specific document.

## **DISCLAIMER NOTICE**

**THIS DOCUMENT IS BEST QUALITY  
PRACTICABLE. THE COPY FURNISHED  
TO DTIC CONTAINED A SIGNIFICANT  
NUMBER OF PAGES WHICH DO NOT  
REPRODUCE LEGIBLY.**

*OR are  
Blank pgs.  
that have  
Been Removed*

**BEST  
AVAILABLE COPY**



**AFAPL-TR-70-27**

# **ELASTROHYDRODYNAMIC LUBRICATION**

## **PRELIMINARY DESIGN MANUAL**

**J. M. McGrew**

**A. Gu**

**H. S. Cheng**

**S. F. Murray**

**Mechanical Technology Incorporated**

**TECHNICAL REPORT AFAPL-TR-70-27**

**November 1970**

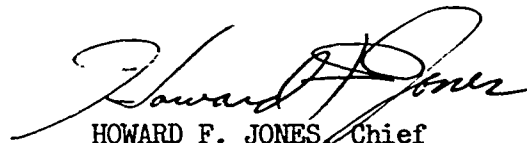
This document is subject to special export controls and each transmittal to foreign governments or foreign national may be made only with prior approval of the Air Force Aero Propulsion Laboratory (APFL), Wright-Patterson Air Force Base, Ohio 45433.

**Air Force Aero Propulsion Laboratory  
Air Force Systems Command  
Wright-Patterson Air Force Base, Ohio**

## FOREWORD

This report was prepared by Mechanical Technology Incorporated, 968 Albany-Shaker Road, Latham, New York under USAF Contract No. F33615-69-C-1305. The contract was initiated under Project No. 3048 Task No. 304806. The work was administered under the direction of the Air Force Aero Propulsion Laboratory, with Mr. M. R. Chasman (APFL) acting as project engineer.

This report covers work conducted from 1 February 1969 - 1 February 1970.



HOWARD F. JONES, Chief  
Lubrication Branch  
Fuel, Lubrication & Hazards  
Division

# I

## I

### ABSTRACT

The available data on elastohydrodynamic lubrication are summarized. Based on an assessment of these data, a design procedure is developed for evaluating the performance of an elastohydrodynamic contact. The procedure includes the calculation of minimum film thickness, real area of contact, traction, pressure distribution, temperature profile, and subsurface stress distribution in the contact, based on either available theory or on experimental data. A computer program listing plus illustrative examples are included. Determination of film thickness and traction are identified as areas in elastohydrodynamic lubrication requiring further investigation.

This abstract is subject to special export controls and each transmittal to foreign governments or foreign nationals may be made only with prior approval of the Air Force Aero Propulsion Laboratory (APFL), Wright-Patterson Air Force Base, Ohio 45433.

#### ACKNOWLEDGEMENT

The authors acknowledge the contribution of Dr. W. O. Winer and Dr. J.P.B. Williamson. Dr. Winer wrote the discussion of temperature and pressure effects on lubricant viscosity and Dr. Williamson consulted on the subject of surface topography.

## TABLE OF CONTENTS

	<u>Page</u>
I. INTRODUCTION AND SUMMARY	1
II. STATE-OF-THE-ART IN ELASTOHYDRODYNAMIC LUBRICATION	4
1. PHYSICAL PROPERTIES OF LUBRICANTS FOR ELASTOHYDRODYNAMIC LUBRICATION	4
a. Development of Synthetic Oils	4
b. Basic Relationships Between Structure and Physical Properties	8
(1) Nominal Viscosity of the Fluid Definition of Viscosity	14
(2) Changes in Viscosity	19
(a) Temperature Effects	20
(b) Pressure Effects	24
(c) Shear Effects	28
(d) Time Dependent Effects	30
(e) Viscoelastic Behavior	33
(f) Combined Effects and Correlations	34
(g) Related Effects	36
(3) Bulk Modulus	36
(4) Lubricant Density	38
(5) Gas Solubility	39
(6) Wetting Effects and Surface Films	40
(7) Thermal Properties	43
(8) Effect of Polar Compounds	44
c. Properties of Some Candidate Lubricants	45
2. FILM THICKNESS	46
a. Film Thickness and Film Shape of Line Contacts	46
b. Film Thickness and Film Shape of Elliptical Contacts	55

# TABLE OF CONTENTS (Continued)

	<u>Page</u>
3. PRESSURE DISTRIBUTION .....	58
a. Theories for Moderately Loaded Contacts .....	60
b. Theories for Heavily Loaded Contacts .....	60
c. Thermal Effects on Pressure Distribution .....	65
d. Pressure Measurement .....	65
4. TEMPERATURE DISTRIBUTION .....	69
a. Approximate Theories .....	77
b. Numerical Solutions to the Energy Equation .....	77
c. Temperature Measurements .....	81
5. FRICTION .....	85
a. Rolling and Sliding Friction .....	85
b. Spinning Friction .....	106
6. STRESS .....	111
a. Calculation of Contact Stresses Without Traction .....	113
(1) Geometric Definitions .....	113
(2) Theory for Line Contact .....	115
(3) Theory for Elliptical Contact .....	119
(4) Controlling Stress for Fatigue .....	119
b. Calculation of Contact Stresses with Traction .....	121
7. SURFACE TOPOGRAPHY .....	126
a. The Area of Contact Between Rough Surfaces .....	127
b. The Shape of Solid Surfaces .....	128
(1) Cumulative Processes .....	129
(2) Extreme Value Processes .....	129
(3) Pure Topographies and Transitional Topographies .....	129
c. Real Area of Contact .....	132
8. EFFECT OF ELASTOHYDRODYNAMICS ON BEARING DYNAMICS .....	132
a. Roller Bearing Dynamics .....	132

## TABLE OF CONTENTS (Continued)

	<u>Page</u>
b. Ball Bearing Dynamics .....	134
(1) The Concept of Raceway Control .....	134
(2) Ball Bearing Solutions .....	137
9. ROLLING ELEMENT BEARING FAILURE MODES .....	142
a. Classification of Failure Modes for Rolling Element Bearings .....	142
b. Contact Failures .....	144
(1) Wear Failures .....	144
(a) Mild Wear Failure Mode .....	144
(b) Severe Wear Failure Mode .....	151
(2) Plastic Flow Failure Mode .....	161
(3) Fatigue Failure Mode .....	162
(a) Subsurface Fatigue .....	162
(b) Surface Fatigue .....	165
(c) Effect of Elastohydrodynamic Lubrication on Fatigue .....	165
c. Effect of Elastohydrodynamic Lubrication on Bearing Life .....	167
III. ELASTOHYDRODYNAMIC PERFORMANCE CALCULATION .....	170
1. FLOW DIAGRAM .....	171
2. ANALYSES .....	171
a. Dimension of the Contact Ellipse .....	171
b. Load and Speed Parameters .....	171
c. Lubricant Parameters .....	174
d. Thermal Parameters .....	174
e. Thermal Reduction Factor .....	175
f. Side Leakage Reduction Factor .....	178
g. Minimum Film Thicknesses .....	178
h. Protrusion Width .....	179
i. Area of Contact .....	186
j. Frictional Coefficient .....	188

# TABLE OF CONTENTS (Continued)

	<u>Page</u>
k. Pressure Distribution.....	196
l. Temperature Distribution.....	197
m. Reduction Ratio for Pressure-Viscosity Coefficient.....	198
n. Stress Distribution.....	199
IV. APPLICATIONS.....	200
1. ELASTOHYDRODYNAMIC PERFORMANCE CALCULATION.....	200
a. Geometry Input.....	200
b. Speed Input.....	200
c. Lubricant Parameter Input.....	201
d. Example 1 - High Speed Deep Groove Ball Bearing.....	204
e. Example 2 - Roller Bearing.....	215
f. Example 3 - Low Speed Angular Contact Bearing.....	220
2. CALCULATION OF FRICTIONAL FORCES AND SPIN TORQUE AT A BALL-RACE CONTACT.....	226
a. Method of Analysis.....	227
b. Results.....	230
V. CONCLUSIONS AND RECOMMENDATIONS.....	234
1. CONCLUSIONS.....	234
2. RECOMMENDATIONS.....	237
VI. REFERENCES.....	240
APPENDICES.....	
I. PROPERTIES OF CANDIDATE LUBRICANTS.....	255
II. PROTRUSION WIDTH.....	268
III. AREA OF CONTACT.....	271
IV. FRICTION ANALYSIS.....	278
V. PRESSURE DISTRIBUTION.....	280
VI. INLET TEMPERATURE ANALYSIS.....	286
VII. ELASTOHYDRODYNAMIC PERFORMANCE COMPUTER PROGRAM.....	289
VIII. FRICTIONAL FORCES AT A BALL-RACE CONTACT COMPUTER PROGRAM.....	321



# LIST OF FIGURES

	<u>Page</u>
1. Steamline or Viscous Flow-----	15
2. Viscosity Characteristics of a Newtonian Liquid-----	17
3. Types of Non-Newtonian Viscous Behavior-----	18
4. Viscosity-Temperature Characteristics of Typical Candidate Lubricants-----	23
5. Viscosity-Pressure Curves for Various Oils at Several Temperatures-----	25
6. Coastdown Characteristics of Rolling Contact Bearings-----	31
7. Film Thickness Comparison-----	49
8. Survey Diagram for Incompressible Isothermal Elastohydrodynamic Lubrication-----	50
9. Comparison of $\phi_T$ with Experimental Data-----	51
10. Circumferential Profiles of Lubricated Rolling Disks-----	52
11. Rolling Point Contacts-----	56
12. Film Thickness Profiles-----	57
13. Pressure Distributions-----	59
14. Pressure Distribution in Contact Zone, Moderately Loaded Contact-	61
15. Film Thickness in the Contact Zone, Moderately Loaded Contact----	62
16. Pressure Distributions for an Incompressible Lubricant-----	63
17. Pressure Distributions for a Compressible Lubricant-----	64
18. Comparison of Pressure Distributions Between the Isothermal Case and the 25 Percent Slip Thermal Case with an Approximately Equal Rolling Velocity-----	66
19. Pressure Distribution, Thermal Theory, with 25 Percent Slip-----	67
20. Details of Pressure Spikes-----	68
21. Measured Variation in Pressure Profile with Disk Loading-----	69
22. Measured Film Pressures Between Crowned Disks Showing Variations with Loading-----	71
23. Measured Film Pressures Between Crowned Disks Showing Variations with Rolling Speed for Two Loadings-----	71
24. Measured Pressure Profiles Between Crowned Rolling Disks-----	72
25. Measured Film Pressures Between Crowned Disks Showing Variations with Temperature and Loading-----	73
26. Measured Film Pressures Between Crowned Disks Showing Variations with Lubricant Type-----	73
27. Pressure Pattern Between Crowned Rolling Disks Showing Variations with Temperature-----	74
28. Comparison of Ball-Race Pressure Pattern in 85 mm Bearing with Lubricant Type, Shaft Speed = 2500 rpm.-----	75
29. Comparison of Ball-Race Pressure Pattern in 85 mm Bearing with Lubricant Type, Shaft Speed = 5000 rpm.-----	76
30. Components of Temperature Increase in Lubricant for a Particular Case -----	78
31. Temperature Distribution for 25 Percent Slip Case, $U = 79.26$ in/sec-	79
32. Lubricant Film Temperature Map-----	80

# LIST OF FIGURES (Continued)

	<u>Page</u>
33. Mid-Film Temperature -----	82
34. Surface Temperature -----	83
35. Thermal Solution to Elastohydrodynamic Problem by Dowson and Whittaker -----	84
36. Calculated and Measured Surface Temperature -----	86
37. Variation in Disk Temperature with Loading -----	87
38. Variation in Disk Temperature with Rolling Speed -----	87
39. The Four Disk Machine -----	89
40. The Two Disk Machine -----	90
41. The Ratio of the Effective Viscosity ( $\bar{\mu}_m$ ) to the Supply Viscosity ( $\mu_o$ ) in Pure Rolling, Calculated from the Visco-Elastic Hypothesis. (a) $G = 1.9 \times 10^8$ dyne-cm <sup>-2</sup> ; $\lambda = 1.9 \times 10^{-4}$ sec; (b) $G = 7.4 \times 10^6$ dyne-cm <sup>-2</sup> ; $\lambda = 1.1 \times 10^{-4}$ sec; (c) $G = 1.4 \times 10^6$ dyne-cm <sup>-2</sup> ; $\lambda =$ $1.2 \times 10^{-4}$ sec. Experimental Points, Load ( $10^7$ dyne-cm <sup>-1</sup> ): $\nabla$ 2.5, $\square$ 2.9, $\Delta$ 14.6. -----	92
42. Frictional Traction as a Function of Sliding Speed (Rolling Speed Constant at 400 cm-sec <sup>-1</sup> ). Load ( $10^7$ dyne-cm <sup>-1</sup> ): (a) 20, (b) 15, (c) 7.5. -----	92
43. Frictional Traction as a Function of Sliding Speed. Load $1.25$ $\times 10^8$ dyne-cm <sup>-1</sup> ; (a) $U = 120$ cm-sec <sup>-1</sup> , $\mu_o \approx 0.4$ P; (b) $U = 200$ cm-sec <sup>-1</sup> , $\mu_o \approx 0.4$ P; (c) $U = 400$ cm-sec <sup>-1</sup> , $\mu_o \approx 0.4$ P; (d) $U = 400$ cm-sec <sup>-1</sup> , $\mu_o \approx 0.7$ P; (e) $U = 600$ cm-sec <sup>-1</sup> , $\mu_o \approx 0.4$ P ---	93
44. The Variation of $\bar{\mu}_m$ with Sliding Speed. Load = $1.2 \times 10^3$ dyne- cm <sup>-1</sup> , $U = 400$ cm-sec <sup>-1</sup> , $\mu_o = 1.4$ P ----- from experiment, ----- calculated. (a) $K_f/\beta_1 = 1.5 \times 10^5$ dyne-sec <sup>-1</sup> ; (b) $K_f/\beta_1 = 7.5 \times 10^4$ dyne-sec <sup>-1</sup> ; (c) $K_f/\beta_1 = 3.75 \times 10^4$ dyne-sec <sup>-1</sup> ---	93
45. Comparison Between Theoretical and Experimental Sliding Fric- tion Factor -----	94
46. Traction Versus Shear Rate -----	94
47. Coefficient of Traction as a Function of Sliding Speed -----	96
48. Variation of Traction with Sliding Speed at Various Contact Pressures -----	96
49. Influence of Rolling Speed and Inlet Temperature Upon the Traction Coefficient -----	97
50. The Influence of Rolling Speed Upon Effective Viscosity -----	97
51. Variation of Traction Coefficient with Sliding Speed Calculated by Crook's Theory, at Various Contact Pressures -----	99
52. Mean Shear Stress as a Function of Shear Plane Temperature -----	99
53. Friction of Smooth and Rough Discs as a Function of Maximum Hertz Contact Pressure -----	100
54. Simplified Elastohydrodynamic Contact: With Temperature Effects and Finite Rate of Increase in Viscosity -----	100
55. Typical Plot of Coefficient of Friction Against the Ratio of Peak-to-Valley Roughness/Theoretical Minimum Film Thickness -----	101

# LIST OF FIGURES (Continued)

	<u>Page</u>
56. Friction vs. Sliding Speed Curve-----	103
57. Apparent Viscosity vs. Mean Rolling Speed-----	104
58. Apparent Viscosity vs. Mean Rolling Speed-----	105
59. Comparison of Calculation in Simplified Theory with Solution Profiles by Cheng-----	107
60. Comparison of Crook Data with Simplified Traction Calculations ---- Crook Data-----	108
61. Comparison of Traction Predictions Using Various Lubricant Models. $U = 157$ in/sec-----	109
62. Spinning Friction Apparatus-----	110
63. Spinning Torque as a Function of Spinning Speed-----	112
64. Point Contact and Contact Ellipse-----	114
65. Line Contact Geometry-----	116
66. Magnitude of the Stresses On and Below Surface Layer-----	118
67. Shear Stress vs. x-Coordinate, at the Depth of Maximum Alter- nating Shear Stress-----	120
68. Range of Orthogonal Shear Stress as a Function of the Ellipti- city Ratio $b/a$ -----	120
69. Ratio of Shear Stress to Maximum Contact Stress vs. Ellipticity Ratio -----	122
70. A Contact Zone with Normal and Tangential Stress Distribution---	124
71. Variation of Shear Stress from Computer Calculations-----	125
72. Contact of Rough Surfaces-----	130
73. Cumulative Height Distribution and Typical Profile of a Ground Surface -----	131
74. Cumulative Height Distributions Showing the Effect of Wear on the Initially Gaussian Height Distribution of a Bead-Blasted Surface-----	133
75. Cage Speed vs. Load and Inner Ring Speed-----	135
76. Illustration of Raceway Control -----	136
77. Ball Loading Assuming Raceway Control of Ball Motion -----	138
78. Forces and Moments Acting on a Ball -----	139
79. Cage/Shaft Speed Ratio vs. Thrust Load per Ball -----	140
80. Influence of Velocity Parameter $(U_2 - U_1)/U_1$ on Wear Modes-----	150
81. Region of Smearing -----	155
82. The Two-Dimensional Plasticity Model -----	160
83. The Effect of a Tangential Force on the Limit of Elastic Behavior and Shakedown Limit -----	163
84. The Intensity of the Bulk Contact Stress -----	164
85. Influence of Elastohydrodynamic Lubrication on Bearing Life -----	168
86. Computer Program Flow Diagram-----	172
87. Protrusion Width -----	179
88. Protrusion Width vs. Velocity Parameter -----	183
89. Effect of Load Parameter on Protrusion Width -----	184
90. Minimum Film Thickness vs. Velocity Parameter -----	185

# LIST OF FIGURES (Continued)

	<u>Page</u>
91. Real Area of Contact vs. Specific Film Thickness -----	187
92. Coefficient of Friction vs. Shear Rate Parameter for Heating Parameter = $5 \times 10^{-7}$ -----	189
93. Coefficient of Friction vs. Shear Rate Parameter for Heating Parameter = $10^{-6}$ -----	190
94. Coefficient of Friction vs. Shear Rate Parameter for Heating Parameter = $5 \times 10^{-6}$ -----	191
95. Coefficient of Friction vs. Shear Rate Parameter for Heating Parameter = $10^{-5}$ -----	192
96. Coefficient of Friction vs. Shear Rate Parameter for Heating Parameter = $5 \times 10^{-5}$ -----	193
97. Coefficient of Friction vs. Shear Rate Parameter for Heating Parameter = $5 \times 10^{-4}$ -----	194
98. Coefficient of Friction vs. Shear Rate Parameter for Heating Parameter = $10^{-3}$ -----	195
99a. Velocities with Respect to Bearing Centerline -----	202
99b. Relative Velocities with Respect to Rolling Element -----	202
100. $\mu_{100}$ vs. $\alpha$ for Lubricants Tested in the ASME Report -----	203
101. Computer Input, Example 1 -----	206
102. Computer Output, Example 1 -----	207
103. Computer Input, Example 2 -----	216
104. Computer Output, Example 2 -----	217
105. Computer Input, Example 3 -----	222
106. Computer Output, Example 3 -----	223
107. A Contact Ellipse -----	228
108. Frictional Torque as a Function of Spinning Velocity -----	231
109. Effects of Spinning Velocity on Frictional Forces and Torque ---	232
II-1. Protrusion Width Diagram -----	268
III-1. Smooth-Film Deformation Shape of an Elastohydrodynamic Line Contact -----	272
III-2a. A Typical Surface Roughness Profile -----	274
III-2b. Abbott's Bearing Area Curve -----	274
III-3. Detail Surface Roughness Shape -----	274
III-4. Surface Roughness Profile and an Elastohydrodynamic Profile -	277
V-1. Grid Spacing Diagram for Pressure Calculation -----	281
V-2. Exit Pressure Calculation -----	284
VIII-1. A Ball-Race Contact -----	322

# LIST OF TABLES

	<u>Page</u>
I. Candidate Synthetic Lubricants .....	7
II. Some Normal Paraffin Hydrocarbons .....	11
III. Viscosity Unit Conversion Table .....	16
IV. Typical Values for Isothermal Bulk Modulus at 25°C and 0 psig .....	37
V. Typical Densities of Various Oils .....	38
VI. Coefficients of Thermal Expansion, for Various Types of Oils .....	39
VII. Solubility of Various Gases in Petroleum Oil or Diesters .....	40
VIII. Typical Thermal Properties of Lubricants .....	44
IX. Measured Film Thickness Between Rolling Disks .....	53
X. Failure Modes of Rolling-Element Bearings .....	143
XI. Classifications of Mild Wear Modes in Rolling Contact .....	150
XII. Surface Distress Data of Bodersiek (Ref. 184) .....	153
XIII. Variation of $f_1$ with Respect to $\alpha^*$ , $\beta'/\alpha^*$ , and $Q_m$ .....	176
XIV. Variation of $f_3$ with Respect to $\alpha^*$ , $\beta'/\alpha^*$ , and $Q_m$ .....	177
XV. Numerical Functions of $C$ , $n_1$ , and $n_2$ .....	178
XVI. Analysis of $\bar{e}$ Based on Cheng's Isothermal Theory .....	180
XVII. Analysis of $\bar{e}$ Based on Cheng's Thermal Theory .....	181
XVIII. Variation of $\epsilon$ and $C'$ with Slip .....	182
XIX. Sample Bearing Number 1, Deep Groove Ball Bearing .....	204
XX. Sample Bearing Number 2, Roller Bearing .....	215
XXI. Sample Bearing Number 3, Low Speed Angular Contact Bearing .....	221
XXII. Sample Bearing Number 3, Low Speed Angular Contact Bearing Film Thickness and Area Ratio as a Function of Oil Temperature .....	226

# NOMENCLATURE

$\bar{A}$	$\frac{1}{2}(\frac{1}{R_{x1}} + \frac{1}{R_{x2}}), \text{ in}^{-1}$
$A_c$	Area of contact, $\text{in}^2$
$a$	Semi-major axis of contact ellipse, in
$b$	$\left\{ \begin{array}{l} \text{Semi-minor axis of contact ellipse, in} \\ \text{Half Hertzian contact width, in} \end{array} \right.$
$B$	$\frac{b^2}{2R'_x h_o}$
$\bar{B}$	$\frac{1}{2R_{y1}} + \frac{1}{2R_{y2}}$
$C_1, C_2$	Specific heat of body number 1 and number 2, $\text{BTU/lb-}^\circ\text{F}$
$C_f$	Specific heat of lubricant, $\text{BTU/lb-}^\circ\text{F}$
$D1$	$\left( \frac{K_f^2}{\pi \rho_1 C_{11} U_1 K_1} \right)^{1/2} \frac{R' E'^3}{4w^3}^{1/4}$
$D2$	Same as D1 except with subscript 2
$E_1, E_2$	Modulus of elasticity of body number 1 and number 2, $\text{lb/in}^2$
$E'$	$2 \left( \frac{1 - \nu_1^2}{E_1} + \frac{1 - \nu_2^2}{E_2} \right)^{-1}, \text{ lb/in}^2$
$\bar{E}$	$\alpha E'$
$e$	Protrusion width, in
$\frac{e}{b}$	$\frac{e}{b}$
$F_x, F_y$	Frictional force in x- and y-direction, lb
$f$	Coefficient of friction
$G$	Shear modulus, $\text{lb/in}^2$
$G_1, G_2, G_3$	Friction parameter

# NOMENCLATURE (Continued)

H	$\frac{h}{h^*}$
h	Film thickness, in
$h_o$	Nominal film thickness (entrance film thickness), in.
$h_{DOW}$	Film thickness calculated by the Dowson and Higginson's formula, in
$h^*$	Film thickness near the exit where pressure gradient vanishes, in
$h_{min}$	Minimum film thickness at exit, in
$K_1, K_2$	Thermal conductivity of body number 1 and body number 2, BTU/°F-hr-ft
$K_f$	Thermal conductivity of lubricant, BTU/°F-hr-ft
k	Wear coefficient
$M_z$	Frictional torque, lb-in
P	Normal contact load, lb
p	Pressure, lb/in <sup>2</sup>
$p_{HZ}$	Maximum Hertzian pressure, lb/in <sup>2</sup>
$p^*$	Cut-off pressure separating the low and high pressure region, in the modified exponential pressure-viscosity law, lb/in <sup>2</sup>
$\bar{p}$	$p \frac{b}{w}$
$Q_c$	$\frac{\rho_o C_f (U_1 + U_2) b^3}{16 K_f R_x'^2}$
$Q_m$	$\frac{2 \rho_o U^2}{K_f T_o}$
R	Radius of ball, in
$R_G$	Radius of race groove, in
$R'$	Effective radius, in

# NOMENCLATURE (Continued)

$R_{x1}, R_{x2}$	Principal radius of body number 1 and number 2 in x-direction, in
$R_{y1}, R_{y2}$	Principal radius of body number 1 and number 2 in y-direction, in
$R'_x, R'_y$	Principal effective radius in x- and y-direction, in
$r$	Radius of race, in
$r_i$	Radius of inner race, in
$r_o$	Radius of outer race, in
$\dot{S}$	Shear rate, $\text{sec}^{-1}$
$s$	$\frac{U_1 - U_2}{U_2}$
$T$	Temperature, $^{\circ}\text{R}$
$T_o$	Inlet temperature, $^{\circ}\text{R}$
$T_1$	Surface temperature of body number 1, $^{\circ}\text{R}$
$T_2$	Surface temperature of body number 2, $^{\circ}\text{R}$
$T_c$	Center film temperature at $\frac{h}{2}$ , $^{\circ}\text{R}$
$U$	$\frac{U_1 + U_2}{2}$ , in/sec
$U_1, U_2$	Rolling speed at contact of body number 1 and number 2, in/sec
$\bar{U}$	$\frac{\mu_o U}{E' R'_x}$
$u_r$	Rolling velocity of race, in/sec
$u, v$	Velocity components in the x- and y-direction, in/sec
$u_s$	$U_2 - U_1$ , in/sec.
$v$	$\frac{V_1 + V_2}{2}$ , in/sec
$V_1, V_2$	Speed perpendicular to the direction of rolling, in/sec
$W$	$\frac{W}{E' R'_x}$



# NOMENCLATURE (Continued)

w	Load per unit length, lb/in
x	Coordinate along the film, in
$\frac{x}{b}$	
x*	Contact zone exit coordinate, in
y	Coordinate across the film, in
$\alpha$	Pressure-viscosity exponent in the visosity function $\mu = \mu_0 \exp[\alpha p + (\beta + \gamma p) (\frac{1}{T} - \frac{1}{T_0})]$ , in <sup>2</sup> /lb
$\alpha_1, \alpha_2$	Pressure-viscosity exponent in the low and high pressure region in the modified exponential viscosity law, in <sup>2</sup> /lb
$\alpha$	$\alpha \frac{w}{b}$
$\beta$	Temperature-viscosity coefficient, °F
$\beta_1$	Temperature-viscosity coefficient in the viscosity function $\mu = \mu_0 \exp[\alpha p - \beta_1(T - T_0)]$ , °F <sup>-1</sup>
$\gamma$	Pressure-temperature-viscosity coefficient, in <sup>2</sup> -°F/lb
$\zeta$	Surface tension, lb/in
$\kappa$	$\frac{\alpha_2}{\alpha_1}$
$\Lambda$	$\frac{12\mu_0 U}{w^2} E' R'_x$
$\lambda$	Relaxation time, sec
$\mu$	Viscosity of lubricant, lb-sec/in <sup>2</sup>
$\mu_m$	Effective viscosity, lb-sec/in <sup>2</sup>
$\mu_0$	Inlet viscosity, lb-sec/in <sup>2</sup>
$\mu$	$\frac{\mu}{\mu_0}$

# NOMENCLATURE (Continued)

$\nu$	Kinematic viscosity, $\text{in}^2/\text{sec}$
$\nu_1, \nu_2$	Poisson's ratio of body number 1 and number 2
$\xi$	$\frac{h}{o}$
$\rho$	Density of lubricant, $\text{lb}/\text{in}^3$
$\rho_o$	Lubricant density at inlet conditions, $\text{lb}/\text{in}^3$
$\rho_1, \rho_2$	Density of body number 1 and number 2, $\text{lb}/\text{in}^3$
$\sigma$	Standard deviation of surface roughness, $10^{-6}$ in
$\sigma_1, \sigma_2, \sigma_3$	Principal normal stress component, $\text{lb}/\text{in}^2$
$\sigma_x, \sigma_y, \sigma_z$	Normal stress components, $\text{lb}/\text{in}^2$
$\tau_o$	Maximum alternating shear stress, $\text{lb}/\text{in}^2$
$\tau_x, \tau_y, \tau_z$	Shear stress components, $\text{lb}/\text{in}^2$
$\tau_{\max}$	Maximum shear stress, $\text{lb}/\text{in}^2$
$\phi_S$	Side leakage factor for film thickness calculation
$\phi_T$	Thermal reduction factor for film thickness calculation
$\phi(z)$	Surface roughness distribution function
$\Omega_i$	Angular velocity of inner race about bearing center, $\text{rad}/\text{sec}$
$\Omega_o$	Angular velocity of outer race about bearing center, $\text{rad}/\text{sec}$
$\omega_o$	Angular velocity of ball/roller about its own center, $\text{rad}/\text{sec}$
$\omega_R$	Orbital velocity of ball/roller with respect to bearing center, $\text{rad}/\text{sec}$
$\omega_S$	Spinning angular velocity of ball, $\text{rad}/\text{sec}$

## SECTION I

### INTRODUCTION AND SUMMARY

Historically, the theoretical evaluation of rolling contact bearings has been mainly a matter of determining the elastic behavior of the contact zone. As loads, speeds, and temperatures have increased, it has been evident that this treatment alone is inadequate. Accurate predictions of bearing behavior under the conditions typical of jet engine applications, for example, require a thorough understanding of the elastohydrodynamic conditions existing in the loaded region. Elastohydrodynamics describes the fluid-mechanical interaction of mating surfaces undergoing elastic deformation in the presence of a lubricant under conditions where both the mechanical properties of the surfaces and the rheological properties of the lubricant contribute significantly to the resultant behavior.

Recent experimental data show that highly loaded angular contact bearings using high temperature synthetic lubricants have much shorter fatigue lives than classical bearing theory (Lundberg-Palmgren) predicts. These failures appear to be due to the inadequate lubricant film in the contact zone. This in turn permits metal to metal contact of local surface asperities, progressive surface damage, and ultimate failure. Thus successful analysis of such applications must include meaningful prediction of the separating film thickness. This in turn requires a thorough knowledge of elastohydrodynamic lubrication and the parameters which govern it. This report is addressed to such predictions.

This problem has been under study for some eighteen years both here and abroad. Gradually considerable insight has been achieved into elastohydrodynamic behavior. Unfortunately, perhaps because of the diverse aspects of this research, there has been little work done in compiling and interrelating the various results obtained and published. A critical study of the current state-of-the-art is both important and timely. It permits optimum utilization of available knowledge and improved planning for continued research. The first result is particularly important, since there is real immediate need for improved predictions of safe operational limits of load, speed, temperature and lubricant for high performance rolling contact bearings. Longer range, as additional information is accumulated, still better techniques for analyzing these variables can be evolved.

This report covers the work conducted during the first phase of a three-phase program in elastohydrodynamic research as follows:

Phase I : Survey, assemble and summarize all available data on elastohydrodynamic lubrication, analyze the data, and prepare a Design Procedure integrating these data and the best current theories. This design procedure would provide a parametric approach to predicting film thickness in the contact zone, percent asperity contact, and the relationship of these factors to bearing life and type of ultimate failure. Also as a result of this analysis, points of conflict between theories or between theory and experiment will be identified and those areas requiring experimental exploration or verification will be determined.

Phase II - Based on the experimental and analytical needs determined as the conclusions of Phase I, experimental program will be carried out determining which factors are significant in defining behavior in actual contact zones, critical lubricant properties, and the interaction between the two. In addition, any necessary extensions of analytical descriptions of contact zone hydrodynamics and the influence of contact zone dynamics on overall ball-bearing dynamics will be carried out.

Phase III - Following completion of the definitive experimental and analytical work of Phase II, the results, together with available data from other sources, will be compiled and analyzed as the basis for generating an improved and more complete description of elastohydrodynamic behavior. This in turn will be interpreted for practical utility as parametric presentations from which significant bearing behavioral information, such as zones of trouble-free operation, can be quickly determined. This final report, essentially a Design Manual, will then form the basis for rational bearing design and selection for aircraft turbomachinery.

The product of the first phase of the program is a Elastohydrodynamic Performance Calculation Procedure based on state-of-the-art data and the best current theories. This design procedure provides a method for predicting film thickness, percent asperity contact, temperature distribution, pressure distribution, and the relation of these factors to bearing life and type of ultimate failure.

The Elastohydrodynamic Performance Calculation Procedure consists of computer program which calculates all major variables in an elastohydrodynamic contact. The input to the program consists of:

1. The radii of curvature in the direction as well as perpendicular to the direction of rolling for both contacting surfaces.
2. The surface speed for both contacting surfaces.
3. The load.
4. Material data.
5. Lubricant data.
6. Surface roughness for both contacting surfaces.

With these input data the program calculates the following quantities successively by means of a series of subroutines:

1. The nominal film thickness based on isothermal theory (the nominal film thickness is the film thickness at the entrance region of the elastohydrodynamic contact).
2. The reduction of film thickness due to thermal and side leakage effects.
3. The exit protrusion width and depth.
4. Percentage of area of contact.
5. Contact friction.
6. Pressure distribution.
7. Mid-film and surface temperatures.
8. Subsurface and surface stress distributions.

The use of subroutines provides a convenient way to replace any old methods of calculation with any new techniques which may be developed in the future for any one of these variables. Using this approach, one does not have to rewrite the main computer program as the state-of-the-art of elastohydrodynamic lubrication advances.

The computer program is primarily intended for use on rolling element bearing contact problems. However, it has been made general enough so that it is applicable to many other heavily loaded concentrated contact problems. Thus, it should also find use in the design of gears, cams, and pivots.

To provide for improvement in the present calculation procedure, four areas of further investigation are identified. These include contact friction, contact film thickness, contact topology, and lubricant rheology.

## SECTION II

### STATE-OF-THE-ART IN ELASTOHYDRODYNAMIC LUBRICATION

The theory of heavily loaded concentrated contacts has been studied extensively in recent years. It is an interdisciplinary theory involving the physics, chemistry, mechanics, and metallurgy of the interacting surfaces. As such, it is not an easy problem to grasp and reduce to practical engineering procedures.

The necessity of extracting useful information from this multidiscipline field has received added impetus as manufacturers operate their equipment at higher loads, temperatures, and speeds. This is particularly true in the aircraft engine field where turbine engine bearings operating at 600 F and DN [Product of the bearing bore in mm times the speed in rpm] values of 2 million are now being considered. Practical design criteria are needed to define potential failure modes and predict the onset of these failure modes.

Because of the multidisciplinary character of this problem and the plethora of literature on the subject, it is extremely difficult for the engineer to digest all of the available information and make practical design judgements from it. To aid the practicing engineer, an attempt is made in this section to survey all of the available data on rolling and sliding contact lubrication and to determine its usefulness for design. In addition, the basis is laid for a preliminary design procedure which is discussed in Section III and attention is focused on those remaining problems which have not yet yielded to the continuing research effort in this field.

#### 1. PHYSICAL PROPERTIES OF LUBRICANTS FOR ELASTOHYDRODYNAMIC LUBRICATION

This chapter has two main objectives. The first is to present engineers with a simplified picture of the chemical and physical behavior of a variety of petroleum and synthetic lubricants, and the second is to summarize the lubricant properties which are known to be important for elastohydrodynamic lubrication.

##### a. Development of Synthetic Oils

Petroleum lubricants are naturally occurring compounds of carbon and hydrogen (hydrocarbons) which can be refined to produce oils having a wide range of viscosities. Although certain molecular structures predominate in these oils, depending on their geographical origin and the refining process, a random sample of petroleum oil will contain hundreds of different molecules in small quantities. Typical analyses will report the percentages of various ring structures and the percent of straight or branch chain hydrocarbons and will ignore the fact that less than one percent of the oil probably consists of a large number of various molecular species of undefined composition. This is reasonable since these trace compounds have no effect on the bulk proper-

ties of the oil such as viscosity, density, etc. However, they do have a strong influence on oxidative stability since many of these compounds are naturally-occurring oxidation inhibitors. They also have a marked beneficial effect on the boundary lubrication characteristics of the oil.

The average molecular weight of the compounds in the oil will determine the viscosity grade, while the predominant molecular structures will govern its physical characteristics.

By chemical synthesis, it is possible to make fluids which have similar, or oftentimes vastly improved, physical and chemical characteristics as compared to petroleum oils. Aside from the fact that synthetic oils are of major interest for aircraft engine application, because of the need for certain physical characteristics and oxidative stability which conventional petroleum oils cannot satisfy, synthetic lubricants may offer many advantages in laboratory studies. These fluids are generally reasonably pure chemical compounds and, in certain cases such as the esters, the fluid is made up of one type of molecule. Thus, the problem of assessing the effect of the complex structures found in petroleum oils can be eliminated or at least reduced.

The need for high performance lubricating oils is a fairly recent development. Up to the time of World War II, conventional petroleum oils were adequate for most machinery. Although synthetic hydrocarbons and polyalkylene glycols were commercially available before 1940, their use was restricted to very specialized applications. Even the petroleum oils that were being used at that time were relatively crude forerunners of the highly compound motor oils that are available today. Many of these oils contain ten to fifteen percent of synthetic compounds, added to improve viscosity characteristics and chemical stability.

During World War II, the synthesis of new fluids as substitutes for petroleum oils was given considerable attention, particularly in Germany. Some work was also done in the United States, mainly on instrument lubricants, but this effort was limited because there was no pressing need for replacing petroleum oils. The development of the aircraft gas turbine engine for military use marked the turning point where the favorable properties of synthetic oils began to overshadow other factors, such as cost and a lack of background experience.

The first aircraft turbine engines were lubricated with grade 1010 petroleum oil. Problems with meeting the  $-65^{\circ}\text{F}$  low temperature starting requirement caused a shift to a grade 1005 petroleum, but this oil was excessively volatile and had very low viscosity at normal engine operating temperatures. It was this low temperature problem, and the need for fluids with lower volatility characteristics, which really sparked the interest in synthetic oils.

The first synthetic oil to be used was a compounded diester-base lubri-

cant, specification MIL-L-7808. Later modifications of this oil (now MIL-L-7808G) include esters other than the diesters. This is classed as a Type I oil. Problems were anticipated with this oil in many turbo-prop and helicopter transmissions because the viscosity at the normal operating temperature was not thought to be high enough to provide adequate lubrication for heavily-loaded gears. A compromise lubricant, the MIL-L-23699 oil was developed by relaxing the low temperature starting requirement from  $-65^{\circ}\text{F}$  to  $-40^{\circ}\text{F}$ . This permitted the use of a higher viscosity ester-base fluid which was thought to be a more effective gear lubricant. This is classed as a Type II oil.

The Air Force also has a specification, MIL-L-9236, for a lubricant capable of operating at bulk oil temperatures on the order of 100F higher than the MIL-L-7808. This 9236 oil has a minimum viscosity requirement of one centistoke at 400F. However, it has been found that the candidate fluids have less resistance to degradation than the MIL-L-7808 when "hot spots" are encountered. A new specification lubricant, MIL-L-27502 is now being developed. This oil will have a low temperature use limit of  $-40^{\circ}\text{F}$ , but will have a minimum viscosity of one centistoke at 500F and will be able to operate at a bulk oil temperature of 425F. For reference purposes, abstracts of these specifications are shown in Appendix I, Table I-V.

All of the oils described above are based on synthetic esters. However, there are also many other classes of synthetic oils which have also been studied extensively. Some of these are listed in Table I. It is difficult to rank these fluids on the basis of physical properties because small changes in structure, or the use of additives, can change the ranking appreciably.

Most of these synthetics are now being used for specialized applications, but each has certain disadvantages which have prevented them from gaining wide acceptance. Of these fluids, the silicones and the polyphenyl ethers are probably of the greatest current interest for high temperature bearing usage.

In the last few years, there has been a growing awareness of the importance of elastohydrodynamic (EHD) effects on the lubrication of rolling contact bearings and gears. Under the extremely high unit pressures which are generated in the contact areas, the lubricant viscosity can increase many-fold, and can thus support appreciable loads. However, the oil will also be subjected to high temperatures and high shear stresses, both of which tend to negate the increases in viscosity with pressure. The combined effect of temperature, pressure and shear on lubricant viscosity is still imperfectly understood. In addition, there are other physical characteristics of the lubricant such as: density, compressibility, dissolved gases, etc., that may play an important role in elastohydrodynamic lubrication.



TABLE I  
CANDIDATE SYNTHETIC LUBRICANTS

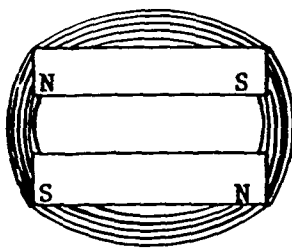
LUBRICANT TYPE	VISCOSITY TEMPERATURE CHARACTERISTICS	THERMAL STABILITY	OXIDATION RATE	BOUNDARY LUBRICATION
Esters	B <sup>(a)</sup>	C-B	C*	A*
Dimethyl and methylphenyl silicones	A	B	B	D
Halogenated silicones	B-A	E	B	B
Silicate esters	A	C-B	C*	C-B*
Fluorinated and chlorinated hydrocarbons	D	C-A	B-A	B-A
Synthetic hydrocarbons and super-refined mineral oils	C-B	B	C*	B-A*
Polyphenyl ethers	D-C	A	C	C
(a) Relative ranking, A is best, D is poorest				
* Good response to use of additives				

b. Basic Relationships Between Structure and Physical Properties

A detailed review of the effect of changing chemical composition or structure on the physical properties of oils is beyond the scope of this discussion. Ref. 1 presents some guidelines which can be used to predict physical properties from chemical structure. However, the important point to bear in mind is that the same basic laws govern both the petroleum oils and the synthetic oils. The magnitude of the attractive forces, the geometrical structure, the flexibility of the molecule, and the freedom of rotation around bonds will determine the physical properties of the oil, regardless of whether it is a natural product or a synthetic. This fact is important to bear in mind because there is a tendency to regard many lubricants, particularly the synthetic oils, as being unique species. As far as physical behavior is concerned, the differences are often more apparent than real. The purpose of this section is to point out the fundamental relationships and differences which do exist among the various lubricating oils and to present as simple a physical picture as possible of the behavior and properties of these liquids. For more detailed discussions of the structure and behavior of liquids, Refs. 2 through 5 should be consulted.

A liquid is made up of a large number of individual molecules. Visualize that, on a submicroscopic scale, each of these molecules has a shape roughly like a broken match stick. The individual molecules occupy a definite physical space and have certain limitations on their geometrical shape. However, they are not rigid, static bodies. Kinetic theory shows that each molecule is constantly in rapid and chaotic motion, just as it would be in a gas, and that this motion is theoretically independent of molecular weight and structure. The motion is governed only by the absolute temperature. Thus, each of these oil molecules is spinning, gyrating, elbowing its nearest neighbors and continually changing its position.

The forces that hold these molecules together to form a liquid are basically electrical in nature. Even though each individual molecule is electrically neutral, shifts in electron density can and do occur within the molecule, and this results in stray fields of forces which induce unbalanced forces in neighboring molecules. This is analogous to the situation where two magnets of equal pole strength are arranged as shown below.



Although these magnets are completely balanced, they still show a residual field of force which can be demonstrated by the use of iron filings. The same condition holds true in a molecule. Stray fields

of electrical force can set up large attractive forces for neighboring molecules. This effect is much more important if the molecules do not have a symmetrical chemical structure. For example, if this molecule with the match stick shape is symmetrical except for a different group of atoms at one end (polar group), there is a built-in electron unbalance (dipole moment) in the molecule, which is much more potent than the induced fields of force (induced dipole moment) described above.

These forces of attraction between molecules in a liquid are only effective over a short range since they vary inversely as the seventh power of the distance between molecules. However, they are actually very large since the distance between molecules is only slightly larger than the diameter of the molecule. Because the forces fall off very rapidly with distance, no long range order exists and, therefore, the liquids can flow in response to any shear stress. Larger molecules will have more volume and surface area. They will, therefore, exert larger attractive forces toward neighboring molecules.

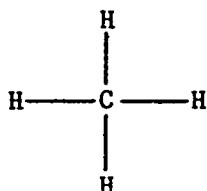
If an attempt is made to compress the liquid, the molecules can squeeze together to some extent, but then forces of repulsion begin to take over and impose a definite limit on the amount of volume change that can be achieved. Unlike gases, where the distance between molecules is large and the volume can be compressed many times before forces of repulsion start to take effect, liquid have very limited compressibility.

Summing up these conditions to this point:

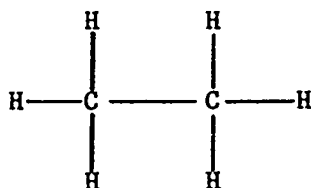
- A liquid is made up of individual molecules which are constantly in rapid and chaotic motion. The kinetic energy of translation of these molecules is governed only by the absolute temperature.
- These molecules are held together by short-range electrical forces of attraction. The distance between molecules is balanced by the attractive forces which hold the molecules together, and the repulsive forces which limit the amount that the volume can be compressed.
- Because these electrical forces fall off very rapidly with distance, liquids have only short range order. Therefore, liquids can respond to any type of shear stress.
- Larger molecules, because of their volume and surface area, exert larger attractive forces (electrostatic).

To illustrate some of the foregoing statements, consider the case of a series of straight chain hydrocarbons (paraffins). The shape of these molecules is very much like a match stick. These molecules consist of a series of carbon atoms arranged in a straight chain with hydrogen atoms attached to each carbon atom to satisfy all of the

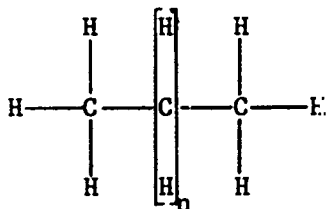
valence bonds. The simplest member of the series is a gas, methane, which consists of one carbon atom surrounded by four hydrogen atoms.



The next member of the series, ethane, has two carbon atoms:



Each succeeding member in the series has an additional carbon atom so that the structure can be represented by:



where n can be any whole number from one on up.

Some of the physical properties of this series are listed in Table II. At room temperature and atmospheric pressure, the short chain members of the series (up to 4 carbon atoms in the chain) are gases. This is because the volume and surface area of the molecules is too small to exert attractive forces large enough to keep the molecules together unless they are forced together under pressure. If the temperature is lowered so that the kinetic energy of the molecules is reduced, then the gases will condense to the liquid state.

As the chain length of the molecule is increased, the forces of attraction between the molecules become larger and liquids are obtained. With molecular chain lengths above seventeen or eighteen carbon atoms, these materials form waxy solids. To convert them to the liquid state, it is necessary to raise the temperature until the kinetic energy of the molecules can overcome the attractive forces, and break up any long range order.

The viscosity of a liquid is basically the resistance of the molecules to move past each other against the attractive forces which are trying to hold the molecules together. Since these forces increase as the size of the molecules increase (increasing molecular weight), the

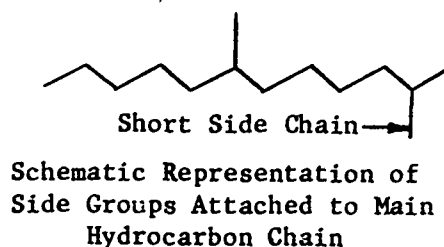
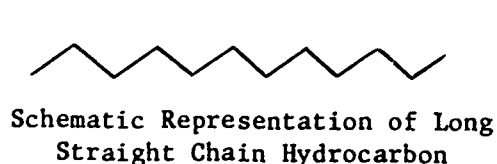
TABLE II  
SOME NORMAL PARAFFIN HYDROCARBONS

Molecular Formula	Name	Boiling Point °C	Melting Point °C	Density at 20°C g/cc
CH <sub>4</sub>	Methane	-161	-184	—
C <sub>2</sub> H <sub>6</sub>	Ethane	-88	—	—
C <sub>3</sub> H <sub>8</sub>	Propane	-45	—	—
C <sub>4</sub> H <sub>10</sub>	n-Butane	+0.6	—	0.60. (at 0°C)
C <sub>5</sub> H <sub>12</sub>	n-Pentane	36	-148	0.631
C <sub>6</sub> H <sub>14</sub>	n-Hexane	69	-94	0.658
C <sub>7</sub> H <sub>16</sub>	n-Heptane	98	—	0.683
C <sub>8</sub> H <sub>18</sub>	n-Octane	126	-98	0.702
C <sub>9</sub> H <sub>20</sub>	n-Nonane	150	-51	0.719
C <sub>10</sub> H <sub>22</sub>	Decane	174	-32	0.747
C <sub>11</sub> H <sub>24</sub>	Undecane	194.5	-26.5	0.758
C <sub>12</sub> H <sub>26</sub>	Dodecane	214-216	-12	0.768
C <sub>13</sub> H <sub>28</sub>	Tridecane	234	-6.2	0.757
C <sub>14</sub> H <sub>30</sub>	Tetradecane	252.5	5.5	0.774 (at m.p.)
C <sub>15</sub> H <sub>32</sub>	Pentadecane	270.5	10	0.776 (at m.p.)
C <sub>16</sub> H <sub>34</sub>	Hexadecane	287.5	18	0.775 (at m.p.)
C <sub>17</sub> H <sub>36</sub>	Heptadecane	303	22.5	0.777 (at m.p.)
C <sub>18</sub> H <sub>38</sub>	Octadecane	317	28	0.777 (at m.p.)
C <sub>19</sub> H <sub>40</sub>	Nonadecane	330	32	0.777 (at m.p.)
C <sub>20</sub> H <sub>42</sub>	Eicosane	205	36.7	0.778 (at m.p.)

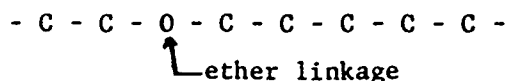
(at 15 mm)

molecules which contain more carbon atoms in the chain are more viscous and have a higher resistance to flow. As the temperature is raised, the kinetic energy of the molecules increases and this thermal agitation reduces the forces of attraction, thus decreasing the viscosity of the liquid.

Up to this point, the discussion has been confined to one molecular geometry and chemical composition, the straight-chain hydrocarbon series. This particular hydrocarbon molecule has a high length to diameter ratio and is very flexible with very little hindrance to free rotation about the carbon-carbon bonds. If short chain or cyclic groups are attached to the long chain, this will affect the geometrical alignment of the molecules and may inhibit the rotation of the carbon-carbon bonds.

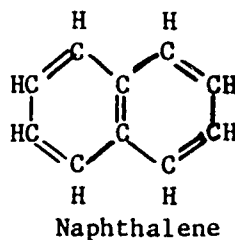
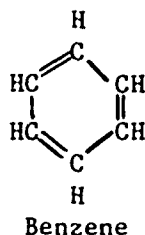


Since the molecules cannot be packed together as neatly with these appendages sticking out of the chain, the molecular spacing will be different. Thus, the force fields holding the molecules together will vary and this will change the melting point, viscosity, and viscosity-temperature characteristics of the oil. Likewise, if other atoms, such as oxygen, are inserted in the main hydrocarbon chain:



the physical properties of the liquid will be different because of changes in the bond rotation.

In addition to the straight-chain, paraffinic hydrocarbons, there are also many hydrocarbons which have a ring structure. From the standpoint of the lubricants, the most important members of this class are the aromatic compounds which are ring structures with a particular type of electronic bonding between the carbon atoms. The basic structures resemble the following atomic arrangements.



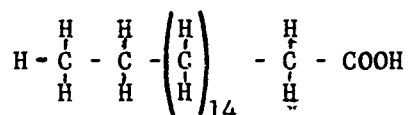
These aromatic compounds have higher attractive forces between molecules than the paraffinic-base oils and, as will be noted later, this influences many of their physical properties.

The point is worth mentioning because petroleum oils can be either predominantly paraffinic (straight chain structures) or aromatic, depending on the particular source of origin and method of refining.

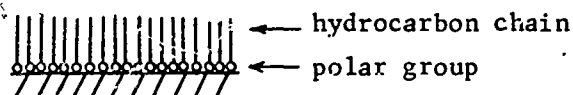
There is one more aspect of molecular structure which should be given more attention because of its importance in boundary lubrication. That is, the polarity of the molecule. As was noted before, if a molecule, such as a hydrocarbon, has a different group of atoms attached at one point, there is generally a built-in electron unbalance in the molecule so that it behaves like a bar magnet with opposite poles, even though the overall molecule is electrically neutral. It has been found that certain groups of atoms are especially important in creating this polarity. These include:

- OH alcohol group
- COOH acid group
- NH<sub>2</sub> amine group
- CONH<sub>2</sub> amide group

These groups could be attached to a carbon atom at any point on the hydrocarbon chain (by substituting the group for a hydrogen atom). However, the greatest benefit in boundary lubrication is achieved by having the group attached at one end. For example, stearic acid has the following structure:



When an oil, which contains some stearic acid in solution, is in contact with a metal surface, these molecules are attracted to the surface with the polar group oriented toward the metal. This forms a layer of molecules which are oriented vertically so that the hydrocarbon



portion stands up away from the surface. The adherence of the layer depends on two factors, the strength of the dipole moment which is pulling the molecule down against the surface and the strength of the lateral forces of attraction which are holding the hydrocarbon portions of the molecules together. Both of these forces are important and it has been shown that good boundary lubrication is only obtained

when the chain length of the hydrocarbon portion of the molecule is greater than 14 carbon atoms.

More detailed descriptions of the mechanisms by which polar molecules function can be found in many publications (e.g. Refs. 4, 6, and 7). The subject is very significant in any work on surface effects such as: partial elastohydrodynamic lubrication, boundary lubrication, corrosion inhibition, detergency, metal passivation, etc.

The physical properties of the lubricant which are believed to be the most significant in EHD lubrication include:

Nominal viscosity of the fluid

Changes in viscosity with temperature, pressure and shear rate

The bulk modulus (compressibility) of the fluid

[The bulk modulus does not enter into the film thickness calculations, but it is believed to be a significant factor which influences both temperature and pressure peaks in the film].

In addition to the above, there are other properties which may have an important influence on the results obtained. These are:

Fluid density

Gas solubility

Wetting effects and surface films

Thermal properties of the oil

Effect of polar compounds

Each of these is discussed briefly in the following paragraphs.

#### (1) Nominal Viscosity of the Fluid

As noted previously, the viscosity of a fluid is basically the resistance of the molecules to move past the force fields of neighboring molecules. Suppose that a film of oil is placed between two parallel planes, as shown in Fig. 1, with the bottom one stationary, and that the upper plane of area  $A$  is moved with a constant velocity of  $U$  by means of a force,  $F$ . The oil molecules slide over one another in layers between the flat planes. Since the oil will "wet" and cling to the two surfaces, the bottom-most layer will not move at all, the uppermost will move with a velocity,  $U$ , and each intermediate layer will move with a velocity directly proportional to its distance from the stationary bottom plane. This orderly type of movement in parallel layers is known as streamline, laminar or viscous flow. The force per unit area ( $\frac{F}{A}$ ) required to impart motion to the layers is called the shear stress, while the movement of one layer of oil relative to another is the shear strain rate. The rate of



shear ( $\dot{S}$ ) of a particular layer, sometimes called the velocity gradient, is defined as the ratio of its velocity to its perpendicular distance from the stationary surface, and is constant

for each layer:  $\dot{S} = \frac{U}{h} = \frac{U_1}{h_1} = \frac{U_2}{h_2}$  etc. Newton correctly deduced

that the force ( $F$ ) required to maintain a constant velocity ( $U$ ) of the upper plane was proportional to the area ( $A$ ) and to the velocity gradient or rate of shear ( $\frac{U}{h}$ ). This, in equation form

is,  $F = \mu A \frac{U}{h}$  where  $\mu$  is the proportionality constant, or the coefficient of viscosity, or simple viscosity of the absolute or dynamic type. By rearranging the equation, absolute viscosity is thus defined as:

$$\mu = \frac{\text{Shear Stress}}{\text{Rate of Shear}} = \frac{\frac{F}{A}}{\frac{U}{h}} \quad (1)$$

If the metric system of units (centimeter, gram, second) is used as shown in Fig. 1, shear stress ( $\frac{F}{A}$ ) is expressed in dynes per square centimeter, rate of shear ( $\frac{U}{h}$ ) in reciprocal seconds, and absolute viscosity in poises or centipoises.

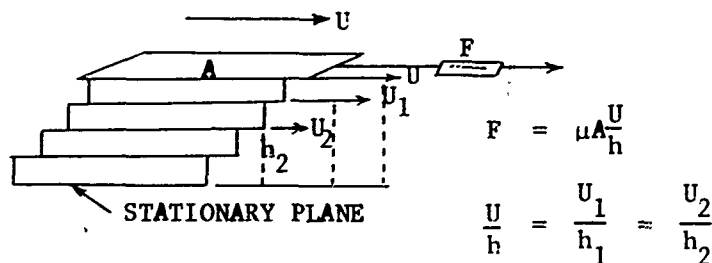


Fig. 1

Factors for converting the various units of viscosity are given in Table III. As shown in Fig. 2, the viscosity of a Newtonian fluid is independent of shear rate and the shear stress is directly proportional to the rate of shear.

TABLE III  
CONVERSION CONSTANTS

Viscosity Conversion Factors

Multiply	By	To Obtain
Stokes (cm <sup>2</sup> /sec)	Density (grams/cc)	Poises (grams/cm-sec)
Poises	100	Centipoises
Centistokes	$1.55 \times 10^{-3}$	(in. <sup>2</sup> /sec)
Centistokes	Density	Centipoises
Centipoises	$1.45 \times 10^{-7}$	Reyns
Centipoises	$1.45 \times 10^{-7}$	Slugs/in.-sec.
Centipoises	$1.45 \times 10^{-7}$	lb force-sec/in <sup>2</sup>
Centipoises	$2.42 \times 10^{-9}$	(lb force-min/in. <sup>2</sup> )
Centipoises	$5.6 \times 10^{-5}$	(lb mass/in.-sec)
Centipoises	$2.088 \times 10^{-5}$	(slugs/ft-sec) or (lb force-sec/ft <sup>2</sup> )
Centipoises	$6.72 \times 10^{-4}$	(lb mass/ft sec) or (poundal-sec/ft <sup>2</sup> )

Power Conversion Factors

Multiply	By	To Obtain
Horsepower	550	ft-lb/sec
Horsepower	0.7457	Kilowatts
Horsepower	0.7068	Btu/sec
Horsepower	2544	Btu/hr

Energy Conversion Factors

Multiply	By	To Obtain
Horsepower-hours	$2.68 \times 10^6$	Joules
Horsepower-hours	$2.74 \times 10^5$	Kilogram-meters
Horsepower-hours	$1.98 \times 10^6$	Foot-lbs
Horsepower-hours	0.7457	Kilowatt-hours

Volumetric Conversion Factors

Multiply	By	To Obtain
Cubic feet	1728	Cubic inches
Cubic feet	7.481	U. S. gallons
Cubic feet	28.42	Liters
Cubic feet	0.02832	Cubic meters

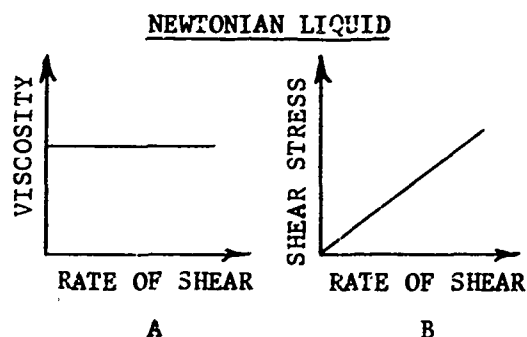


Fig. 2 A. Viscosity independent of shear rate for Newtonian Liquid.

B. Flow curve for same liquid.

Many oils do not show this Newtonian behavior. As the oil is sheared, the viscosity may decrease. Since the viscosity can vary over a wide range, depending on the shear rate, the term Apparent Viscosity is often used. This is the effective viscosity of the oil at some specified shear rate.

The most important types of flow behavior for non-Newtonian lubricants are: plastic, pseudoplastic and thixotropic. Fig. 3 shows the characteristic behavior of these types of lubricants.

Greases are plastic, i.e. a certain yield stress must be applied before they yield and flow. Pseudoplastic lubricants will yield, but the apparent viscosity decreases with increasing shear rate. The higher molecular weight silicones also behave in this manner. Polymer-thickened oils show a decrease in viscosity with shear until some limiting value is reached when they become Newtonian again.

Thixotropic lubricants show a decrease in viscosity with time, even at a constant shear rate. If the lubricant recovers to its original value of viscosity when the shear effect is removed, this is called reversible thixotropy. If not, it is irreversible. Some polymer thickened oils show this type of behavior.

A number of excellent reviews have been written on the subject of oil viscosity and the measurement techniques that are used, e.g. Refs. 8 through 10. Bondi (Ref. 2, pages 40-46) has presented a brief discussion of the theory of viscosity. Ref. 11

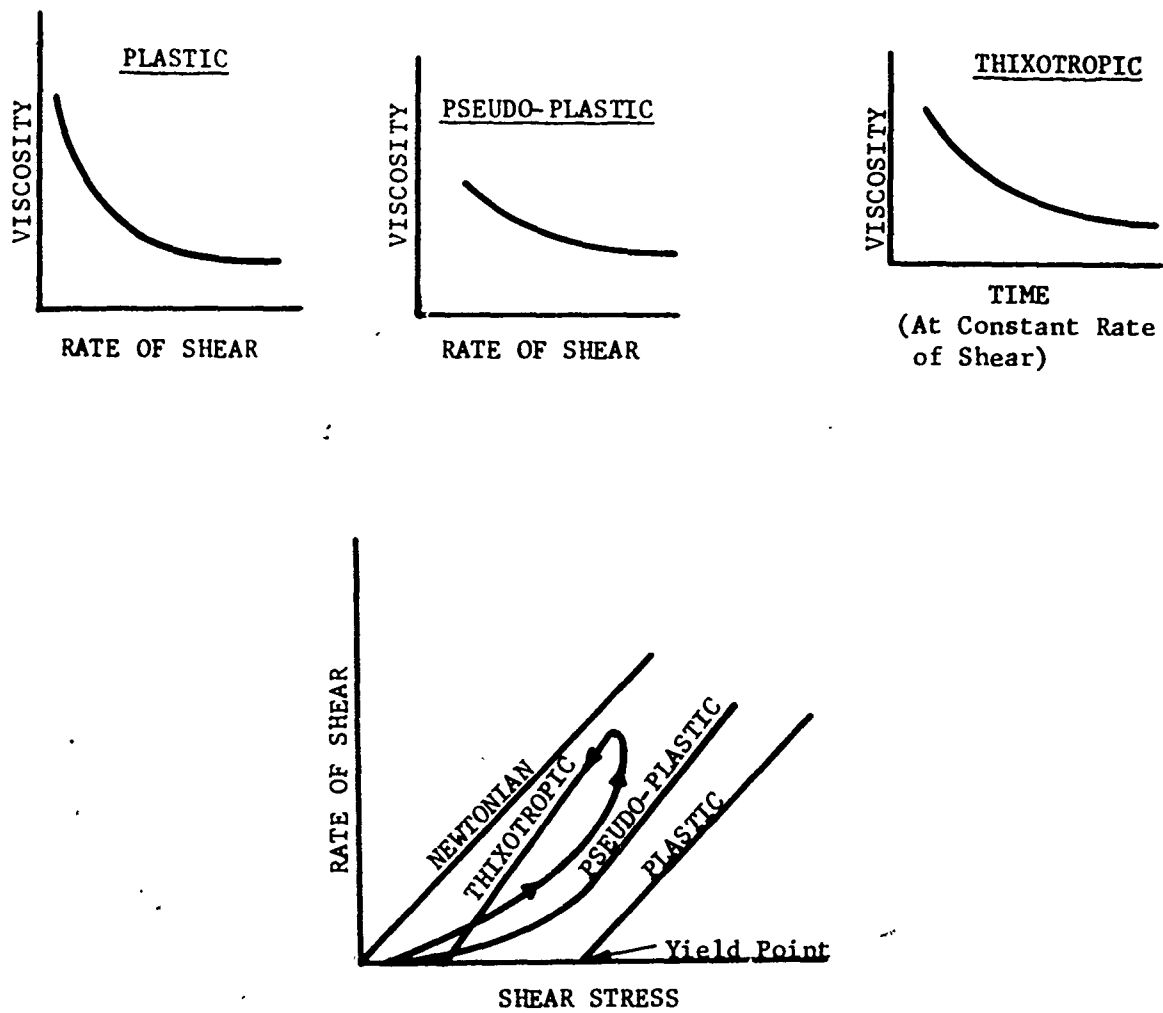


Fig. 3 Types of Non-Newtonian Viscous Behavior

treats the subject from a practical viewpoint. Murphy and Zisman (Ref. 1) discuss the subject as it relates to structural chemistry.

Standard methods are available for the measurement of viscosity as a function of temperature (Ref. 12). Since the attractive forces between molecules determine the viscosity of the fluid, it follows that the higher viscosity oils will have greater proportions of large (high molecular weight) molecules. This fact is the basis for the ASTM method of determining the average molecular weights of petroleum oils from viscosity measurements (Ref. 13). Considerable work has also been done to develop techniques for measuring the effect of shear rate on viscosity, e.g., Ref. 14. Some of this effort is described in greater detail on pages 28-30.

Mention should be made here of the significance of the term "viscoelasticity". If a liquid is stressed rapidly enough, there may not be sufficient time for flow to occur and the liquid will behave partially as an elastic solid. The combined viscous and elastic effects are covered by the term viscoelasticity. This is discussed on page 33.

The bulk viscosity of oils can be adjusted by several techniques. For example, light and heavy stocks of the same type of oil can be blended together. Standard blending charts are available for this purpose. In the case of polymers, such as the silicones or the polyalkylene glycols, the average molecular weight and molecular weight distribution of the molecules can be increased. Finally, small percentages (on the order of 5 - 10%) of very high molecular weight polymers can be added to an oil. This latter technique is being used to blend multigrade motor oils.

Any one of these three procedures could be used to make an oil with a particular bulk viscosity at a specified temperature. However, as will be discussed in the next sections, the behavior of the oil in a practical mechanism, where it is subjected to shear and pressure, may be very dependent on the exact procedure that was used to blend multigrade motor oils.

## (2) Changes in Viscosity

The rheological properties of lubricants, that is, the relation between deformation and stress, is of primary importance in lubrication. The most important rheological property of an oil is viscosity. This varies with temperature, pressure, shear rate or stress, time, past history and molecular type. In the previous sections, the relationship between viscosity and the molecular type of the fluid was discussed and the definition of viscosity was given. In this section, a discussion of the variation of viscosity with each of the other variables, a discussion

of the attempts to understand the combined effects and correlations, and a brief presentation of some less well understood rheological considerations will be given.

The study of the viscous behavior of lubricants dates back to before the beginning of this century. In the early work, much attention was given to the variation of viscosity with temperature and pressure, because viscosity exhibits one of the largest changes with temperature and pressure of all physical properties. Consequently, the variation of viscosity with temperature, and to a lesser extent, pressure, are quite well understood. However, the variation of viscosity with shear rate is considerably more in doubt in spite of the fact that the first studies of this phenomenon also date back to the last century. As pointed out earlier, the variation of viscosity with shear rate is referred to as non-Newtonian behavior. The implications of non-Newtonian behavior in lubrication are only poorly understood and are the subject of much study and controversy (Ref. 15).

#### (a) Temperature Effects

The viscosity of liquids, and the rate of change of viscosity with temperature, decreases with increasing temperature. Within any class of fluids, the higher the viscosity is, the greater will be the rate of change of viscosity with temperature. This is true whether the viscosity increase is due to a lower temperature, a higher pressure or an increased molecular weight. The rate of change of viscosity with temperature for the fluids under consideration in this work ranges from about 6% per °F at 0 F to 2/3% per °F at 300 F. As discussed earlier, when the temperature of the fluid is increased, thermal agitation of the molecules results in a reduction of the forces of attraction between the molecules. Thus, the viscosity or resistance to flow is decreased.

The variation of viscosity with temperature at atmospheric pressure and low shear rates is easily obtained by well-developed techniques. Standard methods for measuring the viscosity are described in detail by the ASTM (Ref. 12). Therefore, these data are generally available from the suppliers of any fluids.

By empirically fitting curves to viscosity-temperature data, the Walther equation can be obtained. It is valid for hydrocarbons and most other materials and is as follows:

$$\log \log (\nu + k_1) = n \log T + C \quad (2)$$

where:  $\nu$  = kinematic viscosity, cs  
 $k_1$  = constant between 0.6 and 0.8  
 $T$  = absolute temperature in degrees Rankine  
 $n, C$  = are constants for the given fluid

The Walther equation has been employed by the ASTM to generate ASTM viscosity-temperature charts, (Ref. 16) which are printed with scales to include the variation of the "constant",  $K$ , in the Walther equation. The viscosity-temperature curves for some of the fluids of interest in this program are shown in Fig. 4.

The advantage of these charts is that the viscosity of virtually all fluids, as a function of temperature, is a straight line over a very wide range of temperatures. This allows the measurement of viscosity at a few temperatures (generally two) to be used to predict the viscosity at other temperatures. Exceptions are fluids which do not give a straight line on the charts, such as certain polyalkylene glycols, and the low temperature behavior of all fluids. As the temperature is reduced, the viscosity of all fluids will, at some temperature characteristic of the fluid, begin to deviate from the straight line relationship on the ASTM charts. This deviation is generally related to phase changes that occur at low temperature, and therefore, is a function of the molecular type and weight of the constituents. In general, cyclic molecules will exhibit phase changes sooner than linear molecules. Higher molecular weight materials have phase changes at higher temperatures within a given class of fluids. The deviation from the straight line behavior always results in the actual viscosity being higher than that predicted by the straight line extrapolation to low temperature. At high temperatures, above 350 F, the actual viscosity is usually lower than the extrapolated values would indicate.

Within a given class of fluids, the cyclic molecules give a greater change of viscosity with temperature than do the straight chain type molecules, and within each of these categories, the higher molecular weight materials show a greater change of viscosity with temperature. The straight chain polydimethylsiloxanes have the least temperature sensitive viscosity of any liquid, at a comparable viscosity.

Several different methods exist to describe the variation of viscosity with temperature. Most of these suffer from a lack of generality and an inability to be readily incorporated into the engineer's physical intuition. The most common system is the Dean and Davis Viscosity Index which is an ASTM method (Ref. 17). This method compares the viscosity variation of the unknown fluid between 100°F and 210°F with that of two sets of standard fluids. One set of standard fluids is arbitrarily said to have zero VI because they have a

large variation of viscosity with temperature and the other is said to have a VI of 100 because it has a relatively small change of viscosity with temperature. One fluid is selected from each of the standard sets so that all three fluids have the same viscosity at 210°F and then the viscosity index of the unknown fluid is defined as the following

$$VI_u = 100 \times \frac{L-U}{L-H} \quad (3)$$

where L, H, and U represent the viscosities of the low VI standard, the high VI standard, and the unknown fluids at 100 F, respectively. With the use of the ASTM publication (Ref. 17), it is necessary only to know the viscosity of the fluid in question at 100°F and 210°F to determine the viscosity index of that fluid from a table. This method was conceived in the early thirties and today it is not uncommon for fluids to have viscosity indices greater than 100 or less than zero. For example, from Fig. 4, the silicone has a VI of 172 and the five ring polyphenyl ether has a VI of -74.

Two other methods are often used to describe the viscosity variation of a fluid with temperature. They are the viscosity-temperature-coefficient (VT-C) and the viscosity-temperature-modulus (VT-M). They are defined as follows:

$$VT-C = 1 - \frac{\text{kinematic viscosity at 210°F, cs}}{\text{kinematic viscosity at 100°F, cs}} \quad (4)$$

$$VT-M = \frac{1}{v} \frac{dv}{dT} = \frac{d \ln v}{dT} \approx \frac{\Delta v}{v \Delta T} \quad (5)$$

The VT-M is a function of temperature and therefore must be specified at a particular temperature. It is also commonly referred to as the viscosity-temperature coefficient. None of these parameters are very useful by themselves.

The Walther equation given above is somewhat cumbersome and difficult to employ in any analytical investigation. There are several other expressions which are useful in representing temperature-viscosity relations and are most applicable. These are valid over much smaller temperature ranges and the smaller the temperature range of interest, the simpler the expression required. Three of these are worthy of mention. They are, in order of decreasing temperature range of applicability,

$$v + A = d^{BT^C} \quad (6)$$



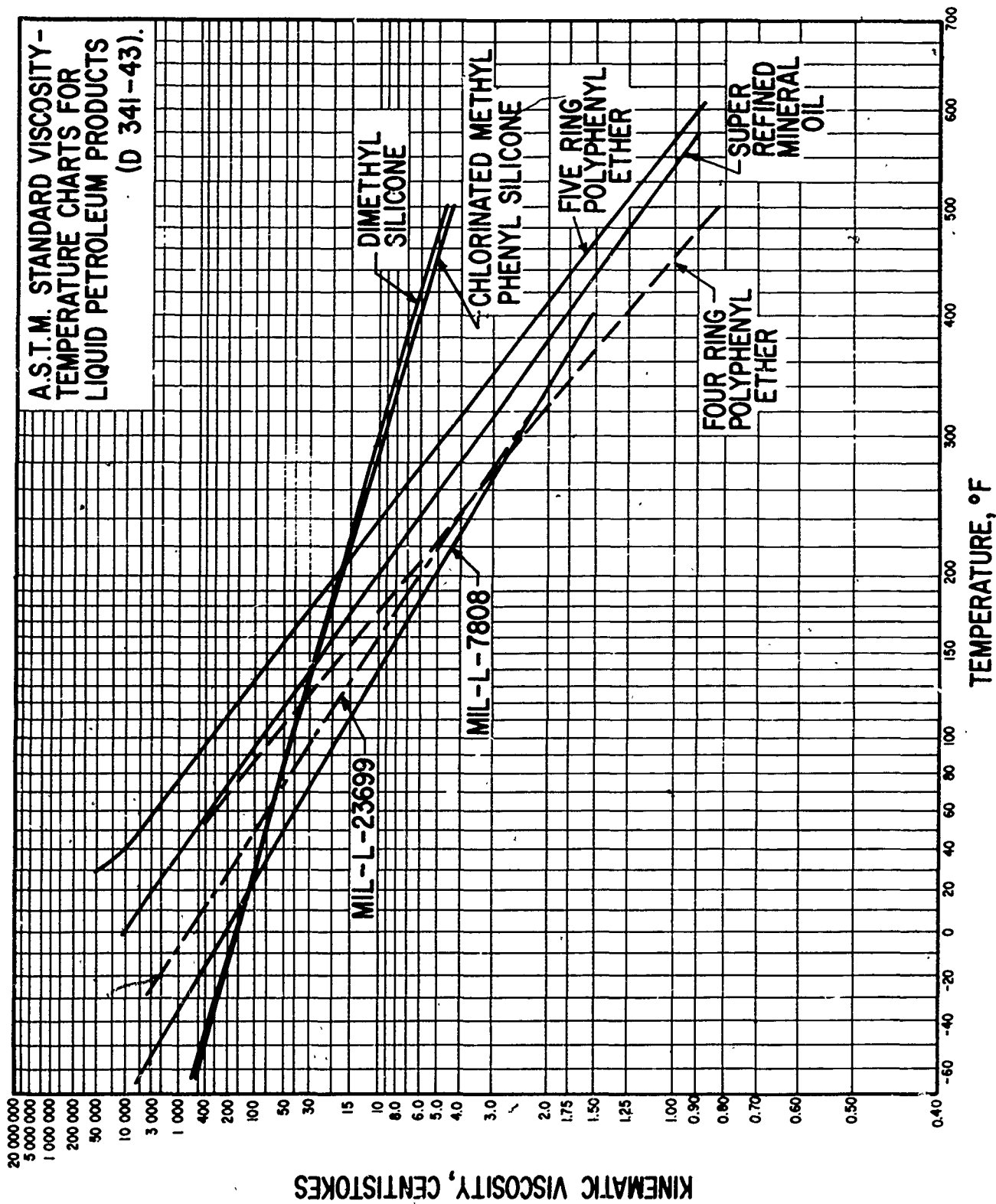


Fig. 4 Viscosity-Temperature Characteristics of Typical Candidate Lubricants  
(Courtesy of ASTM Book of Standards, Vol. 17, 1969).

$$\nu = Ae^{B/T} \quad (7)$$

$$\nu = \frac{1}{AT + B} \quad (8)$$

where A, B, and C are constants which must be determined for each particular case.

The rather large variation of viscosity with temperature can be a source of difficulty in viscometry and lubrication because, in each of these cases, mechanical energy is being dissipated through viscous action into thermal energy. This causes the local temperature to rise, which in turn causes the viscosity to decrease. In low shear rate viscometry, which is the most common, viscous heating is no problem. However, when investigating the effects of shear rate at high shear rates corresponding to practical applications, particular care must be taken to avoid the difficulties associated with viscous heating. In capillary viscometry studies, Gerrard and coworkers (Refs. 18 through 20) have determined the upper limits of energy dissipation where excessive temperature increases occur. They employed the two limiting thermal boundary conditions to find these limits, namely, the isothermal wall and the adiabatic wall cases. Novak and Winer (Ref. 21) have shown that it is possible to make measurements at shear rates higher than the limits given by Gerrard et al. by making the measurements over a very short period of time. The heating problem also exists in rotational viscometers and is discussed in some detail in VanWazer (Ref. 8, pp. 82-85).

The heat of compression, that is the temperature rise resulting from the work done on the fluid during compression, will also cause a change in the viscosity. For typical hydrocarbon fluids undergoing adiabatic compression, this temperature rise is about 10° to 15°F per 10,000 psi pressure increase.

#### (b) Pressure Effects

The effect of pressure on the viscosity of fluids has been studied for many years with P.W. Bridgeman (Ref. 22) as the earliest and most prolific investigator. The ASME study (Ref. 23) was a direct result of Bridgeman's pioneering work and still stands as the most complete study related directly to lubricants. In essence, the effect of pressure on viscosity is determined by the molecular spacing forces and forces of attraction between molecules. As shown in Fig. 5, the viscosity of naphthenic fluids increases more rapidly with pressure than that for paraffinic fluids. This is because the naphthenic fluid molecules have stronger cohesive forces, and are more closely packed, than the

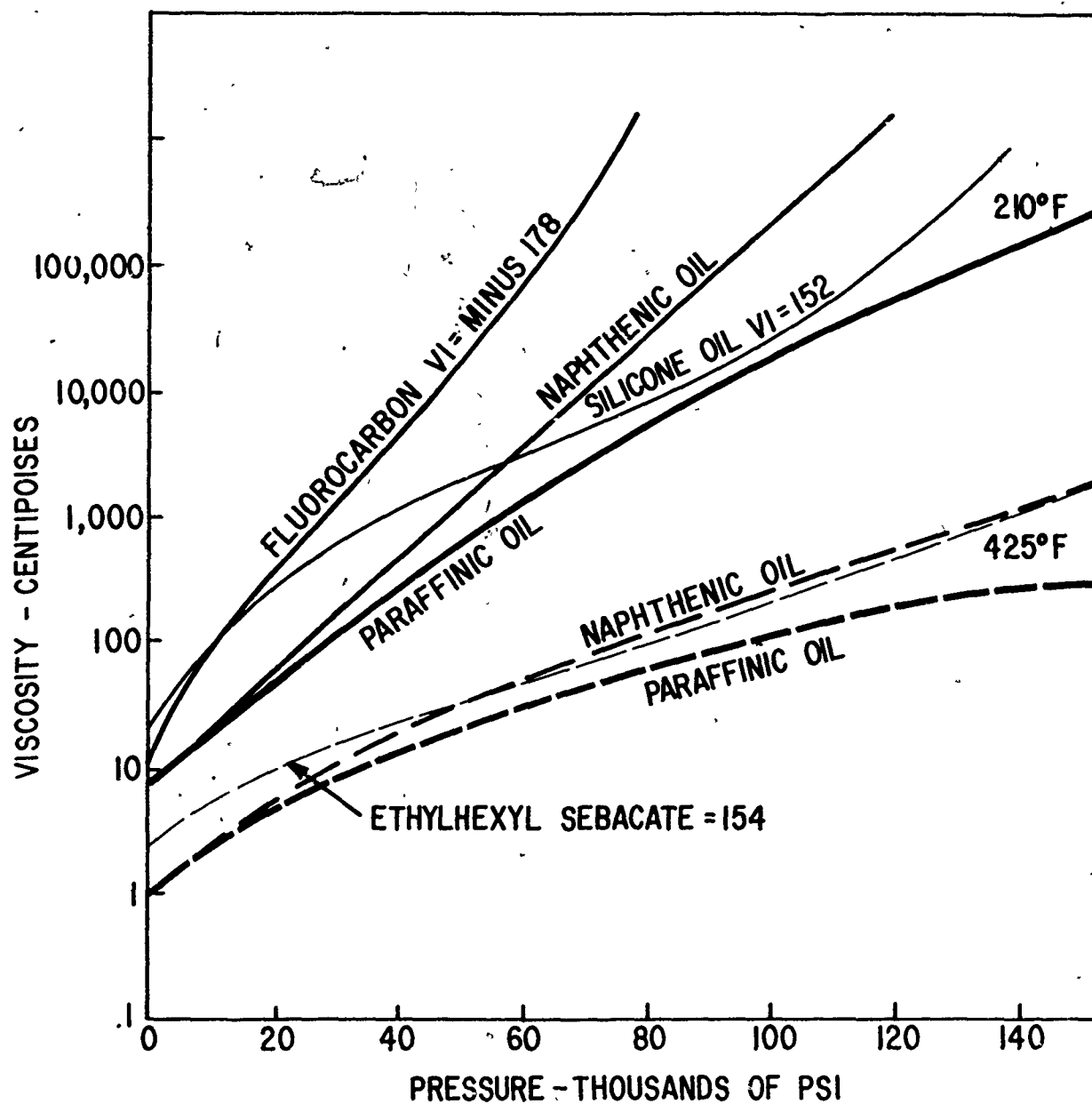


Fig. 5 Viscosity-Pressure Curves for Various Oils at Several Temperatures (Courtesy of ASME Pressure-Viscosity Report, Vol. II, 1954).

paraffinic fluid molecules. In general, it is to be expected that the increase of viscosity with pressure within a given class of fluids will be greater for cyclic molecules than for the linear molecules.

In general, the effect of pressure on viscosity is influenced by the pressure level and the bulk viscosity of the fluid. An increase in pressure at a high pressure level will have more effect on the viscosity than the same increase at low pressure. This is the result of the fact that, at high pressure, most of the free space between the molecules has already been taken up. A fluid of high viscosity (high molecular weight) will show a greater viscosity change than a low molecular weight fluid for the same increase in pressure.

Pressure viscosity data are usually presented as isotherms on a log viscosity versus pressure curve such as that in Fig. 5. To a first approximation, the variation of viscosity with pressure is exponential and, therefore, would be a straight line on a semilog plot. The experimental relation

$$\mu/\mu_0 = e^{\alpha p} \quad (9)$$

is often used because of its simplicity. As seen from Fig. 5, such an approximation can lead to serious errors in predicting the high pressure viscosity of some fluids. The pressure viscosity coefficient,  $\alpha$ , is defined as:

$$\alpha = \frac{1}{\mu} \frac{\partial \mu}{\partial p} \bigg|_T = \frac{\partial \log \mu}{\partial p} \bigg|_T \quad (10)$$

The value of  $\alpha$  used in most elastohydrodynamic analyses is the zero pressure value. Cameron (Ref. 24) has suggested that for fluids which deviate greatly from the straight line behavior, such as the paraffinic fluid in Fig. 5, a simple but better relation for expressing its pressure-viscosity behavior would be the power law relation

$$\frac{\mu}{\mu_0} = (L + C_p)^n \quad (11)$$

where  $C$  and  $n$  are constants to be determined for the fluid. In such cases, the elastohydrodynamic film thickness ex-

pressions should have  $\alpha$  replaced with  $(n-1)C$ . For all fluids investigated to date, the plot of isobars on the temperature-viscosity charts (Fig. 4) are straight lines.

Typical values of the pressure viscosity coefficient,  $\alpha$ , for hydrocarbons are from about 1 to 2 times  $10^{-4}$  psi $^{-1}$ . However, it is likely that the variation of  $\alpha$  for the synthetic fluids used in this program may vary from 1 to 5 or 6 times  $10^{-4}$  psi $^{-1}$ . Appeldoorn (Ref. 25) argues that, in elastohydrodynamics, the variation of viscosity with temperature is more important than the variation with pressure because of the small variation of  $\alpha$  in the hydrocarbon system. Although there may be some basis for this opinion when considering only the hydrocarbons, it should probably not be extended to the broader class of fluids employed as lubricants.

Although the ASME work (Ref. 23) mentioned above is the largest investigation into the effect of pressure on viscosity, a number of other investigations are worthy of note here. Bridgeman (Ref. 26) investigated the behavior of dimethylsiloxane fluids and showed that they exhibited an upturn of viscosity at high pressure ( $> 150,000$  psi). However, there was never any indication of freezing or solidification. Bridgeman's, and most other investigations were performed at very low shear stresses  $\sim (250$  dynes/cm $^2)$ . This raises questions about the relevance of such data to lubrication situations for fluids that are expected to show some non-Newtonian behavior. Two exceptions to this low shear stress limitation are the works of Novak and Winer (Ref. 21) and of Barlow and Lamb (Ref. 27). The first of these combined high shear stresses (to  $10^6$  dynes/cm $^2$ ) and high pressure (to 80,000 psi) in a capillary type viscometer, and the second employed an oscillating crystal type viscometer at very high shear rates (to 78Mc/sec or approximately  $10^8$  sec $^{-1}$ ) and pressures to about 15,000 psi.

Some experimental work has been done to evaluate the importance of pressure-viscosity effects on rolling contacts. For example, Anderson and Carter (Ref. 28) conducted an experimental study of the effect of lubricants on the fatigue life of M-1 steel balls. With a series of paraffinic petroleum fluids they found that the life improved as the bulk viscosity was increased. They also evaluated several types of synthetic fluids and found a trend toward improved fatigue life with higher pressure-viscosity coefficients. The dimethyl silicones gave the best life. It is interesting to note that, although the silicone probably had the highest pressure-viscosity coefficient at atmospheric pressure, it is a fluid whose pressure viscosity behavior deviates considerably from the logarithmic behavior mentioned above, as seen in Fig. 5. Admittedly, other factors could also have

influenced the results but the pressure-viscosity behavior seemed to show significant correlation.

(c) Shear Effects

The various types of shear dependence of viscosity have been described in the earlier section dealing with the definition of viscosity. The pseudoplastic and thixotropic types of non-Newtonian behavior are the most common types of non-Newtonian behavior observed in fluids that are used as lubricants. When the apparent viscosity decreases with increasing shear rate or shear stress, this is defined as pseudoplastic behavior, and will be the subject of this section. Thixotropic behavior is the decrease of viscosity with time at a constant shear rate. This will be discussed in the next section.

Most fluids that are used as lubricants are Newtonian over a very wide range of shear rates. However, many fluids, such as polymer-thickened fluids, or synthetic fluids with a molecular weight distribution that extends into the high molecular weight range, clearly exhibit pseudoplastic behavior, even at moderate shear rates. The pseudoplastic behavior is divided into two distinct categories. The first is that shown by polymer-thickened fluids which may contain 5-10% polymer in the base oil. At low shear rates, the viscosity is Newtonian and then, as the shear rate is increased, the viscosity begins to decrease until it reaches a level known as the second Newtonian. This is usually close to the characteristic viscosity of the base fluid, and it is constant for further increases in shear rate, at least for the range of shear rates which are normally investigated. The second category is that for fluids which are completely polymeric, such as the high molecular weight silicones. These latter fluids again have a first Newtonian but, when the viscosity begins to decrease with increasing shear rate, it continues to decrease and does not reach a second Newtonian within the very wide range of shear rates measured. In both cases, the non-Newtonian behavior is associated with the presence of high molecular weight polymeric material. The shear rate at which the behavior begins to deviate from the first Newtonian is related to the molecular weight of the polymeric material. This critical shear rate decreases as the molecular weight of the polymer increases. This leads to the speculation that, at the high shear rates encountered in elastohydrodynamic lubrication, even the apparently Newtonian low molecular weight materials like ordinary hydrocarbon lubricants may also exhibit some non-Newtonian behavior. This is a much debated and controversial point which is currently receiving some attention.

There is some question about whether to use shear rate or shear stress as the independent variable when discussing non-Newtonian behavior of fluids. This is a minor problem because the viscosity is defined as the ratio of the shear stress to the shear rate at a point and, therefore, if one

has the shear rate, the shear stress is also defined. On the other hand, it can be argued that the shear stress is the more logical variable to use because that is a measure of the force applied to the fluid. The shear rate is a measure of its response to that force.

The measurement of the viscosity at high shear rates or shear stresses must be done with caution because of the possible difficulties with kinetic energy effects and heating effects in the fluid. The kinetic energy effect is easily handled (Ref. 8) and the heating effect has been mentioned above. When dealing with non-Newtonian fluids the shear rate at the wall in either the capillary or the rotational type viscometer is not the same as in the case of the Newtonian fluid. The determination of the correct wall shear rate is straightforward and can be found in VanWazer (Ref. 8). This correction is generally small for lubricating fluids.

A great deal of work on the variation of viscosity with shear rate at atmospheric pressure has been reported in the literature. For example Klaus and Fenske (Ref. 29) have studied the effects of shear rate on mineral oils thickened with polymethacrylate, polybutene, and polystyrene. Selby (Ref. 30) has presented a general discussion of the effect of viscosity index improvers on the behavior of mineral oils at both low and normal temperatures. Philippoff (Ref. 31) studied similar systems and demonstrated the equivalence of result obtained with rotational and capillary viscometers to shear rates of  $10^6 \text{ sec}^{-1}$ .

Wright and Crouse (Ref. 32) have also studied polymer thickened fluids and attempted to correlate the results using the product of the shear rate and the shear stress as a parameter. This is the energy input rate per unit volume. Philippoff (Ref. 33) has employed a reduced variable approach to try to correlate non-Newtonian data.

Viscosity-shear rate data on bulk polymers (fluids consisting of polymer) is abundant in the literature. However, of the particular fluids of interest here, the silicones are the most thoroughly documented. For instance, the work of Currie and Smith (Ref. 34) is an early example. Producers of the dimethylsiloxane fluids supply data sheets showing this behavior, e. g. (Ref. 35).

Greases all exhibit non-Newtonian behavior. Generally, this is of the pseudoplastic variety and often at low shear stress they may also have a yield stress. That is, if stresses less than some critical values are applied to the material it will not flow but rather will behave as an elastic medium. Critical shear stress values for lubricating materials are generally so low that they are only apparent when considering the

stresses due to the forces of gravity.

Because pseudoplastic behavior is closely related to molecular weight, the average molecular weight (weight average, number average, viscosity average or all three) and the molecular weight distribution should be documented when considering the non-Newtonian behavior of any material. This should also be kept in mind when evaluating existing data because these quantities often vary from batch to batch of otherwise seemingly similar material. This is especially true of the molecular weight distribution. The bulk viscosity of a material is correlatable to the average value of molecular weight but the same viscosity and average molecular weight can be obtained with widely varying molecular weight distributions. Therefore the non-Newtonian viscous behavior can be different for two materials of the same chemical type and average molecular weight or bulk viscosity. For example, Porter and Johnson (Ref. 36), when measuring the viscosities of several petroleum oils, found that the viscous behavior was a function of the origin of the fluid and its bulk viscosity. They found that heavy petroleum stocks began to show non-Newtonian behavior at stresses above  $2 \times 10^5$  dynes/cm<sup>2</sup>. Lewis and Murray (Ref. 37) demonstrated that two dimethyl siloxanes of the same nominal viscosity (1000 cs at 25°C) and average molecular weight affected the coastdown characteristics of rolling contact bearings differently as shown in Fig. 6. The fluid blended from a very high molecular weight material and a very low molecular weight material was more sensitive to shear than the fluid with the narrower molecular weight distribution. The latter material was a standard production material, polymerized to give a viscosity of 1000 cs at 25°C, and the other was a blend of 0.65 cs fluid with 2,000,000 cs material to obtain a viscosity of 1000 cs at 25°C. The latter fluid has no practical use, it was prepared simply to illustrate a point.

Similar molecular weight sensitivity is found in other materials as well. No data has been found in the literature for MIL-L-7808 fluid at high shear stresses, but some preliminary measurements on MIL-L-23699 (Ref. 38) showed that, at 100 F, this fluid exhibited pseudoplastic behavior which resulted in a viscosity decrease of about 25 percent over a shear stress range from 1000 to  $4 \times 10^5$  dynes/cm<sup>2</sup> (i.e. a shear rate of  $3 \times 10^3$  to  $2 \times 10^6$  sec<sup>-1</sup>). The effect seemed to be reversible because the bulk viscosity was approximately the same before and after the measurements. This non-Newtonian behavior was probably due to a small percentage of a high molecular weight component in the fluid.

(d) Time Dependent Effects (Non-Viscoelasticity)

This section could also be entitled shear degradation because the type of time-dependent viscous behavior that is of major



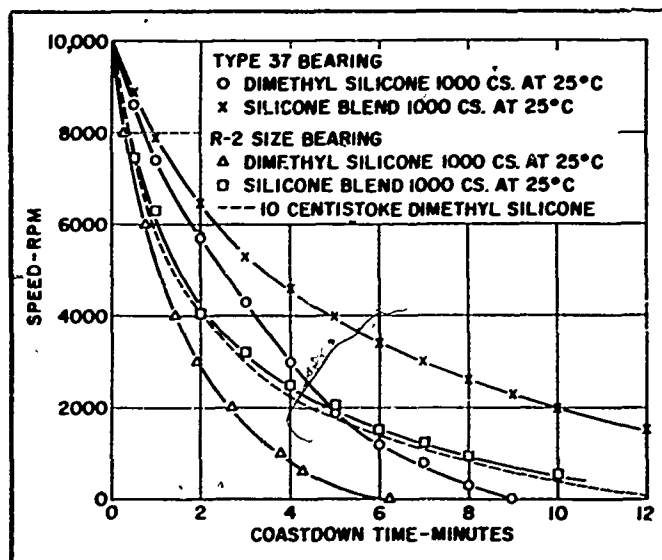


Fig. 6 Coastdown Characteristics of Rolling Contact Bearings  
(Courtesy of Lubrication Engrg., Vol. 18, No. 1, 1962).

importance to lubrication is the thixotropic behavior associated with the mechanical and thermal shear degradation of high molecular weight materials at the high shear flows associated with lubrication. Elastohydrodynamic contacts subject the fluid to very high shear rates and shear stresses, consequently dissipating large amounts of energy in the fluid. This can cause the long chain molecules to be fragmented into smaller molecules, thus resulting in a lower molecular weight material which exhibits different viscous behavior. As would be expected, the higher molecular weight materials will be more susceptible to this shear degradation.

Porter, et al (Ref. 39) have continuously monitored the changes in molecular weight distribution of a polymer-containing system with a gel permeation chromatograph. The fluid was sheared in a concentric cylinder viscometer at high shear rates and laminar flow, and then passed directly into the gel permeation chromatograph. The molecular weight distribution became progressively narrower with time, and the weight average of the distribution shifted to a lower value. This was the result of the higher molecular material being broken into smaller segments. For any given initial distribution and shear conditions there was an equilibrium distribution toward which the molecular weight distribution would progress with time. Wright (Ref. 40) reports shear degradation in high viscosity petroleum base stocks in laminar capillary flow.

Shear degradation has been the source of concern with polymer-thickened motor oils for automotive applications. The ASTM Committee D-2 has studied this question for several years and has published two test methods to be employed in determining shear degradation (Ref. 41). This question is also discussed in Refs. 14, 30, 36 and 42. The ASTM program was primarily concerned with developing a bench test which would satisfactorily simulate the degradation behavior experienced by the fluid in the automobile engine. Shear degradation can easily be obtained in a sonic oscillator, gear pump, or by discharging the fluid through an injection nozzle. The difficulty, which is yet to be satisfactorily overcome, is to correlate the behavior of the fluid in the bench test with its behavior in an application.

It is possible to have the viscosity increase with time in some applications. This is also related to changes in the molecular weight of the fluid. For instance, if the material should increase its average molecular weight through sludge formation or by the loss of low molecular weight material from volatilization, the viscosity would increase.

Shear degradation is related to the energy dissipated per

unit volume per unit time in the fluid. In elastohydrodynamic contacts, the energy input rate is very high and, even though the volume of fluid involved is small, this degradation phenomena probably plays an important role in elastohydrodynamics particularly when polymeric type materials are employed.

(e) Viscoelastic Behavior

If a fluid is stressed rapidly enough, it may behave more as an elastic body than as a liquid, because there is not sufficient time for flow to occur. As the rates of change of stress increase, the elastic behavior becomes increasingly important and the material behaves in both an elastic and a viscous fashion. Its behavior is then described as viscoelastic. This behavior is known to exist in high molecular weight materials such as polymers. Under the conditions of very small strains but very high shear rates, such as exist in the oscillating crystal type viscometer, even hydrocarbon lubricants have been shown to possess viscoelastic properties (Ref. 27). Because of the high shear rates and the very short time the fluid is subjected to them in the elastohydrodynamic contact, there has been much speculation as to the importance of viscoelasticity in elastohydrodynamics. In fact, there has been a tendency by researchers unfamiliar with rheology, to attribute anomalous behavior observed in certain applications to the viscoelasticity of the lubricant. The rheologists concerned with viscoelasticity are not in agreement about what type of constitutive equation should be used to relate the stresses and deformations in viscoelastic fluids, nor on the probable role viscoelasticity plays in lubrication (15).

General viscoelastic theory predicts that there will be both a time-varying shear stress with viscous and elastic components, and normal stresses which are different from the familiar hydrostatic pressure. The attempts of Tanner (43) and Philippoff and Tao (44) indicate that the normal stress effects are apparently not important in lubrication. However, Metzner (45) indicates that this may not be generally true. Dyson (46), in an attempt to employ the data of Barlow, et al (47) to explain the elastohydrodynamic film thickness behavior of silicone fluids, neglected the normal stress effects and considered only viscoelastic shear stress effects. Although his attempt was moderately successful in explaining the observed elastohydrodynamic film thickness data for silicones, his application of oscillatory shear data to the steady shearing conditions of an elastohydrodynamic film is viewed with skepticism by some rheologists.

Many researchers believe that the viscoelastic effect will cause a decrease in film thickness as shown by Dyson (46)

in the case of silicones; however, there are others who have argued to the contrary. For example, Forster (48) has tried to explain that viscoelasticity was responsible for the increased load carrying capacity of spur gears which was observed by Borsoff (49) with increasing speed in the high speed range. Forster claimed that the loading times in the high speed gears was of the order which would result in the viscoelastic behavior of the lubricant.

Metzner (45) has suggested the use of the Deborah Number as a means of obtaining a qualitative assessment of the effect of viscoelasticity in elastohydrodynamic lubrication. The Deborah Number is the ratio of the relaxation time of the fluid to a characteristic process time. For an order of magnitude approximation, the characteristic process time might be the average time the fluid is stressed in the contact region, and the relaxation time might be that measured in the oscillating crystal type viscometer. The elastic effects should become more pronounced as the Deborah Number increases. Some existing viscometric data indicates that the relaxation time decreases for most fluids as the shear rate is increased. Because the shear rates in elastohydrodynamic contacts are very large, this may indicate that the Deborah Number never gets large enough for the viscoelastic behavior to become important. This is clearly an area for further investigation.

Other attempts to relate viscoelasticity to elastohydrodynamics exist in the literature (e.g. Refs. 50 and 51). Lamb (52) presented a discussion of oscillatory shear work and tried to relate it to lubrication. Viscoelasticity of the lubricant obviously remains a major unknown factor in elastohydrodynamic theory at the present time. It is likely to become more important in explaining traction behavior of elastohydrodynamic films than in the case of film thickness analyses.

#### (f) Combined Effects and Correlations

The preceding discussion has been concerned primarily with the rheology of the fluid as a function of each of the independent variables by themselves. Obviously, in an elastohydrodynamic contact, several or possibly all of these variables are changing at once and, therefore, the combined effects on the rheology of the lubricant are important. Very little work has been done to combine more than two of the above independent variables. Exceptions to this are the works of Barlow and Lamb (27 and 52), who combined temperature, pressure and shear rate in the oscillating crystal; and Novak and Winer (21), who employed a capillary type device. The first two had very high shear rates ( $10^5$  to  $10^6$   $\text{sec}^{-1}$ ), but only moderate pressures (15,000 psi),

whereas the latter went to higher pressures (80,000 psi) but was limited to  $10^6$  dynes/cm<sup>2</sup> shear stress (shear rates of only about  $10^4$  or  $10^5$  sec<sup>-1</sup> at high pressure). Qualitatively, nothing unusual occurs when the independent variables are combined, but the quantitative prediction of the behavior of fluids under these combined conditions is yet to be satisfactorily accomplished.

Attempts at correlating the variation of viscosity with more than one independent variable have met with limited success. In most cases, one of the variables is allowed a very limited range. Most of this type of research has been done with variations of both the pressure and temperature. Roelands (53) performed a very extensive evaluation of the previous work in this area and proposed a four constant equation

$$\log(\log \mu + 1.200) = A \left[ \log\left(1 + \frac{T}{135}\right) + [B \left[ \log\left(1 + \frac{T}{135}\right) + C \right] \log\left(1 + \frac{P}{2000}\right) + \log D \right] \quad (12)$$

where  $\mu$  is the viscosity in centipoises, T the temperature in degrees C, p the pressure in kg/cm<sup>2</sup> and A, B, C and D are constants. His equation gives a reasonable prediction of the pressure-temperature-viscosity variation up to the pressure at which the isotherms have an inflection point. At higher pressures, the prediction is in error. However, other notable attempts at correlating this behavior have more serious limitations. For example, the equation proposed by Appeldoorn (54) is only intended to be valid to 15,000 psi, and it only allows isotherms which are straight lines on the log viscosity versus pressure plots. Many fluids show a pronounced curvature of the isotherms at pressures below 15,000 psi. Chu and Cameron (55) presented a correlation which allows for the curvature of the isotherms, but again is unable to allow for an inflection point in the curve.

Barlow and Lamb (27, 47, 52) and Philippoff (33) have successfully employed reduced variables (basically a shift in frequency) to graphically correlate pressure, temperature and shear rate data from the oscillating crystal type viscometer. The data used was limited to pressures below 15,000 psi. They have not attempted to put the data into an expression.

Webb and coworkers (56 and 57) investigated the combined effects of pressure and temperature at low shear stresses in a falling body type viscometer for a number of pure hydrocarbon substances. They attempted to find correlations for the data to relate the observed behavior to

molecular structure and free volume.

Most elastohydrodynamic analysis has been for isothermal conditions, allowing pressure to be the only independent variable affecting the viscosity. Notable exceptions to this limitation are the works of Cheng (58), Dowson (59), and Dyson (46). Cheng and Dowson attempted to include pressure and temperature effects by employing data from measurements on fluids. Dyson, as mentioned above, attempted to employ the viscoelastic data of Barlow and Lamb. Cameron and co-workers (60) presented some discussion on non-Newtonian effects in connection with some experimental elastohydrodynamic measurements. All of these were concerned with film thickness predictions only.

#### (g) Related Effects

A number of related but separate rheological effects have been discussed in the literature with respect to thin film lubrication phenomena. Most of them are directed toward a discussion of boundary lubrication but may be worthy of consideration in elastohydrodynamics as well.

These are usually related to surface effects such as surface viscosity, elasticity or rheology. It is argued that, in very thin films, the molecular force field of the solid may influence the behavior of the lubricant film and possibly make it more rigid. This can be interpreted as an increase in the viscosity of the fluid near the surface which results in a greater load carrying capacity for thin films than would be predicted from the bulk viscosity of the fluid. Criddle (61), Deryagin (62), Cameron (63), and Needs (64) have all presented such concepts in the literature. Their ideas have not been readily accepted as important to practical lubrication situations, but may be worthy of consideration.

Fein (65) has presented the idea of a compressional viscoelasticity which suggests a time delay between the increase in pressure and the increase in viscosity of a fluid in elastohydrodynamic contacts. Indeed, the question is often asked if the data taken at equilibrium pressure is meaningful in elastohydrodynamic applications where the pressure undergoes a very rapid transient. Fein and Kreuz (66) have also presented a somewhat complex model of rheodynamic behavior to explain the mechanisms of boundary lubrication.

#### (3) Bulk Modulus

All oils are compressible. As the molecules are squeezed together, forces of repulsion take over and set very definite limits on the decrease in volume and increase in density that

can take place. Definitions of the various terms used to describe bulk modulus are given by Wright (67). The fractional change in volume with pressure is designated as the compressibility of the oil. The bulk modulus is the reciprocal of compressibility. It is the resistance of the oil to being compressed and can be expressed in several ways such as: adiabatic or isentropic, isothermal, tangent and secant. Adiabatic or isentropic bulk modulus refers to conditions where the pressure change is rapid and heat is not dissipated. Isothermal bulk modulus is obtained by PVT measurements at constant temperature. It can be converted into adiabatic bulk modulus by multiplying by the ratio of specific heats,  $C_p/C_v$ . Secant bulk modulus refers to the overall change in volume between two pressures,  $(p-p_0)V_0/(V-V_0)$ , whereas tangent bulk modulus is the slope of the pressure/volume curve at a specified pressure  $V/(dp/dV)_p$ . Data are usually reported as isothermal secant bulk modulus.

Table IV (abstracted from Ref. 25) shows some typical values for various types of petroleum and synthetic oils. The dimethyl silicone oils have the lowest bulk moduli (68), i.e. they are the most compressible oils.

TABLE IV  
TYPICAL VALUES FOR ISOTHERMAL BULK  
MODULUS AT 25°C AND 0 PSIG

Petroleum Oils	260,000 psi
Diesters	290,000
Phosphate Esters	280,000
Dimethyl Silicones	150,000
Chlorofluorocarbons	240,000
Polyphenyl Ethers	390,000

Wright (67) has developed a method for predicting the moduli and densities of petroleum oils. As the bulk temperature of the oil is increased, the bulk modulus will decrease. For example, Ref. 69 presents data on the isothermal bulk modulus of various oils at temperatures to 700°F. This reference shows that the bulk modulus of a polyphenyl ether at 400°F is the same as a methylphenyl silicone at 100°F. The bulk modulus also varies with pressure.

#### (4) Lubricant Density

The density is the weight of a unit volume of oil at a specified temperature and pressure. It is determined by two factors: the chemical make-up of the oil (i.e., the types of atoms found in the molecule) and the spacing between the molecules.

The density ranges for some typical petroleum and synthetic oils are given in Table V.

TABLE V  
TYPICAL DENSITIES OF VARIOUS OILS

	Density at 60°F* in. grams/cc*
Petroleum	0.80-0.95
Diesters	0.90-0.95
Phosphate Esters	1.06
Polyalkylene Glycols	0.96-1.0
Dimethyl Silicone (Above 15 cs)	0.76-0.95
Chlorofluorocarbons	1.90
* To convert from grams/cc to: pounds/gallon, multiply by 8.35 pounds/cu.in., multiply by 0.036	

The straight chain hydrocarbons (paraffins) have lower densities than the aromatic base petroleum oils because, as noted before, the aromatic hydrocarbons are held together by stronger force fields and are therefore more closely packed.

Since the atomic makeup of the diesters is very similar to the petroleum oils, and the molecular spacing is not too different, the densities of these fluids are in the same range (0.90-0.95) as the petroleum oils.

The atomic makeup of the silicones would seem to indicate higher density since the backbone of the molecule is made up of a repeating -Si-O-Si-O- structure instead of a -C-C-C-C- structure. Both the silicon and oxygen atoms are heavier than carbon atoms. However, the silicone molecules are spaced much further apart and are held together by weaker electrical forces. For this reason, the densities of the dimethyl silicone oils are not high. They fall in the range from 0.76 to 0.95.



Actually, only those oils which contain halogens (chlorine, fluorine, bromine, and iodine) in the molecule are markedly different in density. Like the silicones, these halogenated oils have weak electrical forces holding the molecules together, and the molecular spacing is far apart. However, the halogen atoms replace hydrogen atoms in the molecule and their atomic weight is so much higher than hydrogen that they have a large influence on density.

Temperature has a limited effect on the density of oils. The atomic structure does not change, but thermal agitation of the molecules will increase their spacing. Thus, the volume of oil expands and the density decreases slowly with temperature. The coefficient of expansion  $\alpha = \frac{1}{V} \left( \frac{\partial V}{\partial T} \right)_P$ . Some typical values of  $\alpha$  are shown below in Table VI.

TABLE VI  
COEFFICIENTS OF THERMAL EXPANSION  
FOR VARIOUS TYPES OF OILS

Type of Oil	Coefficient of Expansion, Fractional Volume Change/ $^{\circ}\text{F}$
Aromatic Lubrication Oil	.00040
Paraffinic Bright Stock	.00034
Polyethylene Glycol	.00039
Diester di(2-ethylhexyl sebacate)	.00058
Dimethyl Silicone	.00056
Fluorosilicone	.000526

These changes in volume (spacing between molecules) are small. Otherwise, the oil would vaporize because the forces of attraction fall off rapidly with distance between molecules. Thus, a change in temperature of about  $200^{\circ}\text{F}$  only decreases the density of most oils by about 10 percent on the average.

#### (5) Gas Solubility

An extensive literature survey and experimental evaluation of the solubility of gases in oils is presented in Ref. 70. Although it would appear that gas solubility would affect oil viscosity, foaming, pumping and cavitation, the experimental difficulties involved in measuring the quantities of gases dissolved in various types of fluids, cloud the value of the

data obtained. Henry's Law, which states that the solubility of a gas in a liquid is directly proportional to the pressure of the gas above the liquid at a definite temperature, seems to hold for most of the gas-oil systems although the solubility does decrease at higher pressures, above 75 psia. The solubility of gases in oils generally increases with increasing temperature except for carbon dioxide.

As stated in Ref. 70, for a given set of conditions, say 500 psia and 100 F, the volume percentage of dissolved gas in a petroleum oil or diester is shown in Table VII.

TABLE VII  
SOLUBILITY OF VARIOUS GASES  
IN PETROLEUM OIL OR DIESTERS

Gas	Solubility (% by Vol.)
Helium	2.0
Hydrogen	5.1
Nitrogen	10.0
Air	15.0
Argon	24.5
Carbon Dioxide	94.0

These authors found that the effect of dissolved gases on the viscosity of an oil was significant when the gases argon and carbon dioxide were used at pressures on the order of 500 to 600 psia. An appreciable drop in load carrying capacity should be anticipated with these gases in high pressure systems. The effect of dissolved gases on oil viscosity with helium, hydrogen, nitrogen, and air were much smaller. They did not find a clear relationship between foaming and the type or quantity of gas dissolved in the oil. Similar work has been done by Klaus to determine the effect of dissolved gases on oil viscosity at high pressure.

#### (6) Wetting Effects and Surface Films

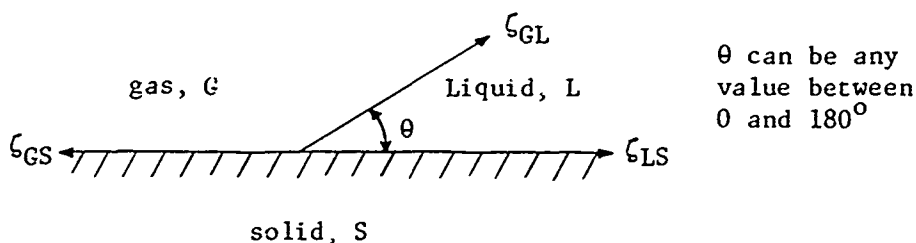
##### The Concept of Surface Tension

A molecule in the interior of a liquid is completely surrounded by neighboring molecules and the forces of attraction which are exerted on this molecule are, on the average, equal in all directions. On the surface, however, there is a resultant attraction inward because the number of molecules per unit volume in

the bulk of the liquid is much greater than the number in the vapor above. Because of this inward attraction, the surface tries to contract to the smallest possible area with the result that the surface behaves as if it were in a state of tension. This force, which is the Surface Tension,  $\zeta$ , has a characteristic value for each liquid. It is the same at every point and in all directions along the surface of the fluid. It may be defined as the forces in dynes acting at right angles to any line of one centimeter length on the surface. The existence of a surface implies an interface between two media, e.g., a liquid and air or a liquid and solid, and the surface tension depends on the nature of both media.

#### Contact Angle and Wetting

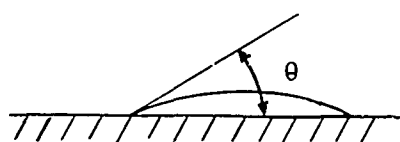
When a drop of liquid is placed in contact with a solid surface, it assumes a characteristic angle of contact equal to the angle  $\theta$  as shown below.



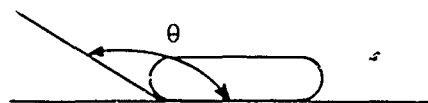
At equilibrium, the forces must balance and

$$\zeta_{GS} = \zeta_{LS} + \zeta_{GL} \cos \theta$$

where  $\zeta_{GS}$ ,  $\zeta_{LS}$  and  $\zeta_{GL}$  are the surface tensions of the gas-solid, liquid-solid and gas-liquid surfaces respectively. The contact angle  $\theta$  depends on the three interfacial tensions, but whether it is greater or less than  $90^\circ$  depends on the relative magnitude of  $\zeta_{GS}$  and  $\zeta_{LS}$ . If the gas-solid tension ( $\zeta_{GS}$ ) is greater than that for the liquid-solid interface ( $\zeta_{LS}$ ), then the  $\cos \theta$  must be positive and  $\theta$  is less than  $90^\circ$ . If the reverse is true, then  $\theta$  must be between  $90^\circ$  and  $180^\circ$ . In the former case, e.g., water on clean glass, the water is said to "wet" the glass. [This is a matter of degree since complete wetting implies a contact angle of  $0^\circ$ ]. In the latter case, e.g., mercury on glass, the liquid is said not to "wet" the glass. These examples can be illustrated as follows:



Wetting, Water on Glass  
 $\theta$  less than  $90^\circ$



Non-Wetting, Mercury on Glass  
 $\theta$  greater than  $90^\circ$

The primary reason for introducing this subject into a discussion of elastohydrodynamic lubrication is because the wetting characteristics of commercial lubricants and bearing surfaces are not well-established or controlled. In both hydrodynamic and elastohydrodynamic calculations, the assumption is made that the layer of oil immediately adjacent to the bearing surface is firmly adherent and immobile. It is also assumed that the properties of the lubricant at the solid-liquid interface are typical of the bulk properties of the fluid. If, for example, a steel bearing surface is being used with a pure lubricant that wets the steel readily, then these assumptions are reasonable. However, if the steel surface is covered with some form of a reaction film, or if the oil contains a surface-active compound which is preferentially adsorbed at the lubricant-metal interface, then the wetting characteristics of the bulk oil and the steel surface can be drastically changed. For conventional hydrodynamic bearings, this would have no significant effect. The magnitude of the film thicknesses involved would mask such thin film effects. However, in elastohydrodynamic lubrication, particularly under marginal conditions, the characteristics of the surface films might be important. If the fluid did not wet the bearing surfaces, or if the physical properties of the fluid were significantly different in the boundary layer (because of preferential adsorption or concentration of surface-active compounds on the surface), then this could affect the film thickness calculations.

Two studies can be cited which show that wetting or surface film formation could be important. In the first study (71) a number of lubricated, instrument size, ball bearings, which appeared to be in satisfactory condition before being put on test, showed surface distress and erratic torque results after short periods of running time. Examination disclosed that the bearings were contaminated with some unknown films and that the bearings were poorly wetted by the lubricant. Once these bearings were cleaned so that good wetting was obtained, no further difficulties were experienced.

Another example of this type was observed in the NASA high temperature ball bearing tests described in Ref. 72. A polyphenyl ether was found to be satisfactory when running in air at 600 F, but failed at the same temperature when run under nitrogen. Johnson (73) has hypothesized that these failures were due to the formation of non-wetting surface films which prevented adequate heat transfer through the oil. It has also been suggested that some form of a contaminant film might inhibit reactions between the lubricant and the bearing surface, thus affecting boundary lubrication. Regardless of the mechanisms involved, these studies show that surface films may play an important role in elastohydrodynamic lubrication.

Similar considerations might explain some of the problems which have been encountered with silicone oil-lubricated ball bearings.

Under heavily loaded, high speed conditions, it has been found that bearings lubricated with silicone oils may show an excessive temperature rise with no tendency for stabilization. This could also be the result of non-wetting or reaction-inhibiting films.

A study of dimethyl silicone oils as lubricants for rolling contact bearings operating in high vacuum is reported in Ref. 74. In these tests, most of which were run at 100 rpm, some surface distress was noted on all of the test bearings. Under the same test conditions, petroleum oils were effective lubricants for at least 1000 hours of running time. These results again suggest the possibility that the elastohydrodynamic characteristics of silicone oils may be influenced by the formation of surface films.

As far as the physical properties of the fluid in the boundary layer are concerned, consider what is known about the mechanism of lubrication by petroleum oils. It has been well established that the boundary lubricating effectiveness of these oils is due to the presence of small concentrations of acidic polar compound, e.g. fatty acids, in the oil. These polar compounds are absorbed on the bearing surfaces and, for the case of reactive metals such as steel or copper, they can chemically react to form metal-organic compounds such as metal soaps. Fein (75) has demonstrated experimentally that during sliding, these soaps can interact with the hydrocarbon carrier to form a gelatinous grease-like structure around the sliding contact areas. He has hypothesized that this is the lubricant film which is functioning in the thin film region. Thus, the oil which is adjacent to the metal surface could have completely different rheological properties than the base oil.

Extreme pressure additives, e.g. compounds containing phosphorous, chlorine and sulfur, function as lubricant additives by decomposing at the hot spots on the sliding surfaces and reacting to form protective inorganic films. These additives will also affect the wetting characteristics of the lubricant and may influence the physical properties of the lubricant adjacent to the bearing surface. Beneficial results have been obtained by immersing ball bearings in hot tricresyl phosphate to pretreat the surfaces before running the bearing on a conventional petroleum oil.

#### (7) Thermal Properties

There is very little that can be done as far as the thermal properties of lubricants are concerned. As shown in Table VIII, the thermal characteristics of most of the oils are so much alike that it would be difficult to use these properties as criteria for the selection of fluids. The only exception would be the chlorofluorocarbons.

TABLE VIII  
TYPICAL THERMAL PROPERTIES OF LUBRICANTS

Lubricant	Specific Heat BTU/lb °F at 100° F	Thermal Conductivity BTU/hr.ft <sup>2</sup> °F/ft at 100° F
Petroleum Oils (Average)	0.43	0.08
Polyalkylene Glycols	0.45	0.09
Dimethyl Silicones	0.35	0.08
Phosphate Esters	0.42	0.07
Diesters	0.46	0.09
Polyphenyl Ethers	0.39	0.08
Chlorofluorocarbon	0.29	0.04
Water	1.0	0.34

The thermal conductivity of an oil decreases with temperature and can be estimated by the following equation:

$$K_f = \frac{0.812}{\rho_{60}} (1 - 0.0003 (T - 32)) \quad (13)$$

where K is in BTU/hr.ft<sup>2</sup> °F/in.

$\rho_{60}$  = density in grams/cc at 60°F

The specific heat increases with temperature according to the following equation:

$$C_f = \frac{(0.388 + 0.00045 T)}{\rho_{60}} \quad (14)$$

where  $C_f$  = specific heat in BTU/lb/°F

A more detailed discussion of the thermal properties of various lubricants is given in Refs. 2, 3, and 25.

#### (8) Effect of Polar Compounds

Earlier in this discussion of lubricant properties, it was pointed out that the presence of polar compounds in the lubricant could have an appreciable effect on the boundary lubricating characteristics of the fluid. For cases where metal to metal contact can occur under heavy loads or high speeds, extreme pressure compounds (compounds containing active ele-

ments such as chlorine, sulfur, phosphorous, etc.) are also used as additives to prevent metal seizure. It is beyond the scope of this discussion to go into any detail on the mechanisms of lubrication in this regime. The subject has been covered very well in many references, e.g. Refs. 3, 4, 6, and 7. However, the fact that the thicknesses of elastohydrodynamic films are often on the same order of magnitude as the surface roughness values indicates that metal to metal contact probably occurs frequently at least to some degree. The influence of these sliding contacts, and subsequent surface reactions, on elastohydrodynamic lubrication has never been resolved. Fein (66 and 75) has pointed out that this could be an important consideration.

#### c. Properties of Some Candidate Lubricants

Among the candidate oils which are being considered in this program, the following lubricants are of particular interest.

- 1) Ester base oils meeting the MIL-L-7808 specification
- 2) Ester base oils meeting the MIL-L-23699 specification
- 3) Mineral oils
- 4) Polyphenyl ethers
- 5) The dimethyl, methylphenyl, and halogenated silicone oils

Some information on the composition and properties of these oils are given in Appendix A. This is by no means an exhaustive survey of the properties of these oils, but should rather be considered as a starting point. As the work progresses, the need for obtaining particular kinds of data will become more obvious. Some of the information will be available in the literature, the rest must be obtained by actual laboratory work.

Based on the results of this survey, conventional physical property data on both petroleum and synthetic lubricants are readily available from suppliers and other laboratory sources. Information on viscosity as a function of shear stress and pressure is needed and, although it is gradually being accumulated from various sources, additional measurements will probably be required to meet the objectives of this program. The most obvious gap in this work is a lack of knowledge of what properties are really important to elastohydrodynamic lubrication. Viscoelasticity, wetting, density, etc., all of these may be relative considerations. Careful experimentation, coupled with analysis, appears to be the best way to resolve this problem.

## 2. FILM THICKNESS

The most important aspect of elastohydrodynamic lubrication is the calculation of film thickness, since in all lubrication processes the primary objective is still the separation of surfaces. The significance of film thickness in relation to all major modes of failures is self-evident. One can almost intuitively expect that a thicker film would improve conditions in every aspect of failure. This is indeed true since all failure records indicate that a thicker film prolongs the fatigue life, diminishes the chance of scoring, and reduces the wear rate for a rolling and sliding contact.

### a. Film Thickness and Film Shape of Line Contacts

Theories and experiments have shown that the film shape of a line contact is reasonably flat throughout the conjunction, with a constricted section at the exit. The minimum film thickness at the exit is approximately 70-75 percent of the nominal film in the flat region.

Since the nominal film thickness determines the level of the separation in the conjunction, the calculation of this quantity has been recognized as the most important problem in elastohydrodynamic lubrication and has received considerable attention. In 1949, Grubin and Vinogradova (82) first successfully obtained the solution of the Reynolds equation at the inlet section by assuming the inlet deformation profile to be identical to the Hertzian profile. This approach circumvents the necessity of solving the coupled elasticity and Reynolds equation and offers great simplicity in determining the separation between the line contacts. Grubin's results can be summarized in the following expression in dimensionless form:

$$\frac{h_o}{R'_x} = 1.95 \frac{(\bar{E}\bar{U})^{\frac{8}{11}}}{\bar{W}^{\frac{1}{11}}} \quad (15)$$

where

$$\begin{aligned} h_o &= \text{nominal film thickness} \\ R'_x &= \text{effective radius} = \frac{R_{x1} R_{x2}}{R_{x1} + R_{x2}} \end{aligned}$$

$$\bar{E} = \alpha E'$$

$$\bar{U} = \frac{\mu_o U}{E' R'_x}$$

$$\bar{W} = \frac{W}{E' R'_x}$$



$$\frac{1}{E'} = \frac{1}{2} \left[ \frac{1-\nu_1^2}{E_1} + \frac{1-\nu_2^2}{E_2} \right]$$

$\alpha$  = pressure-viscosity exponent

$U$  = rolling velocity =  $(U_1 + U_2)/2$

$\mu_0$  = inlet viscosity

$E$  = modulus of elasticity

$\nu$  = Poisson's ratio

Experimental verification of Grubin's results was first provided by Crook (83) who deduced oil-film thickness from measurements of the electrical capacitance between each disk and a lightly loaded pad riding the oil film adhering to the surface of that disk. He also used a second method (84) in which he calculated the oil-film thickness from the capacitance between the two disks, and showed that the results given by this method are in essential agreement with those obtained by the first method.

The second important experimental measurement of film thickness was made by Sibley and Orcutt (85) using an x-ray technique. With the exception that Sibley and Orcutt's results show a slight load dependence, their data are in good agreement with Crook's measurements. It should be noted that both Crook's and Sibley and Orcutt's results were conducted at low or moderate speeds.

After Crook, further experiments on film thickness using the capacitance method were conducted by Archard and Kirk (86), by Christensen (87), and more recently by Dyson et al (88). All results gave further confirmation of Grubin's formula in calculating the film thickness. Very recently Cameron and Gregory (89) initiated a variable magnetic reluctance technique and their results show good correlation with those obtained by capacitance measurements.

Grubin's method gives an accurate prediction of the separation of the film, but not the detailed film distribution. However, he did give a full description of the physical mechanism of the coupled elastohydrodynamic problem. Later his colleague, Petrusevich (90) succeeded in obtaining numerical solutions to the coupled equations for the first time. He predicted that the film thickness is almost constant over most of the conjunction region with a local reduction at the exit. Dowson and Higginson (91), in 1959, intrigued by Petrusevich's work, developed a new numerical approach to the elastohydrodynamic problem and succeeded in obtaining complete solutions of the isothermal film and pressure distributions as functions of dimensionless speed, load and lubricant parameters. Later they also extended their results to include the effect of the lubricant compressibility. An empirical formula was also given by Dowson and Higginson to predict the minimum film thickness of line contacts. Their expression for minimum film thickness is given by the following relationship

$$\frac{h_0}{R_x} = 1.6 \frac{\bar{E}^{0.6} \bar{U}^{0.7}}{W^{0.13}} \quad (16)$$

where the symbols have been defined previously.

Following Dowson and Higginson, Archard, Gair and Hirst (92) also developed a numerical solution which confirms the film shapes shown by Dowson. More recently, Cheng (93) obtained a numerical solution of the full elastohydrodynamic problem by including the thermal effects and his results show that at surface speeds up to 250 in/sec for steel rollers, thermal effects do not have significant influence upon the prediction of the nominal film thickness.

The accuracy of the theoretical investigations in predicting film separation at low and moderate speeds is best illustrated in Fig. 7. It is seen that the experimental results (84, 85) agree very well with the curves (91, 92, 93).

Moes (95) modified the work by Koets (96), shows a comprehensive survey diagram summarizing all theories predicting film thickness for from extremely light loads to heavy loads at low and moderate speeds in terms of three parameters. The diagram and the parameters are shown in Fig. 8. It is seen in the diagram that at the extreme left is the rigid-body theory asymptote by Martin (97) and between this asymptote and the high load region covered by Dowson and Higginson is the numerical method by Weber and Saalfeld (98) for light loads (see discussions on pressure distribution).

In the high speed region the only experimental data are those measured at Battelle Memorial Institute in the past five years (18-23). These data show a drastic reduction of film thickness when speed increases, as indicated in Fig. 9. Furthermore, a strong load-dependence can be seen in Table IX and in the circumferential film profiles shown in Fig. 10.

Since Grubin's analysis is based on the assumption of an isothermal lubricant, it is limited to the conditions where the heating effects of the lubricant are negligible. For high rolling speeds such as those occurring in the rolling-element bearings of jet engines, the reduction of film thickness due to heating is severe and Grubin's formula is no longer valid. To remedy this, the energy equation must be solved in conjunction with the Reynolds equation in the inlet section. Such a thermal Grubin analysis has been recently developed by Cheng (105). The analysis is quite general, and it includes the heat generation due to the compression of the fluid, heat convection, and heat conducted into the solids. Design data and design procedure in determining the thermal inlet film thickness were also generated and included in Ref. 105. A similar Grubin type thermal solution without the effect of heat convection, heat of compression and heat conduction into the boundary were also recently developed by Kannel, et al (104).

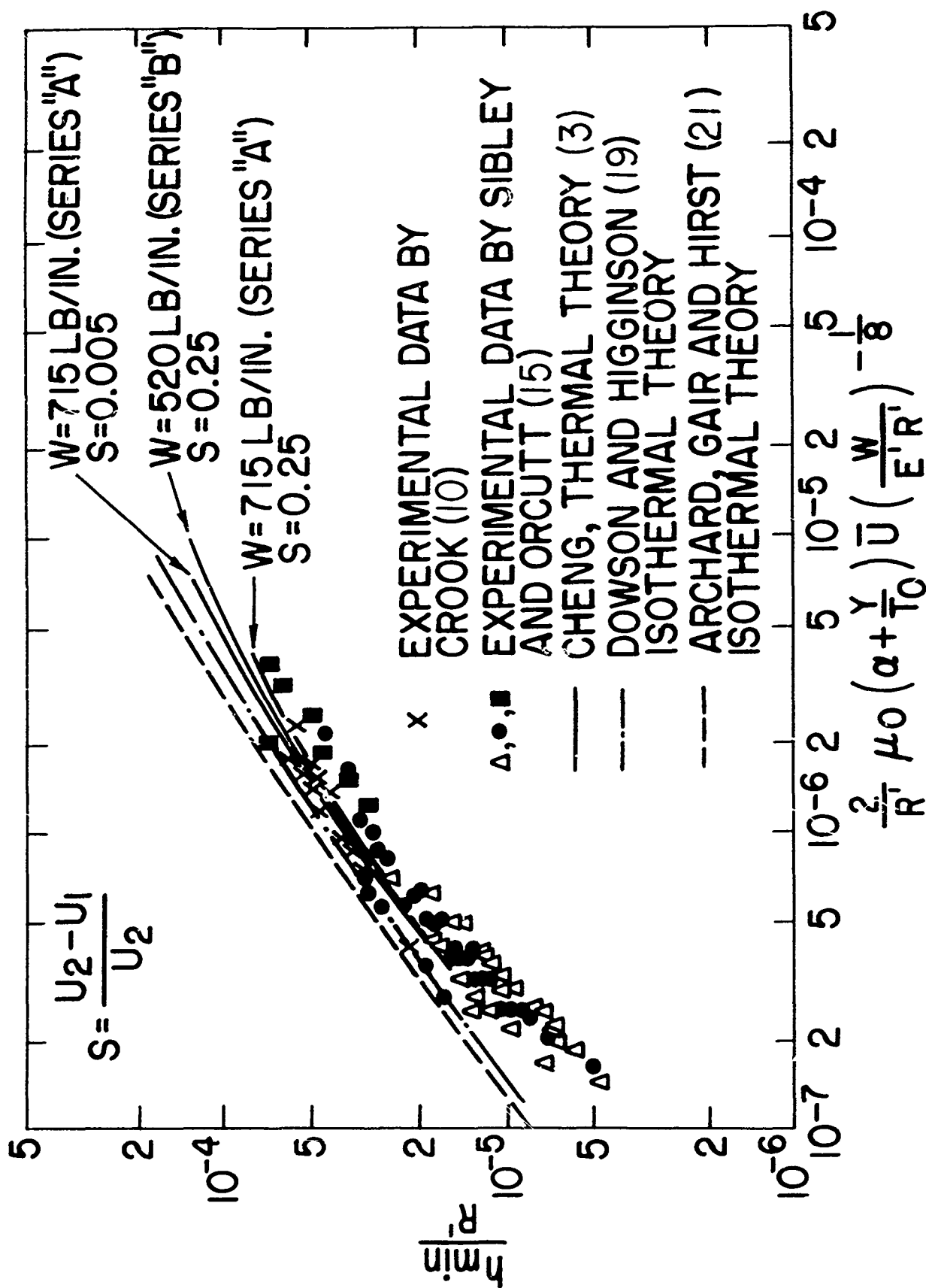


Fig. 7 Film Thickness Comparison

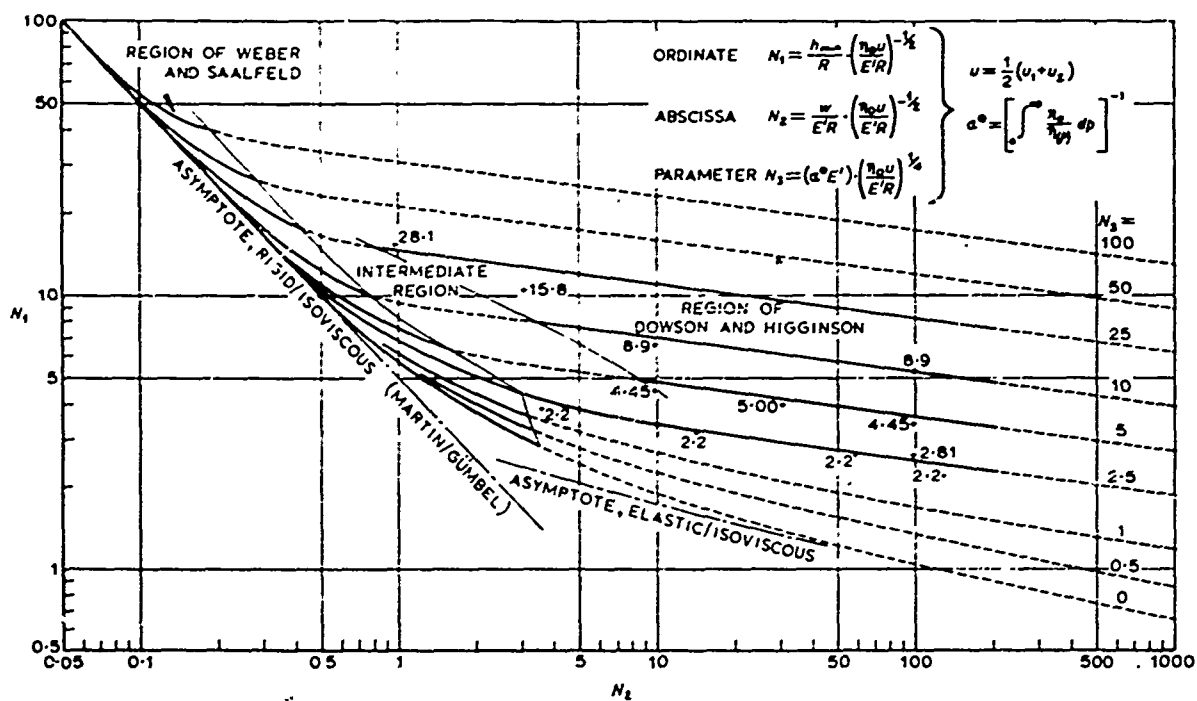


Fig. 8 Survey Diagram for Incompressible Isothermal Elastohydrodynamic Lubrication. (Courtesy of Proc. Instn. Mech. Engrs., 1965-66).

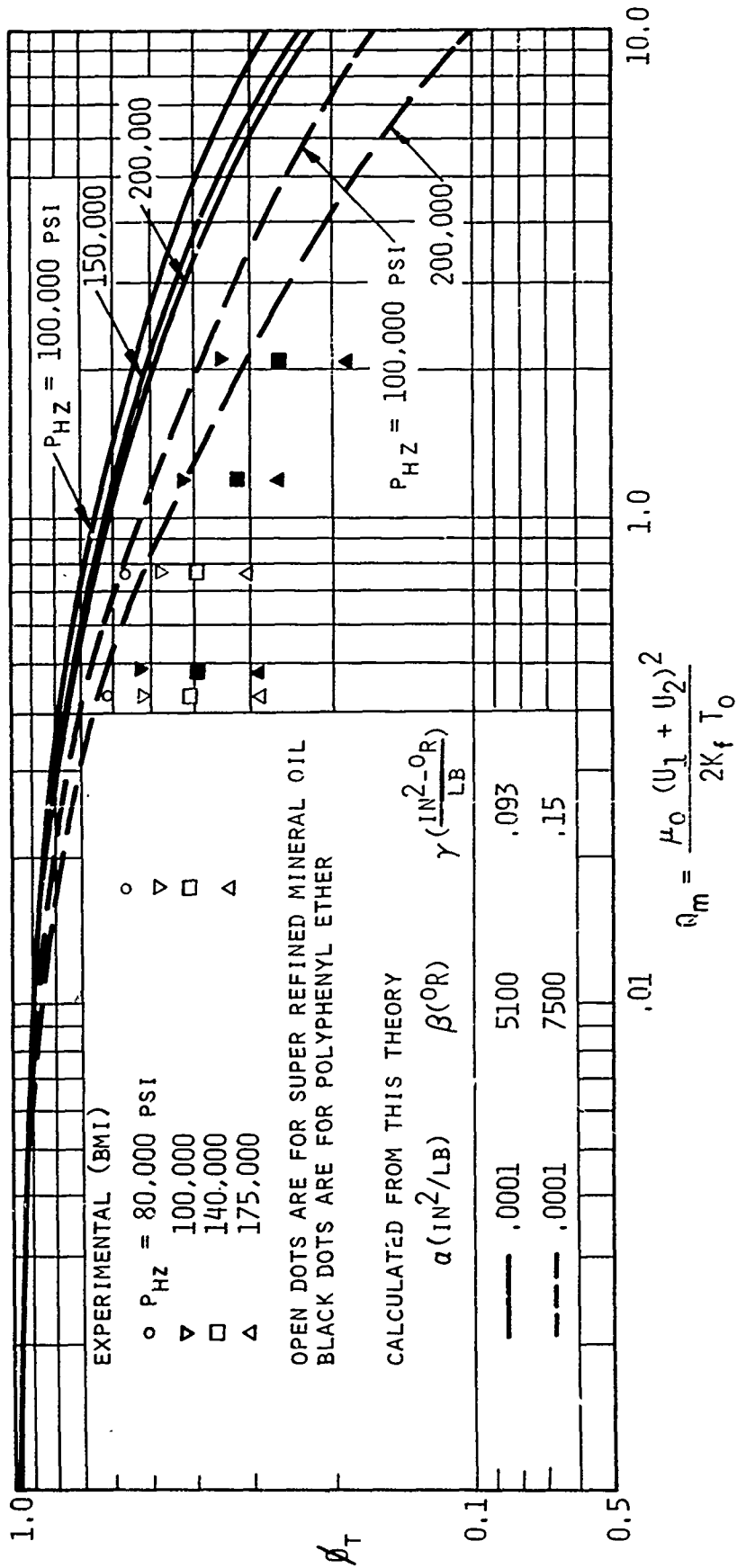


Fig. 9 Comparison of  $\phi_T$  with Experimental Data

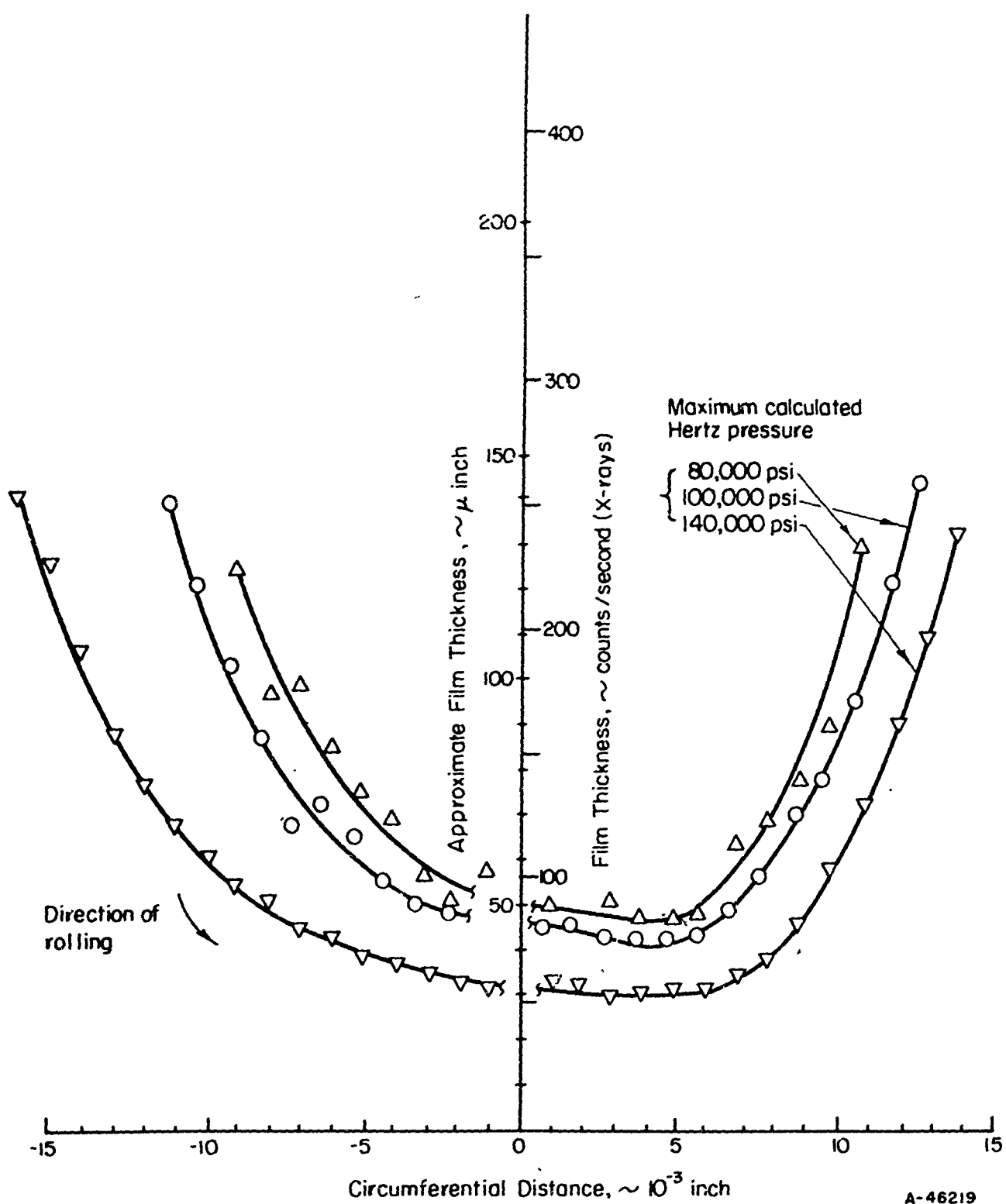


Fig. 10 Circumferential Profiles of Lubricated Rolling Disks.  
(United States Air Force Tech. Report No. ASD-TDR-61-643,  
Sept. 1964).

TABLE IX  
MEASURED FILM THICKNESS BETWEEN ROLLING DISKS  
LUBRICATED WITH A HIGHLY REFINED MINERAL OIL (21)

$T_o$ °R	$\mu_o$ lb-sec in <sup>2</sup>	$\alpha$ in <sup>2</sup> /lb	$P_{HZ} \times 10^{-4}$ psi	$U$ in/sec	$Q_m$	$h$	$h_{DOW} \times 10^6$	$\phi_T$
638	$1.6 \times 10^{-6}$	0.0001	8	860	0.172	22	39.3	0.56
"	"	"	10	"	"	17.5	37.1	0.47
"	"	"	14	"	"	14.0	34.0	0.412
"	"	"	17.5	"	"	9.5	32.0	0.335
"	"	"	8	1360	0.430	33	54.0	0.612
"	"	"	10	"	"	26	51.0	0.51
"	"	"	14	"	"	19	46.6	0.408
"	"	"	17.5	"	"	12.5	44.0	0.284
"	"	"	20	"	"	10	42.6	0.234
"	"	"	8	1820	0.768	35	62.5	0.560
"	"	"	10	"	"	28	59.0	0.475
"	"	"	14	"	"	21	54.0	0.388
"	"	"	17.5	"	"	15.5	51.0	0.304
"	"	"	20	"	"	13	49.3	0.264

$$Q_m = \frac{2\mu_o U^2}{K_F T_o} \quad (17)$$

$$\frac{h_{DOW}}{R'_x} = 1.6 \frac{(\alpha E')^{0.6} \left( \frac{\mu_o U}{E' R'_x} \right)^{0.7}}{0.13 \left( \frac{W}{E' R'_x} \right)} \quad (18)$$

$$\phi_T = \frac{h}{h_{DOW}} \quad (19)$$

Fig. 9 plots two groups of  $\phi_T$  curves, the ratio of the actual film thickness to that predicted by the isothermal theory, calculated from the present theory. The solid curves are for a lubricant with a moderate temperature viscosity exponent, while the dotted curves are for a lubricant with strong viscosity temperature variance. Conditions used in the experiments are listed in Table IX. In the experimental data, the value  $\phi_T$  is assumed to be the ratio of the measured film to that calculated by the Dowson and Higginson formula. These data are also presented in two groups. The open dots are for a super refined mineral oil and the black dots are for polyphenyl ether. It is seen that the data for polyphenyl ether blends smoothly with those obtained for the mineral oil. In general, the trend of the theoretical curves appears to be quite in harmony with the experimental data. However, quantitatively the measured film thicknesses still lie considerably below the calculated value particularly for highly loaded cases. Discrepancies as much as 2.5 to 1 still exist at higher loads. There are several reasons to which this discrepancy may be attributed. First, the fact that the discrepancy becomes greater for thinner film thicknesses suggests rather strongly that the measured film could be somewhat lower than the actual film in the contact due to any slight axial misalignments between the two disks. Secondly, the assumption of a flooded inlet in the theory may be unrealistic. A delayed pressure generation at the inlet due to a restricted lubricant supply or due to early formation of vortices in the inlet region would certainly cause drastic reduction in the calculated film thickness.

In an effort to resolve the discrepancy between the predicted and measured variations of film thickness with load at high speeds, BMI has recently made some new film thickness measurements at moderate speeds to determine whether a strong load-dependance would also exist at lower speeds. Surprisingly, the results, as shown in Ref. 102, at 530 rpm or 106 in/sec show the same degree of load-dependance as those obtained in the high speed data. This rather unexpected new data is now in direct conflict with that found earlier by Crook (84), Christensen (87), Archard and Kirk (106), and Dyson (88) because all the earlier experimental results show no evidence of a strong load dependance even for speeds up to 250 in/sec. It is difficult to speculate what factors may have caused the discrepancy between the x-ray and capacitance measurements. It appears that further examinations of the accuracy of x-ray measurement at very small film thickness is still needed.

To sum up, the film separation between steel rolling and sliding contacts can be accurately predicted by film thickness formulae proposed by Grubin (82) or by Dowson and Higginson (91) for rolling speed up to 250 in/sec. For high speed contacts, the reduction of film thickness due to thermal effects may be determined by the data provided by Cheng (93). However, there is still a disagreement between these data and the BMI measured data with regard to the effect of load. It is uncertain whether the discrepancy is due to certain factors neglected in the analysis or due to the inherent inaccuracy of the x-ray technique at these small film thicknesses.



b. Film Thickness and Film Shape of Elliptical Contacts

The film thickness at the inlet of a ball contact was first analyzed by Archard and Cowking (107). They successfully obtained an analytical solution to the three-dimensional inlet problem by assuming a Hertzian deformation profile. Their results show that the reduction of film thickness due to side leakage is less than 10 percent. However, experiments conducted by Archard and Kirk (86) show that the reduction of film thickness due to side leakage in a ball contact zone is about 40 percent, considerably greater than that predicted by the theory. From the experimental data they found that film thickness follows a simple power law dependence on velocity, load, and material parameters, similar to that of Grubin's.

Recently, a numerical solution was obtained by Cheng (105) to determine the inlet film thickness of an elliptical contact. Results indicate that the numerical solution predicts a film thickness slightly higher than that measured by the experiment. The results are presented in terms of a side leakage factor, which is the ratio of the calculated film thickness and an equivalent line contact film thickness (see Section III).

Interferometry experiments by Gohar and Cameron (108), Foord, Hammen, and Cameron (60), and Hingley (109) were able to obtain a clear map of a ball-on-ball or a ball-on-flat contact. Fig. 11, taken from Ref. 108 shows the development of a point contact film as the rolling speed increases. A schematic drawing of a rolling point contact is presented in Fig. 12. It is interesting to note that the minimum film thickness occurs at the two sides instead of at the exit. The ratio of the minimum to nominal film thickness is, in general, slightly lower than that of the line contact. The results in Ref. 60 also show that load hardly alters the nominal film thickness but does affect the minimum film thickness. At present, theories are available only for calculating nominal film thickness.

For a general elliptical contact, the speeds of two contacting bodies are not directed along either of the axes of the contact ellipse, Snidle and Archard (110) obtained an approximate analytical solution to the film thickness by partially solving a two-dimensional Reynolds equation. The result is as follows:

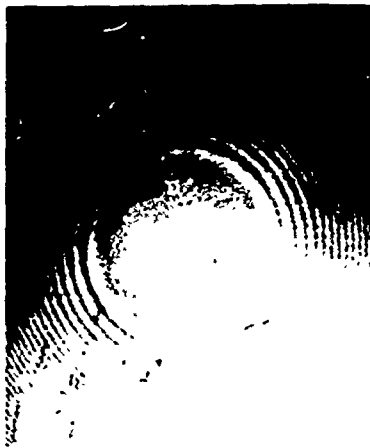
$$h_o = [3.9 U_t \mu_o \alpha]^{2/3} [2R'_x]^{1/3} \left[ \frac{\cos^2 \theta}{(3+2\eta)^2} + \frac{\sin^2 \theta}{\eta(3+\frac{2}{\eta})} \right]^{1/3} \quad (20)$$

$$\text{where } U_t = (U^2 + V^2)^{1/2}$$

$$\theta = \tan^{-1} \frac{V}{U}$$

$$U = \frac{U_1 + U_2}{2}$$

# Elastohydrodynamic Contacts



(a)

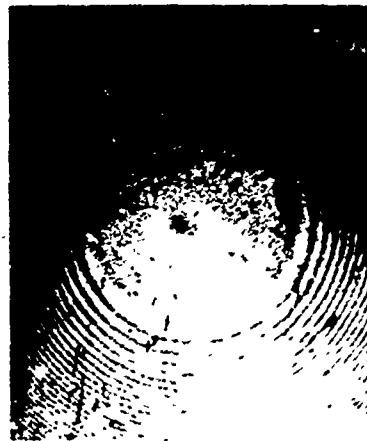


(b)

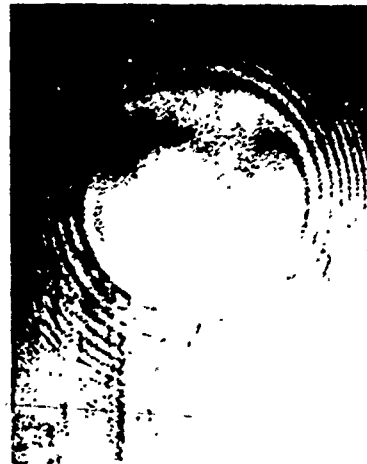


(c)

(a)  $P = 8 \text{ lb}$      $U = 0 \text{ cm/sec}$   
 (b)  $P = 8 \text{ lb}$      $U = 3.2 \text{ cm/sec}$   
 (c)  $P = 8 \text{ lb}$      $U = 32 \text{ cm/sec}$



(a)



(b)



(c)

(a)  $P = 16 \text{ lb}$      $U = 0 \text{ cm/sec}$   
 (b)  $P = 16 \text{ lb}$      $U = 3.2 \text{ cm/sec}$   
 (c)  $P = 16 \text{ lb}$      $U = 28.6 \text{ cm/sec}$

Fig. 11 Rolling Point Contacts. (Courtesy of ASLE Preprint No. 66 LC-21).

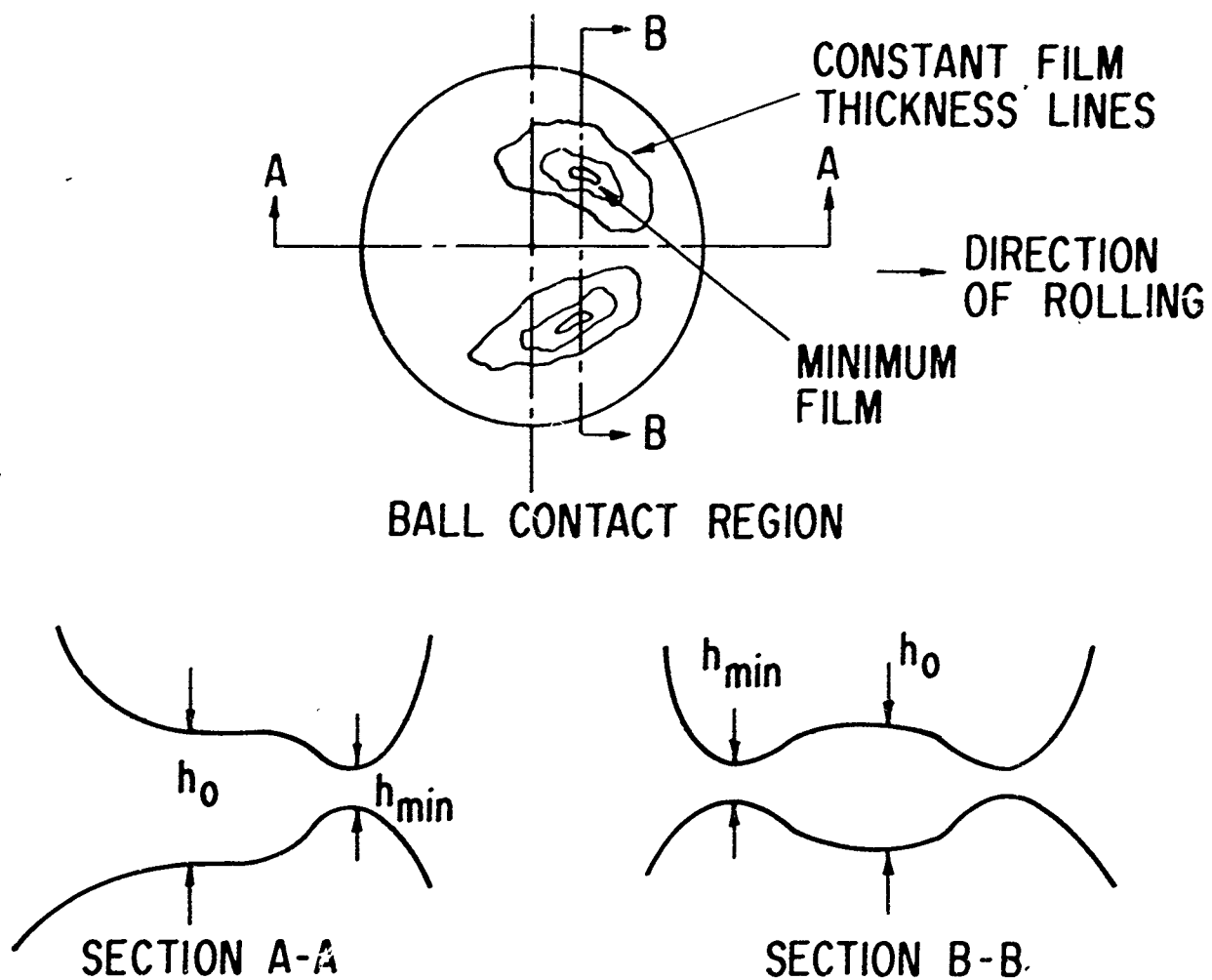


Fig. 12 Film Thickness Profiles

$$V = \frac{V_1 + V_2}{2}$$

$U_1, U_2$  = speeds of the contacting surfaces in x-direction

$V_1, V_2$  = speeds of the contacting surfaces in y-direction

$$\eta = \frac{R}{R' \frac{x}{y}}$$

$R'_x, R'_y$  = principal effective radii of curvature in x- and y-directions, respectively

$\mu_0$  = inlet viscosity

$\alpha$  = pressure-viscosity exponent

Qualitative agreement of the calculated film thickness with measurements with respect to the change of direction of the resolved velocity  $U_t$  was achieved (110).

### 3. PRESSURE DISTRIBUTION

Up until the discovery of elastohydrodynamic lubrication, it was believed that pressure distribution in a lubricated concentrated contact follows the Hertzian elliptical profile. Recent elastohydrodynamic theories show that this Hertzian elliptical profile will be modified considerably by the hydrodynamic effects of the lubricant. The extent of this pressure redistribution due to elastohydrodynamic effects should depend upon the speed, the load, the inlet viscosity, and the pressure-viscosity coefficient of the lubricant. Fig. 13 shows a series of typical elastohydrodynamic pressure profiles with the variable

$$\Lambda = \frac{12\mu_0 U}{w^2} R_x \quad (21)$$

The most unique characteristics of the elastohydrodynamic pressure profile is the sharp pressure peak before the termination of the film. The various effects which influence the location and magnitude of this pressure spike are now well understood - at least within the assumption of a Newtonian lubricant. For a given pressure-viscosity coefficient, the magnitude and location of the pressure peak are governed by the parameter  $\Lambda$  as shown in Fig. 13. As  $\Lambda$  increases, the location of the pressure peak moves toward the entrance region with an increase in intensity of the pressure spike. When  $\Lambda \rightarrow 0$ , the condition corresponds to a dry contact and the pressure profile approaches a Hertzian ellipse. In the other extreme,  $\Lambda \rightarrow \infty$ , the condition corresponds to a rigid cylinder, and the pressure profile approaches the pure hydrodynamic solution. The pressure-viscosity characteristics of the lubricant also

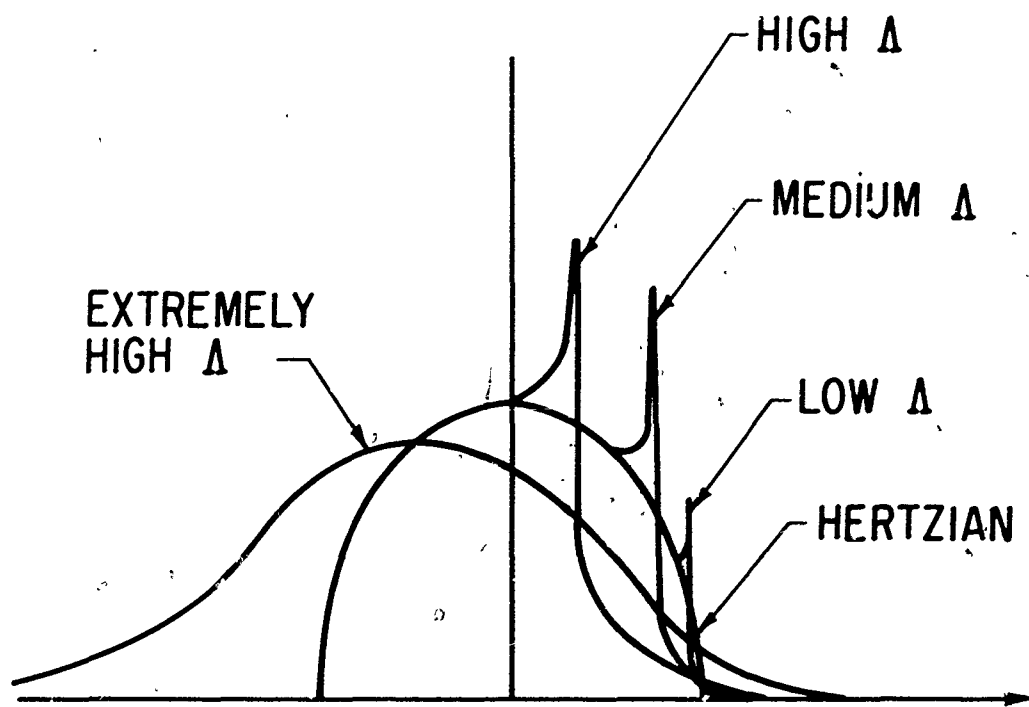


Fig. 13 Pressure Distributions

has a strong influence upon the pressure peak. Increasing the pressure-viscosity exponent has the same influence as increase  $\Lambda$ , it gives rise to a higher peak and moves the peak toward the entrance region.

a. Theories for Moderately Loaded Contacts

At least four theories are available in the moderately loaded region for line contacts ( $p_{H2} < 20,000$  psi). In 1953, Dorr used a power series and developed an analytical solution for an isothermal lubricant under moderate loads. In 1954, Weber and Saalfeld (98) successfully obtained a numerical solution of the coupled elastohydrodynamic equation. They also considered the effect of pressure-dependent viscosity. Figs. 14 and 15 show the compatible pressure and film profiles. One important feature in Weber and Saalfeld's theory is that the coordinate along the film is normalized with respect to the coordinate at the exit of the film. In doing so, they were able to reduce one parameter in the calculation and thus represent the isoviscous elastohydrodynamic solution by one parameter family of curves for the pressure and the film thickness.

In 1961, a more complete numerical elastohydrodynamic solution in the moderately loaded region was provided by Stephenson and Orsterle (112). They employed a direct integration of the Reynolds equation and the film shape by the elasticity equation. Their solution covers a wide range of speeds and loads. The results show that the pressure dependent viscosity has an effect to increase the load capacity for the same minimum film while the compressibility of the fluid has a tendency to decrease the load capacity slightly. The direct iterative elastohydrodynamic theory has also been extended by Wernick (113) for loads heavier than those calculated by Stephenson and Orsterle. Wernick achieved this by using a deacceleration factor to correct the pressure profile in each iteration.

b. Theories for Heavily Loaded Contacts

For heavily loaded contacts, the elastohydrodynamic numerical solution by direct iteration breaks down because of convergence difficulty. This difficulty was first overcome by Dowson and Higginson (91) in which they solved the hydrodynamic equation in the inverse manner in the high pressure region. By comparing the hydrodynamic film thickness obtained from the inverse Reynolds equation and the elastic film thickness obtained from the elasticity equation, the pressure profile is successively corrected in each iteration until convergence is reached. Their results, as shown in Fig. 16 show a sharp pressure peak in the exit region for high pressure dependent viscosities. In a later paper (114) they allowed the lubricant to be compressible and found the pressure was considerably suppressed (Fig. 17).

In 1961 Archard, Gair and Hirst (92) employed the same inverse procedure and found extensive solutions for the heavily loaded cases. They separated the contact zone into four regions, two in the inlet and two in the outlet region. For each of these regions, a different iterative procedure was employed in order to bring convergence. The

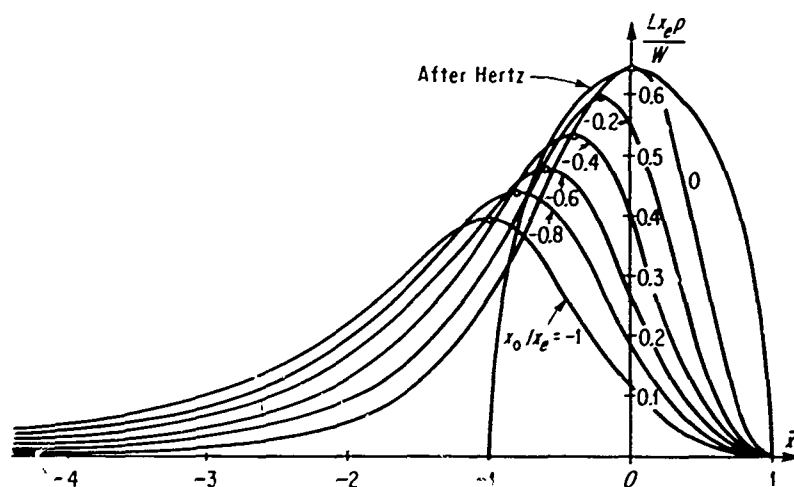


Fig. 14 Pressure Distribution in Contact Zone, Moderately Loaded Contact. (Reference Weber and Saalfeld (98), contained in Theory of Hydrodynamic Lubrication by Pinkus and Sternlicht. Copyright © 1961 by the McGraw-Hill Book Company, Inc. Used with permission of McGraw-Hill Book Company).

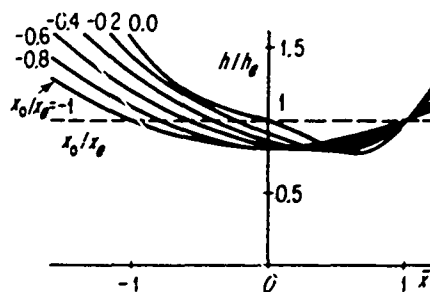


Fig. 15 Film Thickness in the Contact Zone, Moderately Loaded Contact. (Reference Weber and Saalfeld (98), contained in Theory of Hydrodynamic Lubrication by Pinkus and Sternlicht. Copyright © 1961 by the McGraw-Hill Book Company, Inc. Used with permission of McGraw-Hill Book Company).



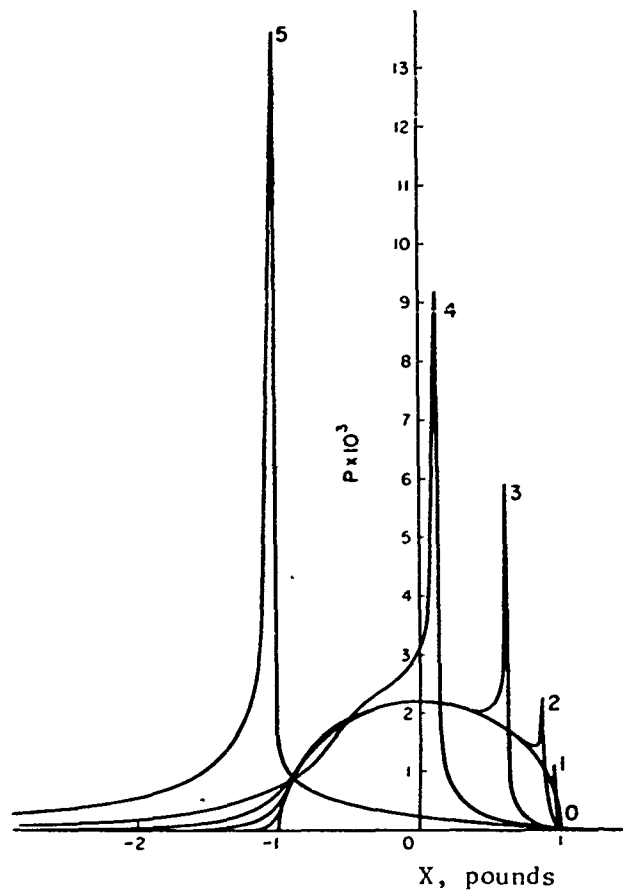


Fig. 16 Pressure Distributions for an Incompressible Lubricant  
 $W = 3 \times 10^{-5}$ ,  $G = 5000$ .  $U = (0) 0$  (dry contact), (1)  $10^{-13}$ ,  
 (2)  $10^{-12}$ , (3)  $10^{-11}$ , (4)  $10^{-10}$ , (5)  $10^{-9}$ .

(Reproduced from the Journal of Mechanical Engineering  
 Science, Vo. 4, No. 2, pp. 121-6 (1962) by kind permission  
 of the Institution of Mechanical Engineers.)

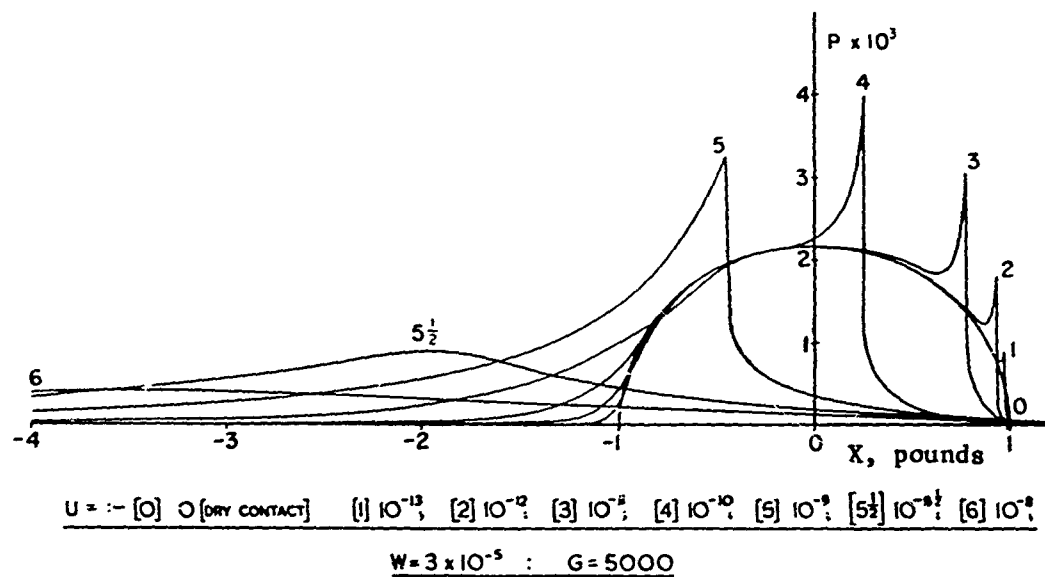


Fig. 17 Pressure Distributions for a Compressible Lubricant

$W = 3 \times 10^{-5}$ ,  $G = 5000$ .  $U = (0) 0$  (dry contact) (1)  $10^{-13}$ ,  
 (2)  $10^{-12}$ , (3)  $10^{-11}$ , (4)  $10^{-10}$ , (5)  $10^{-9}$ , (5 1/2)  $10^{-8\frac{1}{2}}$ ,  
 (6)  $10^{-8}$ . (Reproduced by kind permission from the Proceedings  
 of the Institution of Mechanical Engineers Symposium on Fatigue  
 in Rolling Contact, 1963.)

agreement between the pressure distributions by Dowson and Higginson (91) and by Archard, Gair and Hirst (92) is good except for the intensity of the pressure spike.

#### c. Thermal Effects on Pressure Distribution

The effects of temperature on elastohydrodynamic lubrication were first investigated by Sternlicht, Lewis and Flynn (115), in which they calculated the temperature based on the assumption that all the heat dissipated is entirely convected by the lubricant. This assumption is overly conservative, and it leads to a film thickness considerably thinner than anticipated in practice. As a result, the calculated pressure profiles do not deviate much from Hertzian dry contact profile.

In 1964 Cheng and Sternlicht (58) obtained a numerical solution for the simultaneous hydrodynamic, elasticity, and energy equation. Their solution is particularly applicable for heavily loaded contacts in which the inverse hydrodynamic equation was used. Their results (Fig. 18) show that for heavily loaded contact lubricated with mineral oils at room temperature, the temperature will not remove the pressure peak. On the contrary, Fig. 19 shows that at a higher rolling speed, the thermal effects would tend to shift the pressure peak further toward the inlet and would intensify the pressure spike.

In 1965, Dowson and Whittaker (59) developed another numerical solution to the thermal elastohydrodynamic problem. They found that the temperature effect is not strong enough to remove the pressure spike; however, with a pressure viscosity coefficient slightly smaller than that used by Cheng and Sternlicht (58) they found that the sharpness of the spike is somewhat softened by the increase in temperature at higher sliding speed (Fig. 20).

#### d. Pressure Measurement

Ever since the discovery of a secondary pressure spike in elastohydrodynamic theories, there have been a number of experiments devoted to the hunting of this spike. Early experiments were conducted by Dowson and Longfield (116) and Longfield (117) by using a large rotating disc in pure sliding contact with a stationary conformal surface. Because of the large area of contact due to a conformal contact and the relatively high lubricant temperature introduced by the pure sliding, no secondary pressure peaks were detected. The measured pressure profile show some slight deviation from the Hertzian distribution.

Subsequent attempts were made by Orcutt (118) and Kannel (119) in measuring the pressure distribution in heavily loaded contacts. The pressure sensing in a narrow contact region was made possible by using a vapor deposited manganin strip having approximately .001" in width and a few microinches in thickness. Orcutt's experiment was conducted with a glass disc which limits the maximum contact pressure to about 50,000 psi. At this pressure, he showed that the pressure distribution deviate considerably from Hertzian and indicates some

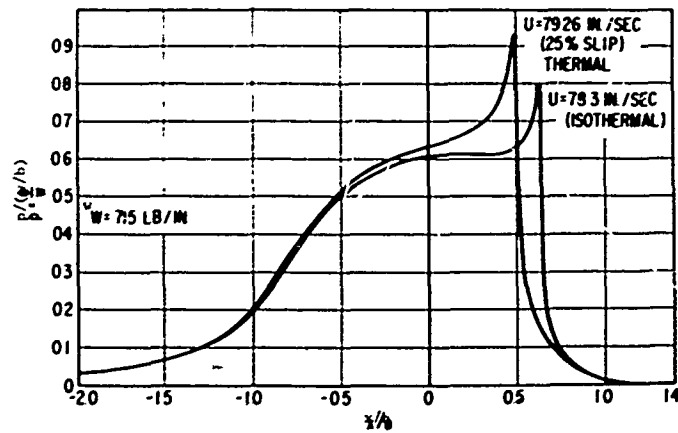


Fig. 18 Comparison of Pressure Distributions Between the Isothermal Case and the 25 Percent Slip Thermal Case with an Approximately Equal Rolling Velocity. (Courtesy of ASME, J. Basic Engrg., Vol. 87D, 1964).

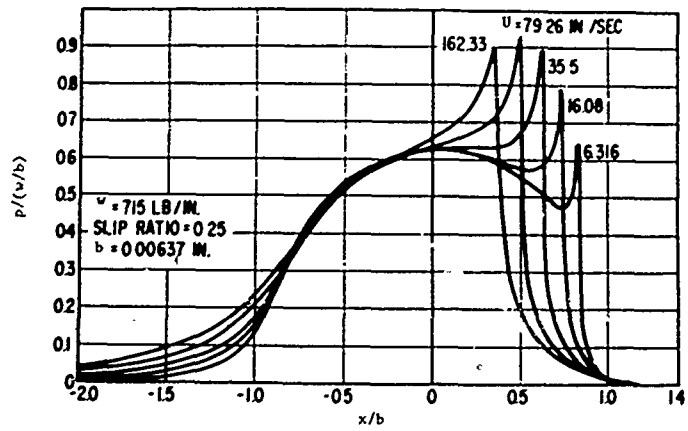


Fig. 19 Pressure Distribution, Thermal Theory, with 25 Percent Slip (Courtesy of ASME, J. Basic Engrg., Vol. 87D, 1964).

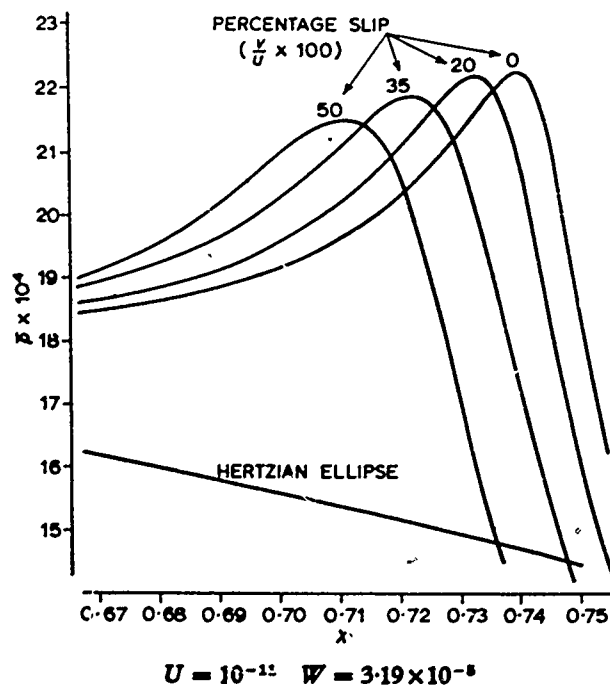


Fig. 20 Details of Pressure Spikes. (Courtesy of Proc. Instn. Mech. Engrg., Vol. 180, Pt. 3B, 1965-66).

marked disturbances at the exit region. However, no evidence of pressure spikes was detected.

In 1965 Kannel used the manganin transducer on a pair of steel discs and obtained pressure profiles which suggest strongly the existence of pressure peaks in elastohydrodynamic contacts. As shown in Fig. 21, at maximum Hertzian pressures above 100,000 psi peaks resembling those predicted by elastohydrodynamic theories are evident. The trend of the effect of load on the location of these pressure peaks also agrees with that predicted analytically.

More recent experiments by Kannel et al (102) have extended the previous data to high loads with a shorter transducer. Moreover, the effects of speed, lubricant inlet temperature and lubricant type have been thoroughly investigated both with cylindrical discs as well as with crowned discs. Figs. 22 through 27 give the measured pressure profiles from Ref. 102. From these data, the following observations can be made:

At higher loads the evidence of the secondary pressure peak appears to be completely removed. The pressure distributions do not deviate much from Hertzian. The only noticeable difference is at the exit where there is a slight build-up in pressure followed by a fast drop to ambient pressure.

There is qualitative agreement between the location of this pressure build-up and the location of the pressure spike predicted by the elastohydrodynamic theory as far as the effects of the rolling speed, load, inlet viscosity, and pressure-viscosity dependence. For example, the pressure build-up tends to push the build-up towards the inlet if the load decreases, the speed increases, the inlet viscosity increases, and the pressure-viscosity coefficient increases.

Recently, Kannel et al (104) measured the pressure distribution between the ball-race contact in an actual 85mm ball bearing. The measurement was taken at a speed up to 5000 rpm and a maximum Hertzian contact pressure of 205,000 psi. As shown in Figs. 28 and 29, that at this high contact pressure, the pressure distribution indeed approaches more to the dry-contact Hertzian shape. There seems to be no significant influence from the speed as well as from the lubricant type.

#### 4. TEMPERATURE DISTRIBUTION

Thermal effects in elastohydrodynamic lubrication have been studied quite thoroughly in the past decade. Approximate solutions to the energy equation have been contributed earlier by Crook (120) and later by Bell et al (121). More recently, complete thermal-elastohydrodynamic theories have appeared in Refs. 58, 59, and 93. In the lubricant film, one is usually interested in the surface temperature distribution for studying the failure by scoring and in the mid-film lubricant temperature for studying the thermal decomposi-

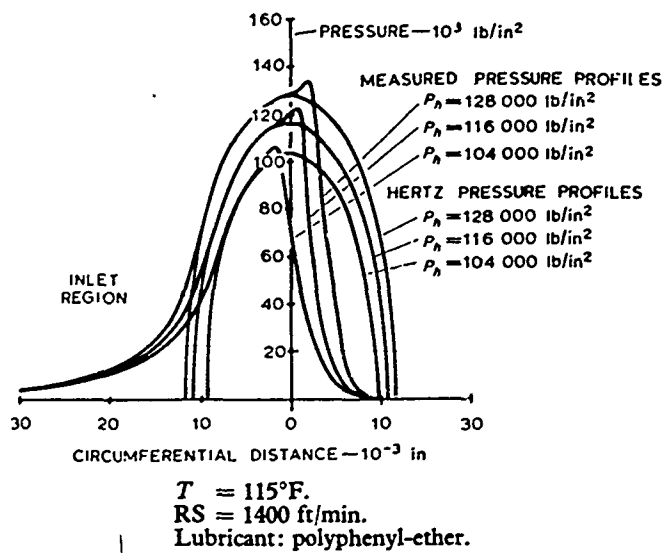


Fig. 21 Measured Variation in Pressure Profile with Disk Loading  
 (Courtesy of Proc. Instn. Mech. Engrg., Vol. 180, pt. 3B,  
 1965-66).



T = 150 F  
 Rolling speed = 4,500 fpm  
 Lubricant: polyphenyl ether

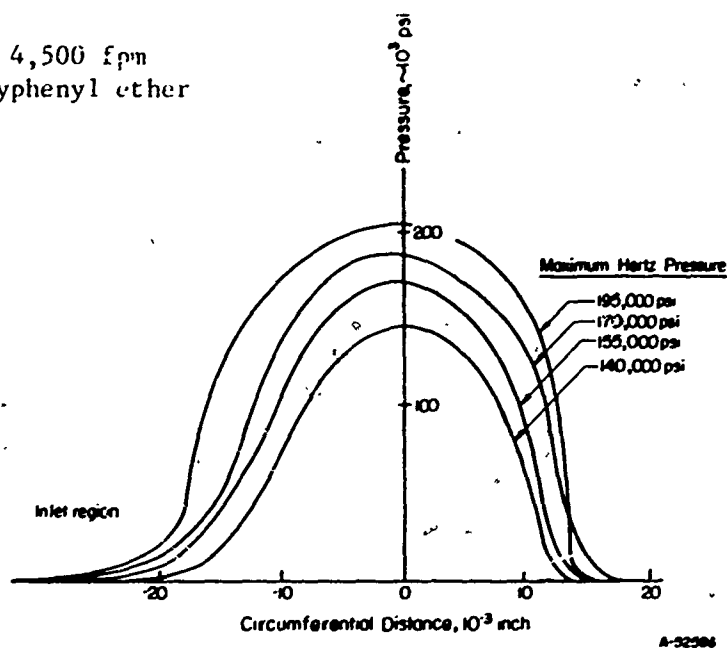


Fig. 22 Measured Film Pressures Between Crowned Disks Showing Variations with Loading. (United States Air Force Tech. Report No. ASD-TDR-61-643, Aug. 1966).

T = 150 F  
 Lubricant: polyphenyl ether

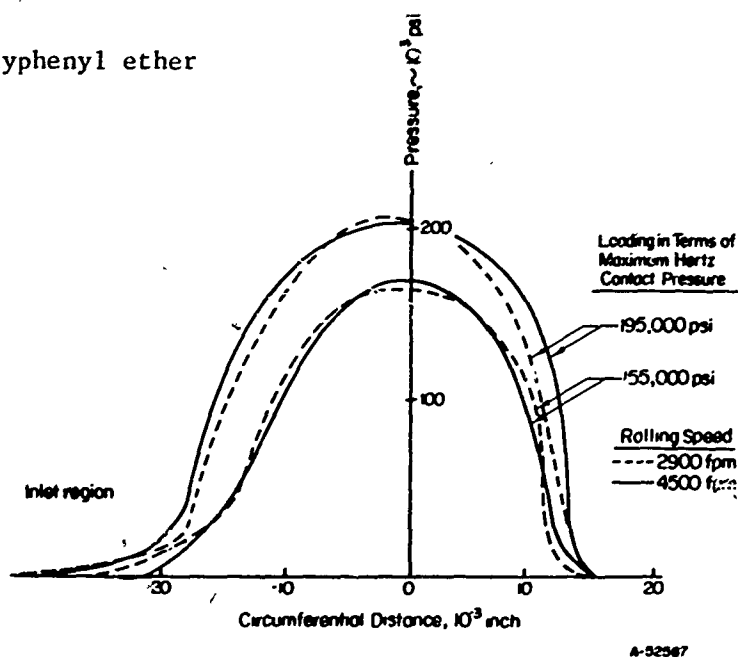


Fig. 23 Measured Film Pressures Between Crowned Disks Showing Variations with Rolling Speed for Two Loadings. (United States Air Force Tech. Report No. ASD-TDR-61-643, Aug. 1966).

Rolling speed = 4150 fpm  
 T = 110 F  
 Lubricant: chlorinated methyl phenyl silicone

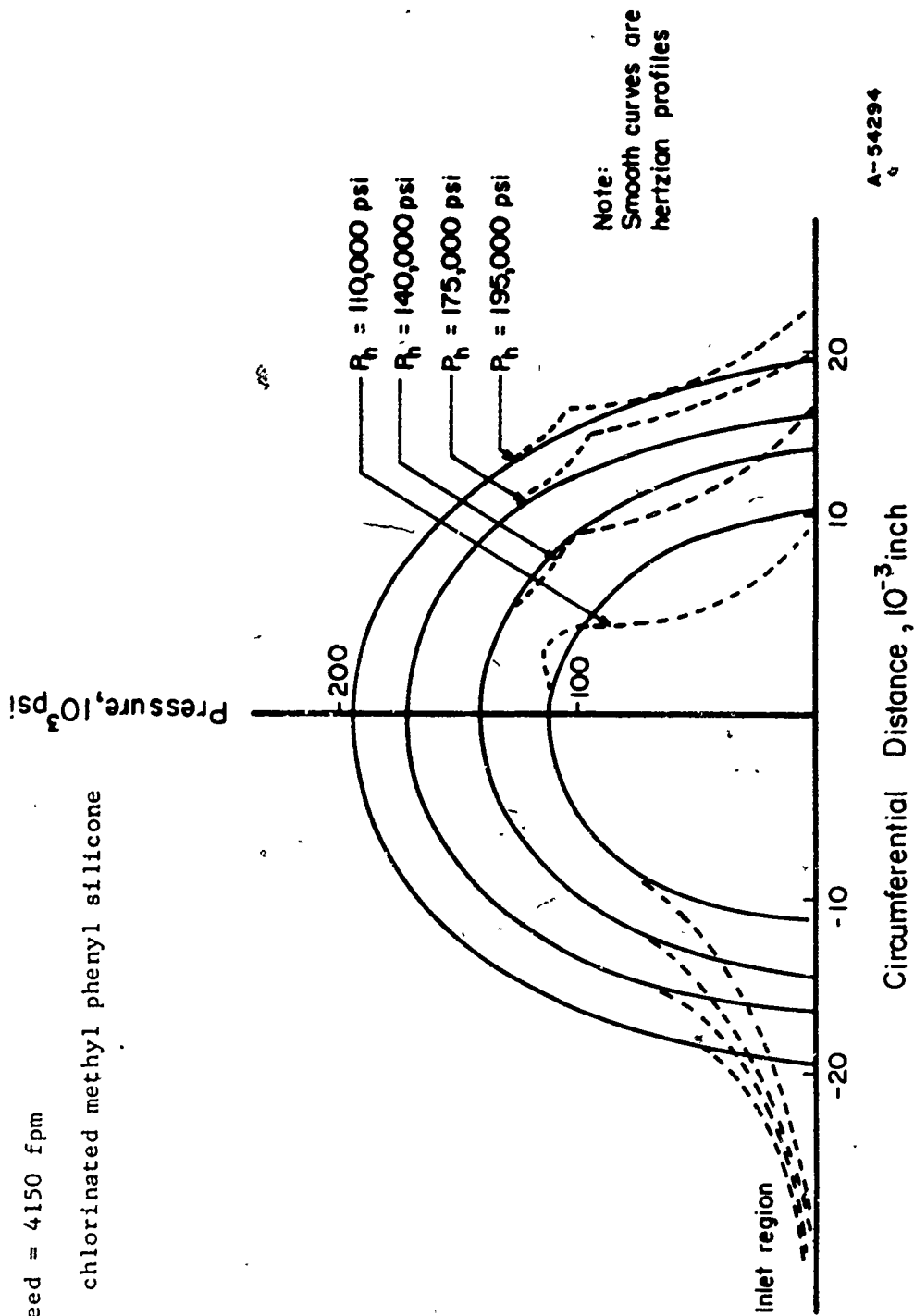


Fig. 24 Measured Pressure Profiles Between Crowned Rolling Disks.  
 (United States Air Force Tech. Report No. ASD-TDR-61-643,  
 Aug. 1966).

Rolling speed = 4,500 fpm  
Lubricant: polyphenyl ether

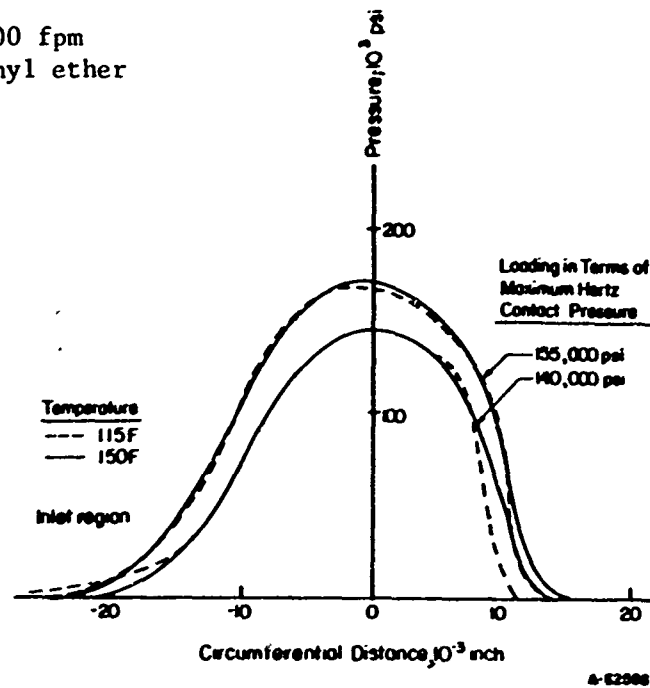


Fig. 25 Measured Film Pressures Between Crowned Disks Showing Variations with Temperature and Loading. (United States Air Force Tech. Report No. ASD-TDR-61-643, Aug. 1966).

T = 115 F  
Rolling speed = 2,900 fpm

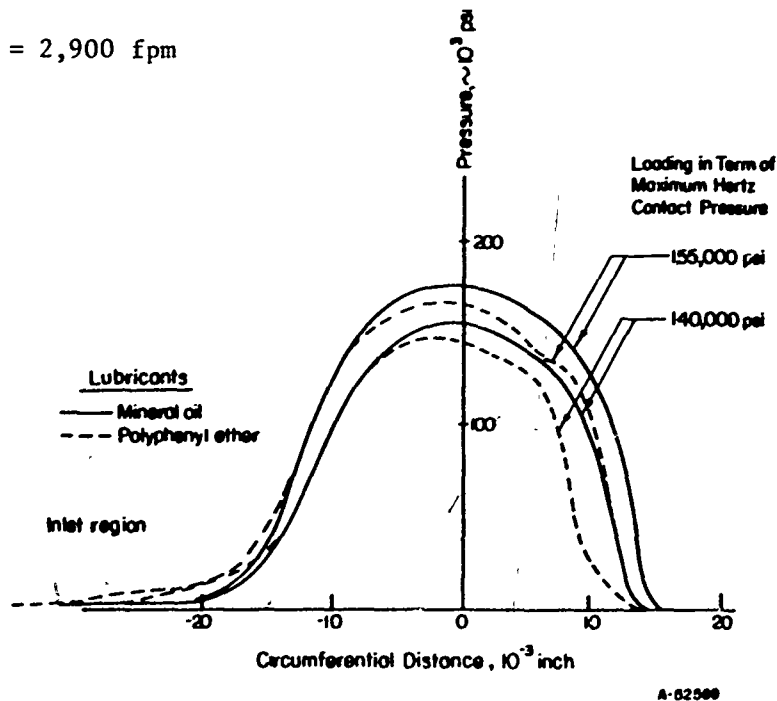


Fig. 26 Measured Film Pressures Between Crowned Disks Showing Variations with Lubricant Type. (United States Air Force Tech. Report No. ASD-TDR-61-643, Aug. 1966).

Rolling speed = 4150 fpm  
 Loading = 140,000 psi Hertz pressure  
 Lubricant: chlorinated methyl phenyl silicone

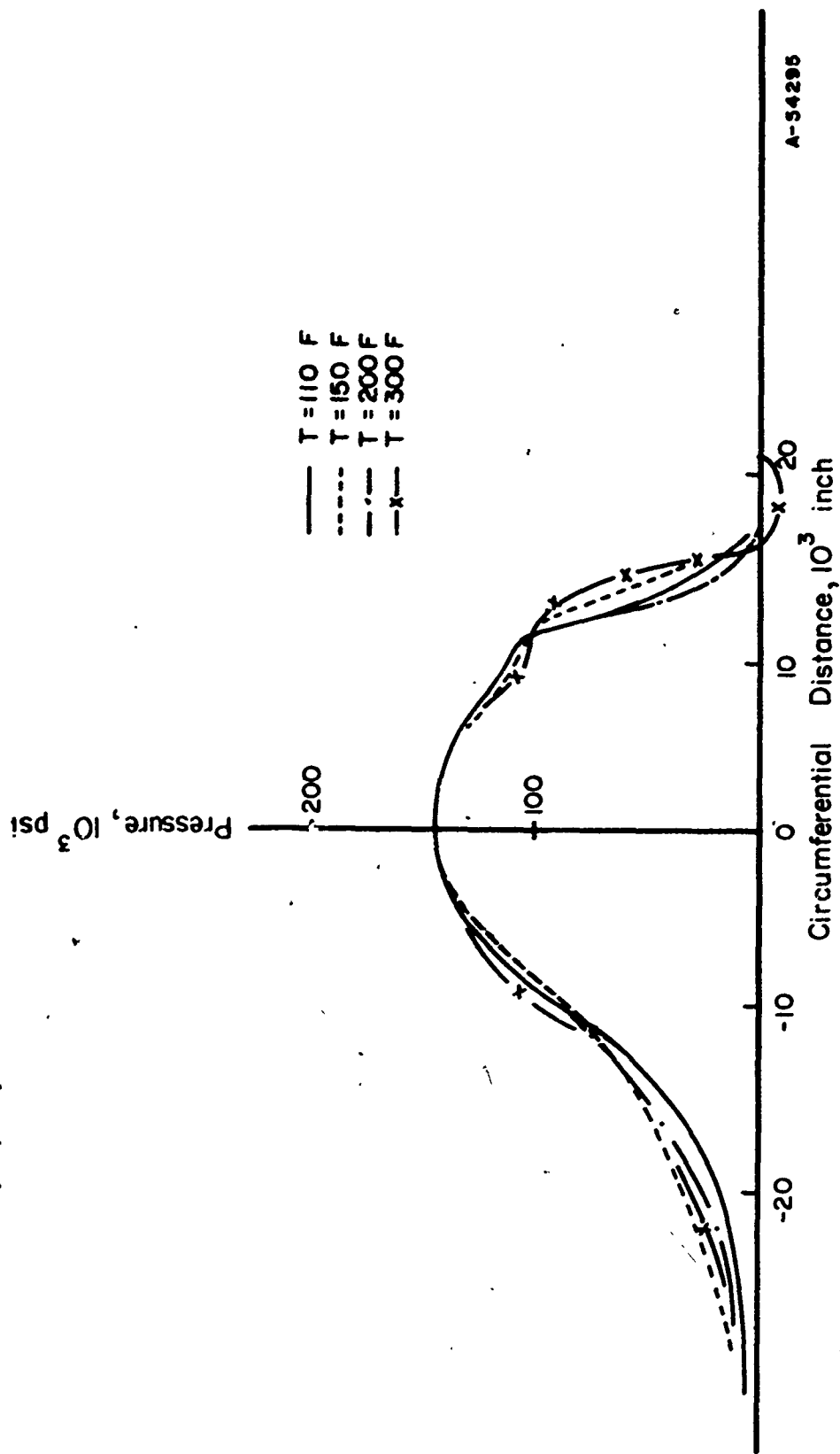
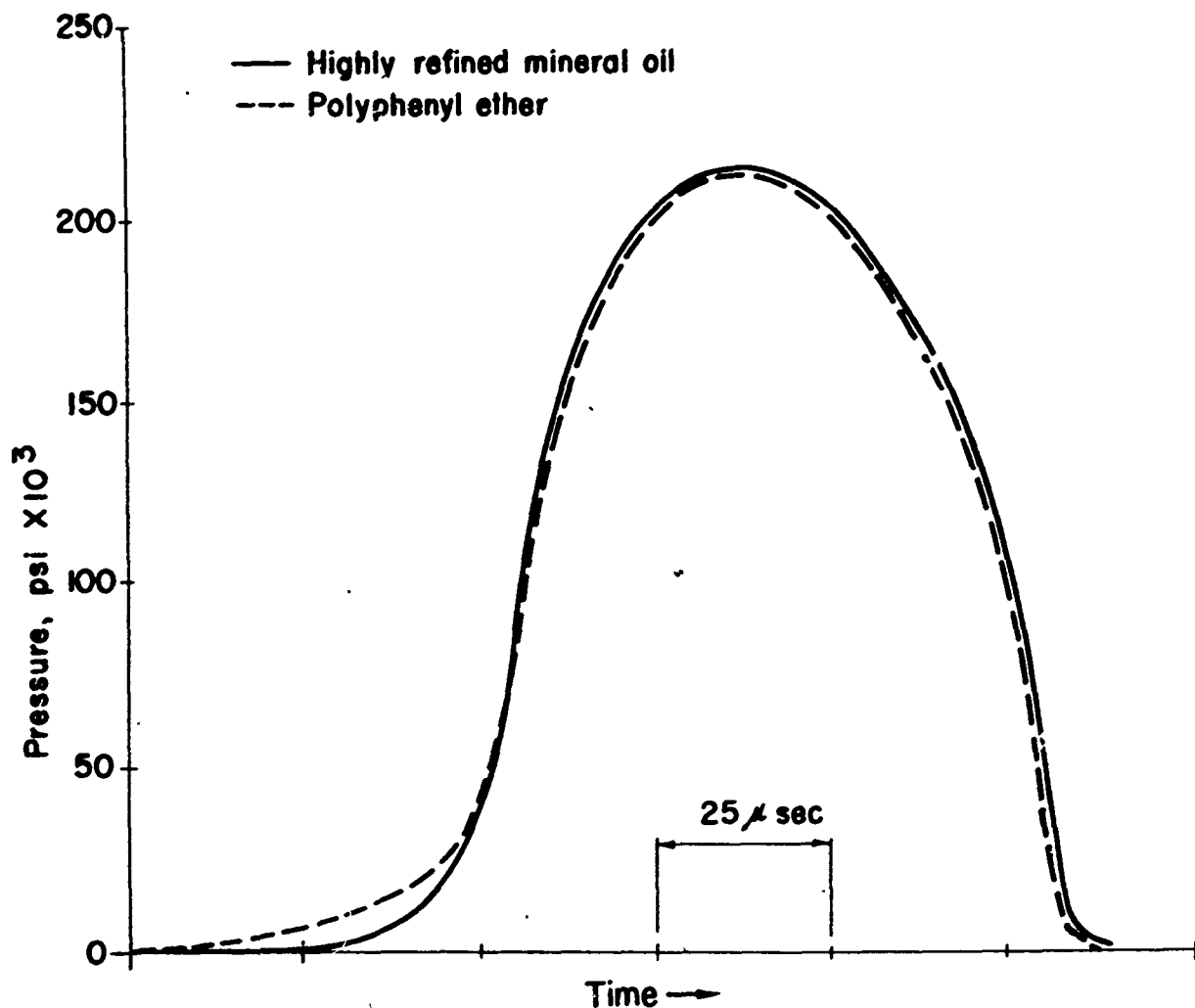
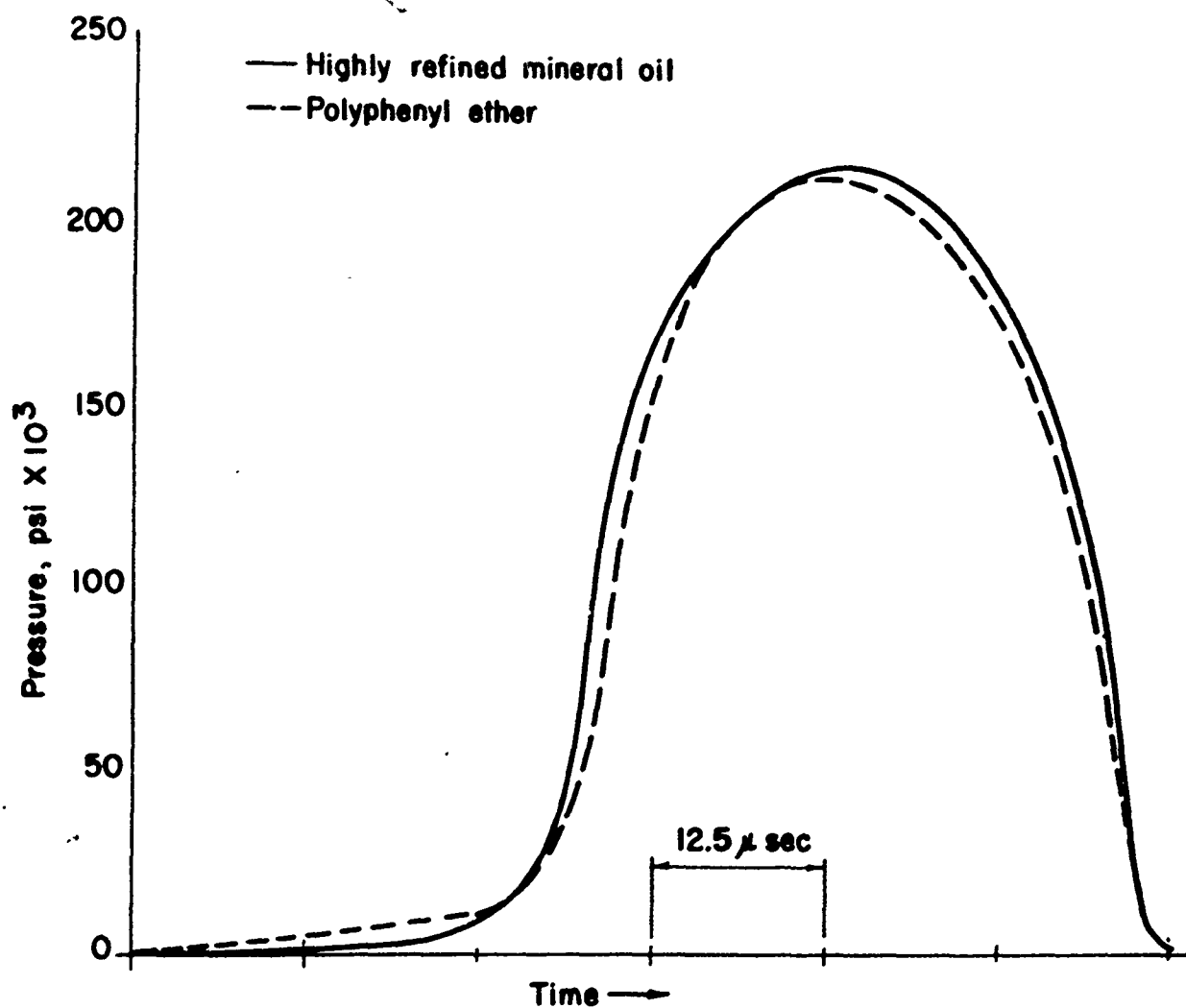


Fig. 27 Pressure Pattern Between Crowned Rolling Disks Showing Variations with Temperature. (United States Air Force Tech. Report No. ASD-TDR-61-643, Aug. 1966).



Shaft Speed  $\sim$  2500 rpm  
 Contact Load - 205,000 psi maximum Hertz pressure

Fig. 28 Comparison of Ball-Race Pressure Pattern in 85 mm Bearing with Lubricant Type, Shaft Speed = 2500 rpm. (United States Air Force Tech. Report No. ASD-TDR-61-643, Aug. 1966).



Shaft Speed  $\sim 5000$  rpm  
 Contact Load - 205,000 psi maximum Hertz pressure

Fig. 29 Comparison of Ball-Race Pressure Pattern in 85 mm Bearing with Lubricant Type, Shaft Speed = 5000 rpm. (United States Air Force Tech. Report No. ASD-TDR-61-643, pt. VIII, 1968).

tion of the lubricant. A brief summary will be given to various theories available in determining the temperature in the lubricant film.

#### a. Approximate Theories

The influence of temperature in elastohydrodynamic lubrication was first asked by Crook (120) and he developed a simplified theory in determining the mid-film temperature by neglecting the surface temperature rise, the viscous heat dissipation due to the pressure flow, and the heat convected by the lubricant. This method yields a reasonably accurate mid-film temperature as long as the speed is not either too high for the heat of convection to be dominant or too low for the surface temperature rise to be of the same order of the film temperature rise. Crook's simplified thermal theory has been widely used in studying the sliding friction.

In 1963, Bell et al (121) developed an analytical solution to the energy equation by neglecting the surface temperature rise and by assuming that the viscosity is thermally independent. They have calculated the temperatures generated separately by viscous heat due to sliding, viscous heat due to rolling, and heat of compression of the lubricant. Fig. 30 gives separate temperature curves for each of the three types of the heat generation. The temperature due to the heat by the rolling action ( $\theta_{mr}$ ) is relatively insignificant at the speed they considered. The temperature due to the sliding heat, ( $\theta_{ms}$ ) occurs mainly in the contact region where the viscosity is high. The heat of compression contributes to a temperature variation which is proportional to the pressure gradient in the contact as indicated by the curve labeled  $\theta_{mc}$ .

#### b. Numerical Solutions to Energy Equation

In 1965 Cheng and Sternlicht (58) developed a numerical solution to the energy equation for calculating the surface as well as the mean-film temperature distributions. In their analysis, the viscosity across the film is assumed to be constant and corresponding to the mean temperature across the film. Typical curves are shown in Fig. 31. This is a case of moderately low speed and the surface temperature rise is of the same order of magnitude of the mean-film temperature.

The assumption of a mean viscosity across the film was later relaxed by Cheng (93), and he developed a rigorous two dimensional finite difference method in determining the temperature distributions across as well as along the film. Typical three dimensional temperature surface within the film for a pair of steel rollers are shown in Fig. 32. In this figure

$$\theta = \frac{\Delta T}{T_o} \quad (22)$$

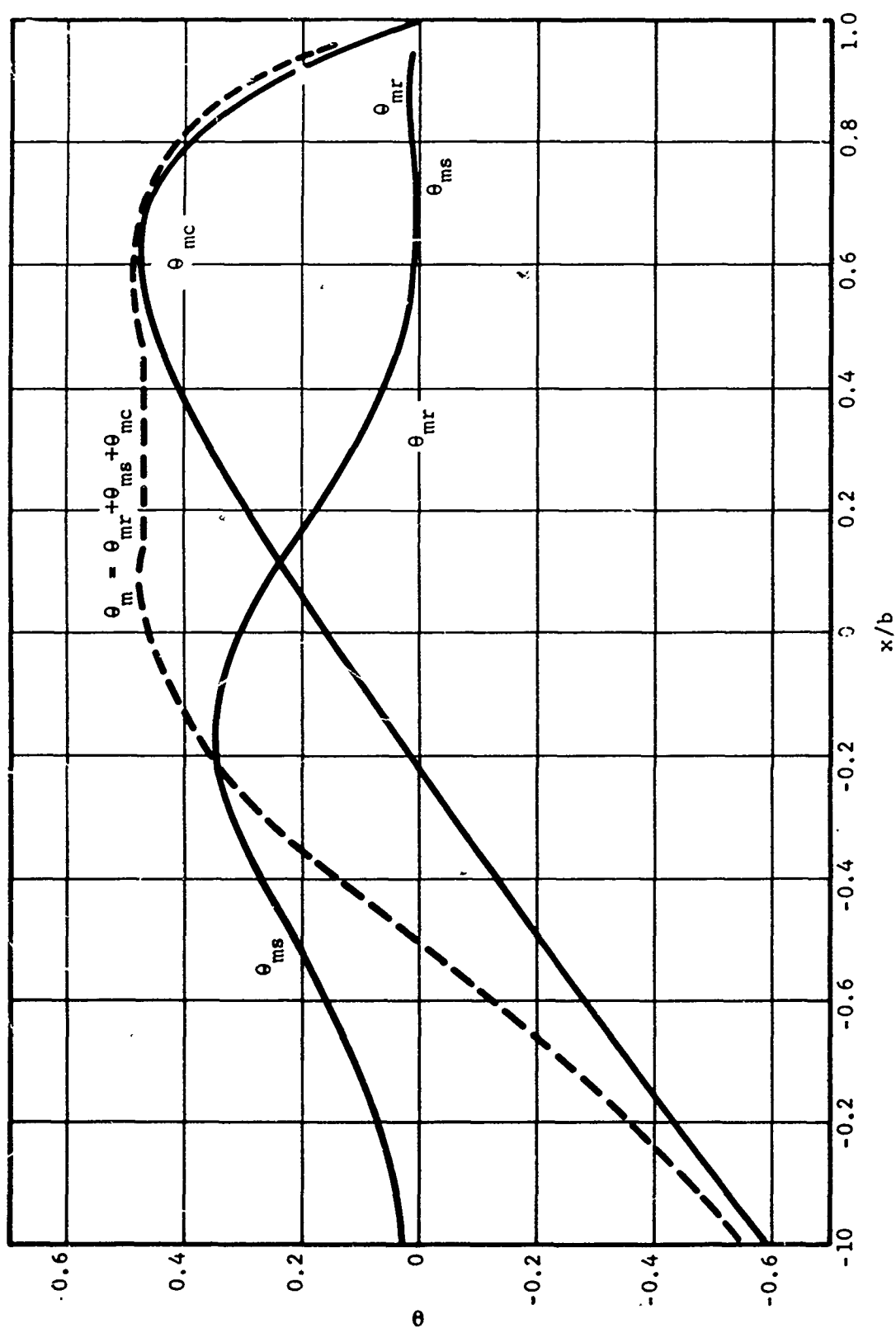


Fig. 30 Components of Temperature Increase in Lubricant for a Particular Case. (Courtesy of ASME, J. Basic Engrg. Series D, No. 3, 1964).



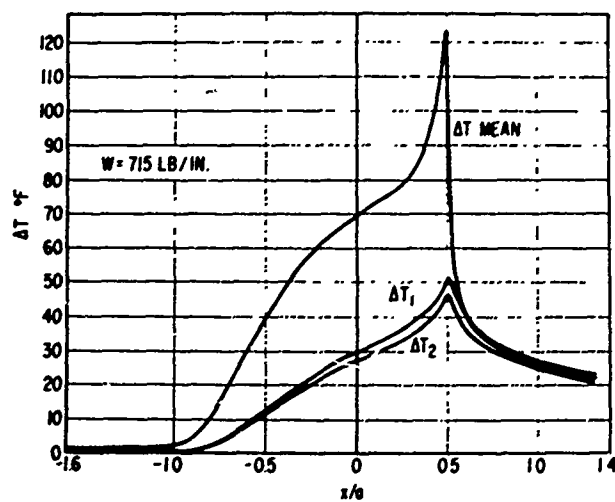


Fig. 31 Temperature Distribution for 25 Percent Slip Case,  $U_j = 79.26 \text{ in/sec.}$  (Courtesy of ASME, J. Basic Engrg. Vol. 87D, 1964).

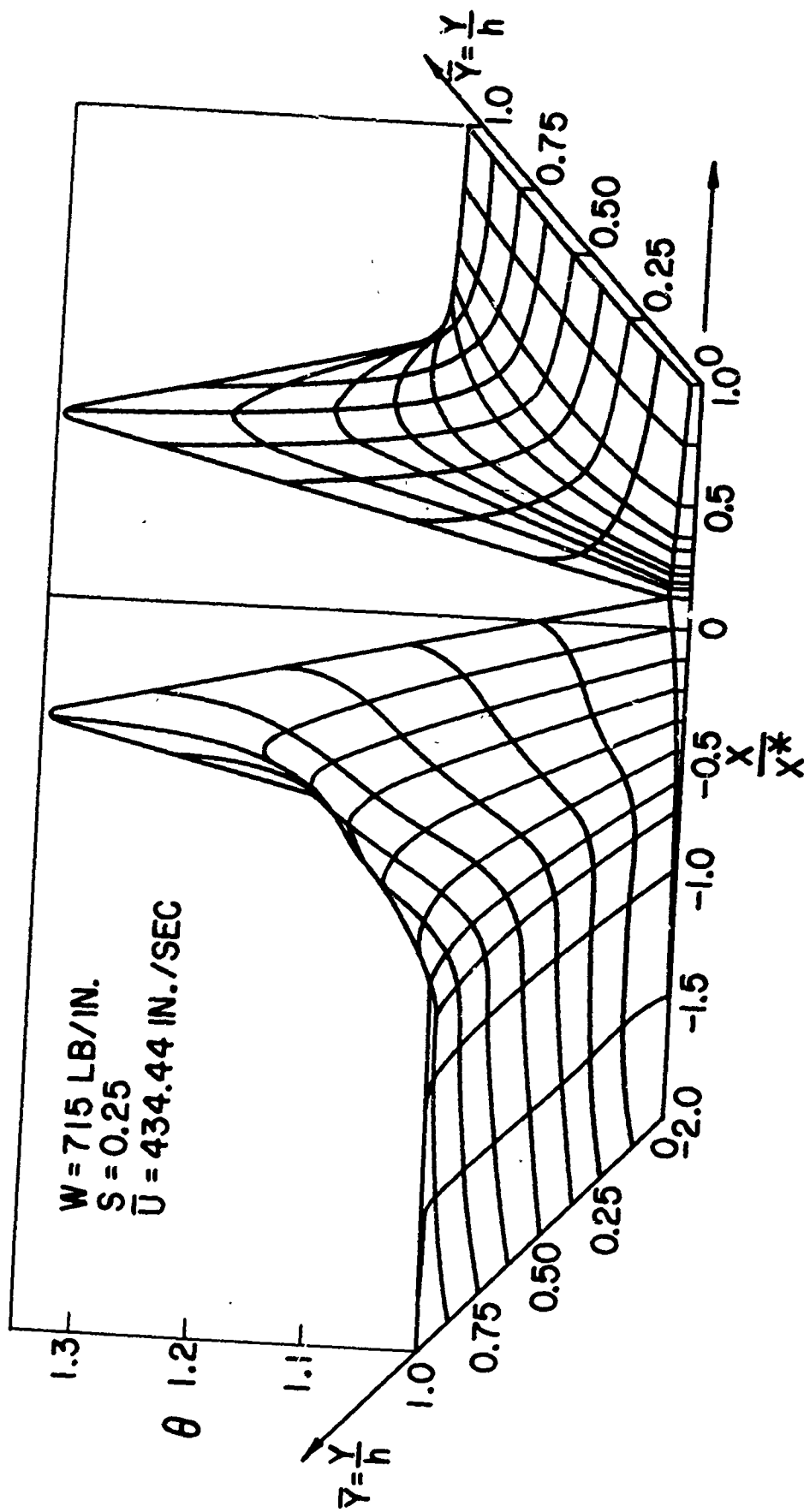


Fig. 32 Lubricant Film Temperature Map

$\Delta T$  = temperature rise,  $^{\circ}\text{R}$

$T_0$  = inlet temperature, for this case  $T_0 = 570^{\circ}\text{R}$

$x^*$  = exit coordinate which is approximately equal to half of the Hertzian width, in.

$x$  = coordinate along the film, in.

$y$  = coordinate across the film, in.

$h$  = film thickness

$s = (U_2 - U_1)/U_2$

The temperature plot is divided into two parts at the pressure peak in order to show the clear details before and after the peak. Since this is a high speed case, the surface temperature rise at  $y = 0$  is practically insignificant comparing to the mid-film temperature rise. The effects of rolling and sliding speed on the surface and mid-film temperature rise are shown in Figs. 33 and 34. For a constant slip ratio, the mid-film temperature always increases with the rolling speed on the surface temperature would depend upon the slip ratio. At high slip ratio, the surface temperature decreases with the rolling speed.

Still another numerical solution for the thermal elastohydrodynamic problem was contributed by Dowson and Whittaker (59). Fig. 35 shows some of their typical temperature maps. Due to the different pressure-temperature viscosity conditions and operating conditions used in two solutions, exact comparison is not possible; however, qualitatively these two solutions are in good agreement.

At extremely high rolling speed, the above thermal theories encounter numerical difficulties at the inlet region where there is a reverse flow. To remedy this, an inlet thermal solution (105) was developed for the purpose of calculating the thermal film thickness at the inlet using the Grubin-type approach. This solution can be used together with one of the contact-zone thermal-elastohydrodynamic solutions to obtain the temperature maps for very high speed and high load cases.

Recently, Kannel et al (103) have formulated the thermal problem at the inlet region and obtained an analytical solution for the case where the convective heat is neglected. This inlet thermal solution has been employed to determine the reduction of inlet film due to temperature effects.

#### c. Temperature Measurements

Measurements of surface temperature have been made by Orcutt (122) by using a platinum wire as the temperature transducer. Typical tempera-

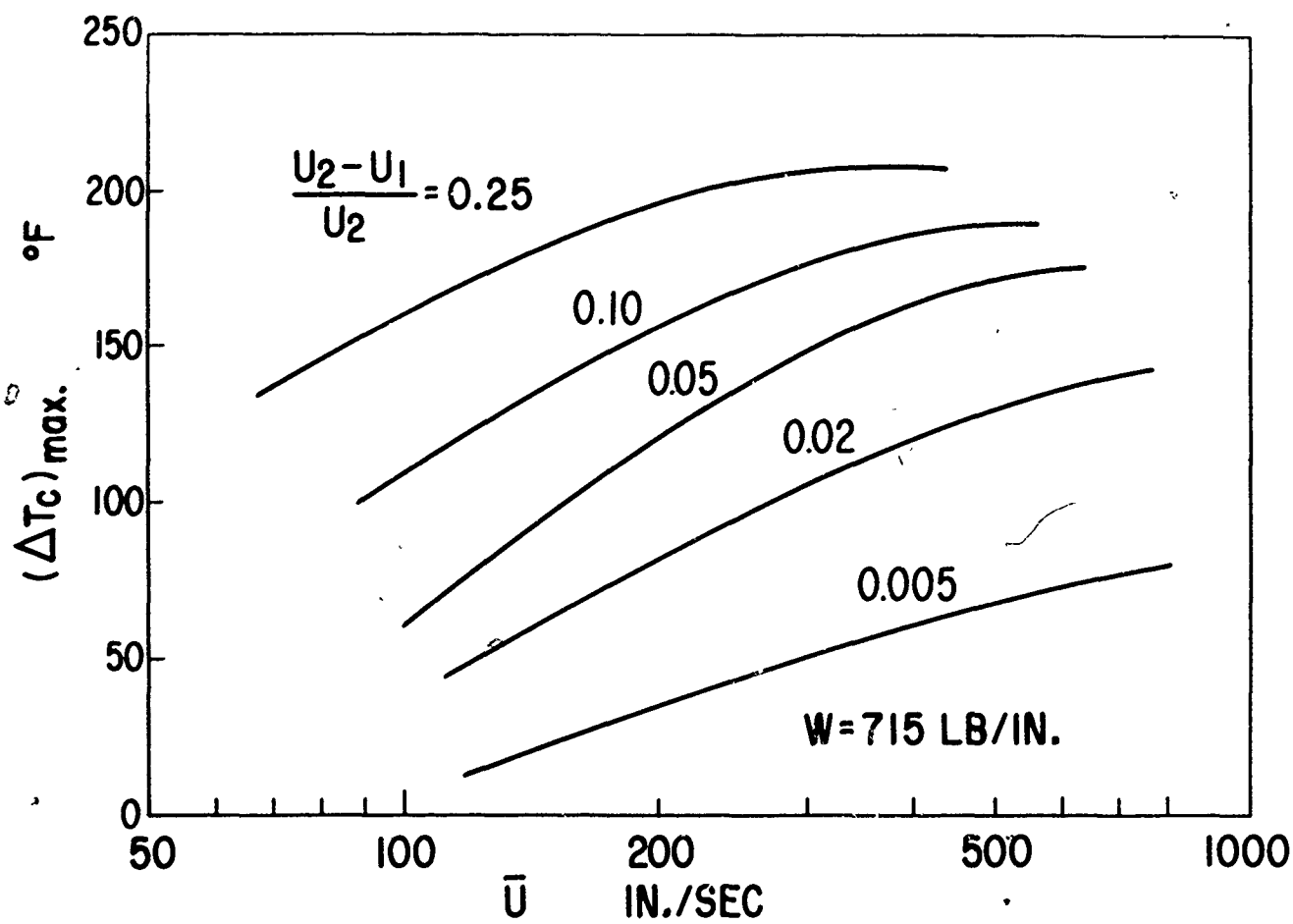


Fig. 33 Mid-Film Temperature

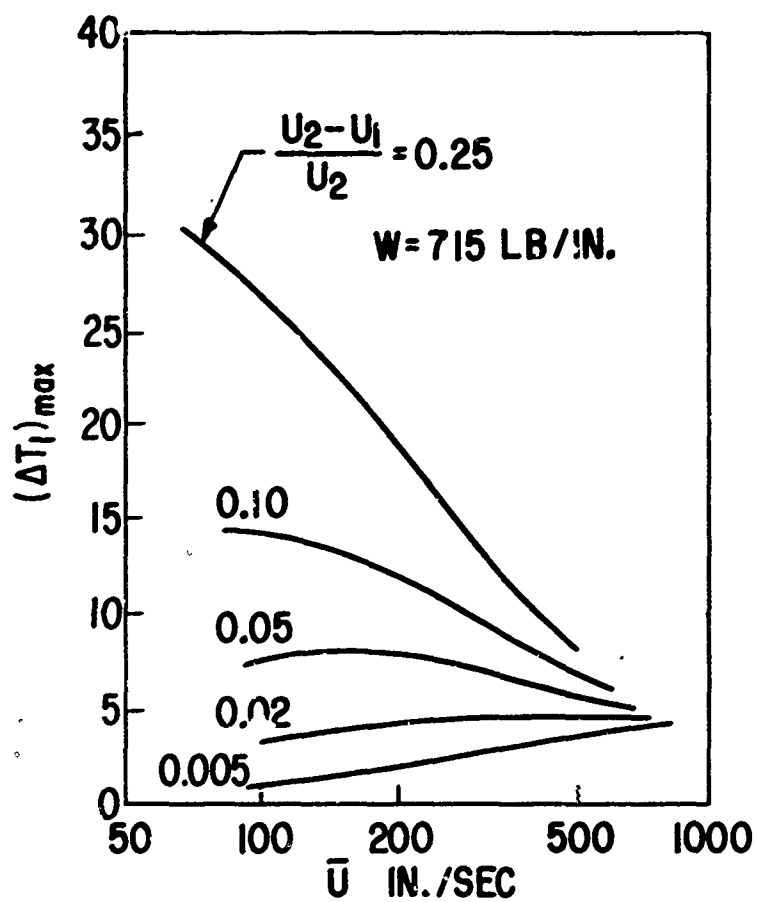


Fig. 34 Surface Temperature

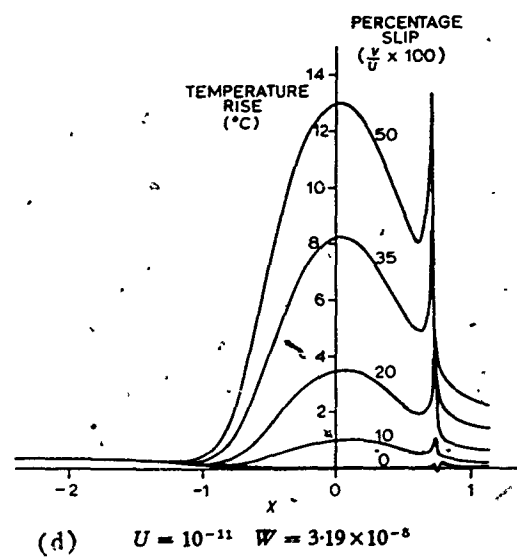
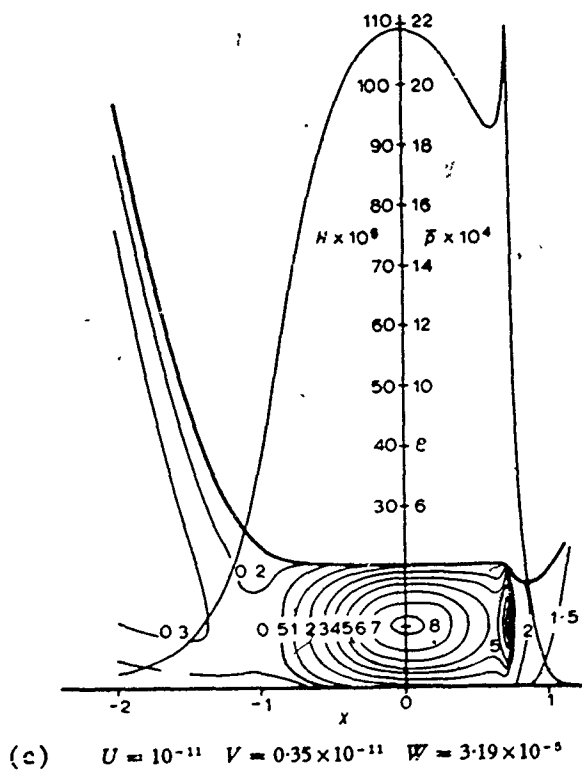
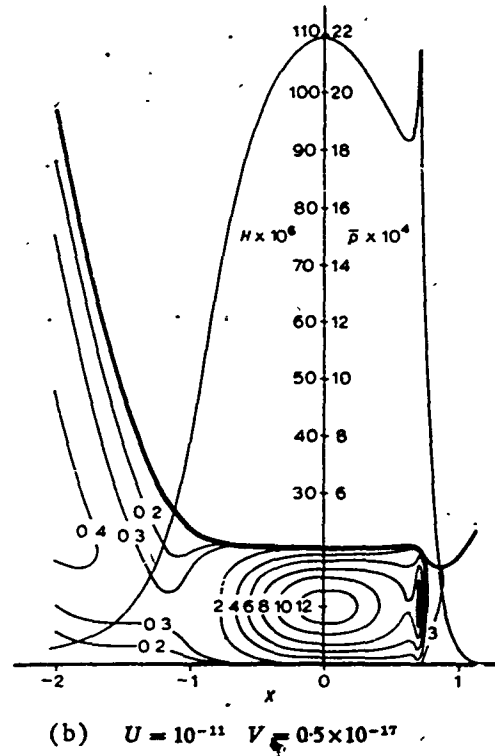
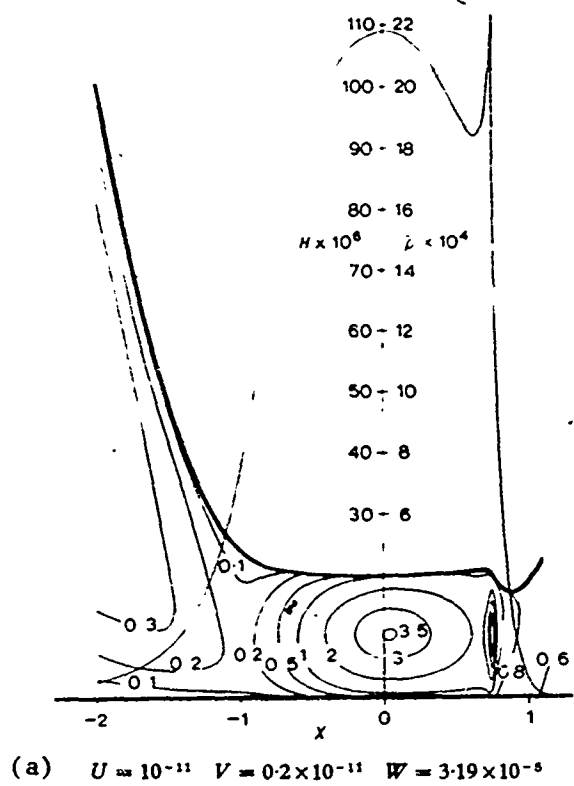


Fig. 35 Thermal Solution to Elastohydrodynamic Problem by Dowson and Whittaker. (Courtesy of Proc. Instn. Mech. Engrs., 1965-66).

ture profiles for a pure rolling case are shown in Fig. 36 in conjunction with measured pressure and film profile. The variation of measured surface temperature against the slip ratio  $(U_2 - U_1)/U_2$  is shown in this figure and they are compared with the theoretical value calculated by the thermal elastohydrodynamic theory. It is seen that the agreement is fair at high slip ratio and rather unsatisfactory at low sliding speeds.

Recently, Kannel et al (102) have made a series of surface temperature measurements under pure rolling conditions and for loads higher than those used by Orcutt. A titanium wire deposited on a silica insulator was used as the sensing element. Figs. 37 and 38 show the effects of load and speed on the surface temperature. In general, the temperature level is considerably higher than those measured by Orcutt.

## 5. FRICTION

One of the most interesting yet perplexing aspects of elastohydrodynamic lubrication is the frictional force developed in shearing a lubricant film in two heavily loaded contacts. Most of the experimental data to date have been obtained from two disc machines in which the friction forces are measured by sliding one disc over the other. Although these data are far from complete, they show a consistent trend of how the frictional force varies with the sliding speed, and beyond this point an increase in sliding speed would cause a decrease in friction. The level of this friction curve is a function of the load, rolling speed, the lubricant inlet temperature and the pressure-temperature viscosity characteristics of the lubricant.

Even though the elastohydrodynamic theory has advanced to a very sophisticated stage, they are far from adequate in predicting the frictional force between two heavily loaded contacts. There are two major reasons for this lack of correlation between the present elastohydrodynamic theories and the measured friction data. First, there is a complete absence of static viscosity data at extremely high pressures. Since the shear stress at a boundary is a product of the viscosity and the shear rate, and since the viscosity is extremely sensitive to both pressure and temperature in the high pressure region, the calculation of friction is inaccurate when using extrapolated viscosity data measured at the moderate pressures or by using an empirical pressure-temperature-viscosity function. A second reason for the lack of correlation is the use of the static viscosity data for conditions where the pressure, temperature, shear stress and shear rate all undergo a tremendous rate of change. Under these circumstances, the flow properties may not have enough time to reach equilibrium and behave in the fashion measured in static experiments. These are the two major reasons which have prevented the development of a satisfactory analytical tool in predicting the traction between elastohydrodynamic contacts. In the following section a brief review will be given to the state-of-the-art of traction in elastohydrodynamic contacts.

### a. Rolling and Sliding Friction

Early measurement of the friction between gear teeth and between circular discs have placed emphasis mainly upon finding empirical corre-

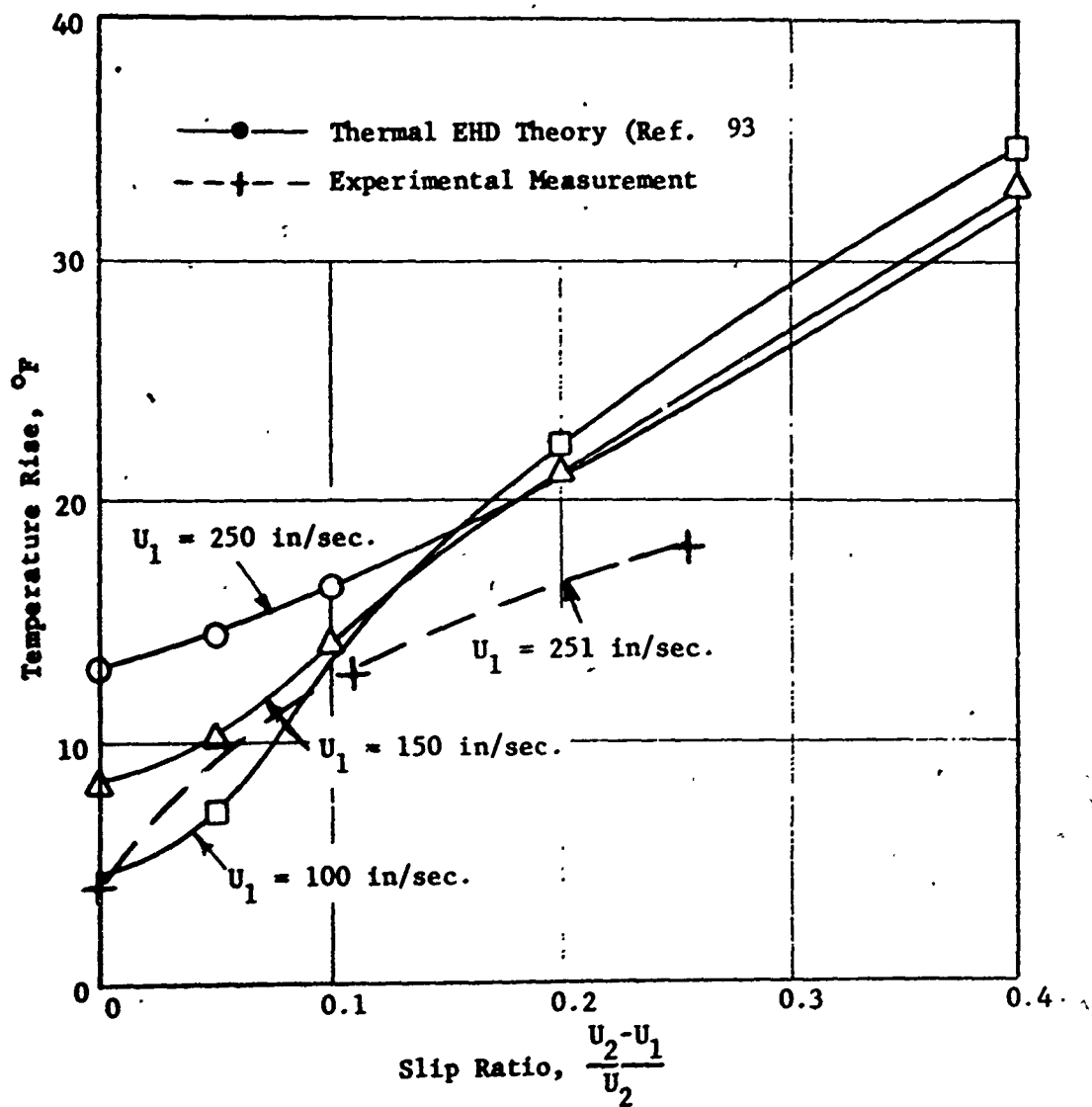
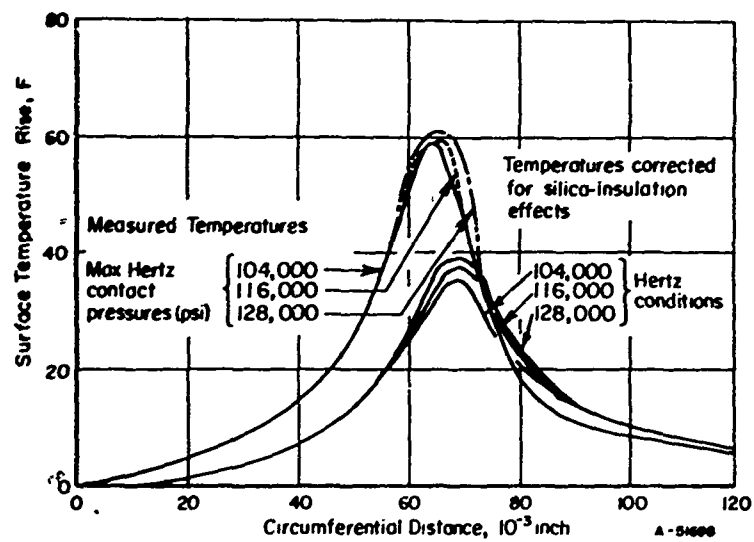


Fig. 36 Calculated and Measured Surface Temperature



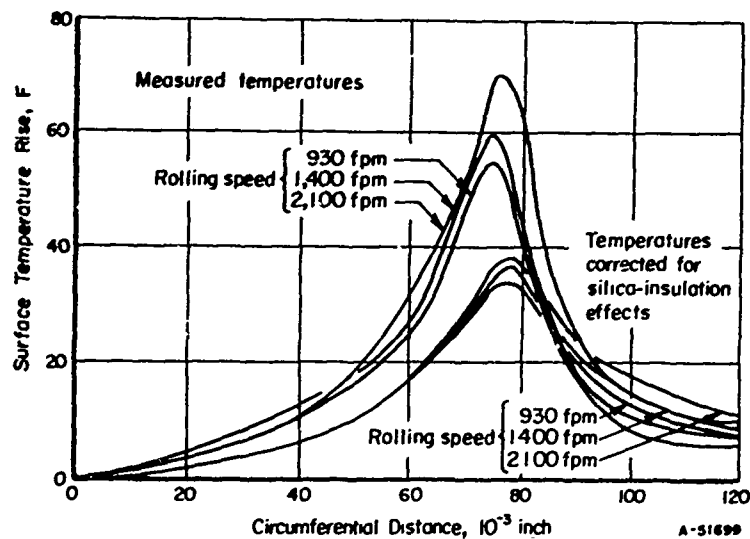


$$T_{\text{amb}} = 115 \text{ F}$$

Rolling speed = 1400 fpm

Lubricant: polyphenyl ether

Fig. 37 Variation in Disk Temperature with Loading  
(United States Air Force Tech. Report No. ASD-TDR-61-643, pt. VI, 1966).



Loading = 116,000 psi (Hertz)

$$T_{\text{amb}} = 115 \text{ F}$$

Lubricant: polyphenyl ether

Fig. 38 Variation in Disk Temperature with Rolling Speed  
(United States Air Force Tech. Report No. ASD-TDR-61-643, pt. VI, 1966).

lations with the design parameters. Typical examples of contributions are by Cameron and Newman (123), Misharin (124), and Benedict and Kelley (125). But none of these papers were designed to promote the basic understandings of the traction between elastohydrodynamic contacts.

Crook (126) used two kinds of rolling disc machines in measuring the friction in the line contact as a function of sliding speed. In the small sliding speed region he used a four disc machine which consists of a center disc surrounded by three equally spaced outer discs (Fig. 39a). Since the center disc is free-floating, the measured torque will not contain any extraneous torque from the supporting bearings. For this reason the four-disc machine gives very accurate friction torque measurement at very small sliding speeds. However, in the region of high slip, the four-disc machine is not suitable because it cannot maintain a stable sliding speed. For high sliding speeds, Crook used the conventional two-disc machine as shown in Fig. 40. In order to investigate how the friction decreases with the sliding speed in the high slip region, the rotation of both discs must be controlled by variable speed motors, one of which acts as a motor and the other acts as a generator. In this manner, Crook was able to measure the friction characteristics throughout the entire region of sliding speed using the four-disc machine in the low slip region and the two-disc machine in the high speed region.

Using the four disc machine, Crook found a profound influence of rolling speed upon the frictional torque in the low slip region. In this region the slope of the traction vs. slip curve is equal to a so-called effective viscosity divided by the oil film thickness. By measuring the slope of the traction curve and by calculating the oil film thickness from the existing elastohydrodynamic theory the effective viscosity can be readily evaluated. If the thermal effects and the non-Newtonian effects of the lubricant are both absent in this region, then the effective viscosity will stay constant as a function of rolling speed. However, this condition was not found in Crook's experimental results. On the contrary, he found a marked influence of the rolling speed on the effective viscosity of the lubricant. As shown in Fig. 41, the ratio of the effective viscosity to the supply viscosity can be reduced by almost two orders of magnitude as the rolling speed increases from 0 to 1200 cm/sec. Such a drastic reduction does not appear to be due to thermal effects only. Crook speculated that it was the visco-elastic effect of the lubricant which prevented it from reaching the static viscosity in the short time interval as it passes through the contact zone. The visco-elastic effect has been more thoroughly investigated analytically by Dyson in a recent paper (128).

By using the two-disc machine, Crook was able to extend the friction data in the high slip region for loads ranging from  $7.5$  to  $20 \times 10^7$  dynes/cm and rolling speed from 400 cm/sec to 1200 cm/sec. All the friction curves showed the same basic trend which is characterized by an ascending portion at a small sliding speed and a descending

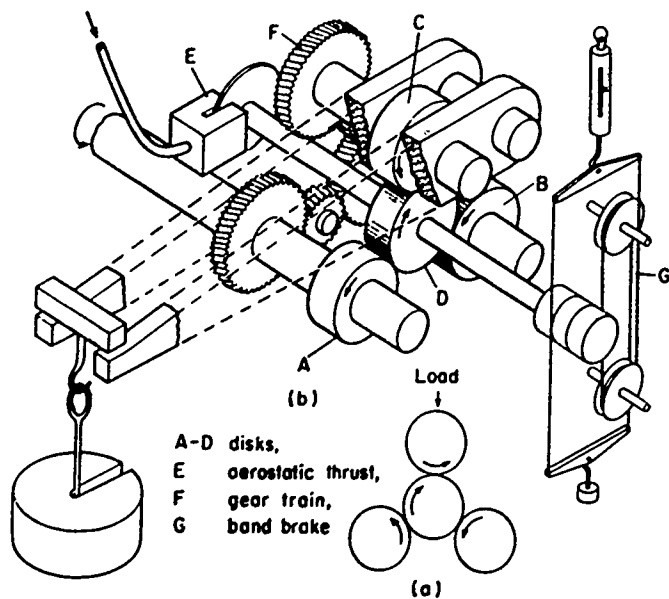
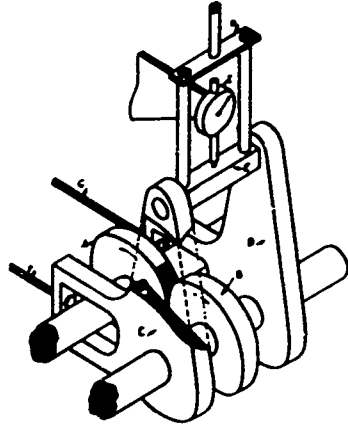


Fig. 39 The Four Disk Machine  
(Courtesy of Philosophical Trans.,  
Series A 255, 281, 1961).



**Fig. 40 The Two Disk Machine**  
(Courtesy of Philosophical  
Trans., Series A255, 281,  
1961).

friction at high sliding speeds. Fig. 42 shows that an increase in load does not change the basic characteristics of the friction curve much, but does increase the level of the friction force. Similarly, in Fig. 43 it was shown that a change in rolling speed also effects the level of the friction force. When the rolling speed increases, the friction level decreases.

Crook also attempted to predict the friction analytically by a simplified thermal friction theory based on the following four assumptions:

1. The film thickness within the contact zone is uniform
2. The pressure distribution in the contact region is Hertzian
3. The heat carried away by the lubricant due to convection is neglected.
4. The temperature rise on the surface of the disc is neglected.

Using this simplified thermal theory, Crook was able to calculate the coefficient of friction or the effective viscosity as a function of sliding speed. Fig. 44 shows the comparison between the calculated effective viscosity and the measured effective viscosity as a function of sliding speed for a load of  $1.2 \times 10^8$  dynes/cm and a rolling speed of 400 cm/sec. There are three calculated curves representing three different values of the ratio of the thermal conductivity of the lubricant to the temperature viscosity coefficient. It is seen that even if this ratio is increased by almost one order of magnitude, it is still not possible to predict the sharp reduction of the effective viscosity at small sliding speeds. Based on this evidence, Crook concluded that the friction force at small sliding speed cannot be accurately predicted by considering the thermal effects only.

In 1965 Cheng (93) employed his full elastohydrodynamic theory in calculating the friction for the conditions corresponding to those used in Crook's experiment. The temperature calculations are based on the finite difference solution of the energy equation and are free from all assumptions made earlier by Crook. It is seen from Fig. 45 that even with this refined thermal analysis there still exists large discrepancy in the low slip region. This strengthens Crook's argument that the thermal effects alone cannot account for the sharp reduction in the low slip region. In 1963 Bell, Kannel, and Allen (121) developed an approximate analysis to predict the temperature rise at low sliding speed. In their analysis they included the heat due to convection of the lubricant and heat generation due to the compression of the lubricant. They also concluded that the temperature effects are too small to account for the loss of effective viscosity at low sliding speeds. In addition to the thermal theory they also developed a non-Newtonian friction theory using a rheological model proposed by Ree Eyring. Fig. 46 shows a typical set of friction curves vs. the dimensionless shear rate parameter. These curves indicate that

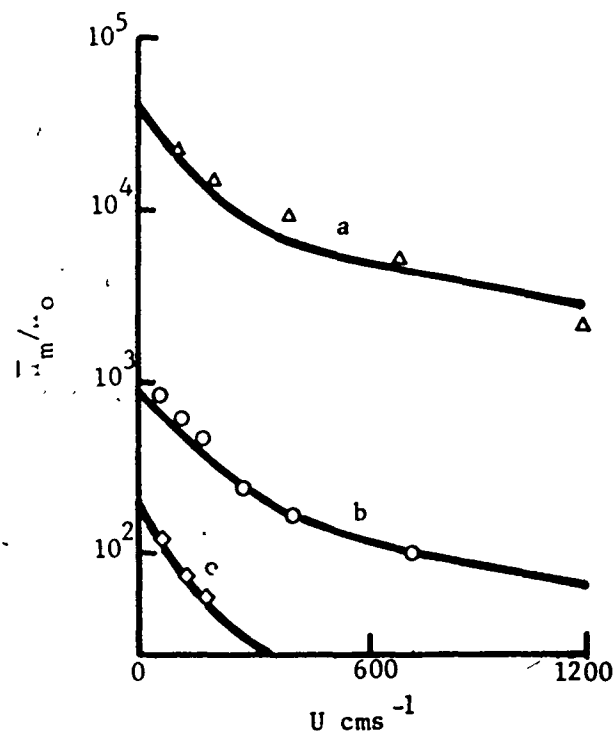


Fig. 41 The Ratio of the Effective Viscosity ( $\eta$ ) to the Supply Viscosity ( $\eta_0$ ) in Pure Rolling, Calculated from the Visco-Elastic Hypothesis. (a)  $G = 1.9 \times 10^8 \text{ dyne-cm}^{-2}$ ;  $\lambda = 1.9 \times 10^{-4} \text{ sec}$ ; (b)  $G = 7.4 \times 10^6 \text{ dyne-cm}^{-2}$ ;  $\lambda = 1.1 \times 10^{-4} \text{ sec}$ ; (c)  $G = 1.4 \times 10^6 \text{ dyne-cm}^{-2}$ ;  $\lambda = 1.2 \times 10^{-4} \text{ sec}$ . Experimental Points, Load ( $10^7 \text{ dyne-cm}^{-1}$ ):  $\Delta$  2.5,  $\circ$  2.9,  $\Delta$  14.6. (Courtesy of Philosophical Trans., Series A255, 281, 1961).

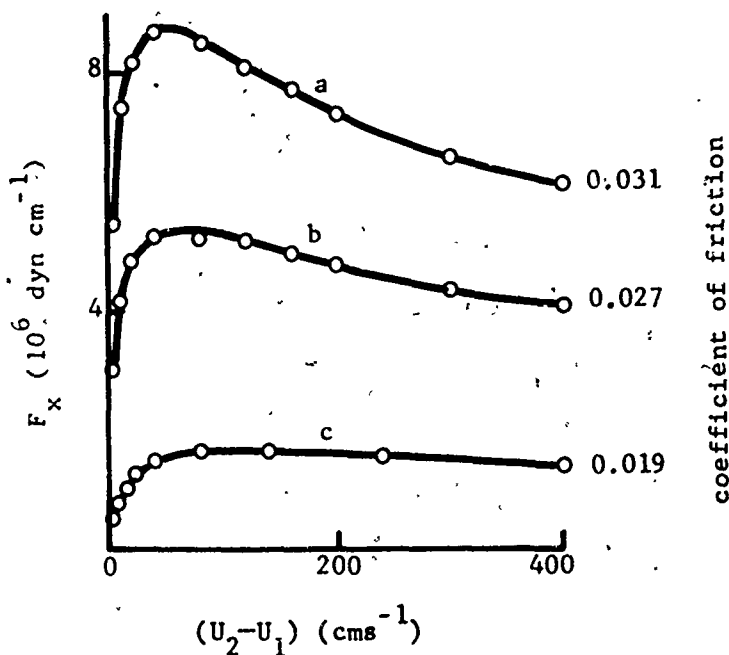


Fig. 42 Frictional Traction as a Function of Sliding Speed (Rolling Speed Constant at  $400 \text{ cm-sec}^{-1}$ ). Load ( $10^7 \text{ dyne-cm}^{-1}$ ): (a) 20, (b) 15, (c) 7.5. (Courtesy of Philosophical Trans., Series A255, 281, 1961).

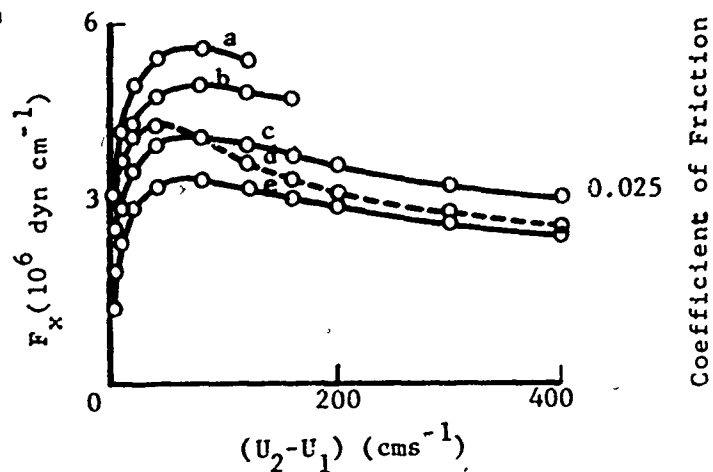


Fig. 43 Frictional Traction as a Function of Sliding Speed. Load  $1.25 \times 10^8$  dyne-cm $^{-1}$ . (a)  $U = 120$  cm-sec $^{-1}$ ,  $\mu_0 \approx 0.4$  P; (b)  $U = 200$  cm-sec $^{-1}$ ,  $\mu_0 \approx 0.4$  P; (c)  $U = 400$  cm-sec $^{-1}$ ,  $\mu_0 \approx 0.4$  P; (d)  $U = 400$  cm-sec $^{-1}$ ,  $\mu_0 \approx 0.7$  P; (e)  $U = 600$  cm-sec $^{-1}$ ,  $\mu_0 \approx 0.4$  P. (Courtesy of Philosophical Trans., Series A255, 281, 1961).

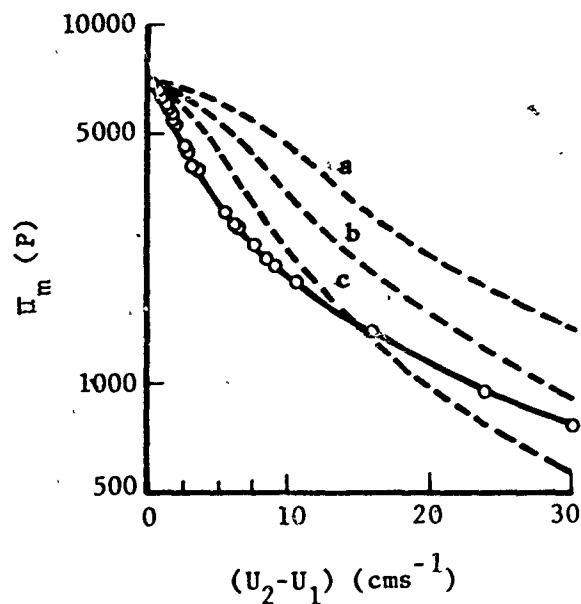


Fig. 44 The Variation of  $\mu_m$  with Sliding Speed. Load =  $1.2 \times 10^3$  dyne-cm $^{-1}$ ,  $U = 400$  cm-sec $^{-1}$ ,  $\mu_0 = 1.4$  P ————o———— from Experiment, ----- Calculated. (a)  $K_f/a_1 = 1.5 \times 10^5$  dyne-sec $^{-1}$ ; (b)  $K_f/a_1 = 7.5 \times 10^4$  dyne-sec $^{-1}$ ; (c)  $K_f/a_1 = 3.75 \times 10^4$  dyne-sec $^{-1}$ . (Courtesy of Philosophical Trans., Series A255, 281, 1961).

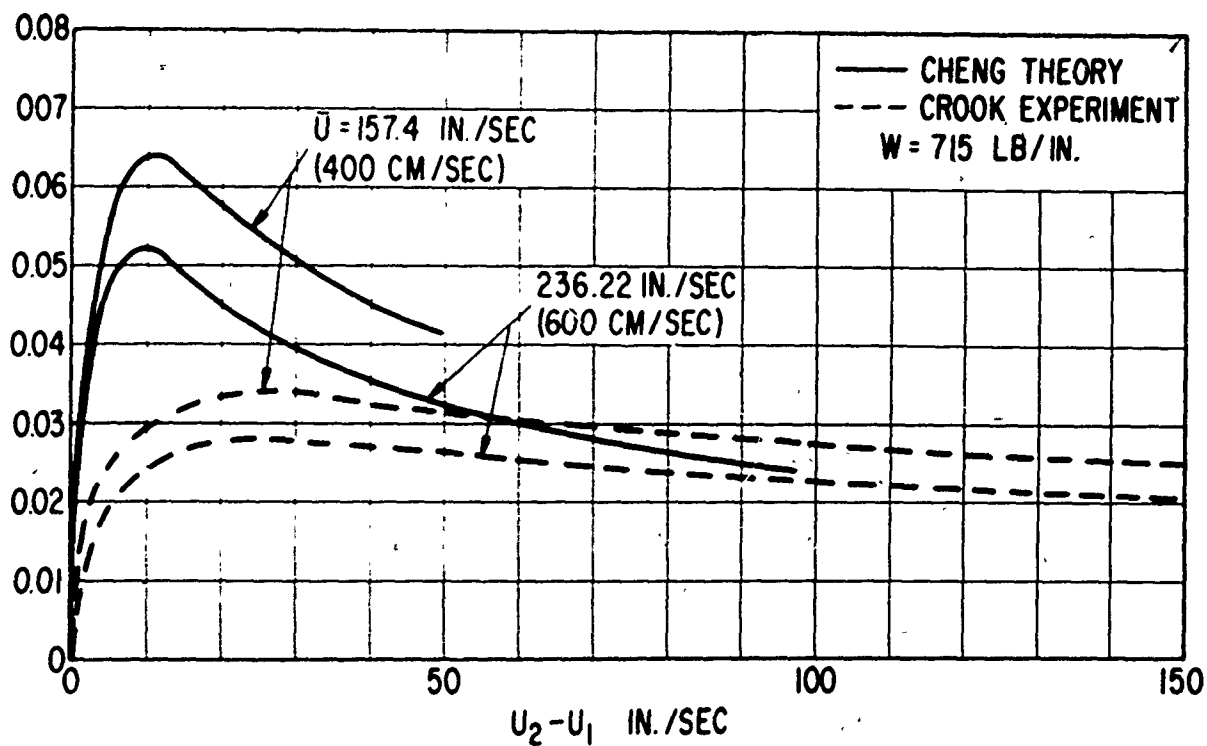


Fig. 45 Comparison Between Theoretical and Experimental Sliding Friction Factor

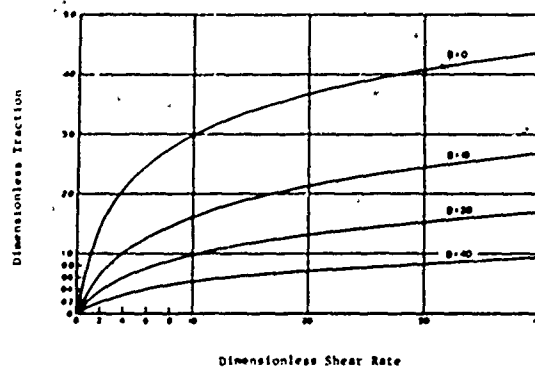


Fig. 46 Traction Versus Shear Rate  
(Courtesy of ASME, J. Basic Engrg., Vol. 86, Series D, No. 3, 423, 1964).



drastic reductions of friction can exist if the lubricant viscosity is shear rate dependent, according to Ree Eyring. However, in all their calculated data the friction force was found to be dependent upon  $1/h$  which means if the rolling speed increases the friction force will fall according to  $1/h$ . On the other hand, all the experimental data gathered thus far have shown the proportionality is far greater than  $1/h$  and in most instances are more nearly proportional to  $1/h^2$ . Thus, one may conclude that the inclusion of the Ree Eyring model in the friction analysis will not be able to predict a reduction of friction force at low rolling speeds. This is really not surprising, since the Ree Eyring model is primarily a shear dependent Newtonian model and is not likely to predict the loss of pressure-viscosity dependence during short transients.

In 1965 F. W. Smith (127) employed a rolling contact machine to measure the friction between two rollers whose axes were skewed at an arbitrary angle. With this skewed arrangement he was able to measure the friction force due to the sliding velocity component. Fig. 47 plots typical friction curves against the sliding speed. These curves show trends similar to that observed by Crook. Smith divided the friction charts into six regions. In regions 1 and 2 friction varies proportionally with the sliding speed and a Newtonian isothermal friction theory is believed to be applicable in this region. Region 3 is the ascending portion of the friction curve in which the friction force increases with sliding speed in a non-linear fashion and Smith believed that the non-linearity is due to the non-Newtonian effects of the lubricant. In regions 4 and 5 he postulated that there exists a shear plane at the center of the lubricant film such that the lubricant film behaves like two layers of solid substance sliding over each other at the shear plane like a plastic solid. Region 6 is where the seizure would take place. He also postulated that the resistance to sliding at the shear plane is dependent upon the shear plane temperature and the hydrostatic stress in the lubricant at the shear plane.

A more comprehensive study of friction covering wide ranges of load, rolling speed, and sliding speed was carried out more recently by Johnson and Cameron (129) using the conventional two-disc machine. The maximum Hertz pressure was varied from 100,000 psi to 200,000 psi; the rolling speed was varied from 8 in./sec; and the inlet film temperature was varied from 30°C to 90°C. Fig. 48 shows the set of friction curves for different loads, and Fig 49 shows the effect of rolling speed and inlet film temperature upon a friction curve. The most striking feature of Johnson and Cameron's data is that there exists a ceiling to all the experimental traction coefficients which cannot be exceeded no matter how the load and the rolling speed are varied. They also took extensive data in the low slip region, and from the slope of the traction and slip curve they were able to calculate the effective viscosity as a function of rolling speed. The loss of effective viscosity due to rolling speed is shown in Fig. 50. They also furnished the most convincing evidence that thermal effects alone cannot account for the experimentally measured friction. Fig. 51 shows two sets of friction curves calculated by using Crook's

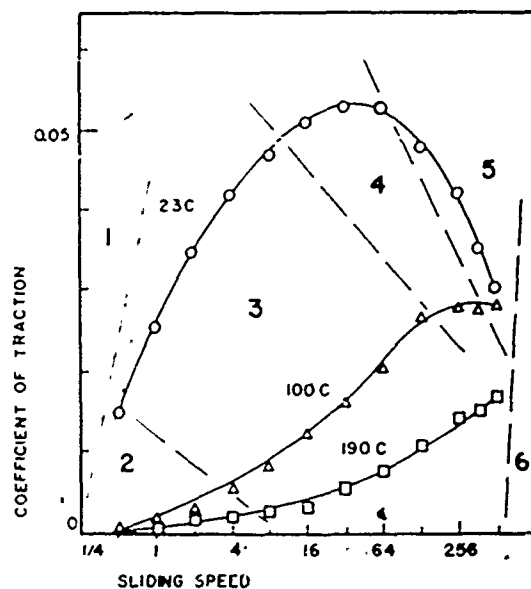


Fig. 47 Coefficient of Traction as a Function of Sliding Speed (Courtesy of ASME, J. of Basic Engrg., Vol. 87, Series D, No. 1, 170, 1965).

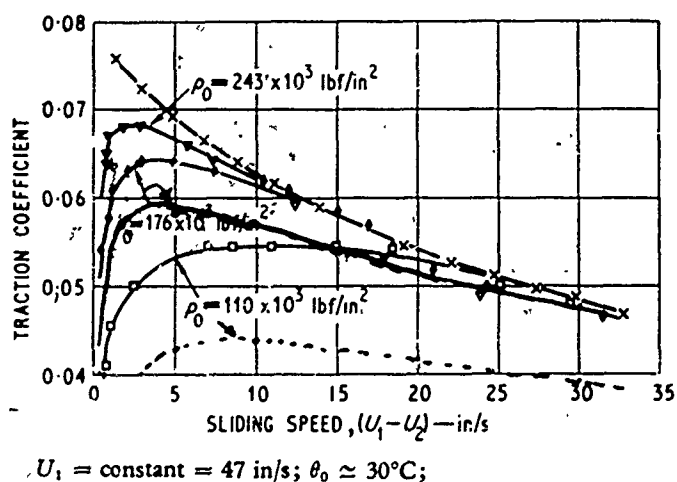


Fig. 48 Variation of Traction with Sliding Speed at Various Contact Pressures. (Courtesy of Proc. of Instn. Mech. Engrs., Vol. 182, 307, 1967-68).

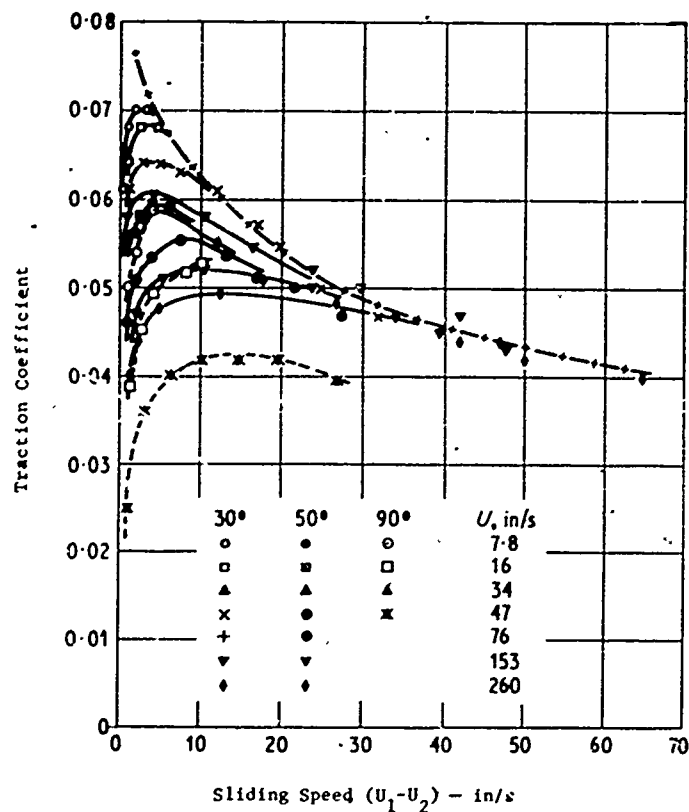


Fig. 49 Influence of Rolling Speed and Inlet Temperature Upon the Traction Coefficient. (Courtesy of Proc. of Instn. Mech. Engrs., Vol. 182, 307, 1967-68).

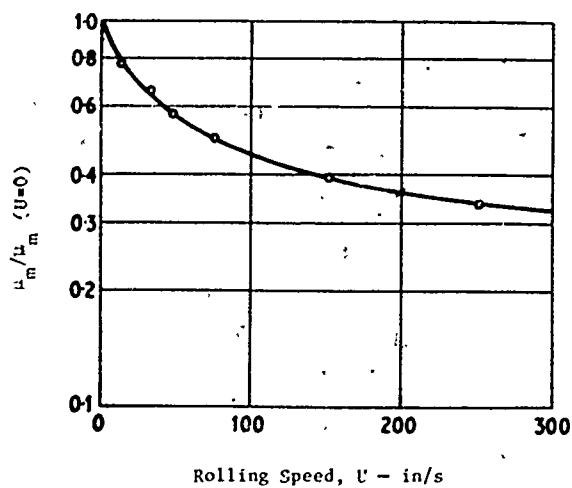


Fig. 50 The Influence of Rolling Speed Upon Effective Viscosity. (Courtesy of Proc. of Instn. Mech. Engrs., Vol. 182, 307, 1967-68).

simplified thermal theory. These curves are for rolling speeds of 16 in/sec and 260 in/sec and are based upon apparent viscosities deduced from the low-slip friction data. It is quite evident that the calculated traction coefficients can be as much as one or more than one order of magnitude higher than the experimental friction data. Discrepancies become larger when the maximum Hertzian pressure becomes greater.

In an effort to explain the discrepancy between the friction calculated by the simplified thermal theory and the experimental friction, Johnson and Cameron resorted to the Smith shear plane concept which states that the traction is limited by the lubricant reaching a critical shear stress at which it shears in the manner of a plastic solid. By plotting the mean shear stress against shear plane temperature at different loads, sliding speed, rolling speed, and inlet film temperature, they have found sufficient evidence that the limiting shear stress is a function of shear plane temperature and pressure only, and is not dependent upon the sliding speed, rolling speed, or the disc temperature. This conclusion was supported by Fig. 52 which shows the mean shear stress can be plotted against the shear plane temperature with the average Hertz pressure as a parameter.

In a sister paper to Johnson and Cameron's work, Jefferis and Johnson (130) investigated the effect of surface roughness upon friction between two lubricated rollers. They concluded that the measured coefficient of traction showed remarkably little variation throughout the whole range of experimental conditions for Hertzian pressure in excess of 175 kpsi as shown in the traction coefficient curve in Fig. 53. At low Hertzian pressures the surface roughness effect can be substantial. This is attributable to the fact that the pressure underneath the asperities for rough surfaces are much higher than those under the smooth surfaces. This is enough to cause a wide variation in overall traction coefficients.

A rather interesting qualitative explanation of the velocity, rate of shear, viscosity, and temperature variations across the film thickness of an elastohydrodynamic contact were offered by Plint (131). These qualitative profiles are shown in Fig. 54. He postulated that at the entrance of the contact zone, the rate of shear, viscosity, and temperature are constant across the film thickness and the velocity profile is linear. As the thermal effects take over, the temperature at the mid film increases and the viscosity becomes lowest at the mid film. This thermal effect causes the velocity profile to distort into a shape such that the rate of shear becomes a maximum at the mid film forming a cusp as shown in Fig. 54. A ceiling curve similar to that of Johnson and Cameron's was also found in Plint's experimental friction data.

Dowson and Holmes (132) modified the Crook's four-disc machine and investigated the effect of surface quality upon traction characteristics of rolling and sliding contacts. By plotting friction against the surface roughness, they showed (Fig. 55) that the friction

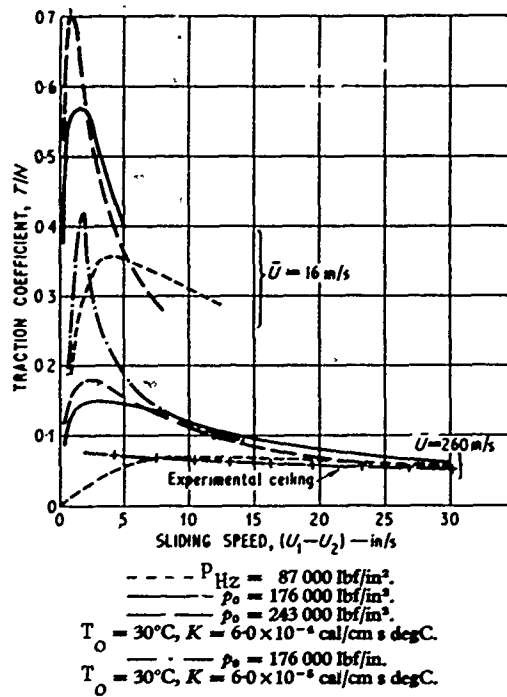


Fig. 51 Variation of Traction Coefficient with Sliding Speed Calculated by Crook's Theory, at Various Contact Pressures. (Courtesy of Proc. of Instn. Mech. Engrs., Vol. 182, 307, 1967-68).

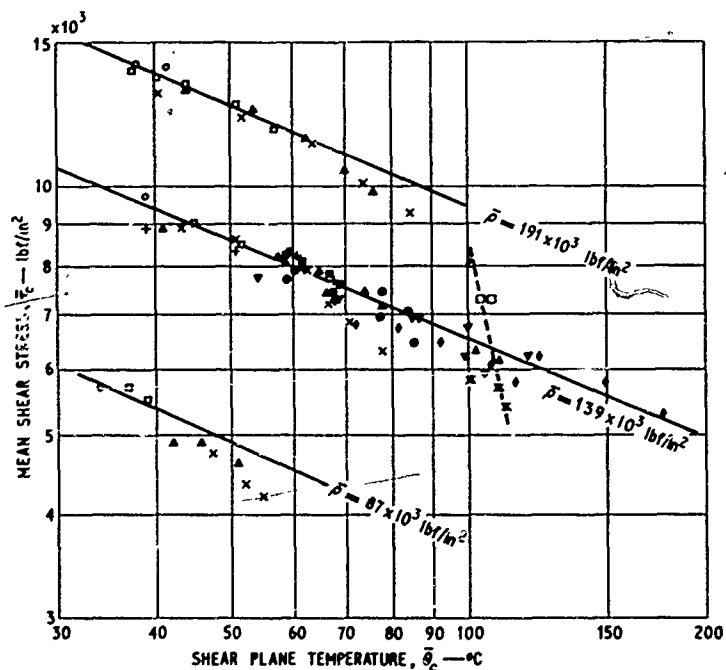
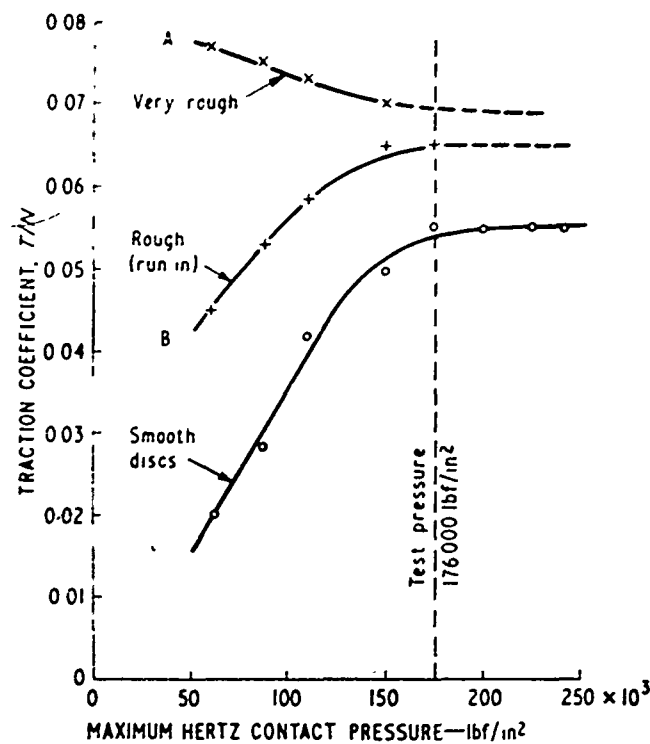


Fig. 52 Mean Shear Stress as a Function of Shear Plane Temperature. (Courtesy of Proc. of Instn. Mech. Engrs., Vol. 182, 307, 1967-68).



$U_1 = 260 \text{ in/s}$ , disc temperature =  $30-40^\circ\text{C}$

Fig. 53 Friction of Smooth and Rough Discs as a Function of Maximum Hertz Contact Pressure. (Courtesy of Proc. of Instn. Mech. Engrs., Vol. 182, 1967-68).

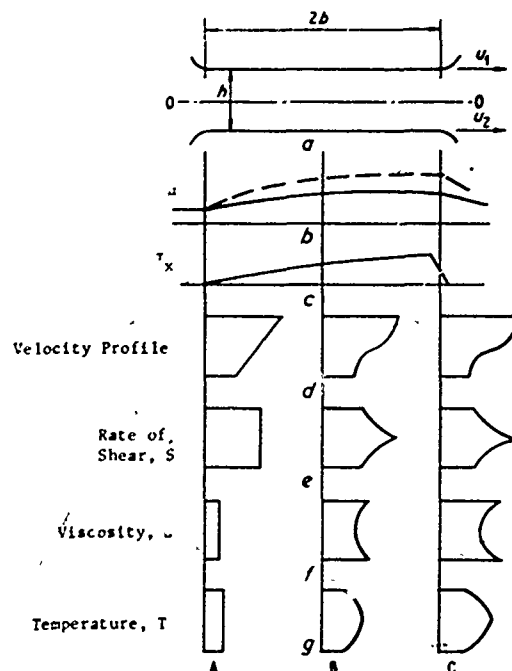


Fig. 54 Simplified Elastohydrodynamic Contact: With Temperature Effects and Finite Rate of Increase in Viscosity. (Courtesy of Proc. Instn. Mech. Engrs., Vol. 182, 300, 1967-68).

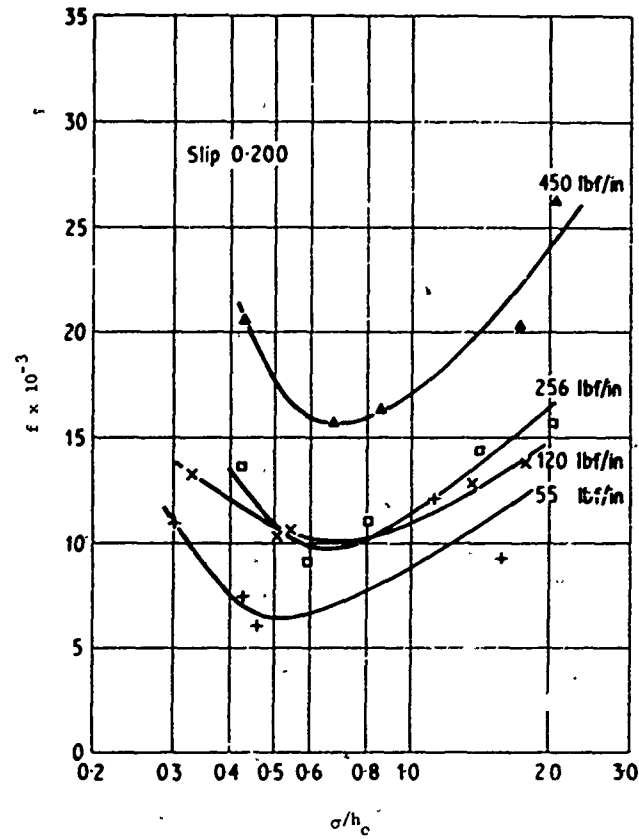


Fig. 55 Typical Plot of Coefficient of Friction Against the Ratio of Peak-to-Valley Roughness/Theoretical Minimum Film Thickness. (Courtesy of Proc. Instn. Mech. Engrs., Vol. 182, 1967-68).

initially decreases with surface roughness, reaches a minimum, and then increases steadily with surface roughness. Unlike Johnson and Jefferies' conclusion on the effect of surface roughness on friction, Dowson and Holmes found that the influence of surface quality is quite pronounced. However, these two results may not necessarily be in direct contradiction because the load used by Dowson and Holmes was much smaller than that used in Johnson and Jefferies' experiments.

In 1969, Dyson (128) analyzed the frictional force in an elastohydrodynamic contact by considering the lubricant as a viscoelastic liquid. He divided the friction vs. sliding speed curve into three regions, as shown in Fig. 56, (1) the linear region, where the frictional force varies linearly with the sliding speed; (2) the non-linear ascending region, where the slope of the friction curve reduces rapidly as the sliding speed increases; (3) the thermal region, where the frictional force decreases with the sliding speed.

In the linear region, he employed the recently developed Barlow-Lamb viscoelastic model (133) and the Maxwell model to calculate the apparent viscosity as a function of the rolling speed. If the viscoelastic effect is absent, then the apparent viscosity should be constant with respect to the rolling speed. Figs. 57 and 58 plot the ratio of the apparent viscosity to that at  $U = 0.2$  in/sec. against the rolling speed  $U$  for the Barlow-Lamb and Maxwell liquids respectively. The variation of this ratio with  $U$  obtained experimentally by Johnson and Cameron was also plotted in these curves for comparison. It is seen that the experimental data agrees better with the curve based on the Barlow-Lamb liquid. However, this agreement is only valid for a static viscosity of  $\mu = 10^6$  P. As the static viscosity increases, the reduction of the calculated apparent viscosity with the rolling speed increases, but this strong dependence upon static viscosity has not been observed by Johnson and Cameron (129).

In the non-linear region, the strain becomes large and the use of the viscoelastic properties as determined in oscillatory shear with small strains becomes questionable. Dyson was able to establish a relation between the shear stress in continuous shear and the properties measured with oscillating crystals under small strains. This relation was obtained for the Barlow-Lamb model as well as for the Maxwell model. He showed that the characteristics of the ascending friction curve can be qualitatively explained better with the Barlow-Lamb model than with the Maxwell model.

In the thermal region, close agreement was found by Dyson between the measured mean shear stress and the limiting shear stress based on the viscoelastic properties from the oscillatory shear. However, he had to postulate that the shear modulus must be dependent upon the contact pressure and mid-film temperature.

Kannel and Walowit (134) recently made several simplified analyses for tractions in elastohydrodynamic contacts. By assuming a Hertzian pressure, a constant film profile in the contact region, and a heat



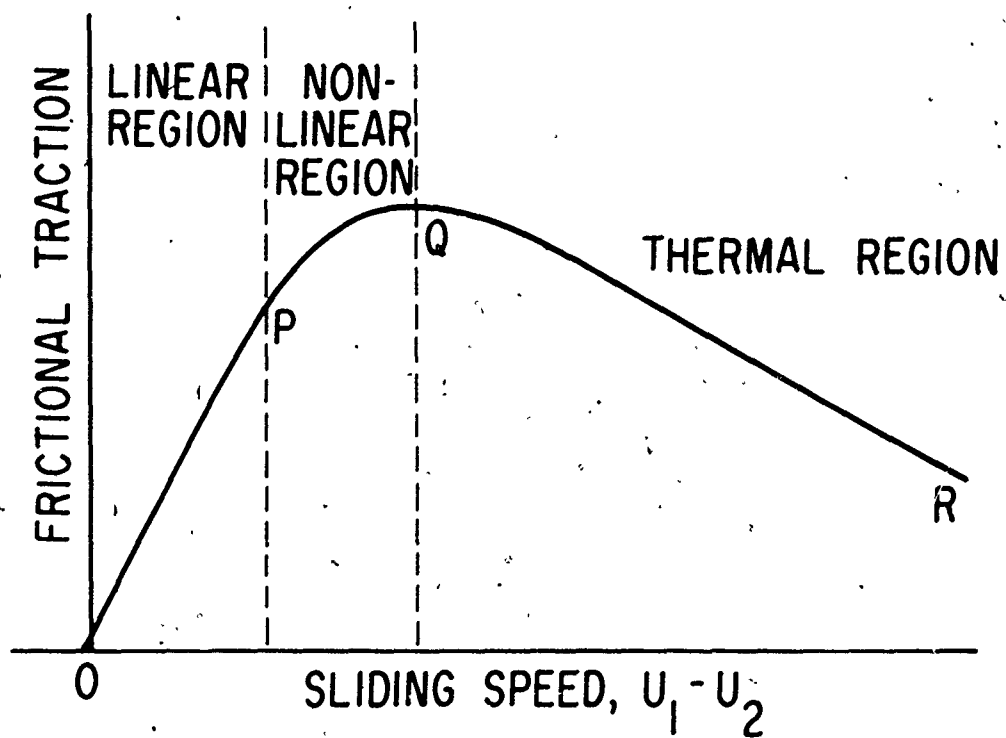


Fig. 56 Friction vs. Sliding Speed Curve.  
(Courtesy of A. Dyson, Paper to  
be published).

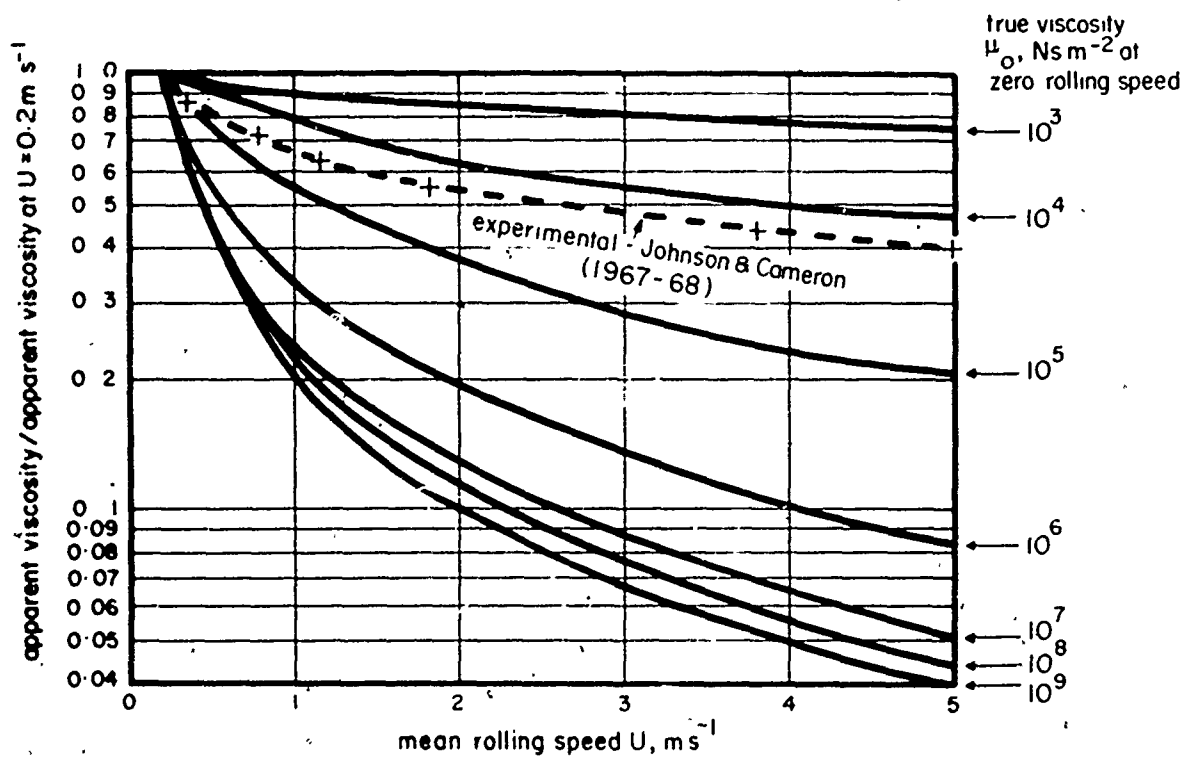


Fig. 57 Apparent Viscosity vs. Mean Rolling Speed, Barlow-Lamb Liquid. (Courtesy of A. Dyson; Paper to be Published).

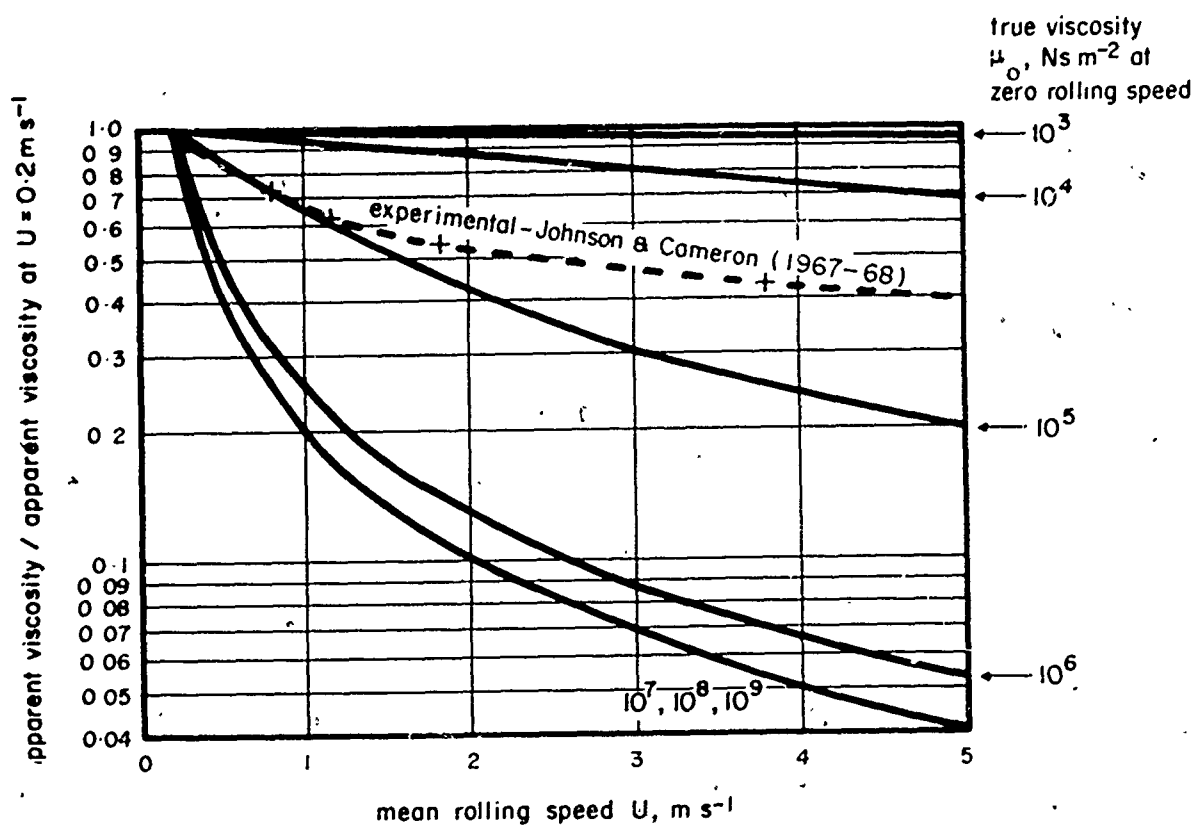


Fig. 58 Apparent Viscosity vs. Mean Rolling Speed, Maxwell Liquid. (Courtesy of A. Dyson, Paper to be Published).

generation due to sliding only, the calculated tractions for the following four viscosity models:

Model 1 - Newtonian

$$\mu = \mu_0 \exp \left( \alpha' p + \frac{\rho'}{T} - \frac{\rho'}{T} + \gamma' \frac{p}{T} \right) \quad (23)$$

where  $\alpha'$ ,  $\rho'$ , and  $\gamma'$  are constants. Fig. 59 shows the friction calculated by their simplified theory agrees very well with those obtained from the full elastohydrodynamic theory (12).

Model 2 - Newtonian

$$\mu = \frac{\mu_0 \exp(\gamma p)}{1 + \delta'(T - T_0)} \quad (24)$$

By adjusting the values for  $\gamma'$  and  $\delta'$  in this model, they showed (Fig. 60), that the calculated friction could be made to agree very closely to those measured by Crook (127).

Model 3 - Maxwell (Non-Newtonian)

$$S = \frac{G^2}{2\mu} \left[ 1 - \sqrt{1 - \left( \frac{2L}{G} \right)^2} \right] \quad (25)$$

where  $S$  is the shear rate,  $G$  is the shear modulus, and  $L$  is the shear stress. By using this model they showed, Fig. 61, that a value of the shear modulus  $G$  of 5000 psi is required to produce significantly different traction than that calculated by the Newtonian model.

Model 4 - Ree-Eyring (Non-Newtonian)

$$S = \frac{G}{\mu} \sinh \left( \frac{L}{G} \right) \quad (26)$$

With this model they found the effect of shear modulus is considerably less than that produced by the Maxwell model.

b. Spinning Friction

Recently, Dietrich, et al (135, 136) conducted a series of experiments on the spinning friction between a ball and a non-conforming groove without rolling between the contacting surfaces. The spinning friction apparatus used is shown in Fig. 62. They showed that

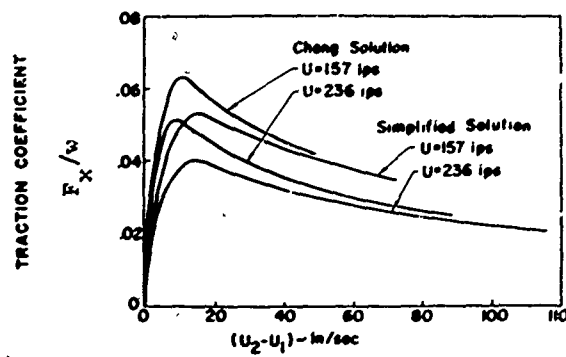


Fig. 59 Comparison of Calculation in Simplified Theory with Solution Profiles by Cheng. (Courtesy of Kannel, J.W. and Walowit, J.A., Paper to be Published in ASME Trans. J. Lubr. Tech.).

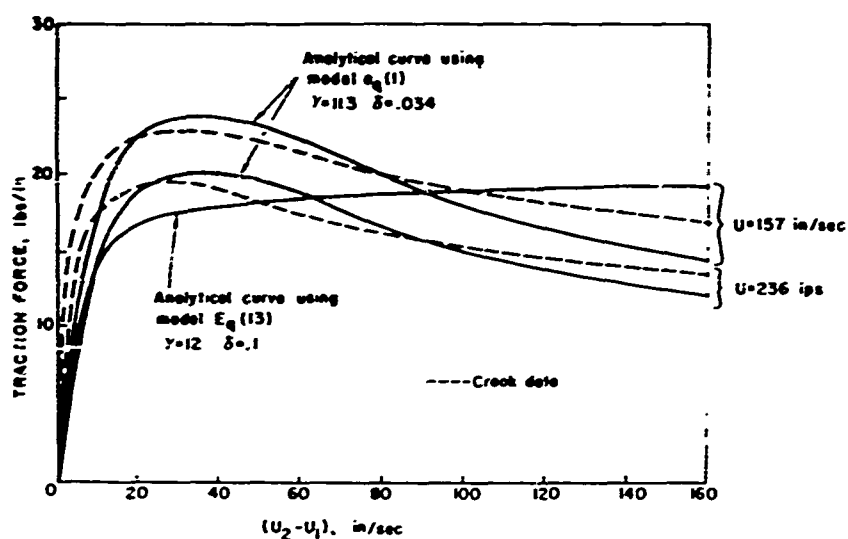


Fig. 60 Comparison of Crook's Data with Simplified Traction Calculations.  
 (Courtesy of Kannel, J.W. and Walowit, J.A., Paper to be Published  
 in ASME Trans. J. Lubr. Tech.).

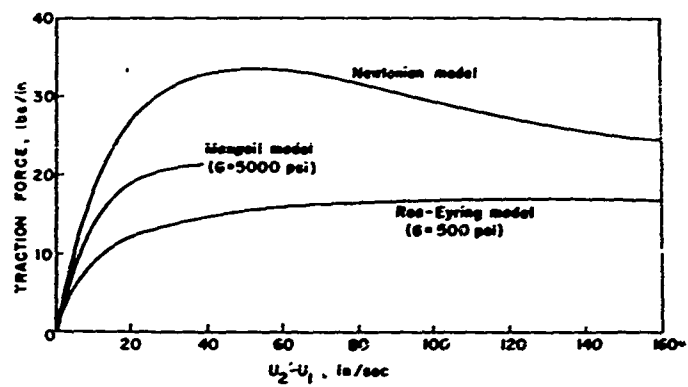


Fig. 61 Comparison of Traction Predictions Using Various Lubricant Models.  $U = 157$  in/sec. (Courtesy of Kannel, J.W. and Walowit, J.A., Paper to be Published in ASME Trans. J. Lubr. Tech.).

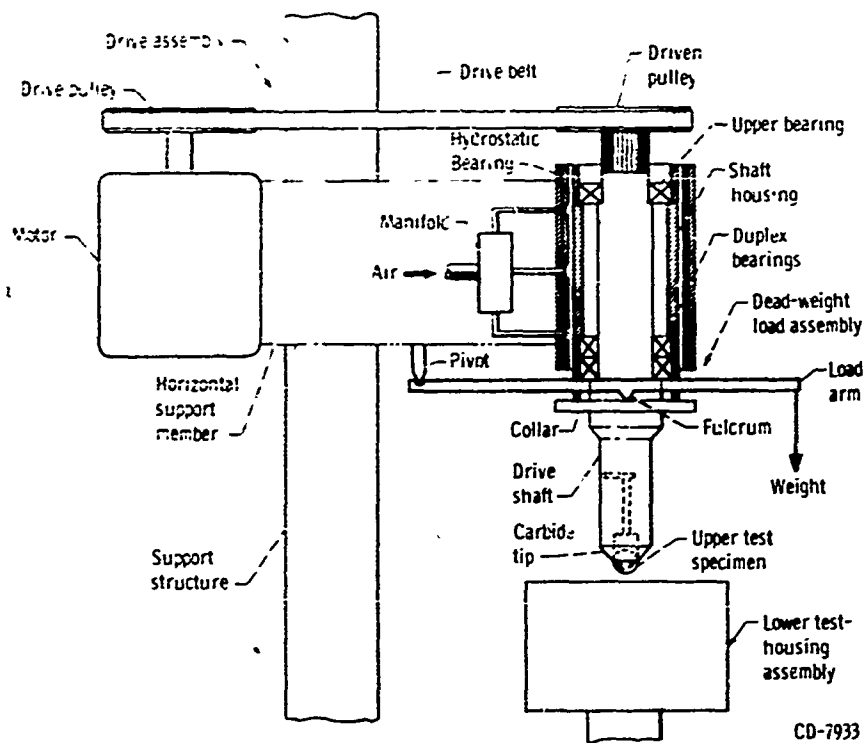


Fig. 62 Spinning Friction Apparatus.  
(Courtesy of NASA TN-D-2796).



frictional torque varies markedly with contact groove geometry, contact stress, lubricant type, and speed.

In order to predict the spinning analytically, Allen, Townsend, and Zaretsky (137) developed a spinning friction theory based on the following three pressure-viscosity relations:

1. Exponential Law

$$\mu = \mu_0 e^{\alpha_1 p} \quad (10)$$

2. Power Law

$$\mu = \mu_0 (1 + Cp)^n \quad (11)$$

3. Modified Exponential Law

$$\mu = \mu_0 e^{\alpha_1 p} \quad \text{for } p \leq p^* \quad (27a)$$

$$\mu = \mu_0 e^{[\alpha_1 p^* + \alpha_2 (p - p^*)]} \quad \text{for } p > p^* \quad (27b)$$

They concluded that the closest agreement between the experimental frictional torque and the calculated torque was found by using the modified exponential law with  $p^* = 60,000$  psi,  $\alpha_1 = 9.2 \times 10^{-5}$  in<sup>2</sup>/lb and  $\alpha_2 = 5 \times 10^{-6}$  in<sup>2</sup>/lb. The lubricant used is a synthetic paraffinic oil without additives. Fig. 63 gives a typical comparison between the spinning friction theory and the experimental friction. With the exception of a very close ball and groove conformity, the agreement is seen to be very close. This technique is used in computer program in Appendix VIII.

## 6. STRESS

When two elastic bodies are in contact with each other under a heavy load, the stresses near the contact region can often reach unusually high values due to large localized pressures in the contact. Materials subjected to these repeated high stresses will gradually develop a crack and eventually chip away from the contacting body. This phenomenon is commonly known as surface pitting which is one of the major failure modes in rolling element bearings. In order to predict the conditions under which pitting occurs, it is necessary first to make accurate calculations of the stress field in the contact. This section deals with the analysis and calculation of these stresses in the contacting bodies.

The first published classical work dealing with stresses in elastic contacts is by H. Hertz of Germany in 1881 (138). He obtained the pressure distribution

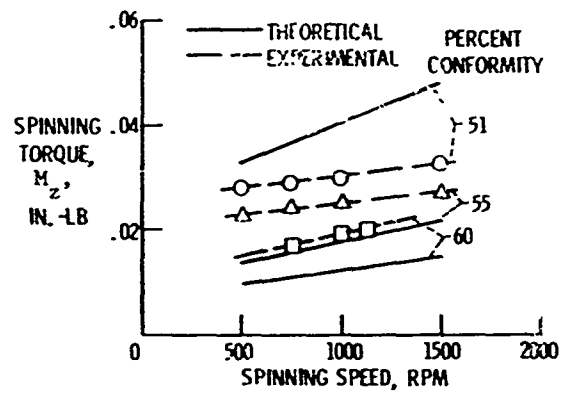


Fig. 63 Spinning Torque as a Function of Spinning Speed.  
(Courtesy of ASME, Paper No. 69-LubS-11).

in the contact for two elastic bodies having counterformal surface. When the surface geometries can be approximated by two paraboloids, the pressure distribution in the contact zone is found to be an ellipsoid. He also solved for the stresses in the body in terms of a potential function. Since Hertz, numerous works have appeared dealing with analytical solutions of stress in the contact. A detailed account of these solutions can be found in a paper by Smith and Liu (139) and in a review by Lubkin (140).

However, these theories are all based on the assumption that the normal or tangential loads in the contact are symmetrical with respect to the center of the contact. This assumption is valid for a dry contact, but it is invalid for a lubricated contact. Recent elastohydrodynamic theories (Refs. 93 and 141) discussed earlier have shown that the pressure distribution including the effects of a lubricant becomes greatly deviated from Hertzian - particularly in the exit of the contact where drastic changes of the pressure profile are found. Moreover, high local frictional forces are shown to exist if a small sliding velocity is introduced in the contact. Consequently, there is a need of a method to calculate stresses in a solid considering an arbitrarily distributed normal and tangential load. We first review the calculation of contact stresses without traction.

#### a. Calculation of Contact Stresses Without Traction

While it is true that all of the principal stress components are compressive when surface traction is not present and have their largest values at the contact surface, the combination of these components results in an induced shear. Because the yielding of steel depends on shearing stress, it is necessary to determine the point within the body at which the maximum shear stress occurs. Thomas and Hoersch (142) give a very complete discussion of the solution to this problem.

##### (1) Geometric Definitions

Figure 64a will aid the reader in visualizing the geometry of the contact between rolling element and race. Two paraboloids made of elastic material are pressed together. The two bodies are initially in contact at a single point. The minimum and maximum radii of curvature of the surface of the upper paraboloid at the point of contact are  $R_{x2}$  and  $R_{y2}$  respectively. These are called the principal radii of curvature of the surface. For the lower toroid  $R_{x1}$  and  $R_{y1}$  are the minimum and maximum radii of curvature, respectively, of the surface at the point of contact. The plane sections in which  $R_{x1}$  and  $R_{y1}$  lie are perpendicular to each other. The signs of  $R_{x1}$  and  $R_{y1}$  are as follows. If the center of curvature is inside the body, the radius is positive; if outside the body, it is negative.

The load  $P$  lies along the axis which passes through the centers of the disks and through the point of contact and is perpendicular to a plane which is tangent to both disks at the point of contact. The effect of the load  $P$  is to

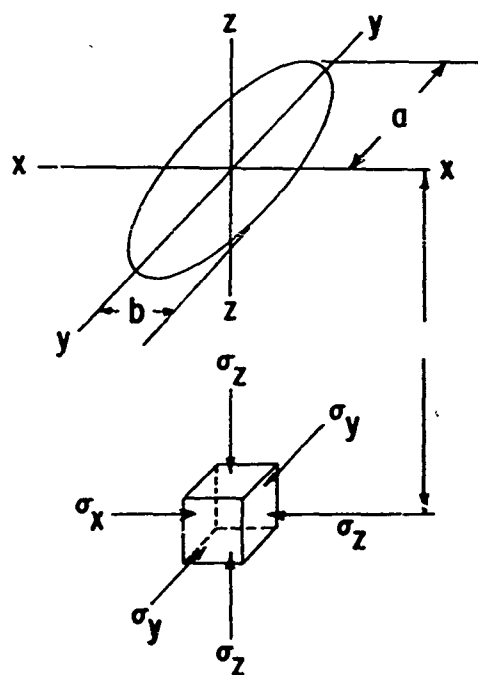
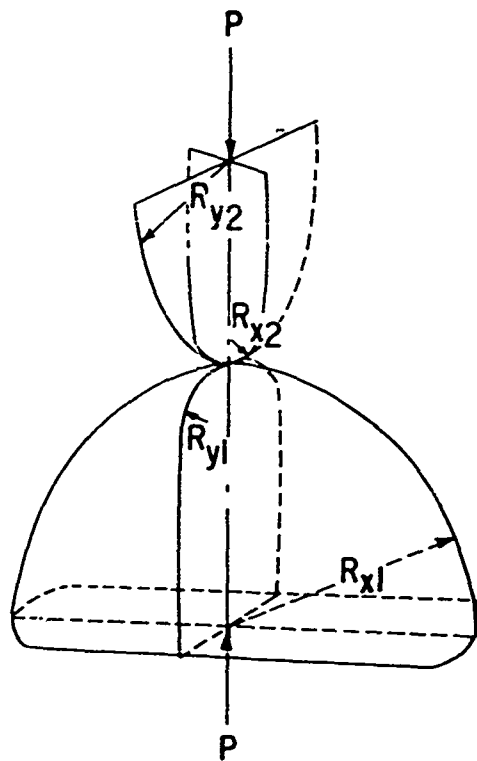


Fig. 64 Point Contact and Contact Ellipse.

cause the surface of the disks to be deformed elastically over a region surrounding the initial point of contact, thereby bringing the two bodies into contact over a small area as shown in Fig. 64b.

(2) Theory for Line Contact (See Figure 65)

For two bodies in line contact, the solution of the contact stress problem is relatively simple. The area of contact when a load of  $w$  lb per unit length is applied is a long narrow rectangle of width  $2b$  in the  $x$  direction and length  $l$  in the  $y$  direction. The stresses at points on the  $z$  axis below the surface are given by:

$$\sigma_x = - \left[ \frac{(\sqrt{1 + (z/b)^2} - z/b)^2}{\sqrt{1 + (z/b)^2}} \right] \frac{b}{\Delta} \quad (28)$$

$$\sigma_y = - 2\nu \left[ \sqrt{1 + (z/b)^2} - (z/b) \right] \frac{b}{\Delta} \quad (29)$$

$$\sigma_z = - \left[ \frac{1}{\sqrt{1 + (z/b)^2}} \right] \frac{b}{\Delta} \quad (30)$$

where

$$b = \sqrt{2w\Delta/\pi} \quad (31)$$

$$\Delta = \frac{1}{(1/2R_{x1} + 1/2R_{x2})} \left( \frac{1 - \nu_1^2}{E_1} + \frac{1 - \nu_2^2}{E_2} \right) = \frac{R'_x}{4E'} \quad (32)$$

The value of stresses at the surface are obtained by setting  $z = 0$ .

(a) Maximum Principal Stresses

The principal stresses  $\sigma_1$ ,  $\sigma_2$ , and  $\sigma_3$  have their maximum numerical value when  $z/b = 0$ , at the contact surface. These stresses are given by

$$\sigma_1 = - b/\Delta \quad \sigma_2 = 2\nu (b/\Delta) \quad \sigma_3 = - b/\Delta \quad (33)$$

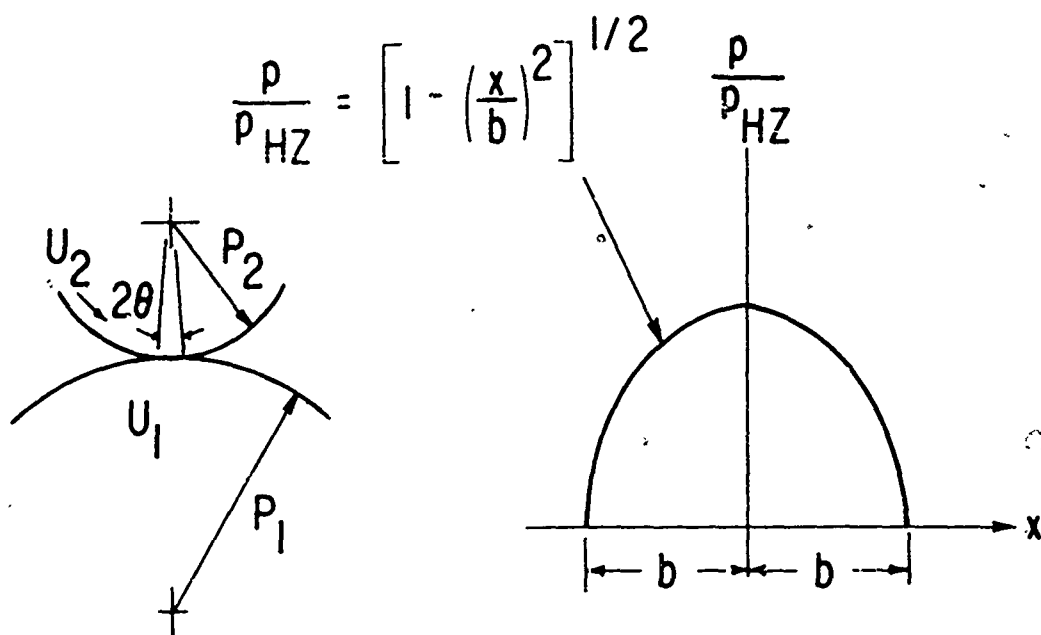


Fig. 65 Line Contact Geometry.

(b) Maximum Shear Stress

The local maximum shearing stress at any point on the z axis is  $\tau = 1/2 (\sigma_1 - \sigma_3)$ . If the expressions for  $\sigma_1$  and  $\sigma_3$  are substituted in the equation for  $\tau$  and the first derivative taken, the maximum value of local maximum shearing stress is found to occur at  $z/b = 0.7861$ . At this point the principal stresses have the values

$$\sigma_1 = -0.1856 \frac{b}{\Delta} \quad (34)$$

$$\sigma_2 = -0.7861 \frac{b}{\Delta} \quad (35)$$

$$\sigma_3 = 0.9718 \nu_1 \frac{b}{\Delta} \quad (36)$$

and

$$\tau_{\max} = 0.3 \frac{b}{\Delta} \quad (37)$$

Fig. 66 is a plot of the magnitude of  $\sigma_x$ ,  $\sigma_y$ ,  $\sigma_z$  and  $\tau$  on and below the surface on the z axis. The value of  $\sigma_{\max}$  refers to the maximum contact stress and is equal to the maximum Hertzian pressure.

(c) Maximum Octahedral Stress

The maximum octahedral shearing stress occurs at the same point as the maximum shear and is given by

$$\tau_{\text{oct}} = 0.27 \frac{b}{\Delta} \quad (38)$$

(d) Effect of Crowning

In order to eliminate the high end stresses that occur with plain rollers, it is possible to crown the roller. This crowning of a roller also provides protection against the effects of misalignment.

The amount of crowning is made just large enough so that the area of contact does not extend beyond the edge of the race. It is shown in Ref. (142) that if the ratio

$$\frac{\bar{B}}{\bar{A}} = \frac{1/R_{x1} + 1/R_{x2}}{1/R'_{y1} + 1/R'_{y2}} > 50 \quad (39)$$

then the maximum stresses can be calculated as for the line contact previously discussed. This means that when the above in-

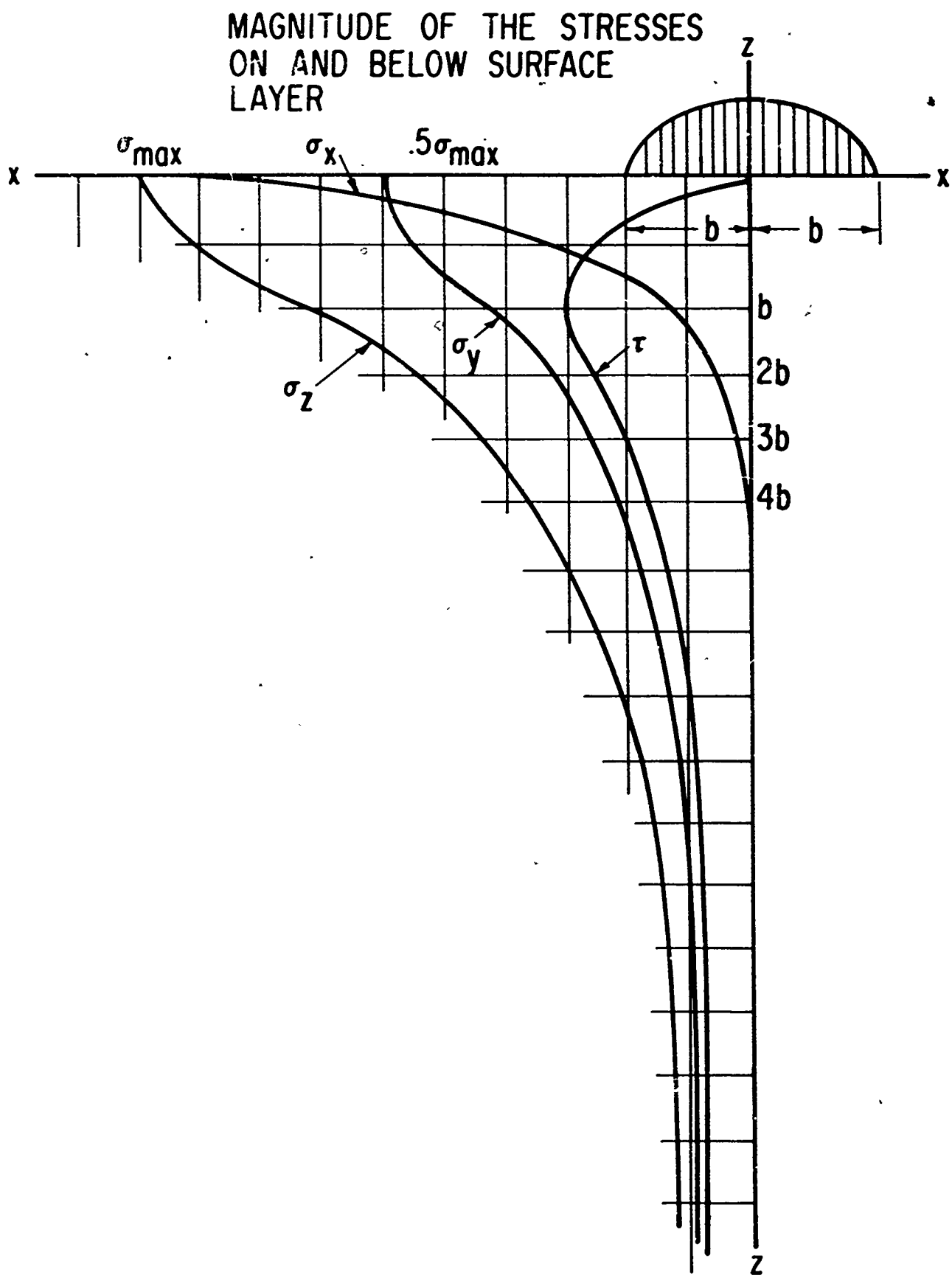


Fig. 66 Magnitude of the Stresses on and Below Surface Layer.



equality is satisfied, the area of contact between the rolling element and race is very nearly a long narrow rectangle. For many cases, this situation holds.

### (3) Theory for Elliptical Contact

If the contacting bodies have curvature in both the x and y directions, then the contact zone will be elliptical in shape. In this case, calculation of the contact stresses is not as simple as for line contact. Solutions for the stresses are given in terms of elliptic integrals which have to be solved with tables (142).

It is shown in Ref. (143) that dimensions of the contact ellipse for a given total load, P, geometry and material properties is given by

$$a = m \sqrt[3]{\frac{3\pi}{4} \frac{P}{(\bar{A} + \bar{B})E'}} \quad (40)$$

$$b = n \sqrt[3]{\frac{3\pi}{4} \frac{P}{(\bar{A} + \bar{B})E'}} \quad (41)$$

where m and n are numerical functions of the variable  $\frac{\bar{A} - \bar{B}}{\bar{A} + \bar{B}}$  tabulated in Ref. (143), and where;

$$\begin{aligned} \bar{B} &= \frac{1}{2R_{x1}} + \frac{1}{2R_{x2}} \quad 1/in \\ \bar{A} &= \frac{1}{2R_{y1}} + \frac{1}{2R_{y2}} \quad 1/in \end{aligned} \quad (42)$$

Eq. 40 and 41 are used to calculate the dimensions of the contact ellipse in the computer program described in Section III.

### (4) Controlling Stress for Fatigue

It has been recognized that subsurface fatigue cracks can be initiated when one of the following two stresses becomes excessive. The first influencing stress is the maximum shear stress, which is half of the differences of the maximum and minimum principal stress. As mentioned earlier, the absolute maximum shear stress occurs at  $x = 0$  and  $z = 0.7861 \times b$ , and has a value equal to 0.3 times the maximum Hertzian pressure. The variation of the maximum stress is from 0 to  $0.3 p_{HZ}$  as the rolling element moves through the contact region.

The second influencing stress is known as the alternating shear stress, which is the shear stress in the orthogonal x-z axis. Figure 67 shows how this shear stress varies with x at the depth  $z_0$  where the greatest value is found. When the contact point rolls along the race, the orthogonal shear stress at the depth  $z_0$  alternating between  $\pm \tau_0$ . As can be seen by comparing Figures 66 and 67, the maximum alternating orthogonal shear stress is larger than the maximum shear stress on

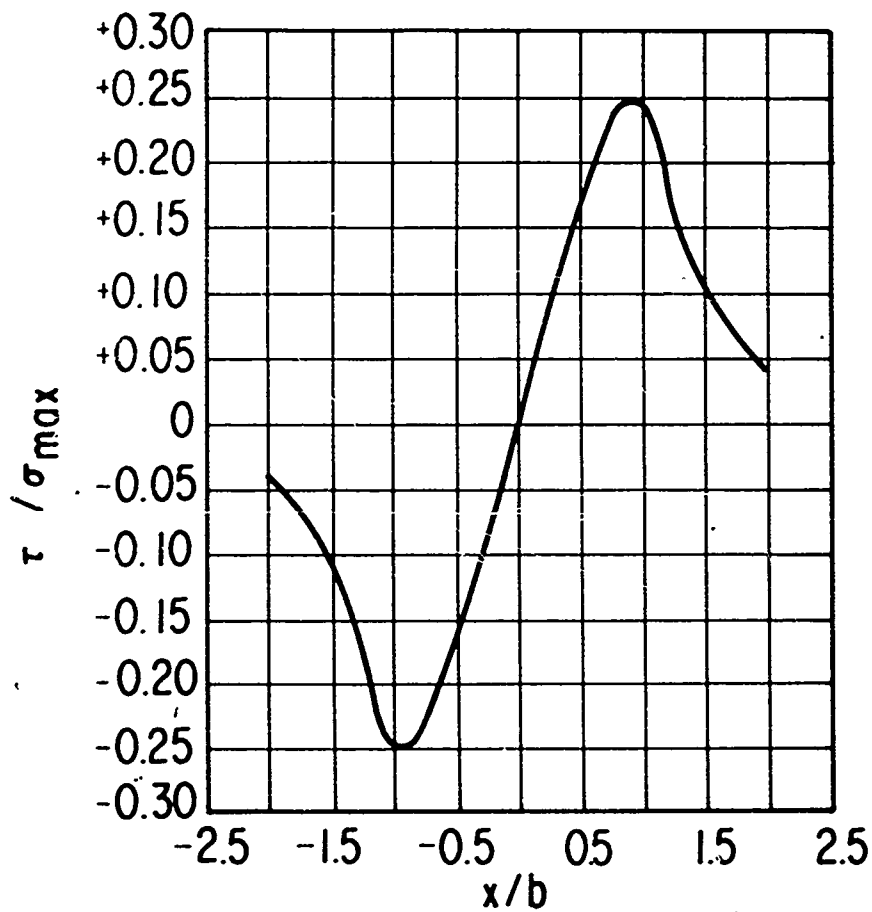


Fig. 67 Orthogonal Shear Stress vs. x-Coordinate, at the Depth of Maximum Alternating Shear Stress.

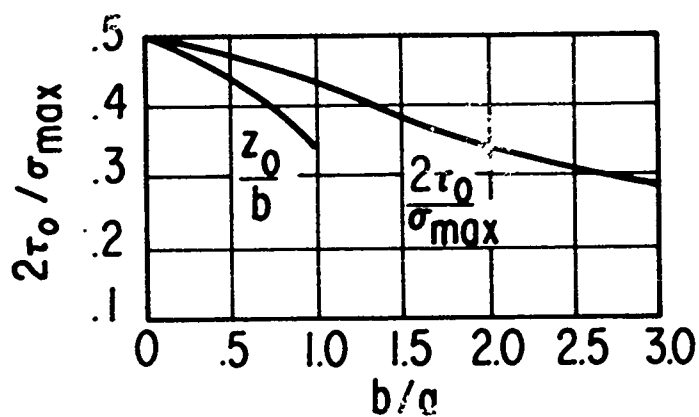


Fig. 68 Range of Orthogonal Shear Stress as a Function of the Ellipticity Ratio  $b/a$ .

the  $z$  axis.

In general, the magnitude of the maximum alternating shear stress depends upon the geometry of the contact zone as illustrated in Figures 68 and 69. It is seen that for the ellipticity ratio ( $b/a$ ) less than 1, which is usually the case for all rolling and sliding contacts, the range of maximum alternating orthogonal shear stress is always greater than the maximum shear stress. Only for the case where  $b/a$  is greater than 2.75, the maximum shear stress overtakes the maximum alternating shear stress. However, for most bearing applications, the ellipticity ratio of this high would not be encountered. Therefore, the maximum alternating orthogonal shear stress is the controlling factor.

This conclusion is borne out by the work of Greenert (146) who obtained excellent correlation of the orthogonal shear stress range with the fatigue life of AISI 52100 rollers.

b. Calculation of Contact Stresses with Traction

The discussion in Section II-6-a applies for the calculation of the stress field due to a normal pressure distribution without a traction.

The stress field for an elliptical normal pressure distribution together with a frictional force governed by the law of Coulomb friction has been investigated in detail by Smith and Liu and also by Poritsky (Refs. 129 and 147).

If a lubricant is introduced in the contact, the normal pressure and the frictional force will be influenced by the hydrodynamic action and the temperature variation of the fluid. The previous discussions have shown that interactions of the elasticity, hydrodynamics and the heat transfer show that the typical elastohydrodynamic pressure distribution deviates considerably from Hertzian and contains abrupt changes as shown in Fig. 13.

To calculate the stress components in the solids for an arbitrarily distributed surface traction, one must resort to numerical solution based on the elasticity solution for an elastic half-space. The development of a numerical method to determine the three principal stresses, the maximum shear stress as well as the octahedral stress for any given point in the solid constitutes the main concern of this section.

If the contacting angle,  $\theta$  (see Fig. 65) is less than 5 degrees, the stress and deformation in the solid can be accurately calculated by neglecting the curvature of the boundary. Using the elasticity solution for a unit load on the boundary of an elastic half-space one obtains:

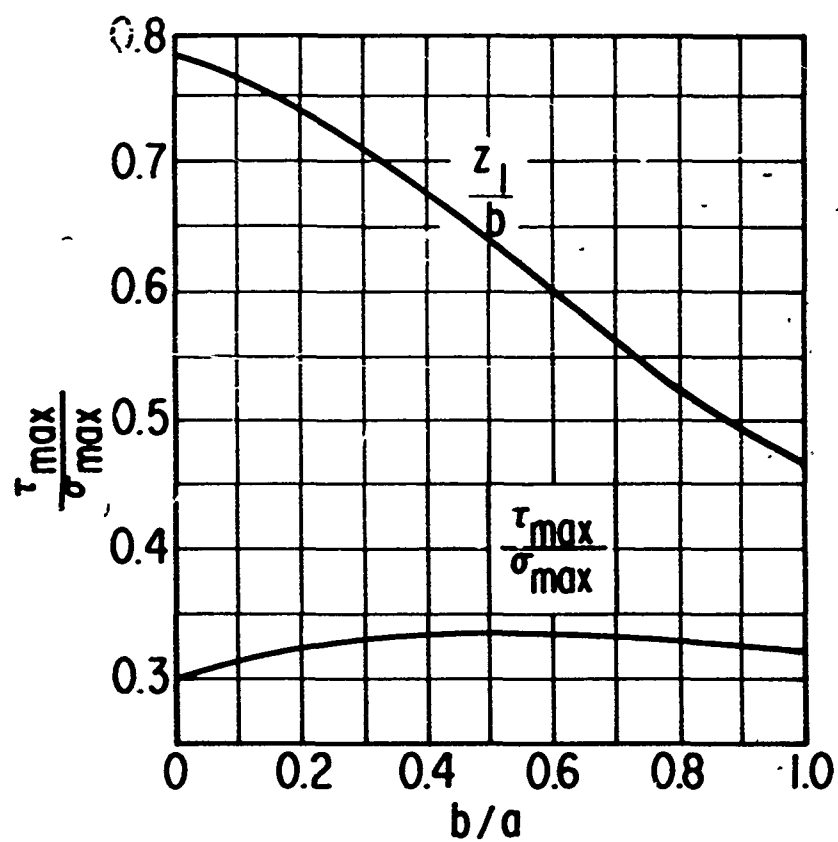


Fig. 69 Ratio of Shear Stress to Maximum Contact Stress vs. Ellipticity Ratio.

$$\begin{aligned}
\delta \bar{\sigma}_{xn}(\bar{x}, \bar{y}, \bar{\xi}) &= \delta \bar{\tau}_{xyt}(\bar{x}, \bar{y}, \bar{\xi}) = -\frac{2}{\pi} \left[ \frac{(\bar{x}-\bar{\xi})^2 \bar{y}}{R^4} \right], \\
\delta \bar{\sigma}_{yn}(\bar{x}, \bar{y}, \bar{\xi}) &= -\frac{2}{\pi} \frac{\bar{y}^3}{R^4}, \\
\delta \bar{\tau}_{xyn}(\bar{x}, \bar{y}, \bar{\xi}) &= \delta \bar{\sigma}_{yxt}(\bar{x}, \bar{y}, \bar{\xi}) = -\frac{2}{\pi} \left[ \frac{(\bar{x}-\bar{\xi}) \bar{y}^2}{R^4} \right], \\
\delta \bar{\sigma}_{xt}(\bar{x}, \bar{y}, \bar{\xi}) &= -\frac{2}{\pi} \left[ \frac{(\bar{x}-\bar{\xi})^3}{R^4} \right],
\end{aligned} \tag{43}$$

where

$\bar{\sigma}_{xn}, \bar{\sigma}_{yn}, \bar{\tau}_{xyn}$  = dimensionless normal and shear stress components due to a unit normal load at  $\bar{x} = \bar{\xi}$ .

$\bar{\sigma}_{xt}, \bar{\sigma}_{yt}, \bar{\tau}_{xyt}$  = dimensionless normal and shear stress components due to a unit tangential load at  $\bar{x} = \bar{\xi}$ .

$$\bar{x} = x/x^*$$

$$\bar{y} = y/x^*$$

$$\bar{\xi} = \xi/x^*$$

$b$  = half of Hertzian width

$-w$  = total normal load per unit axial length

$x^*$  = the exit coordinate

$$R = \left[ (\bar{x}-\bar{\xi})^2 + \bar{y}^2 \right]^{1/2}$$

$$\bar{\sigma}_x = \sigma_x b/w$$

Accordingly, for prescribed normal and tangential loads,  $p(\xi)$  and  $\tau_x(\xi)$ , the normalized stress components become -

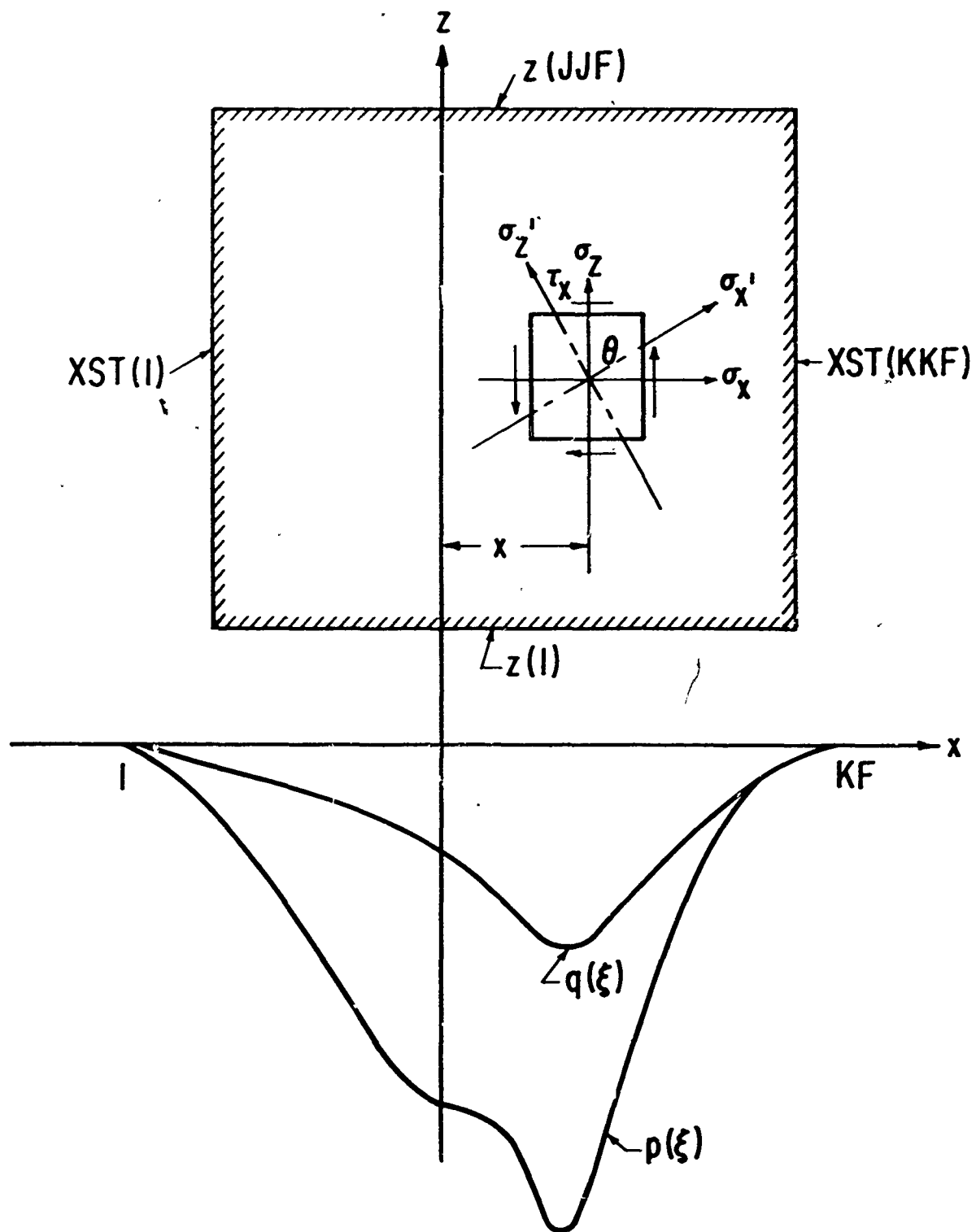


Fig. 70 A Contact Zone with Normal and Tangential Stress Distribution.

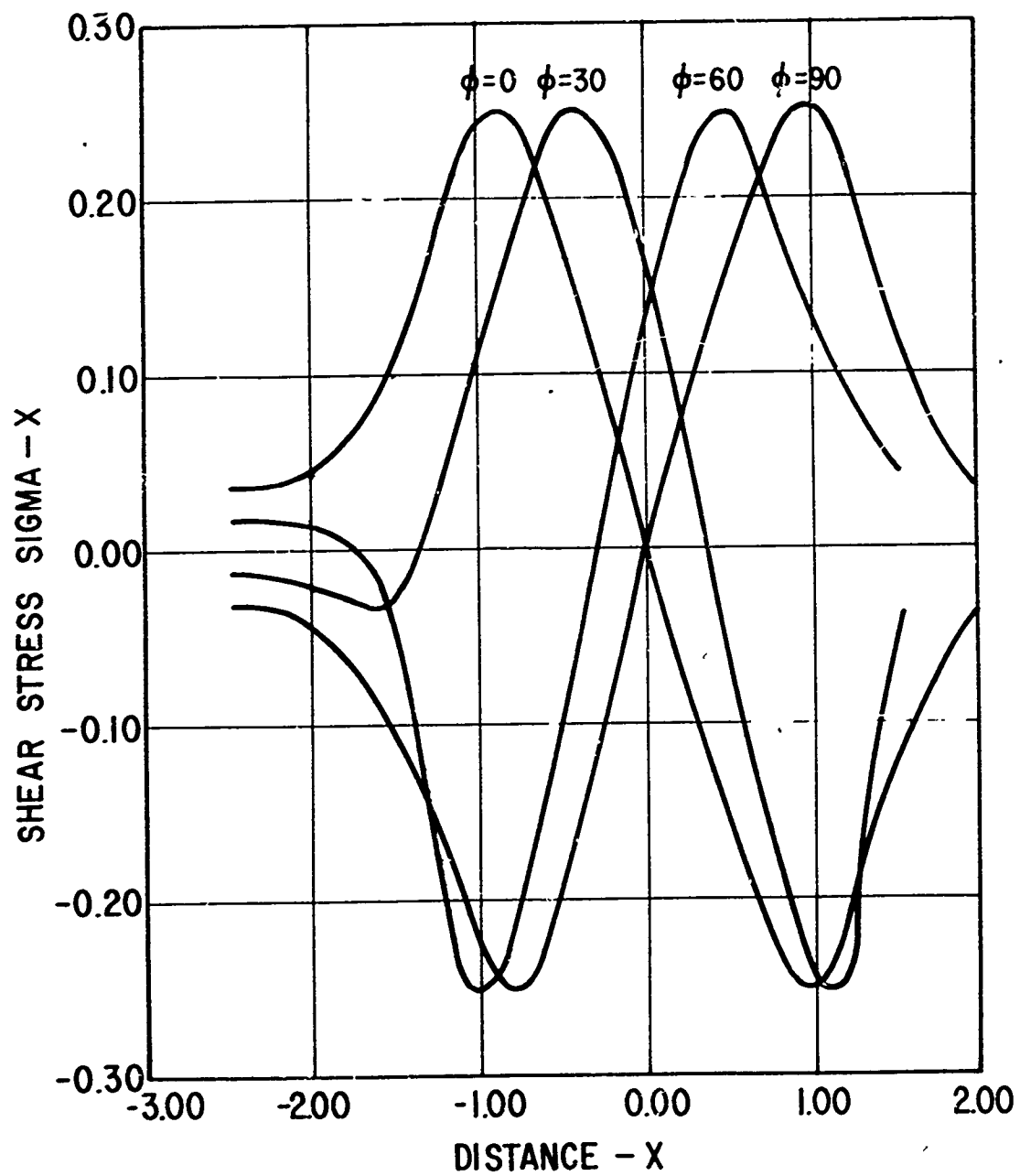


Fig. 71 Variation of Shear Stress from Computer Calculations.

$$\begin{aligned}
\bar{\sigma}_x &= \int_{-\infty}^1 \left[ p(\bar{\xi}) \delta\bar{\sigma}_{xn} + \bar{\tau}_x(\bar{\xi}) \delta\bar{\sigma}_{xt} \right] d\bar{\xi} \\
\bar{\sigma}_y &= \int_{-\infty}^1 \left[ p(\bar{\xi}) \delta\bar{\sigma}_{yn} + \bar{\tau}_x(\bar{\xi}) \delta\bar{\sigma}_{yt} \right] d\bar{\xi} \\
\bar{\tau}_{xy} &= \int_{-\infty}^1 \left[ p(\bar{\xi}) \delta\bar{\sigma}_{xyn} + \bar{\tau}_x(\bar{\xi}) \delta\bar{\tau}_{xyt} \right] d\bar{\xi}
\end{aligned} \tag{44}$$

where

$$\begin{aligned}
p(\bar{\xi}) &= p^{(x)} / \left(\frac{w}{b}\right) \\
\bar{\tau}_x(\bar{\xi}) &= \tau_x^{(x)} / \left(\frac{w}{b}\right) = \frac{\mu_m(U_2 - U_1)}{h(\bar{\xi})} \times \left(\frac{b}{w}\right)
\end{aligned}$$

The integrands in Eq. 44 contain integrable singularities for  $\bar{\xi} = 0$ ,  $\bar{y} = 0$ . For  $y > 0$ , all integrands are free from any singularity, but as  $\bar{\xi}$  approaches zero, these kernel function ( $\delta\bar{\sigma}_{xn}$ , etc), changes very abruptly and exhibit near singular behavior. A conventional integration routine would fail to yield an accurate solution; therefore, special quadratures of the Filon type were developed and the detailed derivations of these quadratures are included in Ref. 148. Using these quadratures, the integration of the stresses can be accomplished by using a computer. A listing of the computer program for accomplishing this is presented in Appendix VII.

To illustrate the use of the program, a sample case was run with no tangential load and a normal loading given by

$$\bar{p} = 1 - \bar{x}^2 \tag{45}$$

This corresponds to simple line contact with no traction. The shearing stresses were computed at  $\bar{z} = 0.25$ , for four different inclination angles ( $\theta = 0, 30^\circ, 60^\circ$ , and  $90^\circ$ ). The  $\theta = 0$  case corresponds to the curve of Fig. 67 and a comparison between them shows that the results are very close.

A stress calculation with tangential load is given in Example 1 on Page 203. In the example the elastohydrodynamic performance computer program incorporating the above-mentioned technique is used.

## 7. SURFACE TOPOGRAPHY

As long as the elastohydrodynamic film thickness exceeds the composite surface roughness of the two surfaces in the contact zone, consideration of the surface topography is not necessary. However, as the elastohydrodynamic film thickness becomes smaller, and the two surfaces approach one another, they



begin to touch at the tips of the higher asperities. The study of the average distance through which the one surface moves into the other surface and the total real area of contact resulting from this movement provides important information about the friction and wear which occurs in the contact zone.

a. The Area of Contact Between Rough Surfaces

The theories of friction and wear are based on the fact that real surfaces are rough so that the area of contact is limited to discrete spots on the two surfaces. It has long been agreed that the most convenient way of explaining Amonton's laws -- that the friction is proportional to the load and independent of the apparent area -- is to take the real area of contact to be proportional to the load.

Many researchers have attempted to explain the proportionality between area of contact and load. If the real area of contact between surfaces is determined by ideal plastic flow of the asperities, then proportionality between the area of contact and the load follows immediately.

If the deformation mode is elastic, or elastic-plastic then it is not possible to explain the proportionality between load and real area of contact. An alternative approach has been offered by Greenwood (149), who showed that the proportionality between load and area of contact can be explained by considering the statistical distribution of heights of the surface asperities. He did this by considering the contact between a rough surface and a smoother one, both nominally flat. The rough surface is represented by taking a large number of asperities of prescribed shape and scattering them over a reference plane. The heights of the asperities will follow some statistical distribution, such as the normal (Gaussian) distribution; the probability of an asperity having a peak height  $z$  above a reference plane is  $\phi(z)$ . The number of asperities with this height is  $N\phi(z)$ . Consider now the approach of the smoother surface, (Fig. 72). When the separation between the smooth surface and the reference plane is  $h$ , there will be contact at all asperities with heights  $z$  greater than  $h$ , there will be deformation of the asperity (and the plane) to accommodate the excess height  $(z-h)$ . Thus, we need the relations governing the deformation of a single contact, in terms of the extra height absorbed in the deformation; that is, the local compliance. This will depend on both the asperity shape and the mode of deformation; or more generally,

$$P = f(\zeta) \quad A_c = g(\zeta) \quad (46)$$

To find the total load and the total area, we substitute the excess height  $(z-h_0)$  for  $\zeta$  and sum over all load-bearing asperities which gives,

$$P = \int_d^{\infty} f(z-h_0) N\phi(z) dz \quad A_c = \int_d^{\infty} g(z-h_0) N\phi(z) dz \quad (47)$$

Thus, when we know (a) the distribution of asperity heights; (b) the deformation law for a single asperity; we can immediately derive the total load and the total area in terms of the separation and from it the load-area relation, itself.

The foregoing formal presentation due to Greenwood (149) includes a large number of different theories. For example, various workers have taken the distribution of heights to be uniform, linear, exponential or Gaussian, the asperities have been taken as spherical caps, wedges, cones, or rods. The usual deformation modes considered are elastic, elastic-plastic, and plastic. Recent advances in surface analysis enable height distributions to be measured, and it is now clear, Tallian, et al (150), that the distribution of many surfaces are more or less Gaussian.

Using a Gaussian surface roughness distribution given by

$$\phi(z) = \frac{1}{\sigma \sqrt{2\pi}} \exp(-z^2/2\sigma^2) \quad (48)$$

Greenwood and Williamson (151) showed that the real area of contact for the elastic deformation was proportional to the load. Greenwood (149) extended the analysis to show that this was a consequence of the statistics of the surface and not the particular mode of deformation.

The foregoing applies to a rough surface and a flat. If both surfaces are rough, the probability of the sum of two heights exceeding the separation must be considered. This however, is exactly equivalent to a different distribution of a single variable. For example, if the two heights are normally distributed with standard deviation  $\sigma$ , their sum follows a normal distribution with standard deviation  $\sigma$ . Thus, the problem of two rough surfaces is equivalent to a rough surface and a smooth surface.

In summary, it has been shown that consideration of the statistical distribution of the heights of surfaces asperities indicates that the average size of the microcontact is almost constant, independent of load. This observation leads to the conclusion that the real origin of the laws of friction is in the statistics of surface roughness and not in a particular mode of deformation.

#### b. The Shape of Solid Surfaces

The use of the Gaussian distribution in the theoretical study of rough surfaces is convenient because it greatly simplifies the

mathematics. It is important to the realism of the theoretical model identify the characteristics of typical surfaces and to determine which of these can accurately be represented by a Gaussian distribution. Williamson et al (152) have divided surface preparation processes into two classes, cumulative and extreme value.

#### (1) Cumulative Processes

A cumulative process is one in which the final shape of the surface is the result of a very large number of events, such as bead blasting, grinding, peening. If the occurrence of these events is random it follows immediately from the Central Limit Theorem of statistics that the topography of the surface will tend toward a Gaussian height distribution.

Some cumulative preparation techniques, however, do not occur randomly. The occurrence of the event may, for example, depend on the microstructure of the material, as when a surface is etched. In general, surfaces of this type are non-Gaussian.

#### (2) Extreme Value Processes

Extreme value processes are ones for which the final surface reflects only the extreme of the events which occurred at each point. Extreme value processes nearly always involve the removal of material such as in grinding or peening. Turning, shaping, and milling are processes in which the events are neither cumulative nor random and create non-Gaussian surfaces. Grinding on the other hand, can yield a height distribution which is approximately Gaussian. In grinding, the grit is located with a Gaussian height distribution, and creates a topography which is the result of many interacting Gaussian probabilities. Its height distribution appears as a gentle curve on probability papers. Fig. 73 which is a distribution presented by Williamson et al (144) supports this argument. For most work there is usually little error in treating ground surfaces as Gaussian. This is fortunate for lubrication engineers, as most rolling element bearing surfaces are finished by grinding.

#### (3) Pure Topographies and Transitional Topographies

Williamson, et al (152) further classified topographies as pure and transitional. A pure topography is one in which the entire surface reflects the action of only one process. The surface of a new bearing prior to running in is approximately a pure topography prepared by grinding.

As the bearing is run, however, its surfaces wear. Fig. 74 shows the height distributions which would be typical as the bearing is run in. Initially the height distribution is Gaussian. As wearing progresses, the transition percentile between the worn topography and the original topography moves steadily lower until the original texture has been almost replaced. This Williamson

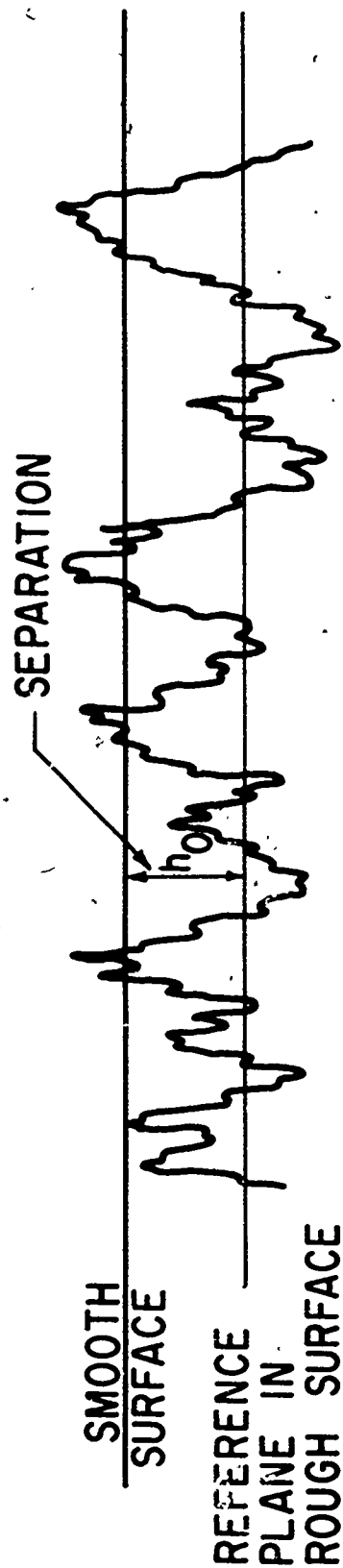


Fig. 72 Contact of Rough Surfaces.

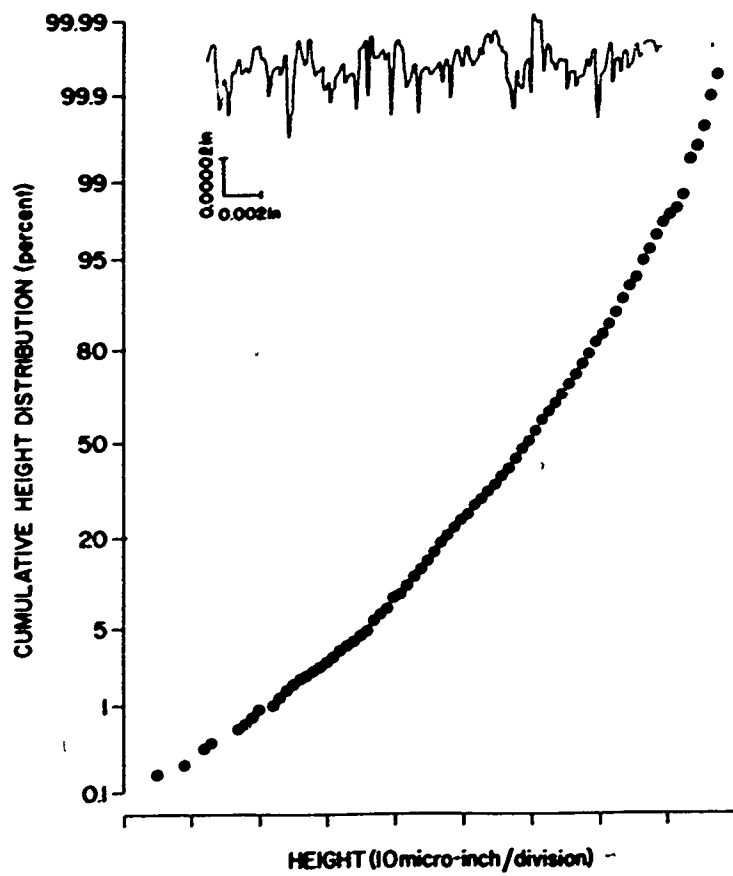


Fig. 73 Cumulative Height Distribution and Typical Profile of a Ground Surface. (Courtesy of Surface Mechanics, ASME).

et al (152) termed a transitional topography.

c. Real Area of Contact

For a Gaussian profile it is a simple matter to find the area of surface above any given height. This figure gives the contact area when such a surface is used in a bearing and wears away from the top as in Fig. 74. It can also be used for any contact, elastic or plastic, provided it is assumed that the displaced asperities move vertically down and do not spread horizontally. With this assumption the relation between the real area of contact and the separation for two Gaussian surfaces is simply

$$A_c = A \int_{h_0}^{\infty} \frac{1}{\sigma\sqrt{2\pi}} e^{-z^2/2\sigma^2} dz \quad (49)$$

$$A_c = A \phi(h_0) \quad (50)$$

This is admittedly a very simple model of the ball-race contact in a rolling element bearing. A subroutine for evaluating Equation (49) is described in Appendix III. More work is needed to develop a more realistic method for prediction of the real area contact for an elastic contact including relative motion between the contacting surfaces.

## 8. EFFECT OF ELASTOHYDRODYNAMICS ON BEARING DYNAMICS

The conventional methods of evaluating (215, 216) rolling element bearing performance do not consider the effect of elastohydrodynamic lubrication in determining the friction forces between the rolling elements and the raceways. As a result it has not always been possible to predict certain rolling element bearing phenomena such as skidding, gyroscopic slip, and certain other bearing instabilities, occurring primarily in high speed applications. Only very recently have analyses become available, which include elastohydrodynamics effects at the raceway.

a. Roller Bearing Dynamics

Because of their relative simplicity the first analyses of elastohydrodynamics effects in bearings were done for roller bearings. Dowson and Higginson (153) showed that for lightly loaded roller bearings, the presence of a lubricant film reduces the angular velocity of the roller about its own center below that expected in pure rolling. This observation suggests that considerable roller slip and some cage slip can be expected in high speed, lightly loaded roller bearings.

For highly loaded bearings, elastohydrodynamic analysis (Dowson and Higginson, 153) shows that the motion of the rolling elements is essentially epicyclic. Calculations show that forces can be trans-

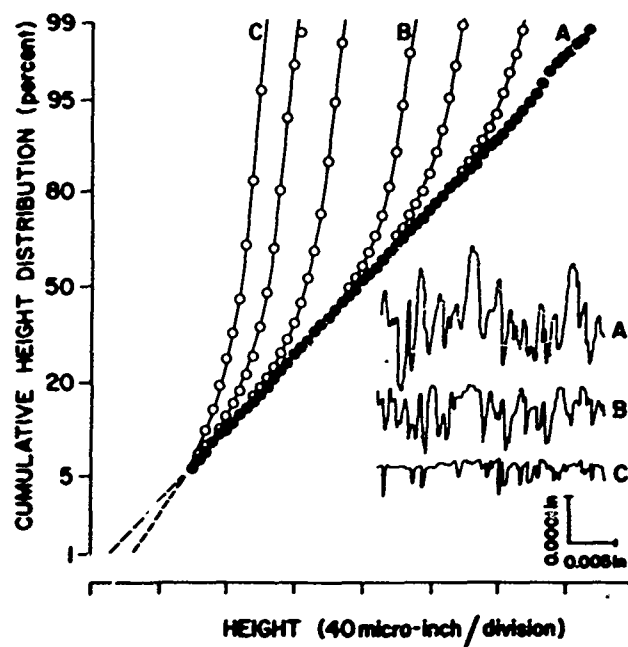


Fig. 74 Cumulative Height Distributions Showing the Effect of Wear on the Initially Gaussian Height Distribution of a Bead-Blasted Surface. (Courtesy of Surface Mechanics, ASME).

mitted through film lubricated contacts between rolling elements and races with negligible slip. Film thickness predictions confirm the presence of a hydrodynamic contact mechanism in rolling element bearings. No detectable cage or rolling element slip can therefore be expected in highly loaded bearings. The actual motion of a rolling element in a given bearing will be located between the limiting cases computed for rigid and elastic components.

Harris (154) using the Dowson and Higginson (153) formulation calculated the cage speed in a high speed cylindrical roller bearing. As illustrated in Fig. 75, he was able to predict quite reasonably the cage speed versus load for a high speed roller bearing. However, discrepancies between theory and experiment occurred at low loads corresponding to the intermediate lubrication regime of rigid bearing surfaces lubricated by an oil having pressure dependent fluid properties.

Boness (155) showed experimentally that oil supply can have a significant effect on cage and roller motion. Using the Dowson and Higginson model (153), Boness calculated the normal and tractive forces at the contact for restricted oil supply to the lubricated contact by varying the location of the point in the oil film where the pressure commences to build up. The theoretical results imply that reducing the oil supply to a minimum value required to maintain full hydrodynamic conditions reduces the cage slip by up to 75 percent of its fully flooded value.

#### b. Ball Bearing Dynamics

Because of the inherently more complicated dynamics of ball bearings, attempts at including the elastohydrodynamic effects in their analysis have been slower in development than for roller bearings. The reason for this is that for the thrust-loaded angular contact bearing, three equations of ball position in addition to equilibrium of forces and moments on the ball must be solved to determine the dynamic performance. Hence, in the most simple case, a system of 9 simultaneous, non-linear equations must be solved, 6 of these equations containing elastohydrodynamic dependent viscous friction forces. Before discussing attempted solutions to this problem, it is necessary to review one basic assumption of the commonly used ball bearing calculation procedures, namely raceway control.

##### (1) The Concept of Raceway Control

Fig. 76 shows a high speed angular contact bearing operating at different contact angles at the inner and outer races. The raceway control hypothesis assumes that the balls will roll relative to one of the raceways and roll and spin with respect to the other. In the example shown, because of the high speed condition, the highest load and therefore the largest contact ellipse exists at the outer race. Raceway control assumes that the ball



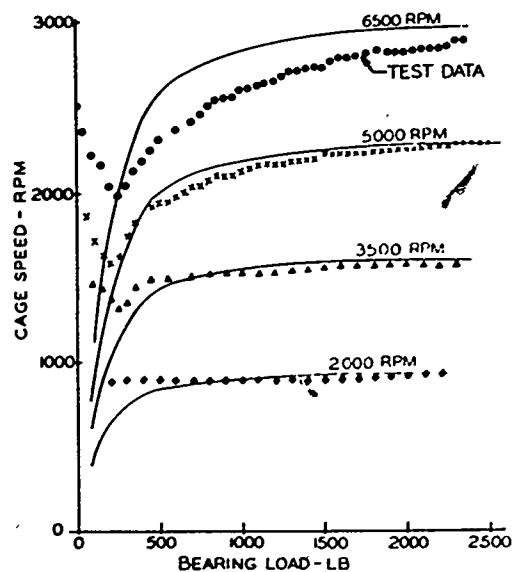


Fig. 75 Cage Speed vs. Load and Inner Ring Speed.  
(Courtesy of ASLE Trans., Vol. 9, 299,  
1966).

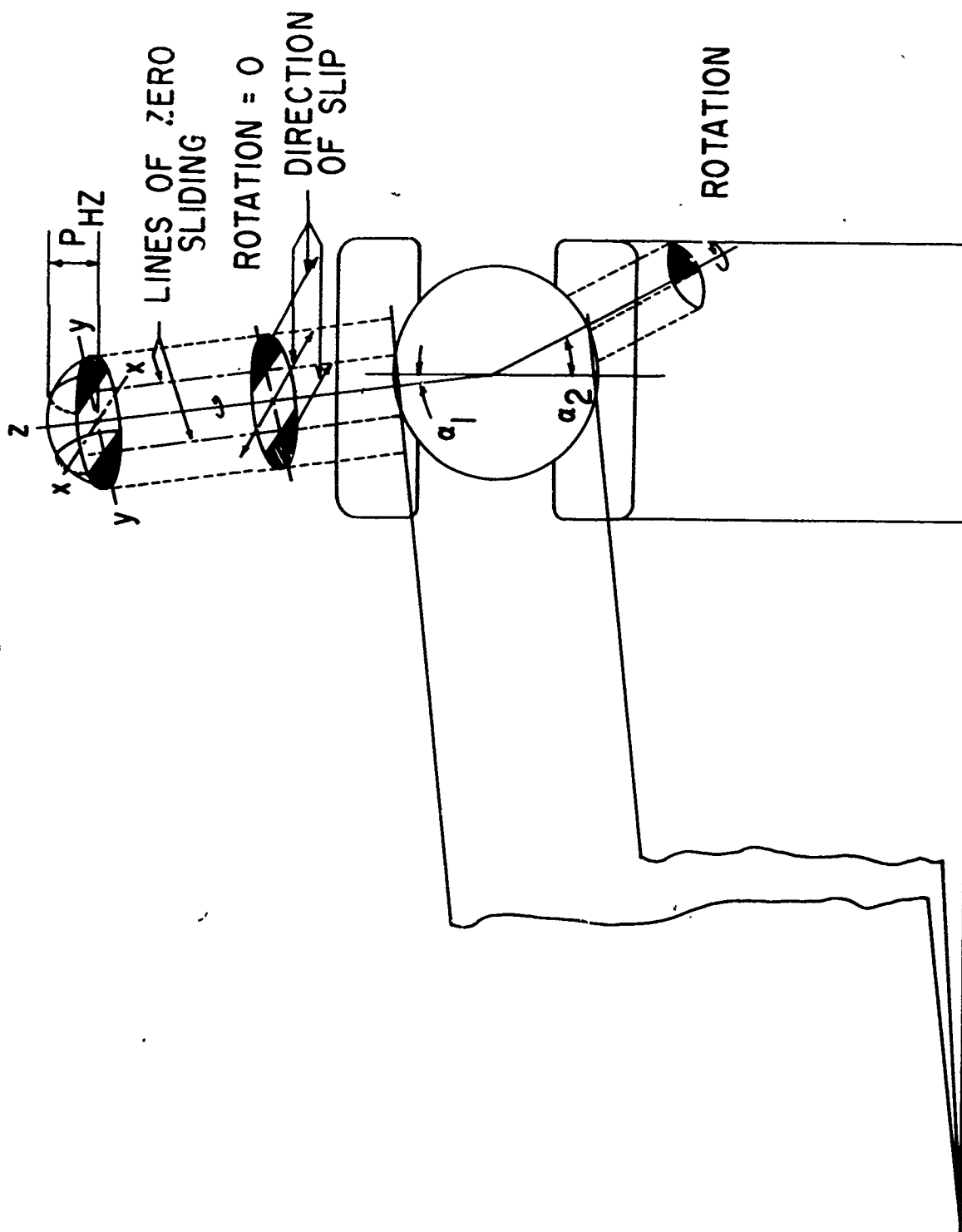


Fig. 76 Illustration of Raceway Control.

will roll at the outer contact and spin and roll at the inner race. The ball motion about its own axes and about the bearing axes is said to be controlled by the raceway at which rolling occurs, the outer raceway in this case. Fig. 77 shows the forces and moments acting on the ball under the influence of raceway control. Eq. 51 from Ref. 216 establishes the criterion for raceway control.

$$P_1 a_1 \bar{\epsilon}_1 (\alpha_2 - \alpha_1) > P_2 a_2 \bar{\epsilon}_2 \quad (51)$$

If the inequality is satisfied, then outer raceway control is assumed to exist. If it is not satisfied, inner raceway control is assumed to exist. If it is not satisfied, inner raceway control is assumed to occur.

The commonly used Jones analysis (215, 216) assumes further that the frictional resistance to the gyroscopic moment shown in Fig. 77 occurs at the controlling raceway only and that gyroscopic slippage does not occur. In a recent paper Harris (156) has refuted this assumption and argues that resistance to gyroscopic slippage motion occurs at both raceways.

## (2) Ball Bearing Solutions

Prediction of the threshold thrust loading below which skidding occurs in thrust loaded angular contact bearings has been impossible using the race control concept. This is illustrated in Fig. 79 where the cage to shaft speed ratio for a bearing tested by Shevschenko and Bolan (157) is shown in comparison to the theoretical values calculated on the basis of the raceway control hypothesis. Similar experimental results have been obtained by Poplawski and Mauriello (158).

Using the Archard (107) isothermal expression for the minimum film thickness in an elliptical contact, and assuming the Hertzian pressure distribution in the contact zone, Harris (155) calculated the cage to shaft speed ratio for the bearing of Ref. 157. The ball force equilibrium model used by Harris is shown in Fig. 78. The results show that the analysis utilizing the elastohydrodynamic lubricant friction forces more correctly predict the trend than the raceway control analytical method.

It should be noted that in Figs. 75 and 79, for both roller and ball bearings, as the thrust load diminishes the deviation between analytical and experimental data increases. Harris presented three possible reasons for

OUTER RACEWAY CONTROL  $\lambda = 0$   
 INNER RACEWAY CONTROL  $\lambda = 0$

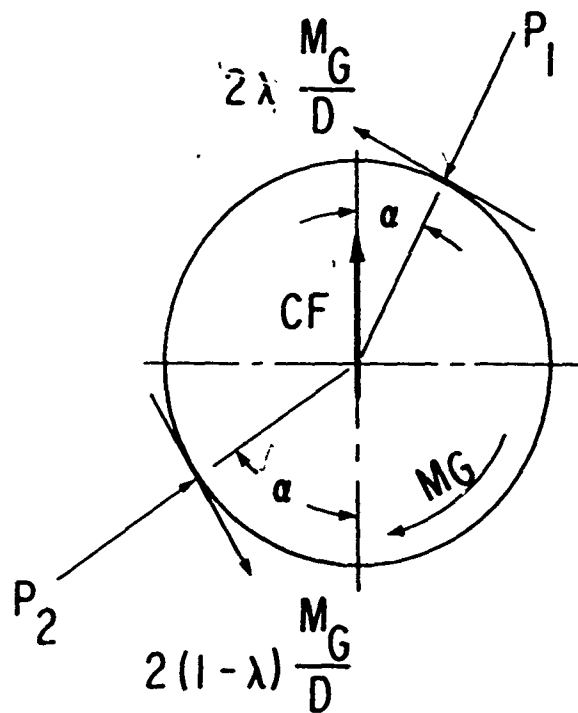


Fig. 77 Ball Loading Assuming Raceway Control of Ball Motion,

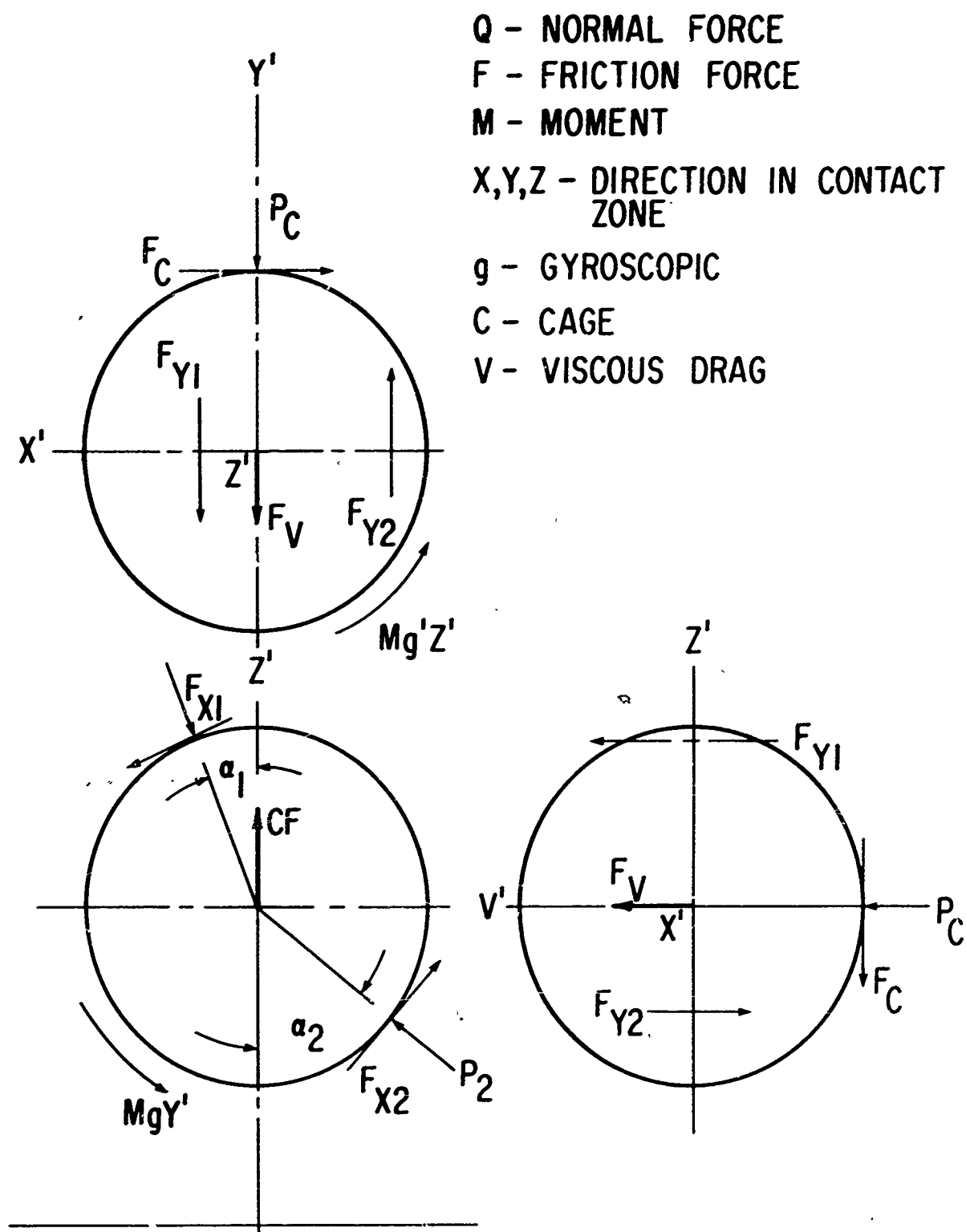


Fig. 78 Forces and Moments Acting on a Ball.

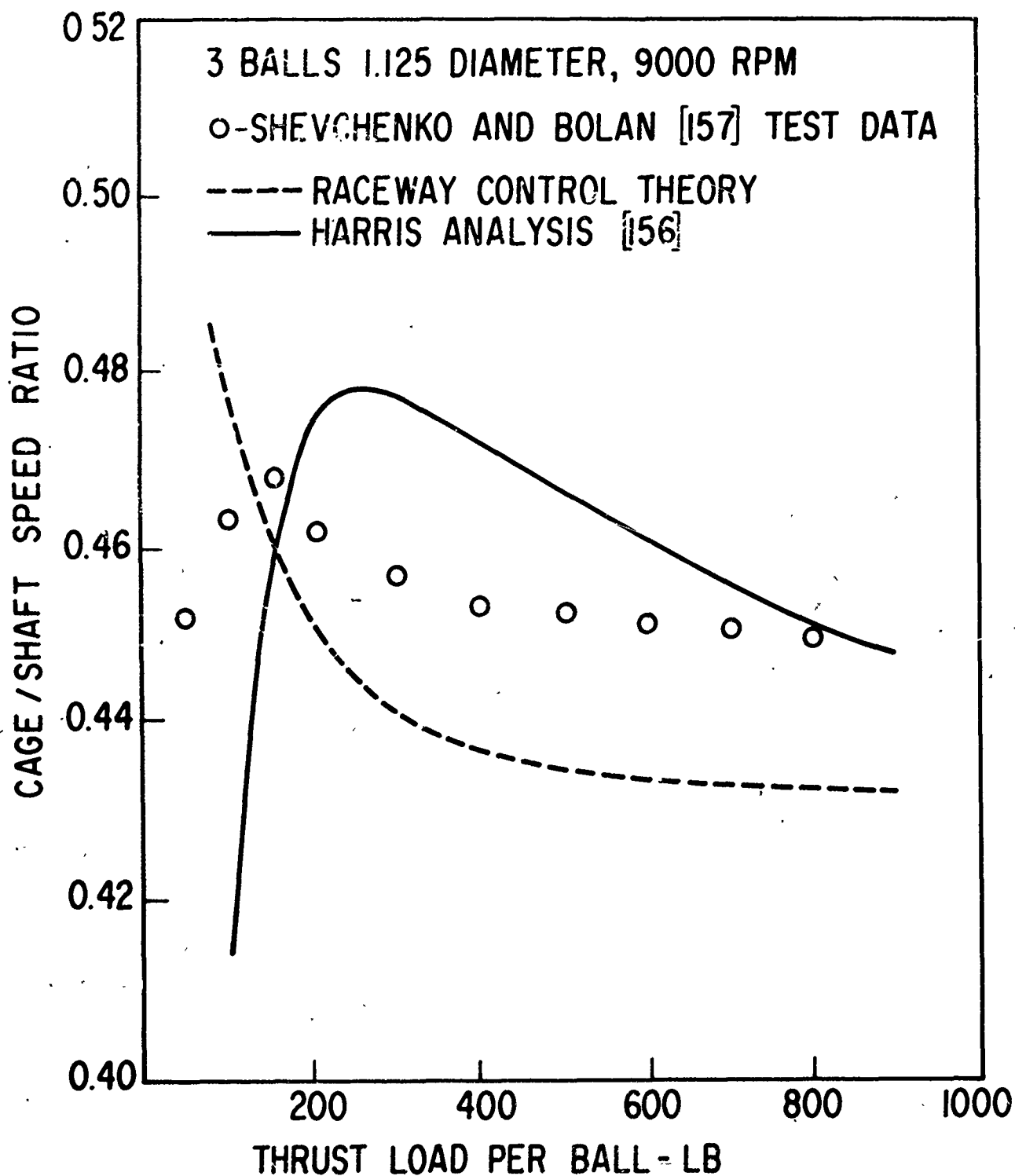


Fig. 79 Cage/Shaft Speed Ratio vs. Thrust Load Per Ball.

this discrepancy

- Differential frictional heat rejection between the inner and outer raceway contacts tends to alter the bearing kinematics and hence frictional forces.
- For lighter loading, the pressure distributions in the contact zones tend to stray from the classical ellipsoidal distributions associated with Hertzian contacts.
- Lubricant behavior tends toward non-Newtonian as sliding speeds increase.

Another important result of Harris' work (155) is his observation that the ball to raceway spin to roll ratio for the Poplawski and Mauriello (157) bearing tests tends to zero only in the region of severe skidding. In fact, the spin to roll ratio at the inner and outer raceways under high loads tended to approach a common value as load was increased in the Poplawski and Mauriello bearing tests. This is in direct contrast with the raceway control hypothesis which states that the spin to roll ratio should be zero on the controlling race and some finite value on the other race. Thus, the Harris analysis indicates that the raceway control hypothesis cannot be valid in the normal operating regimes of fluid-film lubricated, angular-contact ball bearings.

More recently, Walters (159) has presented a comprehensive analysis of the motions of balls and separator motion in ball bearings assuming elastohydrodynamic lubrication at the ball-race contact. The elastohydrodynamic model used was that proposed by Kannel and Walowit (134). Some general results of his calculations for a high speed gyroscope spin-axis bearing include:

- Raceway control does not occur. On the contrary, spinning (or pivoting) is about the same at each contact or the spin vector may oscillate depending on operating conditions. This is in agreement with Kingsbury's observations on a similar bearing (160) and with Harris' analysis.
- The angular velocity vector of the ball does not lie exactly in the plane of the ball mass center and spin axis but lags because of the gyroscopic moment. At 24,000 rpm bearing operation, this amounted to a crossrace ball slip of about 1000 rpm.

- In a perfect geometry bearing under pure thrust load there are no force patterns tending to cause equilibrium in a few revolutions. The meagerness of the lubricant supply complicates the situation because the balls impact the separator causing sharp increases in force and high accelerations. More lubricant tends to soften the impact.
- Static force-balance-type calculations are probably meaningless because for realistic bearings the balls are continuously accelerated and decelerated.

The work of both Harris (158) and Walters (159) confirms the inadequacy of raceway control hypothesis and show the necessity of including elastohydrodynamic lubrication traction forces in both roller and ball bearings.

## 9. ROLLING ELEMENT BEARING FAILURE MODES

Because of their extreme versatility and low operating friction, rolling-element bearings are widely used as a component in gas turbine engines and associated equipment. Failure-rate data for rolling-element bearings is needed to predict the reliability of gas turbine systems. In general, failure-rate data for rolling-element bearings has not been available in the past and, as a result, the ability to predict gas turbine system reliability has been hampered.

Because of the lack of actual failure-rate information for rolling-element bearings, their expected life is usually determined by calculation of a theoretical fatigue life. Unfortunately, most rolling-element bearings do not fail as a result of fatigue. The fatigue failure mode is the limiting mode, but the bearing fails in this way only if all other hazards such as wear, lubrication failure, etc. are avoided.

Before realistic, rolling-element, failure-rate estimates can be made, it is necessary to identify the failure modes other than fatigue which contribute to the overall bearing failure rate, and to categorize available failure information in terms of the various failure modes. Many of these failure modes in addition to fatigue are related to the elastohydrodynamic lubrication process. Therefore, it is necessary to examine the extent to which these failure modes are dependent on elastohydrodynamic lubrication.

### a. Classification of Failure Modes for Rolling-Element Bearings

Classification of rolling-contact failure mechanisms have been made by many different workers in the rolling-element field. Most authorities on rolling-contact bearings - for example, Allan (161) and Palmgren (162) - devote portions of their texts to the illustration of various types of failures. A comprehensive listing of the visual appearance of contact failures is given by Kaufman and Walp (163). Another good reference to rolling-element failure mechanisms is the handbook by Bisson and Anderson (164). Simpson (165) has categorized failures of rolling-contact bearings with illustrations of



TABLE X  
FAILURE MODES OF ROLLING-ELEMENT BEARINGS

I. CONTACT FAILURES

1. Wear Failures
  - a. Mild Wear
  - b. Severe Wear
2. Plastic-Flow Failures
  - a. Cold Flow
  - b. Overheat Softening
3. Contact Fatigue Failures
  - a. Subsurface Fatigue
  - b. Surface Fatigue
4. Electrical and Magnetic Failures

II. NONCONTACT FAILURES

1. Bulk Failures
  - a. Overload Cracking
  - b. Overheat Cracking
  - c. Bulk Fatigue
  - d. Fretting of Fit Surface
  - e. Permanent Dimensional Changes
2. Cage Failures
3. Lubricant Failures

III. PERFORMANCE FAILURES

various faults and defects. Fatigue failures of rolling-element bearings have been systematically classified by Wren and Moyer (166) with illustrative examples of each failure mode. The Russian, Edigaryan (167) claims that the life of rolling-element bearings is dependent on only three basic failure mechanisms. A recent classification of rolling-element failure modes is that by Tallian (168). Other good reviews are given by Cheng and Orcutt (169), Smalley et al (170), O'Connor and Boyd (171), and Moyer and Morrow (172).

Table X represents a classification of failure modes for rolling-element bearings based on the references cited above. The second group collects the noncontact failures into a single category. The last category refers to applications where a bearing may be considered to have failed even though such bearings would still be satisfactory for less exacting applications.

Most of the classifications of rolling-element failure modes emphasize the fatigue failure mode. This, in a sense, is unfortunate since, as estimated by Zaretsky (173) only ten percent of the bearings that fail, fail by fatigue. Although not the most common mode of failure, fatigue is the limiting form of failure in those cases where all environmental factors are controlled. For this reason most bearing manufacturers quote bearing load-carrying capacities in terms of the load that bearings will sustain for a given finite fatigue life.

#### b. Contact Failures

Those failures which originate in the volume of bearing material subject to contact stress, are classified in the Contact Failure Mode. Most of the recent literature is concerned with this general category of failures.

##### (1) Wear Failures

The races and rolling elements of rolling-element bearings undergo wear unless totally separated by a lubricant. The character of the observed wear can be classified as mild or severe.

##### (a) Mild-Wear Failure Mode

In the mild-wear mode the rolling contacts in the bearing wear very slowly, but many bearings have to be replaced prematurely because of this wear due to decreasing work accuracy. The rate of mild wear depends upon three main factors.

##### • Degree of Lubrication

In bearings which are either unlubricated or poorly lubricated such as with jet engine fuel or cryogenic fluids, wear is the predominate failure mode. Wear in these fluids is so great that a sufficient number of cycles never accumulates to form the familiar subsurface spall of contact fatigue.

- Amount of Lubricant Contamination

Significant amounts of wear can also occur if abrasive contaminants are present in the lubricant.

- Amount of Sliding

In rolling-contact bearings, where high rates of slip between the rolling elements and the races occur, rates of wear are correspondingly high. This condition exists primarily in lightly loaded rolling-element bearings.

Tallian (168) characterizes this failure mode by the appearance of wear particles in the lubricant and abrasion of the contact surface. Generally, the surface character is impaired only gradually, and in some rolling bearings, considerable wear can occur before they become unfit for operation. Diagnosis of mild-wear failure can be accomplished by geometrical or weight measurement of the material removed.

The effect of mild wear on rolling-element bearing life has been studied by Eschman (74). He found that more bearings fail from wear than from fatigue. His work indicates that if rolling-element bearings are adequately lubricated and operate in a clean environment, wear is negligible. However, these ideal conditions do not generally prevail in the field, and bearing wear occurs at an accelerated rate. Hence, the environmental conditions are as decisive for the wear failure mode as load is for the fatigue failure mode. Field experience provides many examples for which wear terminates the service life of bearings and it must be considered when evaluating the service life.

In Ref. 175, Brothers and Halling, using model techniques, illustrated the small-scale slip processes which occur between a rolling element and its track. These slip mechanisms arise from applied loading and the geometric conformity of the system. Creep measurements arising from such slip are presented and compared with theoretical predictions. The wear resulting from this slip was determined using the radioactive tracer measurements.

In a concurrent paper, Halling and Brothers (176) also describe an experimental study of the wear in the contact zone between a rolling ball and its track. The ball was subjected to a normal load and a small resisting torque; the rate of wear resulting from the ensuing microslip was determined using a radioactive tracer technique. The effect of load, speed, hardness, and surface finish were investigated, the latter property having negligible effect on the results. The results were used to obtain an equivalent macroscopic-sliding-wear law, which was found to deviate from that normally associated with mild wear, particularly in relation to the effects of load and velocity.

No satisfactory explanation of this velocity dependence was found.

Tallian et al (177, 178), cite experiments in which the rolling-element wear rate was determined for a number of mineral oils and synthetic fluids. The wear rate of a radioactive (activated) ball was measured, using scintillation counting of the lubricant and of washings from the test configuration. A run-in period exists if the test is started with new balls; thereafter, the wear rate becomes steady. The experiments were conducted in the partial elastohydrodynamic range; in this range, the equilibrium wear rate can be expressed as a function of the following variables:

- a. The real area of asperity contact
- b. The slide/roll velocity ratio

For constant geometric conditions - i.e., constant slide/roll velocity ratio and constant contact material - the wear rate can be expressed to good approximation as follows:

$$V = kPl \quad (52)$$

where

$P$  = Load

$V$  = Volume of material worn away

$l$  = Distance slid

$k$  = Wear coefficient dependent on the materials, lubricant, surface condition, and ball spin

The load  $P$  is the fraction of the contact load which is being carried by the contacting asperities. Another fraction of the load  $P$  is, of course, carried by whatever fluid film remains between the two contacting bodies.

Eq. 52 is proposed on the assumption that the real area of contact is proportional to the total load  $P$  applied to all contact zones existing simultaneously; i.e that

$$A_c = k' P \quad (53)$$

This proportionality follows from the statistics of the concluding surfaces as discussed previously on page 128.

Substituting Eq. (53) into Eq. (52) one obtains the wear rate per unit distance travelled.

$$\bar{V} \sim V/l = \left(\frac{k}{k_1}\right) A_c \quad (54)$$

This equation states that the wear rate is, for a given set of conditions, lubricant and surface geometry, proportional to the total area of asperity contacts existing simultaneously.

For sufficiently high surface velocities or low loads, a full film is formed and none of the load is carried by the asperities. In this region, the film thickness is determined by the elastohydrodynamic pressure balance along. As the load increases or speed drops, the film thickness decreases and asperity contacts occur where the local film thickness drops to zero.

The local lubricant film thickness between opposing asperities, as shown in Fig. 72, can be expressed as

$$h(x) = h_0 - y_1(x) - y_2(x) \quad (55)$$

For a function  $h(x)$ , the fraction of the abscissa axis occupied by ordinate values not exceeding a fixed value is given by the cumulative amplitude distribution  $F(h)$ . Therefore, the fraction of the contact area, over which the film thickness does not exceed a given minimum,  $h_0$  is

$$A_c/A = F(h_0)$$

where

$A_c$  = area occupied by film thickness less than  $h_0$

$A$  = total Hertzian contact area

Eq. 49 can be used to calculate  $A_c/A$ .

According to this partial elastohydrodynamic asperity contact model of Tallian, et al (177, 178), the wear rate must go to zero when  $\xi_0$  is so large that no asperity contacts take place. For low enough speeds, the wear rate per unit track length should be expected to reach a value independent of  $\xi_0$ . These postulates appear to be compatible with the experimental results.

The highest wear rate obtained by Tallian, et al (177, 178) was  $10^{-4}$  mg/in track length, and it was observed for  $\xi_0 \approx 1$ . This

amounts to removal of a layer of approximately 400 microinches thickness from the rolling track during the time the balls travel one million inches on each other. This is quite discernible wear for a rolling contact and will, in long run destroy the accuracy of the configuration. Thus, a contact operating under the very high Hertz pressure  $P_{\max} = 680$  kpsi cannot run long with the thin elastohydrodynamic film corresponding to  $\xi_0 = 1$ . For higher values of  $\xi_0 \approx 3$ , the wear rate is about 100 times lower and, at these levels, it is negligible as a failure mode.

The wear law cited states that the wear constant  $k$  is (as a first approximation) independent of the elastohydrodynamic condition, and characterizes wear properties (boundary lubrication properties) of the lubricant/material combination of the rolling contact for the specific geometry and kinematic situation of a test.

The effect of the magnitude of sliding on wear rates seems to depend on the elastohydrodynamic condition. With an almost complete elastohydrodynamic film the effect of sliding on wear seems to be minor. When there is less film and more substantial asperity contact, the wear rate increases by a factor of 10 or more as a ball-to-ball configuration is made to roll with a high amount of sliding (typical of high contact angle ball bearings) instead of zero sliding.

One can use the described concepts of mild wear of well-lubricated rolling contacts to compare lubricants for their wear preventing action in rolling contact, and to predict the wear life of a practical configuration on the basis of relatively simple wear experiments provided that the lubricant, surface geometry, and contact configuration are identical in experiment and practice, and that  $\xi_0$  is known in both cases.

Bamberger et. al. (80) have evaluated the wear preventing action in rolling contact of three advanced lubricants, a synthetic paraffinic oil, a fluorocarbon, and a 5P4E polyphenyl ether. Their results show that if partial elastohydrodynamic conditions prevailed, bearing failure was mainly from wear. They demonstrated that, by reducing bearing load for the paraffinic and fluorocarbon oils to insure a full elastohydrodynamic film, failure was primarily due to fatigue. With the 5P4E polyphenyl ether, wear and surface distress occurred, indicating partial elastohydrodynamic lubrication for all operating conditions. Their results validate the use of the elastohydrodynamic film parameter as criterion for evaluating the effectiveness of an elastohydrodynamic film.

Recent work by Landen (179) presents time rates of mild wear of two cylindrical SAE 8620 steel rollers as a function of film thickness. The rollers were 3.3 and 2.7 inches in diameter and

0.5 inches long. The larger roller was ground with a  $5^\circ$  chamfer on each end to limit the contact length,  $l$ , to 0.180 inches and reduce end effects. Most of Landen's data was taken at a load,  $w$ , of 13,000 lb/in of contact length and at this load the contact width,  $2b$ , was 0.056 inches.

The rollers were carburized to a case depth of .090 to .110 inches with a surface hardness of Rc 61 to 64 and a maximum axial surface finish of 5 to 10 microinches centerline average. A straight mineral oil (SAE 30) was used in his tests.

Landen (179) showed that wear of rolling surfaces is divided into a constant wear mode and a transient wear mode depending on the oil film thickness. For values of specific film thickness less than about 0.2 a constant wear rate prevails but the magnitude of the wear rate depends on operating conditions. For specific film thickness values greater than about 0.2 wear occurs for a short time and exhibits a continual change in the time rate of wear until either a constant rate results or wear stops.

Table XI presents an approximate classification of the various modes as a function of specific film thickness. These classifications can be separated into three classes which are respectively: 1 and 2, constant wear and no rippling; 3 and 4, constant wear with rippling; and, 5 and 6, transient wear with continuous film formation. This grouping is shown in Fig. 80 in which the specific film thickness is plotted as a function of slip. The operating conditions producing constant wear rates are shaded. The beginning of rippling and the beginning of continuous film formation occur at smaller values of calculated oil film thickness as the slip increases from 0.1 to 1.0.

At specific film thickness of roughly 0.16, Landen (179) observed the development of a ripple pattern on the slower moving surface. Both the wavelength and amplitude of this ripple pattern depended upon the value of the slip parameter. Fig. 80 defines the range of film thickness and slip parameter over which this phenomena occurs.

Both Landen (179) and Queener (180) have shown that the total wear can be expressed as the sum of the constant wear  $m_1 = kPl$  and the transient wear  $m_2 = m_0 (1 - e^{-n\ell})$ . The total wear is then

$$m = kPl + m_2 (1 - e^{-n\ell}) \quad (57)$$

The coefficients  $k$  and  $n$  depend upon the specific film thickness and the slip parameter. Unfortunately, Landen's (13) evaluation of these coefficients was not carried out with

TABLE XI

## Classification of Mild Wear Modes in Rolling Contact

$$U_1 = .6 \frac{\text{in}}{\text{sec}} - 72 \text{ in/sec} \quad U_2 - U_1 = 0.1 - 1.0$$

<u>Classification</u>	<u>Approximate Specific Film Thickness</u>
(1) Constant wear rate, distinct surface scratch marks	.02 - .04
(2) Constant wear rate, diffuse surface scratch marks.	.05 - 1
(3) Constant wear rate, ripples on faster surface.	.08 - .16
(4) Small transient, followed by high, constant wear rate ripples on faster surface.	.11 - .22
(5) Large transient followed by small constant, wear or zero wear rate, continuous colored film on $u_2$ surface.	.12 - .24
(6) Small transient followed by small constant wear rate or zero wear rate, continuous colored film on faster surface.	.20 - .40

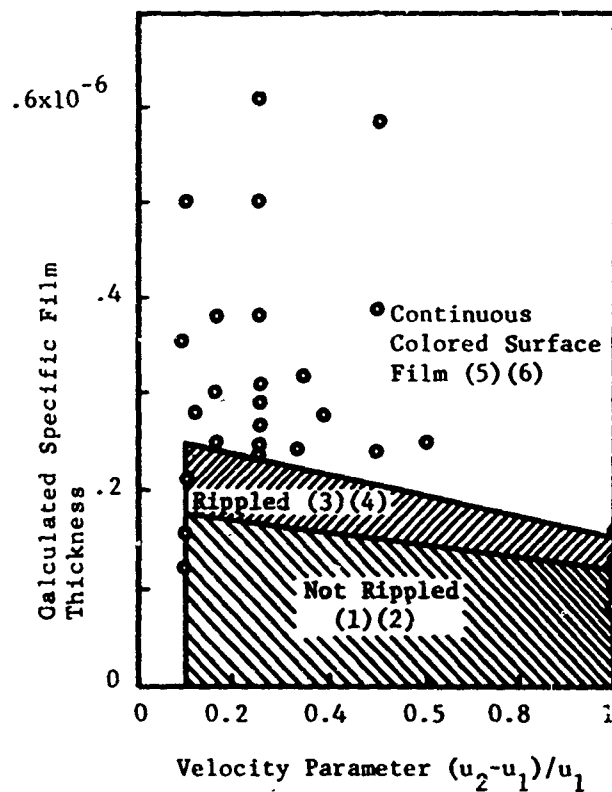


Fig. 80 Influence of Velocity Parameter  $(U_2 - U_1)/U_1$  on Constant Wear, Shaded, and Transient Wear Modes. Surface Conditions Indicated. (Courtesy of ASLE, Trans. Vol. II, 1968)



materials and slip ratios of interest in gas turbine bearing practice. Determination of these coefficients should form a part of any continuing program in the bearing failure area.

In summary, the available literature indicates that mild wear can be a predominate failure mode for bearings under certain conditions. These conditions are confined primarily to rolling element bearings lubricated with solid lubricants or very poor liquid lubricants such as water, liquid metal, or cryogenic fluids. There is a considerable volume of practical test data on hand (Devine, et. al., 181) reporting on wear behavior of solid lubricated bearings but generalizations have not been published that would permit prediction of wear behavior. The other condition, for which mild wear can be a predominate failure mode, occurs when the bearing is operated in a contaminated environment. Eschmann (174) has shown that wear rates can be very high under these conditions leading to early failure of the bearing due to loss of dimensional accuracy.

#### (b) Severe Wear Failure Mode

Severe wear of rolling element contact is usually described by the terms "scoring" or "smearing". No matter what the name, the condition describes a serious failure of Hertzian contacts. It is characterized by a substantial, cumulative transfer of material between areas of moving surfaces. Some degree of sliding is necessary for the onset of this condition and it is, therefore, encountered in rolling contacts in which a high degree of sliding is present. This condition exists in bearings subjected to high angular accelerations or running at extreme speed and low load where, due to the low traction transmitted through rollers or both, they may stop rotation around their own axis and, subsequently, undergo sliding.

Tallian (168) reports that the time to form a smearing failure, if conditions are conducive to smearing, is extremely short. He reports that macroscopically visible metal transfer can occur within inches of sliding after the moment when the onset of severe wear is first indicated by an increase in traction. If this type of failure is allowed to progress, it is generally self-aggravating and leads to rapid destruction of the contact.

The mechanism of smearing is closely related to the basic phenomenon of the collisions of asperities in a heavily loaded rolling and sliding contact. According to Cocks (182, 183), when two asperities slide over each other under a large normal pressure, welded junctions do not subsequently break, but cause one of the asperities (usually the softer one) to undergo a sub-surface plastic shearing in a plane slightly inclined to the direction of motion. Unless this condition is rapidly relieved, it will lead to smear failure.

#### Effect of Lubricant Film Thickness

Since smearing originates from asperity contact, any lubricant film

resulting from elastohydrodynamic action will tend to reduce the chance of smearing.

The specific film thickness  $\xi_0$  is an influential parameter in defining the partial elastohydrodynamic region. In the limit as  $\xi_0 \rightarrow 0$ , more and more asperity contacts occur and substantial transfer of material occurs. Depending upon the bearing load, temperature, and amount of contact slip, operation under this condition leads to severe wear or smearing at best, or to sudden bearing lockup at worst. The influence of the specific film thickness of this region of severe wear has been examined by Bodensiek (184). Bodensiek has concluded that there exists a region of critical specific film thickness below which scoring will occur. Table XII reproduces his summary of how lubricated contact conditions are affected by the specific film thickness. Below about  $\xi_0 \approx 1.2$ , visible signs of surface distress will occur. The severity of the surface distress depends by no means solely on the value of  $\xi_0$ . The temperature and boundary lubrication abilities of the lubricant can retard or promote surface distress in this regime. However, it appears that by maintaining  $\xi_0 > 1.2$ , generalized surface distress is avoided.

Ibrahim and Cameron (185) present some results of film thickness measurements which appear to show a sudden collapse in film thickness coincident with the point of incipient smearing. Their results indicate a film thickness at smearing about equal to the surface roughness which is in general agreement with Bodensiek's conclusions.

In a series of angular-contact ball-bearing (25 mm bore) endurance tests at extreme temperature, Peacock and Rhoads (186) found that smearing failures predominated. Two high temperature lubricants were evaluated, Dupont "Krytox" 143 AC perfluoro alkyl polyether lubricant, and Mobil XRM-177F hydrocarbon lubricant. Their results indicated that Mobil XRM-177F provided marginal lubrication at 700 F and that Krytox 143AC was unsuitable at 600 F under the test conditions used.

In a second phase of the project, lubricant-film-thickness measurements were made in the rolling contacts of ball bearings. Four different types of lubricants (synthetic paraffinic hydrocarbon, improved ester, polyphenyl ether, and perfluoro althyl polyether) were tested at varying speeds (up to 43,000 rpm), loads (up to 250,000 psi maximum Hertz pressure), and temperatures (up to 700 F). It was found that elastohydrodynamic lubricant films exist at these extreme conditions but film thicknesses differ (they are generally lower) from those predicted by isothermal theory and that considerable differences exist in the thickness of films formed by the various types of lubricants.

#### Effect of Maximum Surface Temperature

The important relation between the maximum surface temperature and smearing of rolling and sliding contacts has been recognized by

TABLE XII  
SURFACE DISTRESS DATA OF BODENSIEK (184)

APPROXIMATE $\xi_0$ RANGE	TYPE OF SURFACE DETERIORATION
Over 4.0	None (Full Elastohydrodynamic Lubrication)
1.8 to 4.0	Slight Marking, Mild Wear
1.7 to 1.8	Surface Improvement with Straight Oil
1.6 to 1.8	Surface Improvement with E.P. Additives
Below 1.7 (or 1.6)	Scoring, Spalling, Galling, Scuffing, Seizing
Below 1.4	Pitting (More closely related to surface compressive stress)
Below 1.1	Abrasive Wear
Below .7	Rippling and Ridging

many investigators (187-196) in the well accepted critical temperature concept, which states that smearing occurs when a critical value of peak surface temperature (temperature at inlet plus peak transient temperature in contact) is reached, regardless of the hydrodynamic film thickness. The broad concept of a critical temperature is consistent with modern boundary lubrication theory which says that good lubricants form adsorbed or chemically reacted films on the surfaces. These films protect the underlying surfaces as they slide over one another so that friction is low and surface damage is negligible; however, as the temperature of the surfaces is increased, a point is reached beyond which the films melt, are dissolved by the lubricant, or are desorbed from the surfaces. When this happens, friction goes up, still more heat is generated, and the surfaces eventually weld and tear with catastrophic results if the sliding speeds are high enough.

Generally good correlation between the initiation of smearing and critical temperature is shown by De Crushy and Harrison (187) for rolling-sliding disks, by Leach and Kelley (188) also for disks, and by Matveesky (189) for both roller and disk machines. Leach and Kelley (188) present the most convincing evidence to support the critical temperature concept as a criteria for smearing. Their results indicate that smearing takes place in spite of very large values of specific film thickness.

Fein (190, 191, 192) gives a different interpretation to his experimental results for pin on disc and four ball machines. He presents evidence to show that the critical temperature is influenced by speed, load, and surface material as well as by the lubricant. In some cases, the transition temperature increases with the ratio of speed to load, and in others the critical temperature becomes dependent on this ratio above a certain value. The generality of these results is limited by the fact that the highest speed investigated was 30 IPS, although the occurrence of smearing at such low speeds does extend downwards the speed range in which smearing may be expected.

In the previous discussion, the specific film thickness and the maximum surface temperature have been identified as the major parameters governing smearing. A graphical representation of the region of smearing or severe wear is shown in Fig. 81. This plot uses the inverse of the maximum surface temperature as the abscissa with the specific film thickness as the ordinate.

See next page

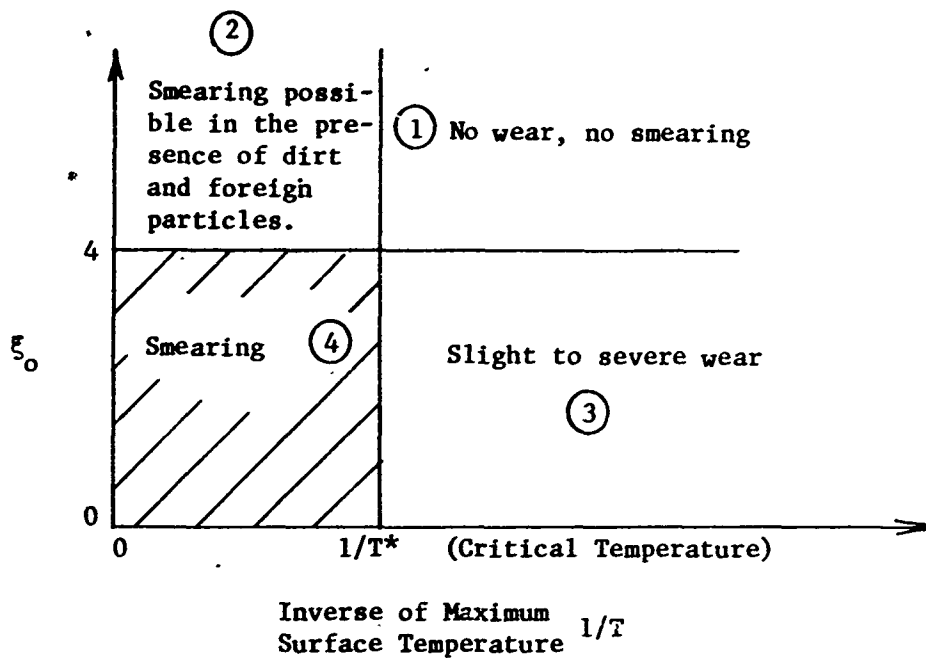


Fig. 81 Region of Smearing

Region 1 represents no wear or smearing because in this region  $\xi_0 > 4$ , the asperities are completely separated by a thick elastohydrodynamic film and the maximum surface temperature is below the critical temperature. In region 2, the maximum surface temperature exceeds the critical temperature even though there is still a thick film. Under this condition, scoring is possible if there are dirt and foreign particles in the film. Region 3 represents operations in the partial film regime, ( $\xi_0 < 4$ ), but below the critical temperature. In this region, abrasive wear will occur instead of smearing and the wear rate will be governed by the load, sliding speed, and the specific film thickness. Region 4 is the dangerous smearing region where the elastohydrodynamic film is not fully present and the maximum surface temperature is above the critical temperature.

As discussed previously, recent developments in elastohydrodynamics have provided reliable formula for prediction of minimum film thickness. At moderate rolling speeds (less than 250 in/sec for mineral oils), the thermal effects have a negligible influence on this calculation of film thickness and the formula derived from the isothermal theory of Dowson and Higginson (153) can be used.

At high speeds, the isothermal theory is no longer adequate and the thermal effects must be included in the calculations of the film thickness. A method to calculate the film thickness at high speeds including the thermal effects will be presented in Section III.

A principal barrier to wide-spread practical application of elastohydrodynamic principles, such as the film thickness formula, is the fact that the surface temperature at the inlet regions must be known with some accuracy in order to establish the inlet viscosity.

Blok (193), as early as 1937, offered formulae for the flash temperature rise occurring in a loaded contact which, if added to the inlet surface temperature or blank temperature, gives the maximum surface temperature in the contact. In spite of the more recent observations by Fein (192) to the effect that a transition temperature criterion is oversimplified, it has great usefulness in judging the likelihood of severe wear failure. Archard (194) has summarized flash temperature calculations for easy practical use. He shows that an upper bound of the attainable flash temperature in a contact can be calculated by assuming that metal to metal contact occurs over a single contiguous area and by assuming that plastic flow takes place over the entire extent of this area.

The difficulty with Archard's simple approach to a transition temperature is that calculated maximum flash temperatures usually turn out to be unrealistically high, presumably because the fully plastic contact hypothesis is clearly in error. Archard (194) also supplies a solution on the assumption that the contact area is a single elastically determined Hertz contact. Tataiah et al (195) have found that the flash temperature calculated on the basis of elastic deformation yields a reasonable estimate of flash temperature at the transition to severe wear if the friction coefficient has been determined.

O'Donaghue and Cameron (196) report that errors involved in contact temperature calculations increase at surface velocity ratios below 0.35. A further source of error arises if the velocities are high, because an appreciable portion of the heat generated may be carried from the contact by the lubricant. Yet another hurdle to the application of such formulae is the problem of obtaining a realistic value of the coefficient of friction. The friction force will be a function of the film thickness, the contact area, the viscosity distribution, and the surface velocities. The results of Smith (197) suggest that the influence of surface roughness is small, and Furey (198) confirms this above a low value of surface roughness. An approach which can bypass the above problems to some extent is to rely on full thermal elastohydrodynamic solutions, such as those published by Cheng and Sternlicht (58), Cheng (93) and Dowson and Whitaker (58).

#### Boundary Lubrication Effects

One of the main conclusions to be gained from an evaluation of the rolling element bearing failure literature is that elastohydrodynamic effects are very important, since no wear failure will occur as long as surfaces are separated by a fluid film. However, if metal to metal contact takes place through the film, then the

conditions of operation will be determined primarily by boundary lubrication effects.

Leach and Kelley (188) have shown that there is a critical temperature which defines the transition between effective boundary lubrication and severe wear (smearing). This transition point is the temperature at which polar constituents in the oil are either melted or de-adsorbed from the contacting surfaces and effective boundary lubrication no longer exists. If an elastohydrodynamic film separates the surfaces, then effective lubrication can persist above this temperature transition point; however, any metal to metal contacts through the film will result in surface damage.

Boundary lubrication is defined as the region in which the bulk properties of the lubricant have a negligible effect on the contact behavior of lubricated surfaces. The chemical makeup of the lubricant and the composition of the bearing surfaces are of major importance. Under these conditions, even minor percentages of certain constituents in the oil can be conducive to the formation of surface films which can prevent high friction and surface damage. The presence of these surface films reduces the friction and amount of surface damage when metal to metal contact takes place.

O'Donaghue and Cameron (196) have attempted to show that, as far as adsorbed surface film characteristics are concerned, there is a similarity between petroleum oils and a solution of a long-chain organic acid in a pure hydrocarbon carrier. From thermodynamic considerations, they concluded that an adsorbed film of this material on a metal surface would have a transition temperature which would not be markedly different than the transition temperature found for the same concentration of pure, long-chain polar organic compounds dissolved in a pure hydrocarbon. This conclusion is of some importance since it permits relating results obtained with pure organic acids in non-polar hydrocarbon solvents with the results obtained with petroleum oils with their completely chemical nature.

The ability to form elastohydrodynamic films is not the sole determining factor in predicting a fluid's success as a bearing lubricant. The previously cited work of Leach and Kelley (188) showed that bearing endurance data does not necessarily correlate with film thickness measurements. The boundary lubrication properties of the lubricant must also be considered.

#### Surface Lubricating Film Breakdown

There are many different types of lubricating films which reduce the amount of contact and adhesion between the surfaces. A list of these films is given below.

## Surface Lubricating Films

- Physically absorbed molecules
- Chemically absorbed molecules
- Decomposition films from lubricant
- Surface-lubricant organic reaction films
- Surface-lubricant inorganic reaction films
- Surface atmosphere inorganic reaction films

Each of these films has its own unique properties and thus, differ in the manner in which it provides surface protection. It would be expected that each has its own unique method of failure. In general, the failures of these films may be categorized as follows:

- Inadequate film thickness for operating conditions
- Destruction of films
- Deformation

### Inadequate Film Thickness for Operating Conditions

When sliding commences between two surfaces, they are usually misaligned and their surface asperities are interlocked. Any films present on the surface at this time will be broken away. However, as sliding proceeds, the surface temperature increases and the surfaces "run in". Surface films are then more easily formed and less likely to be broken away. If the rate of formation is fast enough, effective sliding will result. The rate of formation of films will depend upon the type of film formed. Generally speaking, some sort of a reaction is necessary so the rate of formation is strongly depending upon the temperature and the concentration of reactants in the contact area.

The above also demonstrates the fact that, if the rate of removal exceeds the rate of formation, failure will result. This, of course, is the condition of film wear. One might suggest that, if the rate of formation was adjusted to overcome galling, it should be significantly larger than the rate of removal. However, conditions change drastically after the film is formed (lower friction, lower temperature), so wear may be the dominant factor until metal contact results.

### Destruction of Films

When the sliding or rolling process becomes severe the interface temperatures increase. The interface temperature  $T_i$  can be described qualitatively:



$$T_i \propto \frac{f P_i^n U^m}{K_i} \quad (58)$$

where  $K_i$  = thermal conductivity  
 $P_i$  = load  
 $U$  = velocity  
 $f$  = friction coefficient

$n$  and  $m$  are constants,  $n \leq 1$  depending upon the load  $m \leq 1$  depending upon the velocity and the geometry of the contact. These high temperatures can cause the destruction of the surface film for a variety of reasons:

Melting

Dissolving

Decomposition

Evaporation

The destruction of the film allows metal contact and the possibility of seizure.

#### Deformation

Surface films can also be removed from the surface by a process of fracture or fatigue. Experimental evidence confirms both of these as real failure modes, however, they apply more to the hard oxide films rather than soft lubricating films. The cause of the failure is a function of both the deformation of the film and its basis material as a result of thermal or stress deformations.

#### Material Seizure

Once the fluid film thickness approaches and the protective lubricant films have been broken through, a seizure process can result, under certain conditions. These conditions are a function of the material properties, the friction or adhesion, and the geometry of the contact.

If the model of a soft surface against a rigid one is chosen, then it has been found experimentally (199, 200) that as  $F$ , the tangential force, increases, the area of contact increases, and  $h_f$  decreases. This process continues until slip occurs at the interface (no failure) or fracture occurs away from the interface (metal transfer and failure).

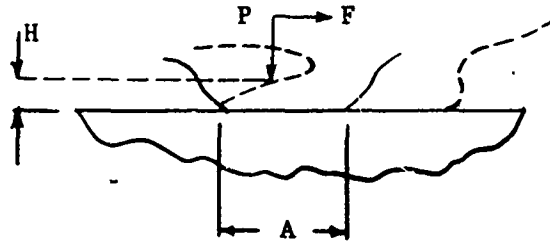


Fig. 82 The Two-Dimensional Plasticity Model

Tabor (201) has treated the problem as one of two-dimensional plasticity and used Hills solution to derive the following expression for the model of Fig. 82.

$$p^2 + 9\tau^2 = 9\tau_m^2 \quad (59)$$

where  $\tau_i$  = interfacial shear strength  
 $\tau_m$  = shear strength  
 $\tau$  = shear stress  
 $p$  = pressure

Since  $\tau_m$  is a material constant this expression demonstrates the experimental observations. As  $F$  increases,  $\tau$  increases;  $p$  must then decrease. The process will continue indefinitely until  $p = 0$ , unless slip occurs at  $\tau = \tau_i$ . This will occur for material combinations of low adhesion (low friction) since  $f = \tau_i/p$ .

If  $\tau_i$  is high the process will continue and necking will occur away from the interface. This will ultimately lead to fracture as shown by the curves dotted lines of Fig. 82. That this process occurs has been experimentally verified by the work of Greenwood (202), Cocks (203) and Antler (204). A precise failure criterion has not been developed; however, it has been suggested that it is associated with the decrease in area in the necking region, the work hardening which strengthens the interface region, or the ductility of the material. Whatever the explicit criterion, it is apparent that it is associated with the ability of the material to deform. This also conforms to common experience — that brittle materials are much better in sliding than a ductile one.

Although our understanding of material seizure is far from complete and not very rigorous, it is clear that there is some friction, deformation, failure criterion. That is, the higher the friction

the more resistant the material must be to deformation to prevent surface damage.

## (2) Plastic Flow Failure Mode

If a rolling-element bearing is overloaded, there will be plastic flow, which, if severe enough, will destroy the intended contact geometry by forming "brinell marks" if the load is stationary, or by distorting the rolling track if the elements roll. Analysis of the damage caused by these plastic indentations has been made by Kaufman (163). By examination of the location and distribution of the ball paths produced on the raceways, the magnitude and direction of the load causing the observed damage can be reduced. These loads may arise from unbalance of rotating parts, unexpected loads, differential thermal expansion, or tight fits resulting in loss of clearance.

Plastic flow on a small scale occurs under quite reasonable loads (162). This has been recognized by defining a "static capacity" for rolling bearings by limiting the magnitude of elastic deformation to an arbitrary but small amount. The static load rating method for bearings is based on a plastic diameter reduction equal to  $10^{-4}$  times the rolling element diameter. For a typical bearing steel this amount of deformation corresponds to a contact stress of approximately 500 kpsi.

If the loading is increased sufficiently, local plastic yielding of the material will occur. It follows from Equation (37) that yield will first occur in a small region beneath the surface which is completely contained beneath the surface. Johnson (205) has shown that this yielding will take one of two forms. The plastic flow which occurs in the first passage of the load will induce a system of residual stresses, and under repeated traversals of the load the material will "shakedown" to a state in which subsequent traversals of the load can be supported by purely elastic stresses. If the load is below this so called shakedown limit, further plastic deformation will cease. On the other hand, at loads greater than the shakedown limit, plastic deformation will take place with every passage of the load.

It has been shown by Johnson (205) that the load at which a metal first yields in rolling contact is given by

$$2.7 \tau_s < \sigma_{\max} < 3.3 \tau_s \quad (60)$$

depending upon which yield criterion is used. Whether or not continuous plastic deformation will occur depends upon whether or not the load exceeds the shakedown limit. In pure rolling the shakedown limit is found to be given by

$$\sigma_{\max} = 4 \tau_s \quad (61)$$

This represents an increase of 66 percent in load carrying capacity above the load for first yield given by Equation (60). Tangential forces introduced by sliding or microslip cause an appreciable reduction in the shakedown limit as shown in Fig. 83.

With a view of establishing a theoretical load capacity of rolling contact including the influence of a lubricant, the shakedown theory has been applied to the elastohydrodynamic stress distribution calculated by Dowson and Higginson (153). This is shown in Fig. 83 where load carrying capacity, expressed by the ratio  $(\sigma_{\max}/\tau_s)$  is plotted versus the pressure distribution parameter  $U/W^2$ .

Points to the left of Fig. 84 correspond to low speed and heavy load and approaches Equation 61 for dry contact. Points to the right correspond to high speed and high viscosity.

Thus, at loads above the shakedown limit, continuous and cumulative plastic deformation is observed; at loads below it, even though they cause some yielding initially; after a few revolutions, the system shakedown to an elastic cycle of stress. The shakedown limit can be regarded as the theoretical ultimate load carrying capacity of a rolling contact. It represents the best that can be achieved if other failure modes such as mild wear, scoring or fatigue did not intrude to cause premature failure.

### (3) Fatigue Failure Mode

The classical failure mode of rolling-element bearings is contact fatigue. From analyses of failed specimens, fatigue failures can be classified into two major categories, those of subsurface origin and those of surface origin.

#### (a) Subsurface Fatigue

The subsurface fatigue is characterized by cracks which are initiated beneath the surface. Under repeated high stress, these cracks gradually grow in length and eventually lead to spalling of metals. Location of these cracks is usually in the vicinity of the maximum shear stress, and their rate of growth depends mainly on the level and the amplitude of the shear stress.

The life of a rolling contact subjected to subsurface fatigue is predictable by the celebrated, classical Lundberg and Palmgren theory (144, 145). They showed that the probability of survival of a rolling element is a power function of the maximum alternating subsurface shear stress, the depth at which this stress occurs, the number of cycles in millions, and the stressed volume. The stressed volume appears because, on the assumption that weakest point is first to produce a flaw, the probability of failure increases with the stressed volume. It is an assumption of this theory that the maximum alternating shear stress does govern

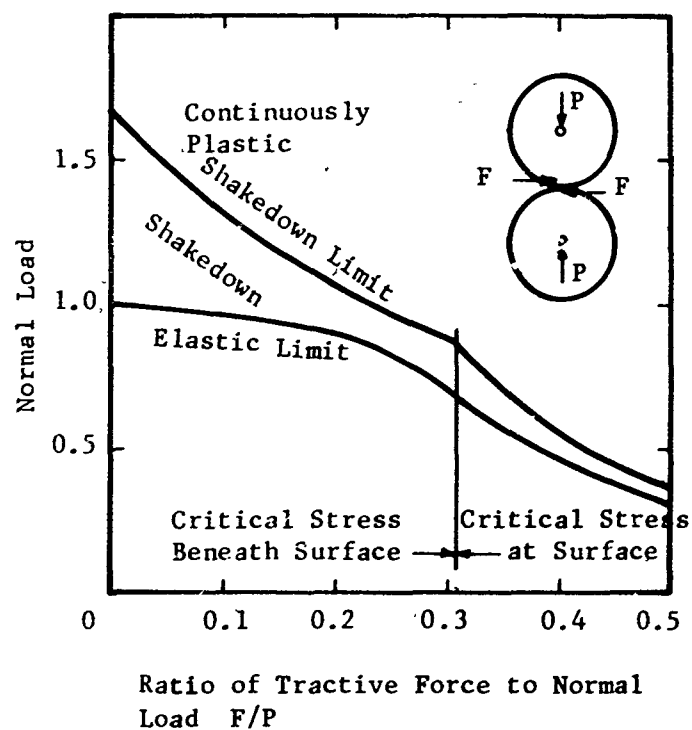


**Fig. 83** The Effect of a Tangential Force on the Limit of Elastic Behavior and Shakedown Limit.  
(Courtesy of WEAR Journal 9, 1966)

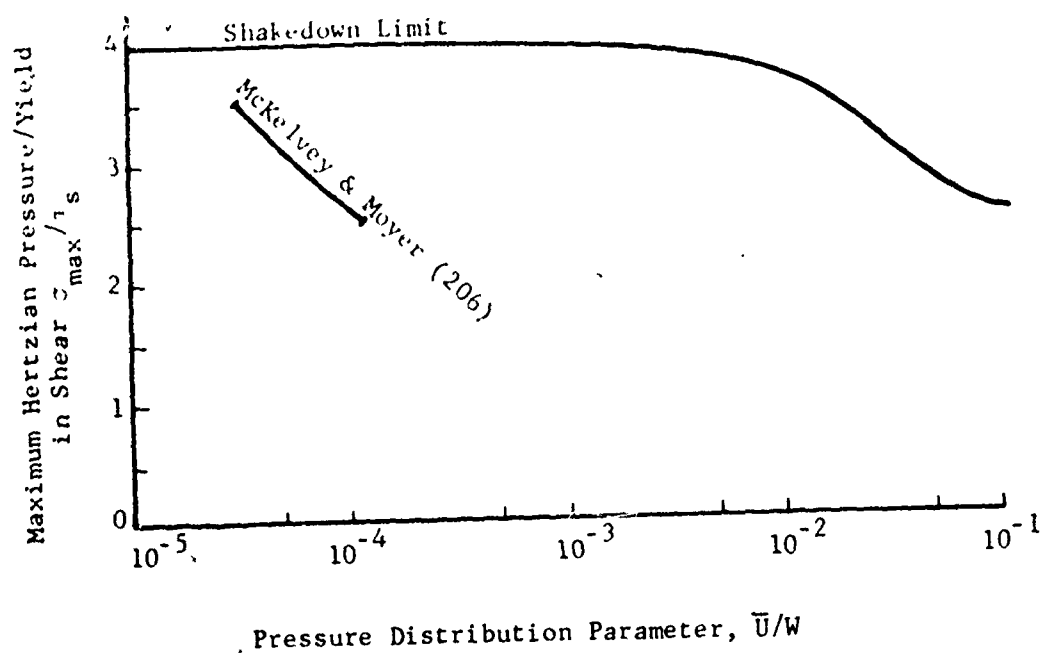


Fig. 84 The Intensity of the Bulk Contact Stress.  
(Courtesy of WEAR Journal 9, 1966)

fatigue failure, and that the stress field is the result of a Hertzian normal pressure distribution. The constant proportionality and exponents need to be determined experimentally, and, therefore, the theory provides a failure criterion rather than absolute values. As such it enjoys popularity and is the basis of conventional life calculations.

It should be noted that Lundberg and Palmgren theory is based on the subsurface stress distribution of a dry contact and does not take into account the effect of lubrication. As many investigations have shown significant dependence of fatigue life to lubricants, it is important to examine how the subsurface fatigue might be affected by the lubrication.

#### (b) Surface Fatigue

Fatigue of the surface origin is distinct from subsurface fatigue in that the cracks are initiated on the surface and propagated in the direction parallel to the surface. These cracks usually do not penetrate deep into the subsurface. As the crack length grows, the metal adjacent to the surface becomes gradually detached chipping away from the surface.

#### (c) Effect of Elastohydrodynamic Lubrication on Fatigue

Both theoretical and experimental evidence shows that fatigue failure is not simply governed by stress distributions resulting from normal Hertzian pressures. Elastohydrodynamic lubrication plays an important role in altering the basic Hertzian stress pattern and hence influencing the fatigue failure.

Under the influence of elastohydrodynamic lubrication, the classical Hertzian stress field will be modified by the following factors:

- The redistribution of the normal pressure profile

- The surface tractions

- The thermal stresses

- The asperity interaction

Modifications due to the first three factors can be readily determined from pressure, surface traction and temperature data obtained by using the computer program of Section III. Since smooth surfaces are assumed in the elastohydrodynamic theories, the modified stresses are only meaningful in the regime of full film elastohydrodynamic lubrication, and they may be termed macro-elastohydrodynamic stresses.

The influence of a sharp secondary peak or severe surface tractions due to viscous shear is similar. Both increase the magni-

tude of the maximum shear and octahedral stress and shift them nearer to the surface. These stress alterations increase the likelihood of surface fatigue. The degree of worsening depends on the operating conditions and the pressure-viscosity exponent of the lubricant. Increase in speed or viscosity in the full film elastohydrodynamic regime tends to increase the magnitude of the secondary pressure peak and hence the maximum stresses. The effect of surface traction is most severe when oils of a high pressure-viscosity exponent are used under small or moderate sliding to roll ratios.

Thermal stresses depend directly on the temperature rise in a contact. For contacts having small sliding to roll ratios, thermal stresses do not have significant influence on the fatigue life.

For contacts involving significant sliding velocity, such as angular contact ball bearings, thermal stresses can reach a significant percentage of the maximum Hertzian stress, which can appreciably influence fatigue life, as life is proportional to the 9th or 10th power of the maximum stress.

In the regime of partial elastohydrodynamic lubrication, stress redistribution from the first three factors based on smooth film elastohydrodynamic analysis becomes overshadowed by the intensified local surface stresses due to asperity contact. These local stresses usually result in surface fatigue of the contacts and may be designated as micro-elastohydrodynamic stresses. Fatigue experiments in this regime have shown that life decreases with decreasing values of the specific film thickness,  $\xi_0$ . Thus, increase in speed and viscosity in the partial film regime will suppress failures due to surface fatigue.

The influence of surface asperities on fatigue has been investigated extensively both by Dawson (208, 209, 210) and by Tallian, McCool and Sibley (177). They both show that life decreases when the specific film thickness decreases. Dawson's experiments, limited to soft steel disks, established an inverse power relationship between life and the inverse of the specific film thickness.

The results of Tallian et al (177) apply to rolling contacts, but are more qualitative. They simply demonstrate that a three fold increase in  $\xi_0$  from 1.7 to 5, induced by varying either the speed or viscosity can increase life by a factor of ten or more. As further support a number of experimental workers demonstrate a general increase of life with viscosity for a particular lubricant type.

The fatigue experiments in the partial elastohydrodynamic regime suggest that the mechanism of two colliding asperities in the presence of a lubricant is extremely important in understanding



fatigue in this regime. Pioneering work in this area has been contributed by Christensen (211, 212). He found that the maximum pressure between two spheres approaching each other under a constant load can exceed the Hertzian pressure if the speed and the pressure-viscosity exponent are large.

To sum up the discussion in this section, the influence of asperity encounter on surface fatigue is definitely significant. A direct measure of the frequency and severity of asperity encounter is the specific film thickness, which depends on the smooth-film elastohydrodynamic or macro-elastohydrodynamic film thickness. The formulae developed by Grubin (82), Dowson and Higginson (153) for line contacts, and Archard for point contacts (86), are therefore, useful in computing the specific film thickness, which determines whether or not asperity interactions are important. The calculation procedure used here is described in Section III.

c. Influence of Elastohydrodynamic Lubrication on Bearing Life

The previous discussion has shown that elastohydrodynamic lubrication has a major influence on the mode of failure in a bearing. Increasing the load of a rolling element bearing, for example, can have a major effect on the magnitude of the elastohydrodynamic film thickness, with the amount of direct metal contact varying from none to a substantial percentage as the load is increased. The effect also increases with temperature, i.e., as the lubricant viscosity dropped.

Fig. 85 has been prepared as a diagrammatic representation of the possible effects of film thickness on bearing-lubricant life. At very high film thickness, skidding may occur and the retainer will travel at too low a speed. This skidding may soon cause sliding metal-to-metal contact, surface damage, and increases in torque. At point A, the film thickness is low enough to cause pure rolling, a full elastohydrodynamic separating film exists, and life is limited only by lubricant supply.

As film thickness is further decreased toward B, a full elastohydrodynamic film separation still prevails, but friction is higher, the temperature increases and the rate of lubricant loss increases. The result is a gradually decreasing life.

Beyond B, the elastohydrodynamic film has decreased to the point where some metal-to-metal contact occurs. The failure mode begins to shift to wear and race damage. The bearing life begins to drop rapidly.

As the film is decreased to C and beyond, substantial ball-race interaction is occurring, and the life continues to drop.

This discussion illustrates the several effects film thickness may have on the life of the bearing-lubricant combination. Im-

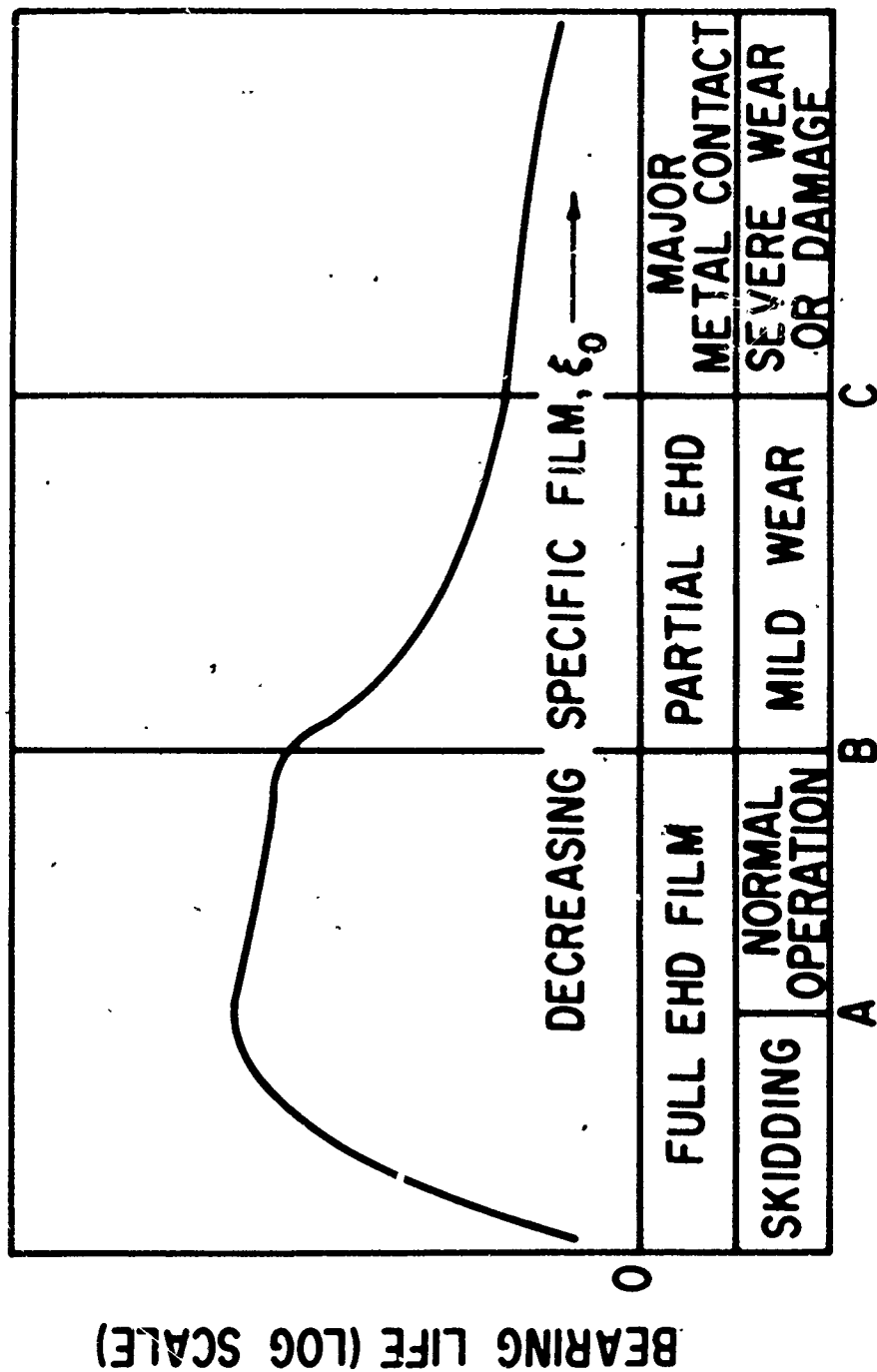


Fig. 85 Influence of Elastohydrodynamic Lubrication on Bearing Life.

plicit in this discussion, however, is the very significant additional fact that the influence of film thickness cannot be considered apart from other variables. For example, the load effect occurs primarily through its influence on lubricant film thickness in the contact zone, and it follows that other variables that also influence that film thickness will shift the failure mode. Thus, increases in speed and in lubricant viscosity, decreases in temperature, and decreases in surface roughness can be expected to shift the transition zones from one failure mode to another.

To aid in predicting the bearing lubrication regime and the failure mode which will dominate in that regime, an Elastohydrodynamic Performance Calculation Procedure has been developed and programmed for the computer. This procedure is discussed in Section III which follows.

### SECTION III

#### ELASTOHYDRODYNAMIC PERFORMANCE CALCULATION

Progress in elastohydrodynamic lubrication has advanced to the stage where development of practical design tools is now possible. The discussion in the previous section has summarized the available knowledge and identified the most modern design approaches. Based on this summary, a calculation procedure has been developed for predicting film thickness, percent of real area of contact, and other major variables in the elastohydrodynamic contact zone. The data calculated by this procedure will serve as a basis on which fatigue life of the contact and other types of ultimate failure can be predicted.

The design tool which has been the major goal of this study consists of a computer program which calculates all major variables in an elastohydrodynamic contact. The calculations are based either on the most reliable theory of elastohydrodynamic lubrication or on the empirical formula derived from the most recent experimental data. As outlined in the previous section, the input to the computer program consists of:

1. The radii of curvature in the direction as well as perpendicular to the direction of rolling for both contacting surfaces.
2. The surface speed for both contacting surfaces.
3. The load.
4. Material data.
5. Lubricant data.
6. Surface roughness for both contacting surfaces.

With these input data the program calculates the following quantities successively by means of a series of subroutines:

1. The nominal film thickness based on isothermal theory (the nominal film thickness is the film thickness at the entrance region of the elastohydrodynamic contact).
2. The reduction of film thickness due to thermal and side leakage effects.
3. The exit protrusion width and depth.
4. Percentage of area of contact.
5. Contact friction.
6. Pressure distribution.
7. Mid-film and surface temperatures.
8. Subsurface and surface stress distributions.

The use of subroutines provides a convenient way to replace any old methods of calculation with any new techniques which may be developed in the future for any one of these variables. Using this approach, one does not have to rewrite the main computer program as the state-of-the-art of elastohydrodynamic lubrication advances.

The computer program is primarily intended for use on rolling element bearing contact problems. However, it has been made general enough so that it is applicable to many other heavily loaded concentrated contact problems. Thus, it should also find use in the design of gears, cams, and pivots.

## 1. FLOW DIAGRAM

The calculations performed in the computer program can be represented by the flow diagram shown in Fig. 86.

## 2. ANALYSIS

The analysis for the variables listed in the flow diagram are described in the following sections.

### a. Dimension of the Contact Ellipse

The semi-major and -minor axes of the contact ellipse for a given total load  $P$ , geometry and material properties are calculated from Equations 40 and 41 on page 119.

### b. Load and Speed Parameters

When the Hertzian pressure distribution of an elliptical contact is replaced by an equivalent line contact with the same total load and maximum Hertz pressure, the effective width of the line contact becomes

$$l_{\text{effective}} = \frac{\frac{2}{3}a}{2} = \frac{4}{3}a \quad (62)$$

The effective load per unit width for an equivalent line-contact is

$$w = \frac{3P}{4a} \quad (63)$$

The dimensionless load parameter for the equivalent line-contact is given by

$$\bar{W} = \frac{w}{E'R'_x} \quad (64)$$

The dimensionless speed parameter is

$$\bar{U} = \frac{\mu_o U}{E'R'_x} \quad (65)$$

where

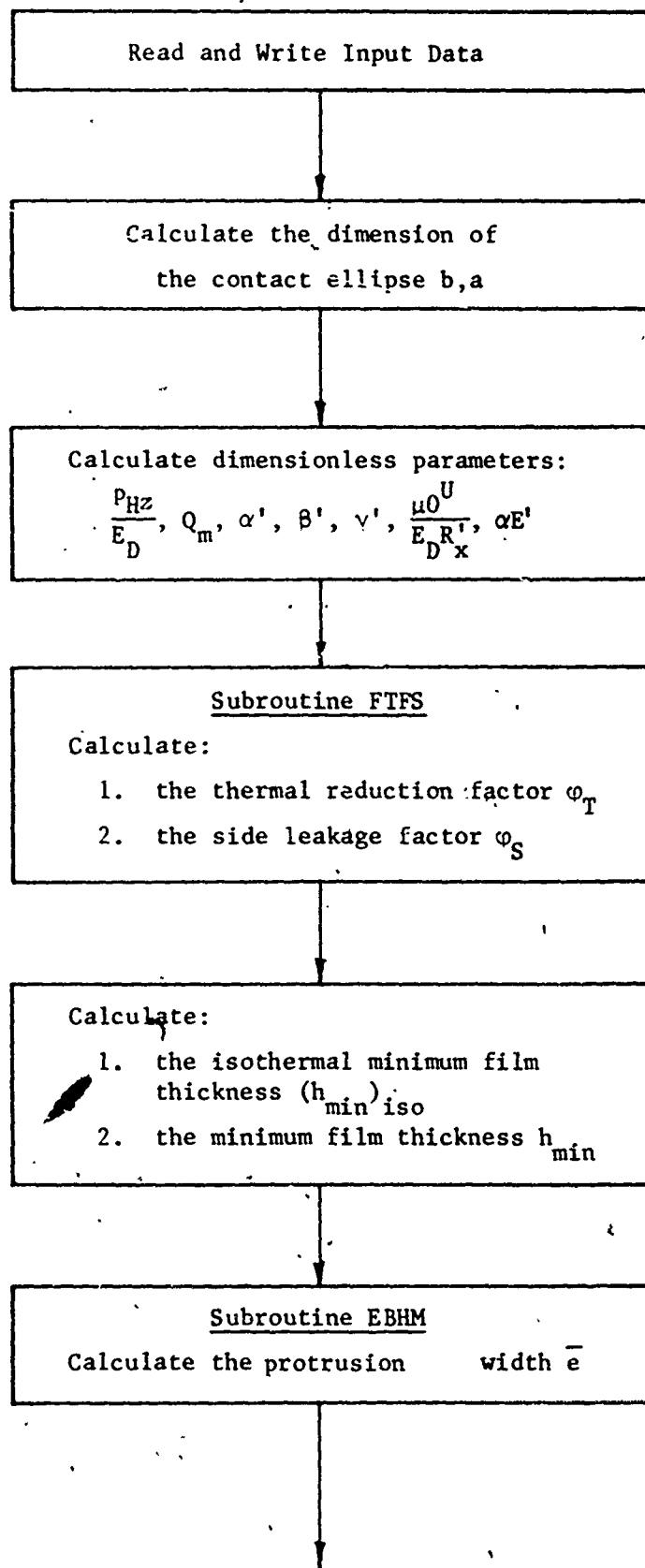


Fig. 86 Computer Program Flow Diagram.

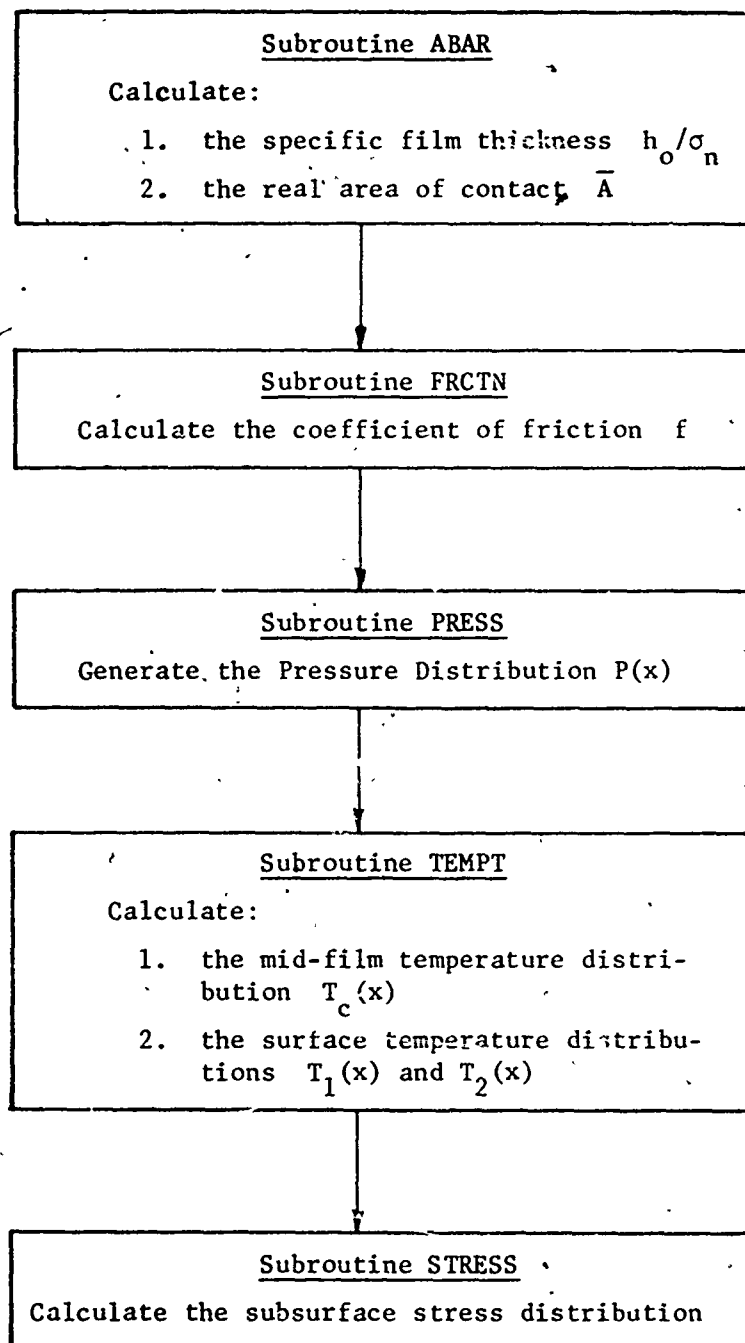


Figure 86 (Continued)

$$\begin{aligned}
 \mu_o &= \text{inlet viscosity} & \text{lb-sec/in}^2 \\
 U &= \text{rolling velocity} & \text{in/sec} \\
 \frac{1}{E'} &= \frac{1}{2} \left( \frac{1-v_1^2}{E_1} + \frac{1-v_2^2}{E_2} \right) & \text{in}^2/\text{lb}
 \end{aligned}
 \quad \left. \vphantom{\begin{aligned} \mu_o \\ U \\ \frac{1}{E'} \end{aligned}} \right\} (66)$$

The maximum Hertz pressure parameter becomes

$$\frac{P_{HZ}}{E'} = \frac{3}{2} \frac{P}{\pi a b E'} \quad \text{for the elliptical contact} \quad (67)$$

and

$$\frac{P_{HZ}}{E'} = \frac{1}{\pi} \sqrt{\frac{w}{E' R'_x}} \quad \text{for the line contact} \quad (68)$$

#### c. Lubricant Parameters

$$\begin{aligned}
 \bar{G} &= \alpha E' \\
 \alpha' &= \alpha \frac{\pi}{2} P_{HZ} \\
 \beta' &= \beta / T_o \\
 \nu' &= \nu \frac{\pi}{2} \frac{P_{HZ}}{T_o}
 \end{aligned}
 \quad \left. \vphantom{\begin{aligned} \bar{G} \\ \alpha' \\ \beta' \\ \nu' \end{aligned}} \right\} (69)$$

#### d. Thermal Parameters

$$\begin{aligned}
 Q_m &= \frac{\mu_o (U_1 + U_2)^2}{2 K_f T_o} \\
 Q_c &= \frac{\rho c f U_a^3}{8 K_f R'_x} \\
 D_1 &= \left( \frac{K_f^2}{\pi \rho_1 C_1 U_1 K_1} \right)^{1/2} \left( \frac{R'_x E'}{4 w^3} \right)^{1/4} \\
 D_2 &= \left( \frac{K_f^2}{\pi \rho_2 C_2 U_2 K_2} \right)^{1/2} \left( \frac{R'_x E'}{4 w^3} \right)^{1/4}
 \end{aligned}
 \quad \left. \vphantom{\begin{aligned} Q_m \\ Q_c \\ D_1 \\ D_2 \end{aligned}} \right\} (70)$$



#### e. Thermal Reduction Factor

The calculation of the thermal reduction factor  $\phi_T$  is based on the numerical data developed by Cheng (105). In that report, the value  $\phi_T$  is plotted against the viscous heating variable  $Q_m$  with the following variables as parameters:

$$\alpha^* = \alpha \cdot \frac{\pi}{2} \cdot 10^5$$

$$\beta' = \frac{\beta}{T_o}$$

$$\frac{P_{HZ}}{E'} = \text{dimensionless Hertz pressure}$$

$$s = \text{slip ratio} = \frac{U_2 - U_1}{U_2}$$

In the analysis of the thermal film thickness, the heat convected by the lubricant and the heat conducted by the discs are both considered. In accounting for the heat conduction to the solids, the thermal properties ( $K_1$ ,  $\rho_1$ ,  $C_1$ ) of steel are used in the calculations. However, it was found that the surface temperature rise due to the heat of conduction to the solids at high speeds is insignificant compared to the film temperature rise. Consequently, these data should be also applicable to contacting materials whose thermal properties are not drastically different from those of the steel. To include the heat of convection, the thermal properties of mineral oils are used. As discussed in Section II, these properties do not vary greatly and the data in Ref. 105 should be good for all lubricants.

In Ref. 105, the curves for  $\phi_T$  indicate that the most influential parameters is the viscous heating parameter  $Q_m$ . The other four parameters,  $\alpha^*$ ,  $\beta'$ ,  $\frac{P_{HZ}}{E'}$ , and  $s$  all play secondary roles in governing the thermal reduction factor. In particular, the influence of the slip ratio is very mild. A review of these curves shows that within the range of the parameters investigated, the thermal reduction factor can be represented by

$$\phi_T = f_1 (1 - 0.1 s) (1 + f_3 \frac{P_{HZ}}{E'}) \quad (72)$$

where  $f_1$  and  $f_3$  are numerical functions of  $Q_m$ ,  $\alpha^*$ ,  $\beta'$ , and are tabulated in Tables XIII and XIV.

These numerical data are programmed within the subroutine FTFS, and  $\phi_T$  is calculated by linear interpolation within the range listed in the tables and by linear extrapolation outside the range.

TABLE XIII  
VARIATIONS OF  $f_1$  WITH RESPECT TO

$\alpha^*$ ,  $\frac{\beta'}{\alpha^*}$ , and  $Q_m$ .

$$(\alpha^* = \alpha \cdot \frac{\pi}{2} \cdot 10^5, \beta' / \alpha^* = \frac{\beta}{\alpha} \cdot \frac{1}{T_{o2} \cdot \frac{\pi}{2} \cdot 10^5})$$

$\beta' / \alpha^*$	15.71	15.71	15.71	23.56	23.56	23.56	31.42	31.42	31.42
$Q_m$	0.35	0.5	0.75	0.35	0.5	0.75	0.35	0.9	0.75
0.0	1.0	1.0	1.0	1.0	1.0	1.0	1.0	1.0	1.0
0.01	.99	.98	.98	.99	.97	.97	.98	.98	.98
0.02	.98	.96	.96	.98	.95	.94	.96	.95	.94
0.05	.96	.94	.93	.95	.92	.90	.93	.90	.89
0.1	.93	.9	.89	.9	.87	.84	.90	.85	.82
0.2	.89	.86	.81	.86	.81	.76	.84	.78	.74
0.5	.8	.78	.66	.77	.7	.72	.75	.66	.59
1.0	.72	.65	.56	.67	.6	.50	.66	.56	.46
2.0	.62	.53	.44	.57	.47	.36	.56	.45	.35
5.0	.47	.37	.3	.44	.32	.24	.43	.31	.23
10.0	.36	.27	.22	.34	.22	.17	.34	.21	.15

TABLE XIV  
 VARIATION OF  $f_3$  WITH RESPECT TO  
 $\alpha^*$ ,  $\beta'/\alpha^*$ , and  $Q_m$

$$(\alpha^* = \alpha \frac{\pi}{2} \cdot 10^5, \beta'/\alpha^* = \frac{\beta}{\alpha T_{o2} \frac{\pi}{2} \cdot 10^5})$$

$\beta'/\alpha^*$ $Q_m$	$\alpha^*$ 15.71			23.56			31.42		
	0.35	0.5	0.75	0.35	0.5	0.75	0.35	0.5	0.75
0.0	0.0	0.0	0.0	0.0	0.0	0.0	0.0	0.0	0.0
0.5	0.0	3.6	3.95	0.0	3.78	4.34	0.0	8.3	4.6
1.0	0.0	12.8	12.4	0.0	11.4	8.2	4.1	12.4	12.0
5.0	47.5	48.8	40.7	26.5	17.6	30.1	12.9	13.75	19.4
10.0	107.8	75.6	51.4	52.9	26.5	25.6	25.6	20.9	19.5

f. Side Leakage Reduction Factor

The side leakage reduction factor for an elliptical contact is determined by the formula proposed by Cheng (213) based on a numerical solution to the hydrodynamic equation in the inlet region of an elliptical contact. According to Ref. 213, the dimensionless film thickness can be expressed as

$$\frac{h_o}{R'_x} = C \left[ \frac{\mu_o U \alpha}{R'_x} \right]^{n_1} \left[ \frac{p_{HZ}}{E'} \right]^{n_2} \quad (73)$$

where C,  $n_1$ , and  $n_2$  are numerical functions of  $a/b$ . These values are shown in Table XV.

TABLE XV  
NUMERICAL FUNCTIONS OF C,  $n_1$  AND  $n_2$

$\gamma' = a/b$	C	$n_1$	$n_2$
5	1.625	0.74	-0.22
2	1.56	0.736	-0.209
1	1.415	0.725	-0.174
0.5	1.132	0.688	-0.066

Assuming that the film thickness at  $a/b = 5$  approaches that of a line-contact, then the side leakage reduction factor becomes

$$\varphi_S = \frac{C}{C_{\gamma'=5}} \left[ \frac{\mu_o U \alpha}{R'_x} \right]^{n_1 - (n_1)_{\gamma'=5}} \left[ \frac{p_{HZ}}{E'} \right]^{n_2 - (n_2)_{\gamma'=5}} \quad (73)$$

g. Minimum Film Thickness

In calculating the minimum film thickness for the isothermal case, the formulas proposed by Dowson and Higginson (153) based on their numerical solution is used.

$$(h_{min})_{iso} = R'_x \left[ 1.6 \frac{(\alpha E')^{0.6} \left( \frac{\mu_o U}{E' R'_x} \right)^{0.7}}{\left( \frac{w}{E' R'_x} \right)^{0.13}} \right] \quad (74)$$

multiplying this by the thermal and side leakage reduction factors, one obtains the actual film thickness

$$h_{\min} = (h_{\min})_{\text{iso}} \phi_T \phi_S \quad (75)$$

#### h. Protrusion Width

In determining the real area of contact in an elastohydrodynamic contact, it is necessary to know the extent of the protrusion at the exit of the contact. As indicated by all elastohydrodynamic theories, the film profile consists of a parallel portion at the entrance followed by a protrusion with an approximately half-sinusoidal or parabolic profile. To date there has been no analysis available to predict the width of this protrusion. To fill this gap, analysis is made in Appendix II, and it shows that the protrusion width can be represented by an expression similar to that of the Dowson-Higginson's film thickness formula (153).

$$\bar{e} = \frac{K}{24I_1} (\alpha E')^{0.2} \left[ \frac{\mu_0 U}{E' R'_x} \right]^{0.4} W^{-0.76} \quad (76)$$

where K is a proportional constant and

$$I_1 = \int_0^1 \left( \frac{H_1 - 1}{H_3} \right) d\eta \quad (77)$$

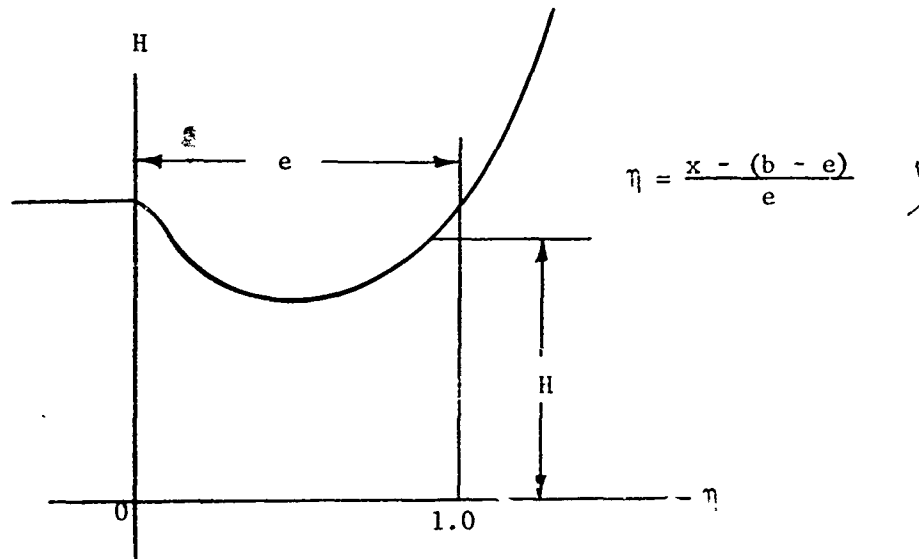


Fig. 87 Protrusion Width

TABLE XVI  
ANALYSIS OF  $\bar{e}$  BASED ON CHENG'S ISOTHERMAL THEORY (REF. 93)

$s = 0.0$	$\frac{u_o}{E'R'_x}$	$\frac{w}{E'R'_x}$	$\alpha E'$	$\bar{e}$	$\bar{H}_e = \frac{h_e}{h_o}$
0.0	$.38 \times 10^{-11}$	$2.828 \times 10^{-5}$	5650	.198	.861
0.0	$1.22 \times 10^{-11}$	$2.828 \times 10^{-5}$	5650	.35	.861
0.0	$3.00 \times 10^{-11}$	$2.828 \times 10^{-5}$	5650	.51	.863
0.0	$6.21 \times 10^{-11}$	$2.828 \times 10^{-5}$	5650	.715	.870
0.0	$11.75 \times 10^{-11}$	$2.828 \times 10^{-5}$	5650	.890	.875

TABLE XVII  
ANALYSIS OF  $\bar{e}$  BASED ON CHENG'S THERMAL THEORY (REF. 93)

$s = \frac{U_2 - U_1}{U_2}$	$\bar{U} = \frac{\mu_0 U}{E' R'_x}$	$\frac{w}{E' R'_x}$	$\alpha E'$	$\bar{e} = e/b$	$H_e = \frac{h_e}{h_o}$
0.005	$2.87 \times 10^{-11}$	$2.828 \times 10^{-5}$	4473	.49	.854
0.005	$6.01 \times 10^{-11}$	$2.828 \times 10^{-5}$	4473	.65	.859
0.005	$11.662 \times 10^{-11}$	$2.828 \times 10^{-5}$	4473	.81?	.859
0.005	$18.00 \times 10^{-11}$	$2.828 \times 10^{-5}$	4473	1.03	.849
0.020	$2.715 \times 10^{-11}$	$2.828 \times 10^{-5}$	4473	.465	.854
0.020	$5.360 \times 10^{-11}$	$2.828 \times 10^{-5}$	4473	.65	.854
0.020	$9.91 \times 10^{-11}$	$2.828 \times 10^{-5}$	4473	.83	.849
0.020	$16.38 \times 10^{-11}$	$2.828 \times 10^{-5}$	4473	1.04	.838
0.050	$2.50 \times 10^{-11}$	$2.828 \times 10^{-5}$	4473	.49	.838
0.050	$4.87 \times 10^{-11}$	$2.828 \times 10^{-5}$	4473	.65	.838
0.050	$8.34 \times 10^{-11}$	$2.828 \times 10^{-5}$	4473	.835	.838
0.050	$14.55 \times 10^{-11}$	$2.828 \times 10^{-5}$	4473	1.02	.832
0.100	$2.238 \times 10^{-11}$	$2.828 \times 10^{-5}$	4473	.50	.827
0.100	$4.434 \times 10^{-11}$	$2.828 \times 10^{-5}$	4473	.667	.838
0.100	$7.611 \times 10^{-11}$	$2.828 \times 10^{-5}$	4473	.85	.832
0.100	$12.61 \times 10^{-11}$	$2.828 \times 10^{-5}$	4473	1.04	.827
0.250	$1.76 \times 10^{-11}$	$2.828 \times 10^{-5}$	4473	.50	.795
0.250	$3.62 \times 10^{-11}$	$2.828 \times 10^{-5}$	4473	.667	.805
0.250	$5.85 \times 10^{-11}$	$2.828 \times 10^{-5}$	4473	.833	.805
0.250	$5.52 \times 10^{-11}$	$2.828 \times 10^{-5}$	4473	1.00	.805

It is noted that if the normalized protrusion shape  $H(\eta)$  does not vary much with the operating conditions, the  $I_1$  will not be a function of  $\alpha E'$ ,  $\frac{\mu U}{E' R'_x}$ , and  $W$ . Consequently, the above exponential relations should give the correct variation of the  $\bar{e}$  with the speed, load and pressure-viscosity parameter.

To validate this approximate theory, the current protrusion-width data were plotted in Figs. 88 and 89. Fig. 90 shows the relation between  $\bar{e}$  and the speed parameter. It was found that the Dowson-Higginson (153), Dowson-Whittaker (114), and Cheng's (105) data all give a slope almost exactly equal to 0.4, thus validating the exponential relation with the speed parameter. Fig. 90 plots  $\bar{e}$  against  $W$  for two values of  $\bar{G}$ . These curves give an exponent between -0.79 and -0.85 for  $w$  and an exponent between +.13 and +.21 for  $G$ , which agree well with that arrived from the analysis.

In Cheng's thermal elastohydrodynamic data (93), it is shown that the  $\bar{e}$  also varies slightly with the slip ratio  $(U_2 - U_1)/U_2$ . The value of  $\bar{e}$  along with the protrusion depth are tabulated in Tables XVI and XVII. Based upon these data, the protrusion width data can be put in the following final form.

$$\bar{e} = C' (\alpha E')^{0.2} \left[ \frac{\mu U}{E' R'_x} \right]^\epsilon \left[ \frac{W}{E' R'_x} \right]^{-0.76} \quad (78)$$

where the value of  $\epsilon$  and  $C'$  are listed in Table XVIII.

TABLE XVIII  
VARIATION OF  $\epsilon$  AND  $C$  WITH SLIP

$\frac{U_2 - U_1}{U_2}$	$\epsilon$	$C'$
0.0	0.4	0.51
0.05	0.41	0.704
0.10	0.42	0.958
0.25	0.43	1.30

These values are used in the computer program to predict the protrusion width.

Fig. 88 also plots the variation of  $H_{\min}$  or protrusion depth with  $\bar{U}$



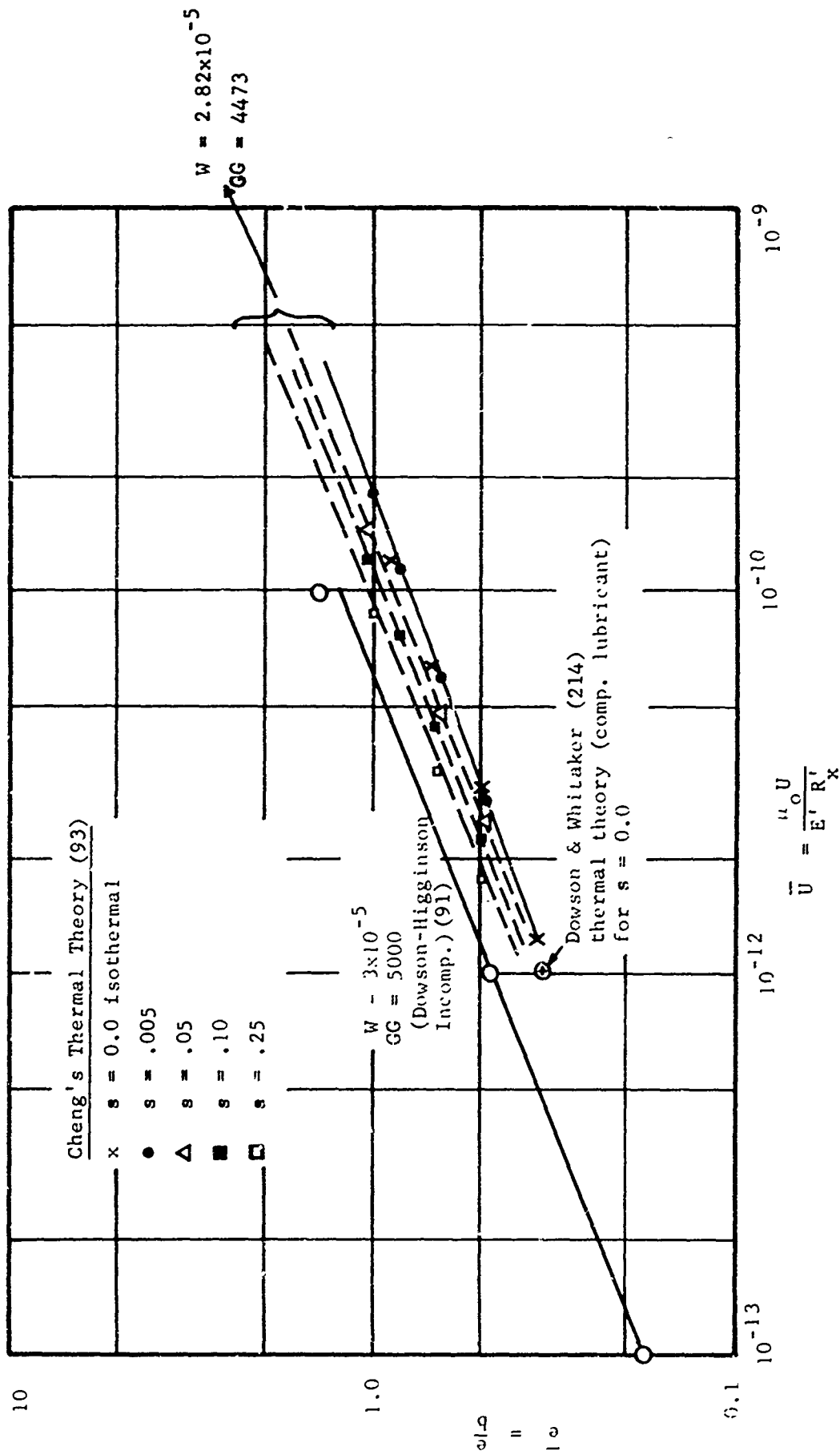


Fig. 88 Protrusion Width versus Velocity Parameter

# EFFECT OF $W$ ON $\bar{e}$

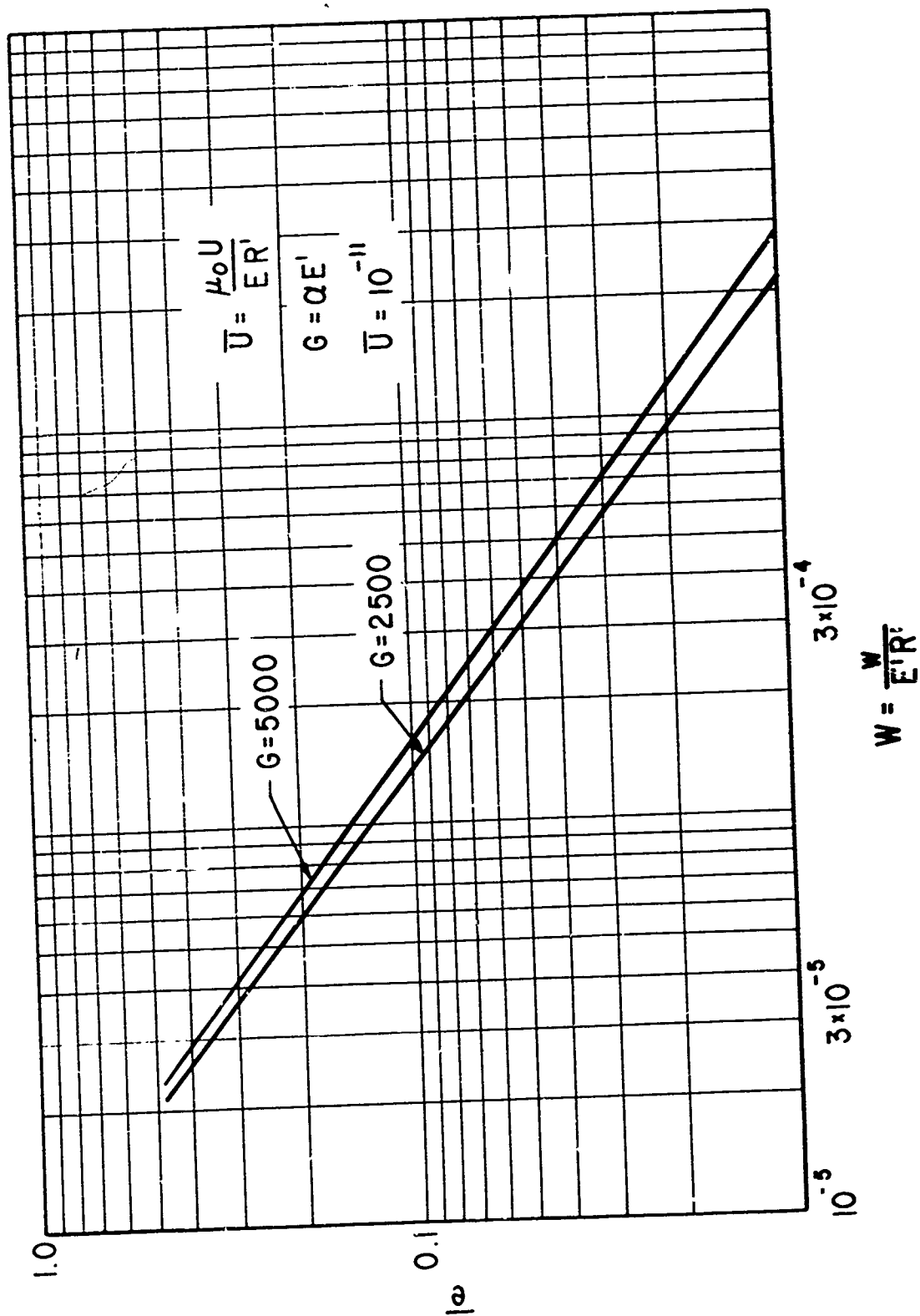


Fig. 89 Effect of Load Parameter on Protrusion Width.

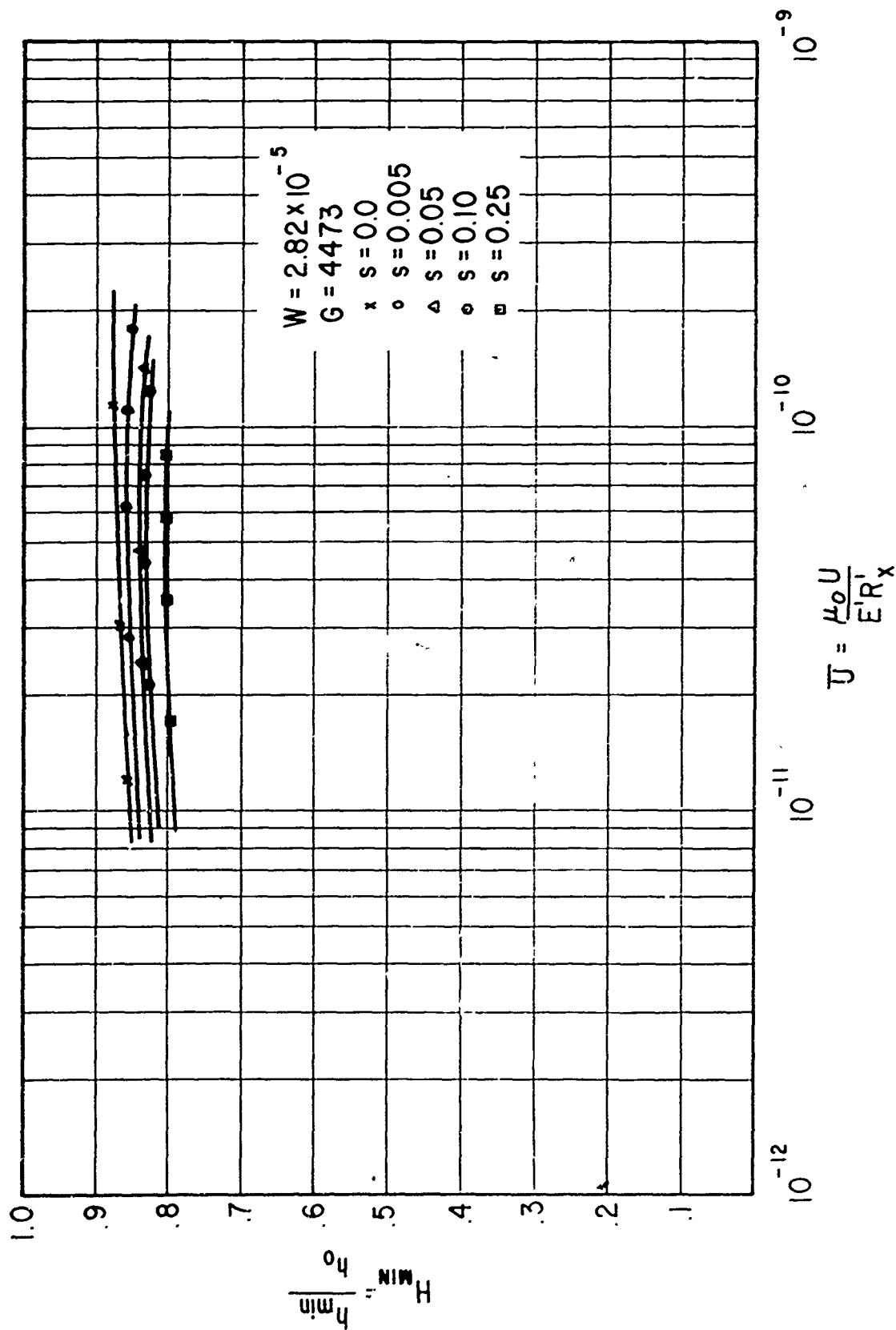


Fig. 90 Minimum Film Thickness vs. Velocity Parameter.

for various slip ratios. It is seen that  $H_{\min}$  is close to 0.8, which is the value used in the computer program regardless of the operating parameters.

#### i. Area of Contact

Whenever the ratio of the nominal film thickness to the effective root mean square value of the surface roughness of an elastohydrodynamic contact is smaller than 4, there will be occasional surface contact. The extent of the contact area is dependent upon the ratio of the elastohydrodynamic film thickness to surface roughness, the shape of the elastohydrodynamic film distribution, and the surface topography. Tallian, et al (177) have developed a combined graphical-numerical approach to predict the extent of the surface contact for surface topography either determined experimentally or generated by a random process. Their method gives the relation between the contact duration, that is the fraction of time during which there is at least on asperity in contact, and the specific film thickness. While this method has an advantage of being able to accommodate any arbitrary surface topography, it lacks simplicity and is somewhat inconvenient for extended computations. There is a need for a simple analysis to study the extent of surface contacts in a partial elastohydrodynamic contact. The analysis described here is aimed at achieving this objective.

This simple analysis is based upon the following two major assumptions:

- 1) The shape of the protrusion from the smooth film elastohydrodynamic theory is approximated by a half-sine wave where the amplitude and the half-wave length correspond to the depth and width of the protrusion.
- 2) The height distribution of the surface roughness is Gaussian and the surface roughness is two dimensional with a roughness profile made of straight line segments.

Based on the detail analysis described in Appendix III, a computer subroutine named ABAR was written which calculates the real area of contact for a given specific film thickness ratio, protrusion width, and protrusion depth.

Typical results are shown in Fig. 91 which plots the percentage of the area of contact  $A_r$ , against the normalized film thickness  $h_0/\sigma$  where  $h_0$  is the smooth film elastohydrodynamic film thickness at the inlet, and  $\sigma$  is the combined standard deviation of both surfaces,  $\sigma = (\sigma_1^2 + \sigma_2^2)^{1/2}$ . Four cases are shown in this probability plot. The straight line is for the condition of zero protrusion width. The other three cases indicate the effect of the protrusion width or depth on  $A_r$ . It is seen that for  $A_r > 20\%$ , the increase in area of contact due to the protrusion is negligible. In the region of high  $h_0/\sigma$ , that is the transitional zone between the full-film and partial-film elastohydrodynamic lubrication, the protrusion has a pronounced effect

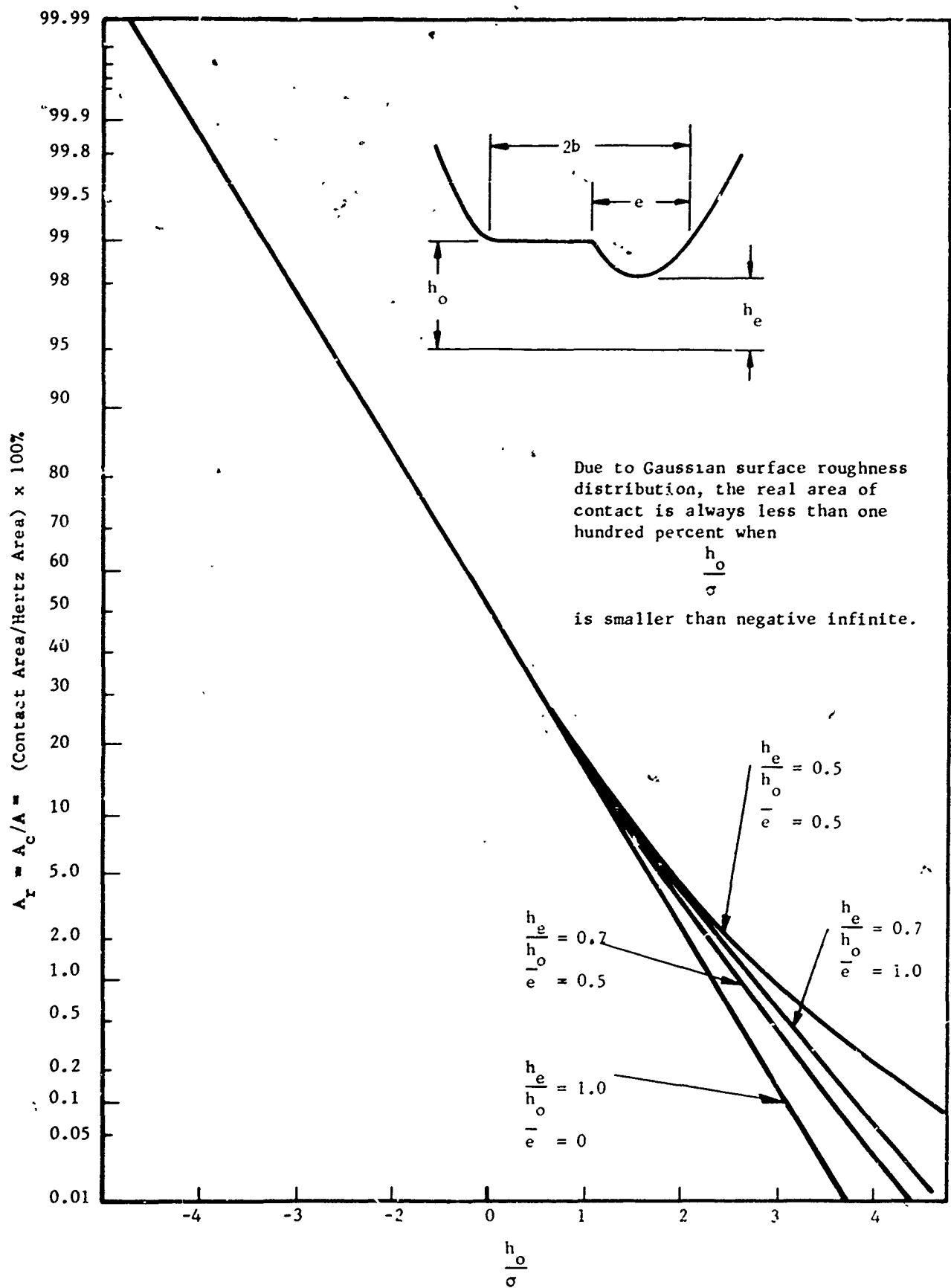


Fig. 91 Variation of Area of Contact Ratio with  $\frac{h_o}{\sigma}$

upon the area of contact. These curves also indicate that the protrusion depth has a stronger effect than the protrusion width,

#### j. Frictional Coefficient

Even though the state-of-the-art of elastohydrodynamic theory has advanced to a fairly sophisticated stage, there exists no reliable theory to predict friction between two heavily loaded sliding contacts. Because of the lack of accurate friction analysis, the determination of the coefficient of friction in this program is achieved empirically based on the experimental data of Johnson and Cameron. (129). Since Johnson's experimental data covers only a restricted range of rolling and sliding speeds and lubricant parameters, the application of their data to conditions other than those used in the experiment must be achieved by plotting their data on the pertinent dimensionless parameters governing friction. In order to identify these pertinent dimensionless parameters it is necessary to perform a simplified analysis of friction similar to that developed by Crook (126). The analysis is summarized in Appendix IV.

It is seen from Appendix IV, the coefficient of friction,  $f$ , is governed by three parameters:

$$\left. \begin{aligned} G_1 &= \frac{\mu_o u_s}{p_{HZ} h} \\ G_2 &= \frac{\beta_1 \mu_o u_s^2}{8K_f} \\ G_3 &= \alpha p_{HZ} \end{aligned} \right\} \quad (79)$$

Physically,  $G_1$  measures the effect of shear rate, whereas  $G_2$  and  $G_3$  represent the thermal heating effect and pressure-viscosity effect respectively.

Graphs of frictional coefficient as a function of  $G_1$  and  $G_3$  for a given  $G_2$  are shown in Figs. 92 through 98. In all the graphs the solid portion of the curve is plotted from Johnson and Cameron's experimental data, whereas the dotted curve is an extrapolation of the experimental data to cover broader ranges of speed, load, and lubricant parameters. It is seen that at small values of  $G_1$  all curves have a 45 degree slope. This corresponds to the fact that at small sliding speeds the frictional coefficient varies linearly with sliding speed. In each graph all curves merge at large values of  $G_1$ , to a common value, which is the so-called "ceiling" found by Johnson and Cameron and also by Plint (131) as shown in Fig. 49. The "ceiling" decreases with increasing  $G_2$ . The existence of a ceiling in friction suggests that there is a limiting shear stress in a lubricant

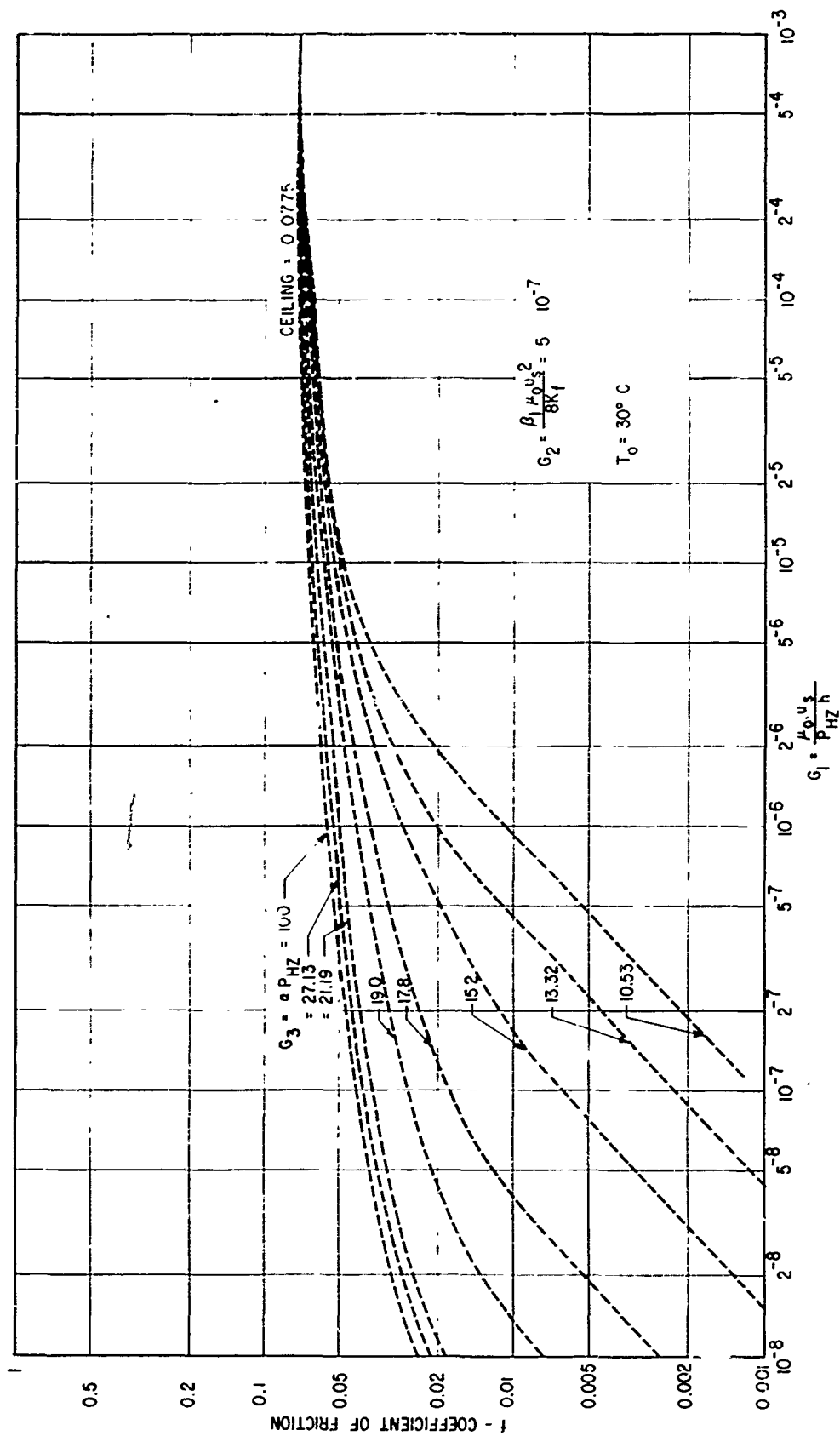


Fig. 92 Coefficient of Friction vs. Shear Rate Parameter for Heating Parameter =  $5 \times 10^{-7}$ .

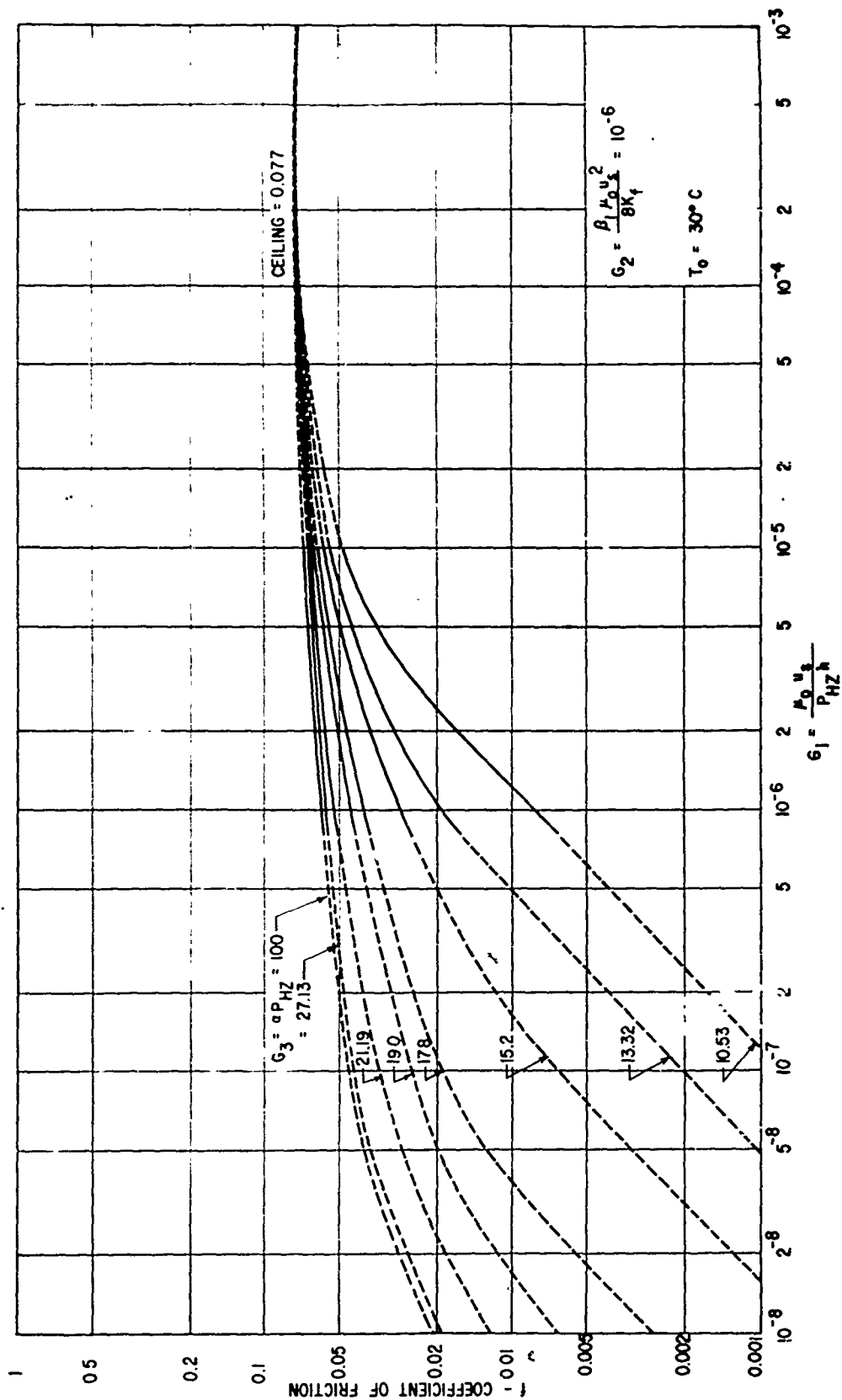


Fig. 93 Coefficient of Friction vs. Shear Rate Parameter  
for Heating Parameter =  $10^{-6}$ .



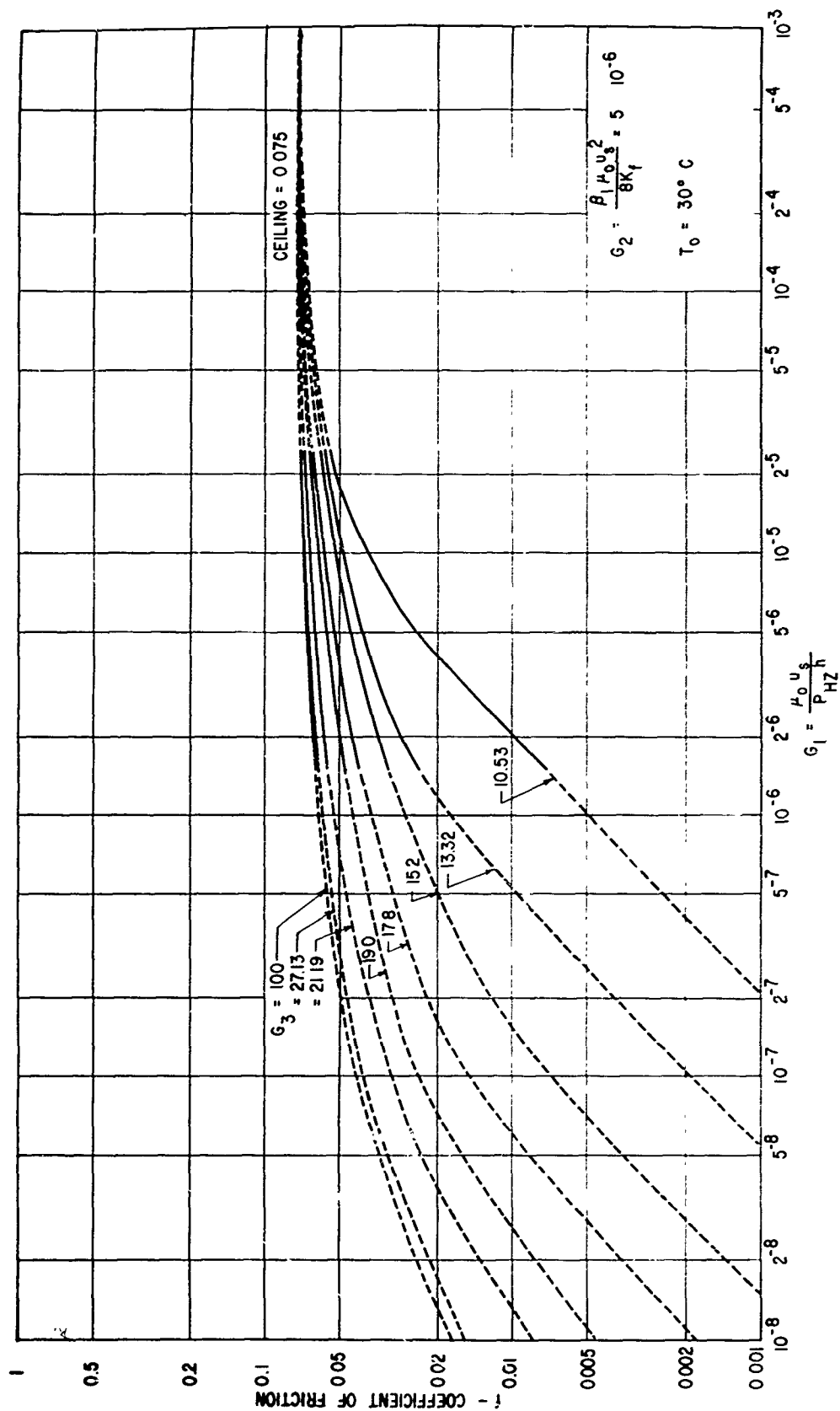


Fig. 94 Coefficient of Friction vs. Shear Rate Parameter for Heating Parameter =  $5 \times 10^{-6}$ .

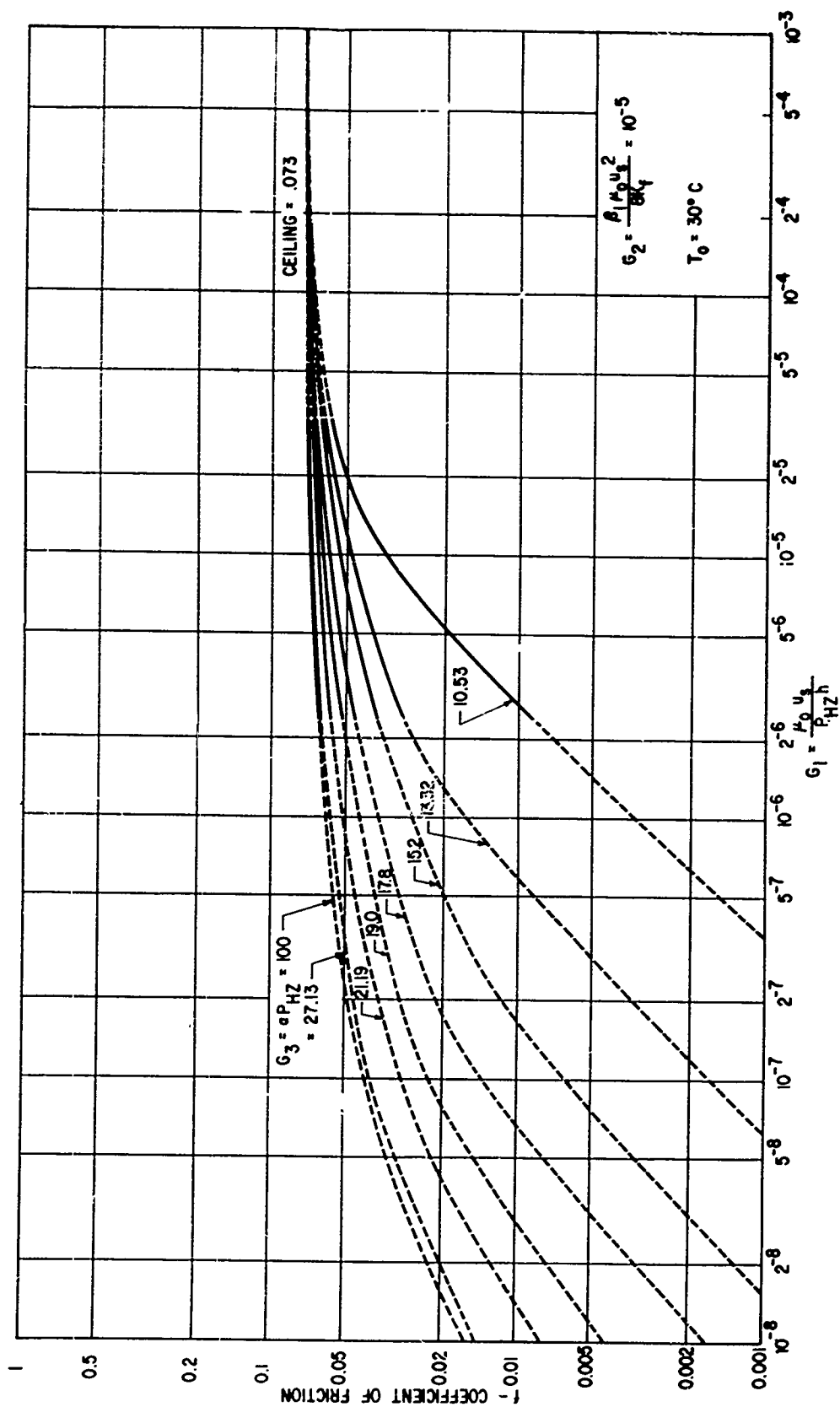


Fig. 95 Coefficient of Friction vs. Shear Rate Parameter for Heating Parameter = 10-5.

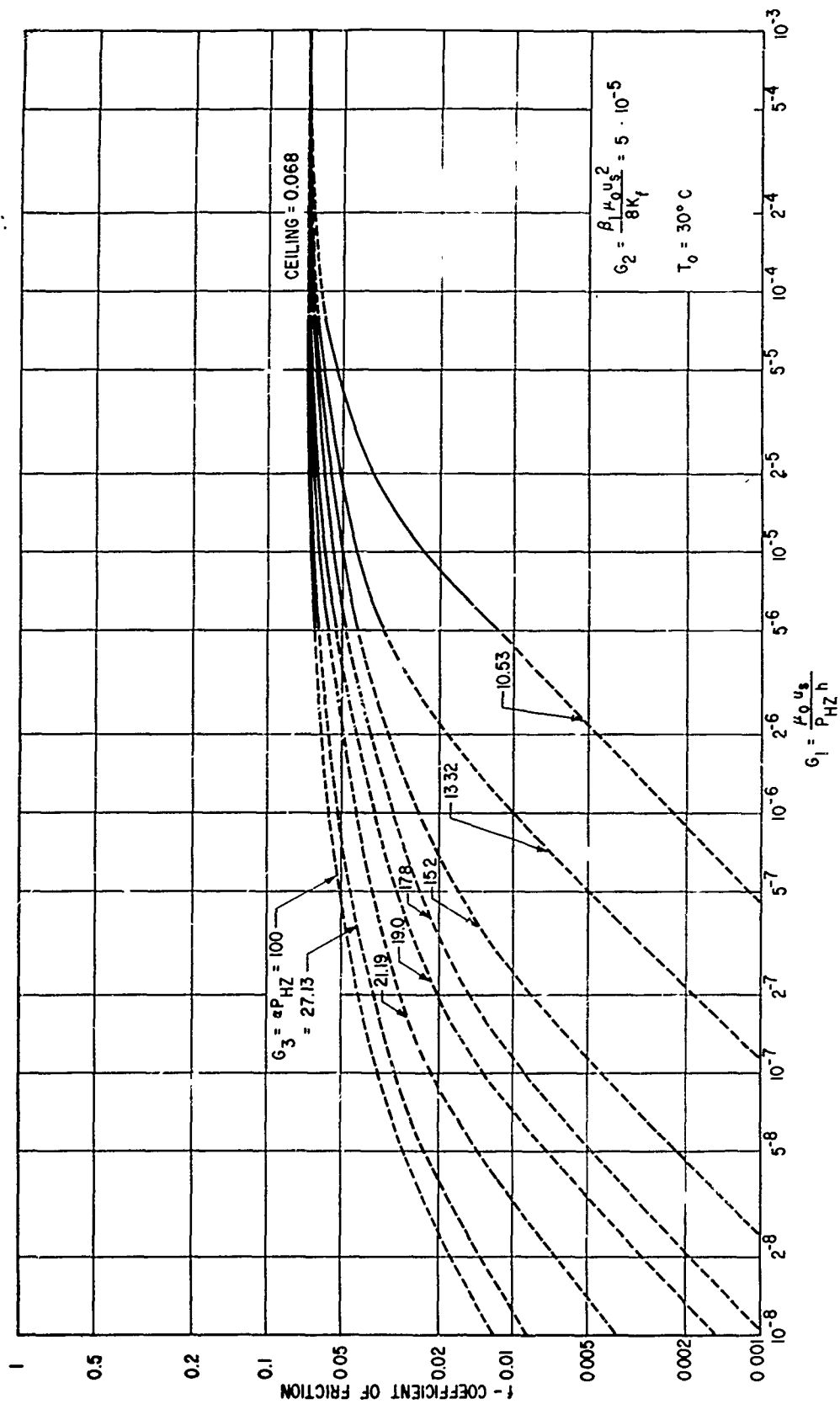


Fig. 96 Coefficient of Friction vs. Shear Rate Parameter for Heating Parameter =  $5 \times 10^{-5}$ .

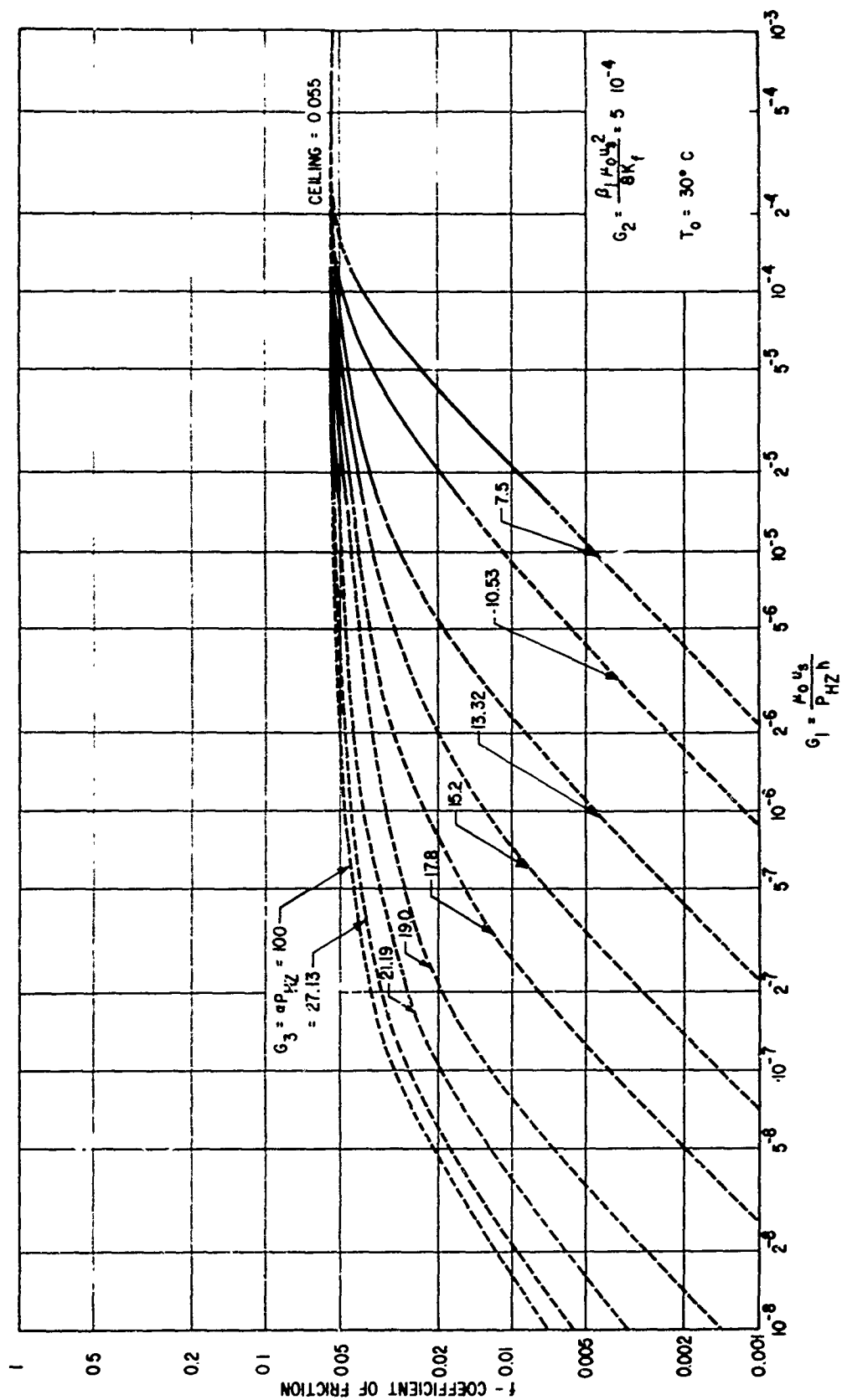


Fig. 97 Coefficient of Friction vs. Shear Rate Parameter for Heating Parameter =  $5 \times 10^{-4}$ .

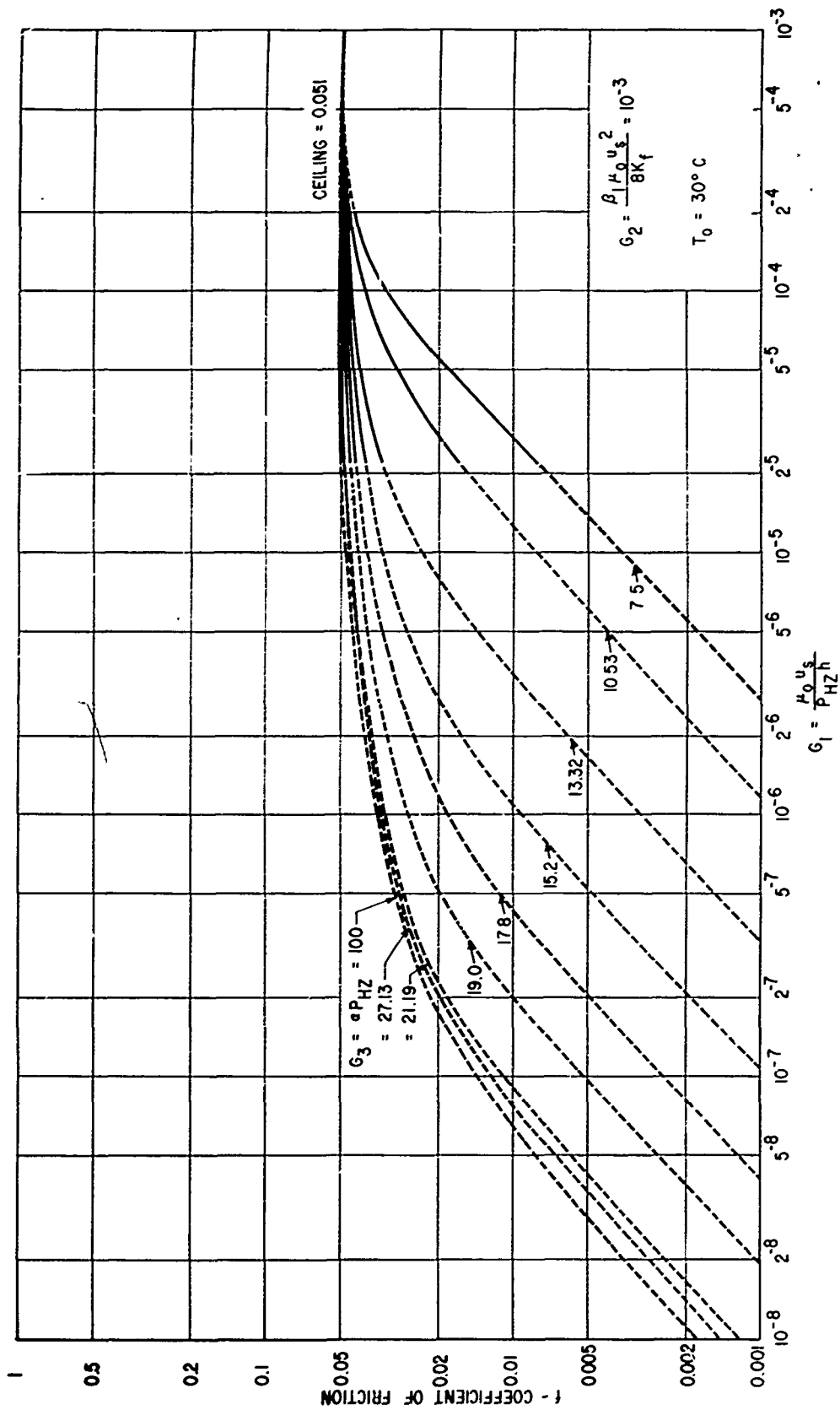


Fig. 98 Coefficient of Friction vs. Shear Rate Parameter for Heating Parameter =  $10^{-3}$ .

film.

It should be noted that all the frictional coefficient graphs are for a given inlet lubricant temperature, 30°C. Change of inlet temperature affects the frictional coefficient due to the dependence of the limiting shear stress upon the inlet temperature. Johnson and Cameron (129) and Plint (131) investigated this inlet temperature effect. Plint's experiment shows that the variation of frictional coefficient with inlet temperature is approximately linear and the slope does not seem to vary much with either rolling or sliding speed. The slope was found to be  $-0.001/^{\circ}\text{F}$ . This fact is used in Appendix IV to predict frictional coefficients for inlet temperature other than 30°C.

#### k. Pressure Distribution

Almost all elastohydrodynamic theories thus far have shown that the pressure profile for heavily loaded contacts does not deviate much from the Hertzian elliptical pressure profile. The deviation occurs mainly in the inlet and the exit regions. Due to the elastohydrodynamic action there is a gradual build-up in pressure ahead of the Hertzian region which is absent in the case of a dry contact. In the contact zone the pressure profile is essentially Hertzian. In the exit region, the elastohydrodynamic theories show that there exists a pressure spike right at the point the protrusion begins. After the pressure spike, the pressure decays extremely rapidly to the ambient pressure. This has been previously illustrated in Fig. 13.

Unfortunately, the exact details of the pressure profile at the inlet and near the pressure spike can only be obtained by solving numerically the simultaneous elasticity, hydrodynamic and energy equations. Such an iterative numerical solution for the pressure profile required a large amount of computation time and the convergence of the solution is not necessarily guaranteed particularly at high speeds and high loads. For this reason the full elastohydrodynamic solution has not been chosen at this time to obtain the pressure profile for this preliminary design tool. Instead, an approximate pressure profile is computed in this program and it is based upon the following assumptions:

- The pressure build-up at the inlet is calculated by assuming that the deformation profile follows the Hertzian elasticity solution.
- The pressure spike occurs exactly at the point where the protrusion begins.
- Pressure increase before the spike and the pressure decay after the spike are assumed to be parabolic.
- The magnitude of the spike is determined by assuming that the

integration of the pressure profile between the center line of the contact and the exit is equal to half of the load.

Details regarding the calculation of this approximate pressure profile are included in Appendix V.

#### 1. Temperature Distribution.

In calculating the surface and film temperature distributions in an elastohydrodynamic contact, the available numerical methods are reasonably complete and accurate. These methods can be divided into two categories. The first category is only applicable to the inlet region and the second category is for the contact region. The inlet thermal methods are for moderate pressure only, and they contain special numerical treatments which avoid the numerical instability associated with the reverse flow in the inlet region. The methods for the contact region are specially designed for high pressure, and are not suitable for calculations at the inlet where there is a negative flow. The descriptions of these methods are given below.

##### (1) Mean Viscosity Method (For the Contact Region Only)

The thermal analysis for this method is based upon the assumption that the viscosity across the film is constant and corresponds to the mean temperature across the film. Using this assumption, the temperature across the film can be integrated analytically. With this analytical integration, the finite difference approximation is only necessary along the contact region but not across the bearing surfaces. This permits one to solve for the surface temperature and the mid-film temperature distribution along the contact region, without the calculation of the detailed temperature across the lubricant film.

This numerical method has been tested successfully for speeds up to 2000 in/sec and loads up to 300,000 psi without encountering any convergence difficulties. However, as mentioned earlier, this approach is only applicable to regions where there is no reverse flow. For low and moderate speeds, the temperature built up in the region of reverse flow at the inlet is insignificant. Therefore, it is entirely adequate to use this program alone by starting the temperature calculations at the point where the reverse flow terminates. However, at high speeds the build up of temperature in the region of reverse flow is quite significant, and this program must be used together with an inlet program in order to yield accurate temperatures in the contact zone. A detailed thermal analysis based on a mean viscosity across the film is fully described in Ref. 59.

##### (2) Two-Dimensional Finite Difference Method (For the Contact Region Only)

In this program, the assumption of a mean viscosity across the

film is removed by employing a finite difference approximation of the temperature derivatives across the film. With the finite difference formulation, the viscosity variation across the film can be incorporated. This program has been used in solving the thermal elastohydrodynamic problem in Ref. 93, which also gives a detailed account of the numerical analysis.

The limitations of this thermal program have not been fully explored. So far, no convergence difficulties have been experienced for maximum Hertz pressure up to 200,000 psi and speeds up to 800 in/sec. Beyond 800 in/sec, isolated cases of convergence difficulties have been encountered particularly for the combination of high speeds and high loads.

(3) Integral Thermal Analysis (For the Inlet Region Only)

This program is primarily written to supplement the mean viscosity method. Its purpose is to determine the increase in temperature in the reverse flow region and to calculate the initial temperature required to start the calculation in the contact zone. The integral thermal analysis is based on the assumption of a parabolic temperature profile across the lubricant film. By assuming a parabolic temperature profile, the energy equation can be readily integrated across the film to yield a first order differential equation which can be solved for the mid-film temperature. Details of this simplified analysis are included in Appendix VI.

(4) Two-Dimensional Finite Difference Method (For Inlet Region Only)

This program is designed especially for obtaining the temperature field in a rapidly convergent lubricant film such as that in the inlet region of an elastohydrodynamic contact. When the film decreases rapidly there is reverse flow at the center of the lubricant film and the presence of this negative velocity leads to a numerical instability if the conventional technique is employed in solving the energy equation. In this program the difficulty of numerical instabilities in the inlet region is removed by using a repetitive forward and backward marching procedure. Details of this numerical treatment can be found in Ref. 105.

In selecting the tools for calculating the temperature distributions in this preliminary design program, Program 1 and 3 are chosen mainly because: the analysis is simple, the computation time is far less than that required for Program 2 and 4, and the results are sufficiently accurate for preliminary design purposes.

m. Reduction Ratio for Pressure-Viscosity Coefficient

In a sliding contact, the calculation of friction and temperature



is critically dependent upon the value of pressure-viscosity coefficient  $\alpha$  at high pressure and temperatures defined in Equation (10) on page 26. It has been shown by Crook (126) and Johnson (129) that if the value of  $\alpha$  is independent of pressure, both the calculated friction and temperature will be too high. This discrepancy becomes increasingly worse as the contacting pressure increases. Recently, Allen, Zaretsky, and Townsend (137) have shown that by using a reduced pressure-viscosity coefficient at higher pressures, good agreement between the calculated and measured friction can be obtained. This composite pressure-viscosity model is adopted in this preliminary design program to calculate temperature profiles in the contact.

Using the composite pressure-viscosity model of Equations (27a) and (27b), on page 111, the viscosity can be expressed as follows.

$$\ln\left(\frac{\mu}{\mu_0}\right) = \alpha_1 p + (\beta + \gamma_1 p) \left(\frac{1}{T} - \frac{1}{T_0}\right) = VS \quad (80)$$

$$\text{for } p < p^*$$

$$\ln\left(\frac{\mu}{\mu_0}\right) = VS + \kappa \alpha_1 (p - p^*) + [\beta + \kappa \gamma_1 (p - p^*)] \left(\frac{1}{T} - \frac{1}{T_0}\right) \quad (81)$$

$$\text{for } p > p^*$$

where  $\kappa$  is the reduction ratio of the pressure-viscosity coefficients.

$$\kappa = \frac{\alpha_2}{\alpha_1} = \frac{\gamma_2}{\gamma_1} \quad (82)$$

This viscosity model is used in the thermal calculations. The value of  $\kappa$  is determined iteratively by requiring that the calculated thermal friction be equal to the friction found empirically from Johnson's data.

#### n. Stress Distributions

Once the normal pressure and tangential traction are calculated in the program, the surface and subsurface stress distributions are evaluated by using a subroutine STRESS for calculating stress in a line contact under arbitrarily distributed normal and tangential load. This calculation is only valid for cases of larger values of  $a/b$  where the stresses at the center can indeed be approximated by a line contact theory. For elliptical contacts approaching a circular contact zone, one should either bypass the stress calculations or consider these values as estimated stresses only.

A summary of the background, governing equations, and method of solutions for the stress calculation has already been discussed on page 121.

## SECTION IV

### APPLICATIONS

In the earlier sections of this report, the subject of elastohydrodynamic lubrication has been reviewed and a calculation procedure developed based on the best available data and theories. We now turn to the application of the calculation procedure to an actual rolling element bearing. This will serve as a demonstration of the procedure and will guide the reader in the future use of the program.

#### 1. ELASTOHYDRODYNAMIC PERFORMANCE PROGRAM

Three examples are given in this section to illustrate the use of the Elastohydrodynamic Performance Program. Typical bearings from high, moderate, and low speed applications have been selected to demonstrate features of the program and its various input-output options. Detailed input and output instructions along with the program listing are given in Appendix VII. First, however, some supplementary input instructions specifically for a roller-race or a ball-race contact are listed below.

##### a. Geometry Input (Card 1): RX1, RX2, RY1, RY2

The sign of a radius of curvature should be positive if the center of curvature lies within the body, negative if outside the body. For a roller-race contact: (if roller is assigned as body number 1 and race as body number 2)

RX1 = radius of roller, positive.

RX2 = radius of race, positive for inner race and negative for outer race.

RY1, RY2 = are not used in the calculation, any numbers can be used as the input.

For a ball-race contact: (if ball is assigned as body number 1 and race as body number 2)

RX1 = radius of ball, positive.

RX2 = radius of race, positive for inner race and negative for outer race.

RY1 = radius of ball, positive.

RY2 = radius of race groove, negative.

##### b. Speed Input (Card 9): U2, U1

The input should be the linear velocities of the two contacting bodies at the point of contact. In bearing applications, it is often necessary to perform a coordinate transformation so that the center of the ball/roller is fixed in the transformed coordinates in order to compute

the linear velocities of the ball/roller and of the contacting race. This is illustrated in Fig. 99.

In Fig. 99,  $\Omega_o$  and  $\Omega_i$  are the angular velocities of the outer and inner races with respect to the bearing center.  $\omega_R$  is the orbital velocity of the ball/roller with respect to the bearing center and  $\omega_o$  is the angular velocity of the ball/roller about its own center. In a reference frame in which the ball/roller center, O, is stationary the angular velocities of the ball/roller and of the races are shown in Fig. 99b.

The two surface velocities at a contact can then be easily calculated. For example, at the outer race contact the two speeds are  $(\Omega_o - \omega_R)r_o$  and  $\omega_o R$ . The larger one should be assigned as  $U_2$ . The smaller one should be  $U_1$ .

c. Lubricant Parameter Input (Card 10) VIS, ALF, BET, GAM

The lubricant properties consist of the following four constants:

$$\begin{aligned} \text{VIS} &= \mu_o, \text{ inlet viscosity of the lubricant, lb-sec/in}^2 \\ \text{ALF} &= \alpha, \text{ pressure-viscosity coefficient for } T = T_o, ^\circ\text{R} \\ \text{BET} &= \beta, \text{ temperature-viscosity coefficient, } ^\circ\text{R} \\ \text{GAM} &= \gamma, \text{ pressure-temperature-viscosity coefficient, in}^2\text{-}^\circ\text{R/lb} \end{aligned}$$

The viscosity is assumed to vary with pressure and temperature exponentially in the following manner

$$\mu = \mu_o e^{[\alpha p + (\beta + \gamma p)(\frac{1}{T} - \frac{1}{T_o})]} \quad (83)$$

In general, these constants are not available from the lubricant vendor. In order to determine these constants from the standard viscosity data which are generally available from the vendor, the pressure-temperature-viscosity data in the 1953 ASME pressure-viscosity report (23) have been analyzed by a least square fit type of regression program based on the above viscosity model.

Using the results from this regression analysis, the following procedure can be used to determine  $\alpha$ ,  $\beta$ , and  $\gamma$  from the standard lubricant data given by the vendor which consists of

$$\mu_{100} = \text{viscosity at } 100^\circ\text{F}$$

$$\mu_{210} = \text{viscosity at } 210^\circ\text{F}$$

$$\text{VI No.} = \text{the viscosity index number}$$

- (1) Use Fig. 100 to determine  $\alpha_{100}$ , the value of  $\alpha$  at  $T_o = 100$  F. If the VI number is in the neighborhood of 70-100, use the curve for paraffinic oils. If the VI number is around 0-20, use the curve for napthenic oils. For intermediate VI numbers, extra-

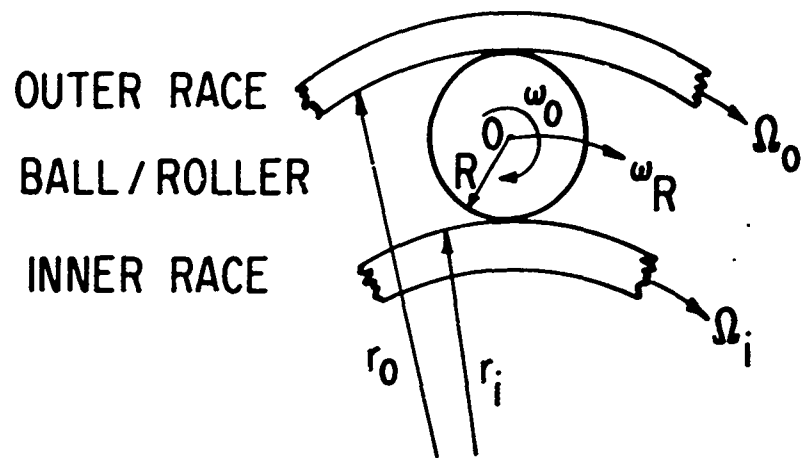


Fig. 99a Velocities with Respect to Bearing Centerline.

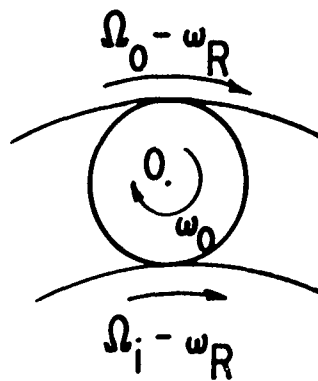


Fig. 99b Relative Velocities with Respect to Rolling Element.

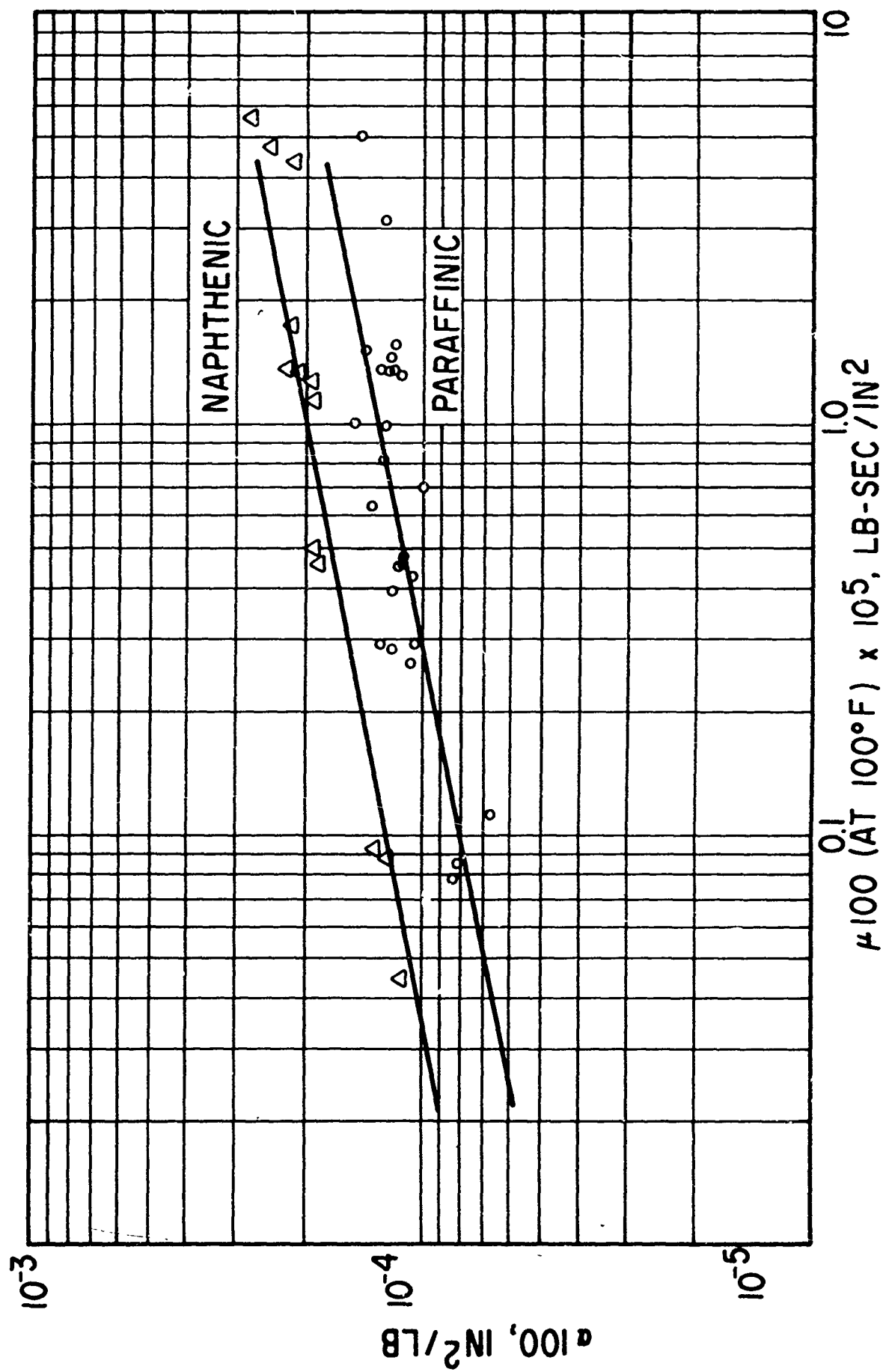


Fig. 100  $\mu_{100}$  vs.  $\alpha$  for Lubricants Tested in the ASME Report.

MTI-9672

polate between these two curves.

(2) Calculate  $\gamma$  by

$$\gamma = 930 \alpha_{100} \quad (84)$$

(3) Calculate  $\alpha$  for  $T = T_o$  by

$$\alpha = \alpha_{100} + \gamma \left( \frac{1}{T_o} - \frac{1}{560} \right) \quad (85)$$

(4) Calculate  $\beta$  by

$$\beta = 3400 \log_e \left[ \frac{\mu_{100}}{\mu_{210}} \right] \quad (86)$$

(This is derived from the relation

$$\mu_{210} = \mu_{100} e^{\beta \left( \frac{1}{670} - \frac{1}{560} \right)}. \quad (87)$$

d. Example 1 - High Speed Deep Groove Ball Bearing

For the first example we consider a deep groove, split inner race ball bearing running at 15,100 rpm and lubricated with MIL 7808 oil at 220 F. The specific bearing dimensions are summarized in Table XIX.

TABLE XIX

SAMPLE BEARING NUMBER 1  
DEEP GROOVE BALL BEARING

Diameter of Ball	= 0.719 inch
Number of Rolling Elements	= 20
Contact Angle	= 25°
Inner Race Curvature	= 0.52
Outer Race Curvature	= 0.515
Pitch Diameter	= 5.431

With the above geometrical data, the necessary speed input information for the ball outer race contact can be calculated by the method described on page 200. The results are summarized below

Ball radius,  $R = 0.3593$  in.

Outer race radius,  $r_o = 2.991$  in.

Spinning velocity of ball about its own center  $\omega_o = 53,000$  rpm.

Angular velocity of outer race  $\Omega_o = 15,100$  rpm.

Orbital angular velocity of ball  $\omega_R = 8400$  rpm.  
 Speed of ball at contact (Body No. 1)  $U_1 = \omega_o \cdot R \cdot \frac{2\pi}{60}$

$$= 1995 \text{ in/sec.}$$

Speed of outer race at contact (Body No. 2)  $= U_2 = (\Omega_o - \omega_R) \cdot r_o \cdot \frac{2\pi}{60}$

$$= 2099 \text{ in/sec.}$$

The individual ball loads were determined from the bearing internal load distribution for a thrust load of 1560 pounds. The computer input for the elastohydrodynamic performance program is shown in Fig. 101.

The output sheet is presented in Fig. 102. Some important results are:

- Maximum Hertz pressure = 201,733 psi
- Minimum film thickness =  $1.69 \times 10^{-5}$  in
- Percentage of area of contact = 0.16%
- Specific film = 2.98819
- Friction in rolling direction = frictional coefficient x total load  
 $= 0.0352367 \times 310$   
 $= 10.94 \text{ lb}$
- Maximum temperature rise in lubricant =  $0.1557968 \times (220 + 460)$   
 $= 106^\circ\text{F}$ , occurring at  $x/b$   
 $= 0.90677$
- Maximum temperature rise on the ball surface (body number 1)  
 $= 0.0485398 \times (220 + 460) = 33 \text{ F}$ , occurring at  $x/b = 0.93785$
- Maximum temperature rise on the race surface (body number 2)  
 $= 0.0448378 \times (220 + 460) = 30.5 \text{ F}$ , occurring at  $x/b = 0.93785$
- Maximum normal compressive stress in the ball at  $(y/b = 0.01) =$   
 $0.65253 \times \frac{\pi}{2} \times 2.01773 \times 10^5 = 2.062 \times 10^5 \text{ psi}$ , occurring at  
 $x/b = 0.$
- Maximum shear stress in the ball at  $(y/b = 0.01) = 0.08003 \times$   
 $\frac{\pi}{2} \times 2.01773 \times 10^5 = 2.54 \times 10^4 \text{ psi}$ , occurring at  $x/b = 0.90677$

The program has the option of printing out the pressure, temperature, and stress distribution. This option has been exercised in this example and the complete output has been shown.

In addition to the above there are several other points to note on the output sheets. The ellipticity of the contact zone  $a/b$  is very low. In general, this is true of most rolling element bearings. As a consequence, the side leakage factor is 1.0.

```

3.595E- 1-2.441E 0 3.545E- 1-0.374E 0 4. E 0 4. E 0
3. E 7 3. E 7 0.333E 0 0.333E 0 0.333E 0 0.283E 0
2.6 E 1 2.6 E 1 0.105E 0 0.105E 0 0.283E 0 0.283E 0
0.001E- 1 0.005E- 1 0.1 E 0
20 10 1 0 0
2 3
0.01 E 0 0.02 E 0
A BALL-OUTER HACE CONTACT IN THE HIGH SPEED BALL BEARING
3.01 E 2 2.20 E 2 2.099E 3 1.995E 3
4.35 E- 7 1.2 E- 4 6.12 E 3 1.116E- 1 0.084E 0 0.5 E 0 2.99 E- 2
6. E 4 0. E 0
0 1 0

```

Fig. 101 Computer Input, Example 1.



PERFORMANCE OF AN ELASTOHYDRODYNAMIC CONTACT  
\*\*\*\*\*

A BALL-OUTER RACE CONTACT IN THE HIGH SPEED BALL BEARING

GEOMETRIAL DATA

RAD. OF BODY 1,2 IN THE DIRECTION OF ROLLING.(IN)	3.59500E-01	-2.99100E+00
RAD. OF BODY 1,2 NORMAL TO ROLLING.(IN)	3.59500E-01	-3.74000E-01
R.M.S. SURFACE ROUGHNESS OF BODY 1,2.(MICRO IN)	4.00000E+00	4.00000E+00

MATERIAL DATA

MODULI OF ELASTICITY OF BODY 1,2.(PSI)	3.00000E+07	3.00000E+07
POISSONS RATIO OF BODY 1,2.	3.33000E-01	3.33000E-01
THERMAL CONDUCTIVITY OF BODY 1,2.(B/DEG.F-IN-FT)	2.60000E+01	2.60000E+01
SPECIFIC HEAT OF BODY 1,2.(B/LB-DEG. F)	1.05000E-01	1.05000E-01
DENSITY OF BODY 1,2.(LB/IN**3)	2.83000E-01	2.83000E-01

OPERATING CONDITIONS

TOTAL LOAD.(LB)	3.01000E+02	
INLET TEMPERATURE OF THE LUBRICANT.(DEG. F)	2.20000E+01	
SURFACE VELOCITY OF BODY 1,2.(IN/SE)	1.99500E+03	2.09900E+03

LUBRICANT DATA

Fig. 102 Computer Output, Example 1.

LUBRICANT DATA

INLET VISCOSITY.(LB-SEC/IN\*\*2) 4.35000E-07  
 PRESSURE-VISCOITY COEF.\*(IN\*\*2/LB) 1.20000E-04  
 TEMPERATURE-VISCOSITY COEF.\*(DEG. R) 6.12000E+03  
 PRESSURE-TEMPERATURE-VISCOSITY COEF.(IN\*\*2-DEG.R/LB) 1.11600E-01  
 THERMAL CONDUCTIVITY OF LUB.\*(B/DEG.F-HR-FT) 8.40000E-02  
 SPECIFIC HEAT OF LUB.\*(B/LB-DEG.F) 5.00000E-01  
 DENSITY OF LUB.\*(LB/IN\*\*3) 2.99000E-02

THERMAL PARAMETERS

1.10017E+01  
 4.78517E-03

QM  
 D1

208

CALCULATED PARAMETERS

2.95493E-01 CONV  
 4.90831E-03 D2

CONTACT DIMENSION

HALF HERTZ WIDTH(ROLLING DIA.),IN. 9.77394E-03  
 B/A 7.49992E+00  
 HALF HERTZ WIDTH(PERP. TO ROLLING),IN. 7.28743E-02  
 M 3.33072E+00

Fig. 102 (continued)

## LOAD, SPEED, AND LUBRICANT PARAMETERS

[illegible]

## REDUCTION FACTORS

THERMAL REDUCTION FACTOR	8.06785E-01	SIDE LEAKAGE FACTOR	1.00000E+00
ISOTh. MIN. FILM(IN)	2.09520E-05	MIN. FILM(IN)	1.69038E-05

## DIMENSIONLESS PROTRUSION PARAMETERS

PROTRUSION WIDTH	1.24300E-01	PROTRUSION DEPTH	2.00000E-01
PERCENTAGE OF AREA CONTACT	1.63398E-01	SPECIFIC FILM	2.98819E+00

Fig. 102 (continued)

FRICITIONAL COFF.

3.52367E-02

ABAR	NORMLZD FILM	PRESSURE
-4.00000E+00	9.50206E+01	0.
-3.50000E+00	6.98739E+01	4.42364E-05
-3.00000E+00	4.83352E+01	1.32663E-04
-2.50000E+00	3.04642E+01	3.41905E-04
-2.00000E+00	1.63683E+01	1.00378E-03
-1.75539E+00	1.09076E+01	1.81967E-03
-1.51078E+00	6.45148E+00	3.98478E-03
-1.38847E+00	4.62702E+00	6.39044E-03
-1.26617E+00	3.09717E+00	1.16232E-02
-1.20501E+00	2.45311E+00	1.66364E-02
-1.14386E+00	1.89871E+00	2.54753E-02
-1.08271E+00	1.44579E+00	4.29198E-02
-1.02155E+00	1.11746E+00	8.30198E-02
-1.01078E+00	1.07617E+00	9.63367E-02
-1.00000E+00	1.04140E+00	1.11758E-01
-9.89223E-01	1.01461E+00	1.25775E-01
-9.78446E-01	1.00000E+00	1.31463E-01
-9.47870E-01	1.00000E+00	2.02864E-01
-9.17293E-01	1.00000E+00	2.53510E-01
-8.86717E-01	1.00000E+00	2.94318E-01
-8.56140E-01	1.00000E+00	3.28969E-01
-7.94987E-01	1.00000E+00	3.86190E-01
-7.33835E-01	1.00000E+00	4.32474E-01
-6.11529E-01	1.00000E+00	5.03708E-01
-4.89223E-01	1.00000E+00	5.55234E-01
-3.66917E-01	1.00000E+00	5.92218E-01
-2.44612E-01	1.00000E+00	6.17280E-01
-1.22306E-01	1.00000E+00	6.31841E-01
7.10543E-15	1.00000E+00	6.36620E-01
1.87850E-01	1.00000E+00	6.25287E-01
3.75700E-01	1.00000E+00	5.89982E-01
5.63549E-01	1.00000E+00	5.25901E-01
7.51399E-01	1.00000E+00	4.20072E-01
7.82474E-01	1.00000E+00	4.27741E-01
8.13549E-01	1.00000E+00	4.50748E-01
8.44625E-01	1.00000E+00	4.89093E-01
8.75700E-01	1.00000E+00	5.42775E-01
9.06775E-01	8.58578E-01	1.72910E-01
9.37850E-01	8.00000E-01	7.68490E-02
9.68925E-01	8.58579E-01	1.92122E-02
1.00000E+00	1.00000E+00	1.98933E-19

-0.01261    -0.04919    0.01261

Fig. 102 (continued)

ITRDU= 1 RDU= 6.00000E-01 ERFR= 9.58697E-02

ITRDU= 2 RDU= 9.43725E-02 ERFR= 1.19505E-01

ITRDU= 3 RDU= 1.10075E-01 ERFR=-3.83023E-03

XBAR	PRESSURE	T MEAN	T1	T2	SHEAR FORCE
-4.0000000	0.0000000	1.0000000	1.0000000	1.0000000	.0000001
-3.5000000	.0000442	1.0000000	1.0000000	1.0000000	.0000001
-3.0000000	.0001327	1.0000000	1.0000000	1.0000000	.0000002
-2.5000000	.0003419	1.0000000	1.0000000	1.0000000	.0000003
-2.0000000	.0010038	1.0000000	1.0000000	1.0000000	.0000005
-1.7553885	.0018197	1.0000000	1.0000000	1.0000000	.0000008
-1.5107770	.0039848	1.0000000	1.0000000	1.0000000	.0000015
-1.3884712	.0063904	1.0000000	1.0000000	1.0000000	.0000023
-1.2661655	.0116232	1.0000000	1.0000000	1.0000000	.0000042
-1.2050126	.0166364	1.0000000	1.0000000	1.0000000	.0000065
-1.1438547	.0254753	1.0000000	1.0000000	1.0000000	.0000117
-1.0827069	.0429198	1.0216980	1.0031770	1.0035762	.0000235
-1.0215540	.0830198	1.0229076	1.0038152	1.0045935	.0001319
-1.0107770	.0963367	1.0222911	1.0042680	1.0052270	.0002256
-1.0000000	.1117582	1.0206154	1.0040450	1.0050759	.0004217
-.9892230	.1251752	1.0181391	1.0039000	1.0049105	.0007542
-.9784460	.1314434	1.0159084	1.0039288	1.0047531	.0009779
-.9478696	.2024044	1.0260675	1.0042932	1.0048624	.0094563
-.9172931	.2535101	1.0351692	1.0048400	1.0052921	.0107644
-.8867167	.2943174	1.0421713	1.0057875	1.0061514	.0119035
-.8561403	.3249092	1.0402935	1.0068147	1.0071079	.0129327
-.7949874	.3861907	1.0522368	1.0086013	1.0087877	.0147707
-.7338345	.4324740	1.0669035	1.0107027	1.0107956	.0163146
-.6115288	.5037079	1.0809667	1.0142557	1.0142089	.0187841
-.4892230	.5552337	1.0921962	1.0181928	1.0180183	.0205137
-.3669173	.5922180	1.1008261	1.0216633	1.0213838	.0216910
-.2446115	.6172802	1.1073439	1.0251012	1.0247248	.0223640
-.1223058	.6318406	1.1117529	1.0279280	1.0274739	.0226242
.0000000	.6366200	1.1143629	1.0306670	1.0301409	.0224642
.1878498	.6252867	1.1145677	1.0334348	1.0328368	.0215256
.3756996	.5849822	1.1100147	1.0357424	1.0350877	.0196540
.5635494	.5254006	1.1018770	1.0366109	1.0359346	.0168537
.7513992	.4200724	1.0870119	1.0363340	1.0356656	.0129184
.7824743	.4217413	1.0874367	1.0372978	1.0366082	.0133365
.8135494	.4507400	1.0887879	1.0369032	1.0362221	.0143571
.8446245	.4490925	1.0892383	1.0370079	1.0363237	.0160302
.8756996	.5421748	1.0906748	1.0375263	1.0368300	.0184569
.9067747	.61729102	1.1557968	1.0468519	1.0430894	.0006244
.9378498	.0768490	1.1159051	1.0485398	1.0448378	.0000509
.9689249	.0192122	1.0825523	1.0468971	1.0437742	.0000095
1.0000000	.0000000	1.0641181	1.0436982	1.0411402	.0000049

ARRAY OF X-COORD. FOR STRESS CALCU.

-1.00000E+00	-9.89223E-01	-9.78446E-01	-9.47870E-01	-9.17293E-01	-8.86717E-01
-8.56140E-01	-7.94987E-01	-7.33835E-01	-6.11529E-01	-4.89223E-01	-3.66917E-01
-2.44612E-01	-1.22306E-01	7.10543E-15	1.87850E-01	3.75700E-01	5.63549E-01
7.51399E-01	7.82474E-01	8.13549E-01	8.44625E-01	8.75700E-01	9.06775E-01
9.37850E-01	9.68925E-01	1.00000E+00			

Fig. 102 (continued)

ARRAY OF Y-COORD. FOR STRESS CALCU.  
1.00000E-02 2.00000E-02

Y= 1.00000E-02

XST	SX	SY	SXY	PSX	PSY	PSZ	PTXY	OS
-1.00000	-.00401	-.01433	.00052	-.00399	-.01835	-.00744	.00718	.00612
SHEAR STRESS AT EVERY 45.00000 DEGREES								
.00052	.00716	-.00052						

XST	SX	SY	SXY	PSX	PSY	PSZ	PTXY	OS
-.98922	-.02141	-.03216	.00206	-.02103	-.03254	-.01784	.00575	.00631
SHEAR STRESS AT EVERY 45.00000 DEGREES								
.00206	.00537	-.00206						

XST	SX	SY	SXY	PSX	PSY	PSZ	PTXY	OS
-.97845	-.06343	-.01220	.00702	-.05954	-.07609	-.04516	.00828	.01264
SHEAR STRESS AT EVERY 45.00000 DEGREES								
.00702	.00439	-.00702						

XST	SX	SY	SXY	PSX	PSY	PSZ	PTXY	OS
-.94787	-.15265	-.18717	.00926	-.15032	-.18950	-.11316	.01959	.03117
SHEAR STRESS AT EVERY 45.00000 DEGREES								
.00926	.01726	-.00926						

XST	SX	SY	SXY	PSX	PSY	PSZ	PTXY	OS
-.91729	-.26473	-.24559	.00349	-.20443	-.24588	-.14996	.02072	.03928
SHEAR STRESS AT EVERY 45.00000 DEGREES								
.00349	.02043	-.00349						

XST	SX	SY	SXY	PSX	PSY	PSZ	PTXY	OS
-.88672	-.24592	-.28838	.00048	-.24591	-.28838	-.17792	.02124	.04550
SHEAR STRESS AT EVERY 45.00000 DEGREES								
.00048	.02123	-.00048						

XST	SX	SY	SXY	PSX	PSY	PSZ	PTXY	OS
-.85614	-.24114	-.32415	-.00223	-.28102	-.32427	-.20156	.02162	.05082
SHEAR STRESS AT EVERY 45.00000 DEGREES								
-.00223	.02151	.00223						

XST	SX	SY	SXY	PSX	PSY	PSZ	PTXY	OS
-.79499	-.34018	-.38252	-.00598	-.33935	-.38335	-.24066	.02200	.05966
SHEAR STRESS AT EVERY 45.00000 DEGREES								
-.00598	.02117	.00598						

XST	SX	SY	SXY	PSX	PSY	PSZ	PTXY	OS
-.73383	-.38861	-.42932	-.00914	-.38665	-.43128	-.27237	.02231	.06692
SHEAR STRESS AT EVERY 45.00000 DEGREES								
-.00914	.02036	.00914						

Fig. 102 (continued)

XST	SX	SY	SXY	PSX	PSY	PSZ	PTXY	OS
-.61153	-.46488	-.50105	-.01330	-.46051	-.50542	-.32166	.02245	.07822
SHEAR STRESS AT EVERY 45.00000 DEGREES								
-.01330	.01509	.01330						
XST	SX	SY	SXY	PSX	PSY	PSZ	PTXY	OS
-.48922	-.52193	-.55283	-.01651	-.51477	-.56000	-.35790	.02262	.08660
SHEAR STRESS AT EVERY 45.00000 DEGREES								
-.01651	.01545	.01651						
XST	SX	SY	SXY	PSX	PSY	PSZ	PTXY	OS
-.36692	-.56442	-.58991	-.01864	-.55458	-.59975	-.38439	.02258	.09273
SHEAR STRESS AT EVERY 45.00000 DEGREES								
-.01864	.01275	.01864						
XST	SX	SY	SXY	PSX	PSY	PSZ	PTXY	OS
-.24461	-.59515	-.61508	-.02026	-.58254	-.62769	-.40301	.02258	.09704
SHEAR STRESS AT EVERY 45.00000 DEGREES								
-.02026	.00996	.02026						
XST	SX	SY	SXY	PSX	PSY	PSZ	PTXY	OS
-.12231	-.61531	-.62971	-.02132	-.60001	-.64501	-.41459	.02250	.09972
SHEAR STRESS AT EVERY 45.00000 DEGREES								
-.02132	.00720	.02132						
XST	SX	SY	SXY	PSX	PSY	PSZ	PTXY	OS
.00000	-.62568	-.63458	-.02195	-.60773	-.65253	-.41967	.02240	.10089
SHEAR STRESS AT EVERY 45.00000 DEGREES								
-.02195	.00445	.02195						
XST	SX	SY	SXY	PSX	PSY	PSZ	PTXY	OS
.18785	-.62264	-.62338	-.02227	-.60073	-.64529	-.41492	.02228	.09976
SHEAR STRESS AT EVERY 45.00000 DEGREES								
-.02227	.00037	.02227						
XST	SX	SY	SXY	PSX	PSY	PSZ	PTXY	OS
.37570	-.59548	-.58832	-.02166	-.56995	-.61385	-.39420	.02195	.09490
SHEAR STRESS AT EVERY 45.00000 DEGREES								
-.02166	-.00358	.02166						
XST	SX	SY	SXY	PSX	PSY	PSZ	PTXY	OS
.56355	-.53882	-.52441	-.02093	-.50948	-.55374	-.35405	.02213	.08563
SHEAR STRESS AT EVERY 45.00000 DEGREES								
-.02093	-.00720	.02093						

Fig. 102 (continued)

XST	SX	SY	SXY	PSX	PSY	PSZ	PTXY	OS
.75140	-.45101	-.42128	-.01575	-.41449	-.45780	-.29047	.02166	.07091
SHEAR STRESS AT EVERY 45.00000 DEGREES								
-.01575	-.01486	.01575						

XST	SX	SY	SXY	PSX	PSY	PSZ	PTXY	OS
.78247	-.44898	-.42693	-.01010	-.42302	-.45291	-.29168	.01494	.07003
SHEAR STRESS AT EVERY 45.00000 DEGREES								
-.01010	-.01101	.01010						

XST	SX	SY	SXY	PSX	PSY	PSZ	PTXY	OS
.81355	-.45717	-.44958	-.00730	-.44515	-.46160	-.30195	.00822	.07170
SHEAR STRESS AT EVERY 45.00000 DEGREES								
-.00730	-.00379	.00730						

XST	SX	SY	SXY	PSX	PSY	PSZ	PTXY	OS
.84462	-.46406	-.48683	-.00839	-.46131	-.48959	-.31665	.01414	.07574
SHEAR STRESS AT EVERY 45.00000 DEGREES								
-.00839	.01138	.00839						

XST	SX	SY	SXY	PSX	PSY	PSZ	PTXY	OS
.87570	-.41039	-.49244	-.05946	-.37918	-.52365	-.30064	.07224	.09236
SHEAR STRESS AT EVERY 45.00000 DEGREES								
-.05946	.04102	.05946						

XST	SX	SY	SXY	PSX	PSY	PSZ	PTXY	OS
.90677	-.27814	-.18467	-.06496	-.15138	-.31144	-.15412	.08003	.07481
SHEAR STRESS AT EVERY 45.00000 DEGREES								
-.06496	-.04674	.06496						

XST	SX	SY	SXY	PSX	PSY	PSZ	PTXY	OS
.93785	-.15949	-.07132	-.02078	-.06667	-.16414	-.07686	.04874	.04375
SHEAR STRESS AT EVERY 45.00000 DEGREES								
-.02078	-.04408	.02078						

XST	SX	SY	SXY	PSX	PSY	PSZ	PTXY	OS
.96892	-.10105	-.02076	-.01380	-.01845	-.10336	-.04056	.04245	.03596
SHEAR STRESS AT EVERY 45.00000 DEGREES								
-.01380	-.04015	.01380						

XST	SX	SY	SXY	PSX	PSY	PSZ	PTXY	OS
1.00000	-.06964	-.00077	-.00446	-.00048	-.06993	-.02345	.03472	.02889
SHEAR STRESS AT EVERY 45.00000 DEGREES								
-.00446	-.03443	.00446						

102 (continued)



The thermal reduction factor is significant, .81, which means that the actual film thickness is 19 percent less than isothermal theory would predict.

This particular bearing's failure history was one of fatigue. This is borne out by the elastohydrodynamic calculation which indicates ample film thickness and essentially no metal-to-metal contact. The maximum temperature in the film is less than the flash temperature for this oil-material combination and the bearing is operating in region 3 of Fig. 81 on page 155. Thus, fatigue is the expected mode of failure.

e. Example 2 - Roller Bearing

The second example is a roller bearing operating at 4500 rpm with MIL-L-7808 oil at an inlet temperature 220 F. The bearing geometry is summarized in Table

TABLE XX  
SAMPLE BEARING NUMBER 2  
- ROLLER BEARING

Roller Diameter =	0.3150 inches
Number of Rolling Elements =	20
Pitch Diameter =	2.5595 inches
Mounted Radial Clearance =	0.0012 inches
Total Roller Length =	0.315 inches
Flat Length of Roller =	0
Crown Radius =	15.0 inches
End Radius =	0.020 inches

As in the previous example, knowledge of the bearing geometry, internal load distribution, and speed permits calculation of the elastohydrodynamic input data for the inner race as shown in Fig. 103. The output data is presented in Fig. 104. The pressure, temperature, and stress distribution are not shown to conserve space. A summary of the output parameters includes the following important results.

- Maximum Hertz Pressure = 233,313 psi
- Minimum Film Thickness =  $3.69 \times 10^{-6}$  in
- Percentage of Area Contact = 25.7975%
- Specific Film = 0.652562
- Friction in Rolling Direction Per Unit Length of Roller =  
 $0.0524 \times 1400 = 73.4$  lb/in
- Maximum Temperature Rise on the Roller Surface (Body Number 1)  
 $= 0.014715 \times (220 + 460) = 10^{\circ}\text{F}$ , occurring at  $x/b = 0.94815$ .
- Maximum Temperature Rise on the Inner Race Surface (Body Number 2) =  $0.013929 \times (220 + 460) = 9.5^{\circ}\text{F}$ , occurring at  $x/b =$

```

1.575E- 1 1.122E 0 1.  E 3 1.  E 3 4.  E 0 4.  E 0
3.  E 7 3.  E 7 0.133E 0 0.333E 0
2.6  E 1 2.6  E 1 0.105E 0 0.105E 0 0.283E 0
0.001E- 1 0.005E- 1 0.1  E 0
20 10 1 0 0
2 3
0.01 E 0 0.02 E 0
A ROLLER-INNER RACE CONTACT IN THE HEAVILY LOADED ROLLER BEARING
1.4  E 3 2.2  E 2 3.  E 2 2.9  E 2
4.35 E- 7 1.2  E- 4 6.12 E 3 1.110E- 1 0.084E 0 0.5  E 0 2.99 E- 2
6.  E 4 0.  E 0
1 1 1 0

```

Fig. 103 Computer Input, Example 2.

PERFORMANCE OF AN ELASTOHYDRODYNAMIC CONTACT  
\*\*\*\*\*

A ROLLER-INNER RACE CONTACT IN THE HEAVILY LOADED ROLLER BEARING

GEOMETRIAL DATA

RAD. OF BODY 1,2 IN THE DIRECTION OF ROLLING, (IN)	1.57500E-01	1.12200E+00
R.M.S. SURFACE ROUGHNESS OF BODY 1,2, (MICRO IN)	4.00000E+00	4.00000E+00

MATERIAL DATA

MODULI OF ELASTICITY OF BODY 1,2, (PSI)	3.00000E+07	3.00000E+07
POISSONS RATIO OF BODY 1,2,	3.33000E-01	3.33000E-01
THERMAL CONDUCTIVITY OF BODY 1,2, (B/DEG.F-IN-FT)	2.60000E+01	2.60000E+01
SPECIFIC HEAT OF BODY 1,2, (B/LB-DEG. F)	1.05000E-01	1.05000E-01
DENSITY OF BODY 1,2, (LB/IN**3)	2.83000E-01	2.83000E-01

OPERATING CONDITIONS

LINE CONTACT LOAD, (LB/IN)	1.40000E+03	
INLET TEMPERATURE OF THE LUBRICANT, (DEG. F)	2.20000E+02	
SURFACE VELOCITY OF BODY 1,2, (IN/SEC)	2.90000E+02	3.00000E+02

Fig. 104 Computer Output, Example 2.

LUBRICANT DATA

INLET VISCOSITY, (LB-SEC/IN\*\*2) 4.35000E-07  
 PRESSURE-VISCOITY COEF., (IN\*\*2/LB) 1.20000E-04  
 TEMPERATURE-VISCOSITY COEF., (DEG. R) 6.12000E+03  
 PRESSURE-TEMPERATURE-VISCOITY COEF., (IN\*\*2-DEG.R/LB) 1.11600E-01  
 THERMAL CONDUCTIVITY OF LUB., (B/DEG.F-INCH-FT) 8.40000E-02  
 SPECIFIC HEAT OF LUB., (M/L-H-DEG.F) 5.00000E-01  
 DENSITY OF LUB., (LB/IN\*\*3) 2.99000E-02

THERMAL PARAMETERS

QM 8.28541E-01  
 D1 1.75092E-02

CALCULATED PARAMETERS

CONTACT DIMENSION

HALF HERTZ WIDTH (ROLLING DIR.), IN. 3.82004E-03

Fig. 104 (continued)

LOAD, SPEED, AND LUBRICANT PARAMETERS

UBAR	2.7536E-11	AFA	4.39786E+01
GG	4.04899E+03	GMA	6.01473E+01
BTA	9.00000E+00	WBAR	3.00421E-04
EQUIV. LINE CONTACT LOAD (LH/IN)	1.40000E+03	PHZ/ED	4.40203E-03
HERTZ PRESSURE (PSI)	2.33313E+05	SLIDE TO MULL	3.38983E-02
R=2.0*W <sub>W</sub> /EP/SH	1.43112E+01		
AM=6.*VIS*(U1+U2)*EP*WXP/W**0.2	5.75116E-03		

219

REDUCTION FACTORS

THERMAL REDUCTION FACTOR	9.83109E-01	SIDE LEAKAGE FACTOR	1.00000E+00
ISOTH. MIN. FILM (IN)	3.75487E-06	MIN. FILM (IN)	3.69145E-06

DIMENSIONLESS PROTRUSION PARAMETERS

PROTRUSION WIDTH	6.91344E-02	PROTRUSION DEPTH	2.00000E-01
PERCENTAGE OF AREA CONTACT	2.57975E+01	SPECIFIC FILM	6.52562E-01

Fig. 104 (continued)

0.94815

• Maximum Temperature Rise in Lubricant =  $0.0253456 \times (220 + 460)$   
=  $17.3^{\circ}\text{F}$ , occurring at

$x/b = 0.94815$

• Maximum Normal Compressive Stress in the Roller at  $(y/b = 0.01)$   
=  $0.6712 \times \frac{\pi}{2} \times 2.333 \times 10^5 = 2.46 \times 10^5$  psi, occurring at  $x/b$   
= 0

• Maximum Shear Stress in the Roller at  $(y/z = 0.01) = 0.08629 \times \frac{\pi}{2}$   
 $\times 2.333 \times 10^5 = 3.16 \times 10^4$  psi, occurring at  $x/b = 0.94815$

Bearings in this application exhibited a shorter fatigue life than the already short life predicted using conventional techniques (215, 216). A possible reason for this can be traced to the low specific film,  $\xi_0 = .65$ , and large percentage of area of contact, 26%.

The elastohydrodynamic lubrication is in the partial film region in this application. In the partial elastohydrodynamic film regime, the load is shared by the hydrodynamic fluid film and the contacting asperities with a majority of the load supported by the fluid film. The effectiveness of hydrodynamic action is measured by the specific film thickness, first introduced by Dawson (208, 209, 210). Dawson arrived at this parameter in a series of fatigue tests designed to study the effect of surface finish on fatigue life. He discovered the important fact that in the partial film regime there exists a straight line relation between fatigue life and specific film thickness on a log-log basis. This means that pitting fatigue life,  $N$  ( $N$  being the number of cycles to pitting), can be expressed in terms of  $\xi_0$  by a power relation

$$N = c\xi^a \quad (88)$$

where  $c$  and  $a$  depend on the material properties of the solids, speeds, loads, geometry, and lubrication in the partial-film regime.

Values of  $c$  and  $a$  for the material lubricant combinations of interest in this study have not yet been measured but Equation 88 corroborates the reduction in fatigue that was experienced in practice.

Also note that the maximum film temperature is very low so smearing failure would not be expected.

#### f. Example 3 - Low Speed Angular Contact Bearing

Using the Elastohydrodynamic Performance Program as illustrated in the previous two example, the contact of the ball and the outer race of a low speed angular contact was analyzed for the conditions of Table XXI below.

TABLE XXI  
SAMPLE BEARING NUMBER 3  
LOW SPEED ANGULAR CONTACT BEARING

Bore	= 3.54 inches
Outer Diameter	= 5.51 inches
Number of Balls	= 16
Ball Diameter	= 0.534 inch
Contact Angle	= 25°
Load	= 30 pounds thrust (nominal)
Lubricant	= mineral oil impregnated phenolic retainers at 22°F
Speed	= 60 rpm
Inner Race Curvature	= .52
Outer Race Curvature	= .52

The input and output data for the sample calculation are shown in Figs. 105 and 106. Several conclusions can be drawn from this data. First, internally generated thermal effects are unimportant since the thermal and isothermal film thicknesses are almost identical. Additional pertinent information is summarized below.

- Maximum Hertz Pressure = 47,222 psi
- Minimum Film Thickness =  $9.94372 \times 10^{-6}$  in
- Percentage of Area Contact = 4.6%
- Specific Film = 1.75782
- Friction in Rolling Direction = 0
- Since the Normalized Protrusion Width  $\frac{e}{b} = 0.553517$ , the  
Pressure Calculations Breaks Down. A Message was Printed Out.

Due to the low loading, the calculated fatigue life of this bearing is extremely long. Because it is operating close to the partial elastohydrodynamic region, mild wear is a possible failure mode. To investigate this failure mode, the elastohydrodynamic program was repeated for different loads and oil temperatures. The results are summarized in Table XXII.

```

2.67 E- 1-2.755E 0 2.67 E- 1-2.63 E- 1 4. E 0 4. E 0
2.9 E 7 2.4 7 0.24 E 0 0.24 E 0
1.4 E 1 1.4 E 1 0.11 E 0 0.11 E 0 0.28 E 0 0.28 E 0
0.001E- 1 0.005E- 1 0.1 E 0
20 10 1 0 0
2 3
0.01 E 0 0.02 E 0
A BALL-OUTER WACE CONTACT IN THE VERY LIGHTLY LOADED BALL BEARING
1.876E- 0 1.0 E 2 6.75 E 0 6.75 E 0
2.99 E- 5 1.25 E- 4 5.5 E 3 1.16 E- 1 0.085E 0 0.433E 0 3.25 E- 2
6. E 4 0. E 0
0 0 0 0

```

Fig. 105 Computer Input, Example 3.



PERFORMANCE OF AN ELASTOHYDRODYNAMIC CONTACT  
\*\*\*\*\*

A BALL-OUTER RACE CONTACT IN THE VERY LIGHTLY LOADED BALL BEARING

GEOMETRIAL DATA

RAD. OF BODY 1,2 IN THE DIRECTION OF ROLLING,(IN)	2.67000E-01	-2.75500E+00
RAD. OF BODY 1,2 NORMAL TO ROLLING,(IN)	2.67000E-01	-2.83000E-01
R.M.S. SURFACE ROUGHNESS OF BODY 1,2,(MICRO IN)	4.00000E+00	4.00000E+00

MATERIAL DATA

MODULI OF ELASTICITY OF BODY 1,2,(PSI)	2.90000E+07	2.90000E+07
POISSONS RATIO OF BODY 1,2.	2.90000E-01	2.90000E-01
THERMAL CONDUCTIVITY OF BODY 1,2,(B/DEG.F-HR-FT)	1.40000E+01	1.40000E+01
SPECIFIC HEAT OF BODY 1,2,(B/LB-DEG. F)	1.10000E-01	1.10000E-01
DENSITY OF BODY 1,2,(LB/IN**3)	2.80000E-01	2.80000E-01

OPERATING CONDITIONS

TOTAL LOAD,(LB)	1.87600E+00
INLET TEMPERATURE OF THE LUBRICANT,(DEG. F)	1.00000E+02
SURFACE VELOCITY OF BODY 1,2,(IN/SEC)	6.75000E+00 6.75000E+00

Fig. 106 Computer Output, Example 3.

# LUBRICANT DATA

INLET VISCOSITY (LN-SEC/IN\*\*2) 2.99000E-05  
 PRESSURE-VISCOSITY COEF. ((IN\*\*2/LN) 1.25000E-04  
 TEMPERATURE-VISCOSITY COEF. ((DEG. K) 6.50000E+03  
 PRESSURE-TEMPERATURE-VISCOSITY COEF. ((IN\*\*2-DEG. K/LN) 1.15000E-01  
 THERMAL CONDUCTIVITY OF LUB. ((B/DLG-F-IN\*\*F1) 4.50000E-02  
 SPECIFIC HEAT OF LUB. ((1/LN-DEG.F) 4.33000E-01  
 DENSITY OF LUB. ((LN/IN\*\*3) 3.25000E-02

## THERMAL PARAMETERS

2.07023E-04 CONV  
 1.07576E+00 U2

3.80941E-04  
 1.07576E+00

## CALCULATED PARAMETERS

### CONTACT DIMENSION

HALF HERTZ WIDTH (ROLLING DIR.), IN. 1.77042E-03  
 B/A 5.05154E+00

HALF HERTZ WIDTH (PERP. TO ROLLING), IN. 1.07140E-02  
 2.91865E+00

Fig. 106 (continued)

# LOAD, SPEED, AND LUBRICANT PARAMETERS

UBAR	2.15597E-11		
GG	3.95786E+03	AFA	9.27206E+00
BTA	1.16071E+01	GMA	1.53651E+01
EQUIV. LINE CONTACT LOAD(LB/IN)	1.31324E+02	WBAR	1.40785E-05
HERTZ PRESSURE(PSI)	4.72221E+04	PHZ/ED	9.49455E-04
B=2.0*W*W/EP/SHM	5.31073E-01	SLIDE TO ROLL RATIO=2(U2-U1)/(U2+U1)	0.
AM=6.*VIS*(U1+U2)*EP*W*W/****2	2.06501E+00		

## REDUCTION FACTORS

THERMAL REDUCTION FACTOR	9.99384E-01	SIDE LEAKAGE FACTOR	1.00000E+00
ISOTH. MIN. FILM(IN)	9.94985E-06	MIN. FILM(IN)	9.94372E-06

## DIMENSIONLESS PROTRUSION PARAMETERS

PROTRUSION WIDTH	5.53517E-01	PROTRUSION DEPTH	2.00000E-01
PERCENTAGE OF AREA CONTACT	4.60901E+00	SPECIFIC FILM	1.75782E+00

FRICTIONAL COEF. 0.

THE PROTRUSION WIDTH IS GREATER THAN 0.5  
PRESSURE, TEMPERATURE, AND STRESS CALCULATIONS ARE BYPASSED

MTI-9592

Fig. 106 (continued)

TABLE XXII  
SAMPLE BEARING NUMBER 3  
LOW SPEED ANGULAR CONTACT BEARING FILM  
THICKNESS AND AREA RATIO AS A FUNCTION OF OIL TEMPERATURE

		$h_o$ ( $\mu$ in)			$\xi_o$			$A_c/A$		
Load	Race	0°C	22°C	50°C	0°C	22°C	50°C	0°C	22°C	50°C
30	Outer	30.2	9.94	4.11	5.35	1.76	0.725	0	.046	.243
30	Inner	28.2	9.25	3.82	4.99	1.64	0.656	0	.059	.264
60	Outer	28.5	9.37	3.87	5.05	1.66	0.666	0	.054	.261
60	Inner	26.5	8.71	3.61	4.69	1.54	0.620	0	.068	.276
120	Outer	26.8	8.82	3.66	4.75	1.56	0.629	0	.063	.273
120	Inner	24.7	8.20	3.39	4.41	1.45	0.599	0	.078	.283

This table shows that at the upper end of the temperature range, the film thickness is small compared to the surface roughness, resulting in a high degree of asperity contact. At the low end of the temperature range, the film thickness is large, implying that wear will not occur. Such a range of alternatives suggests a great need for careful temperature control if this bearing is to operate successfully.

The table suggests one other important point, the surface finish is a major parameter and must be carefully measured and controlled. A change from a 4  $\mu$ in to a 2  $\mu$ in finish would probably reduce the wear rate, initially at least by about 2/3.

As discussed in Section II, Tallian, et al studied rolling and sliding wear using a rolling four ball apparatus. They found that the wear divided by the rolled over track and the total asperity contact area equalled a constant,  $k$ , of approximately 10 micrograms per cubic inch.

Using Equation (52) of Section II, the amount of wear to be expected over the life of the bearing can be calculated provided the wear coefficient  $k$  is known for the particular material-lubricant combination. Dimensional changes due to wear can be as high as .001 or .002 inches over the life of the bearing in applications of this type.

## 2. CALCULATION OF FRICTIONAL FORCES AND SPIN TORQUE AT A BALL-RACE CONTACT

In the previous examples, only rolling and slip in the direction of motion have been considered. The discussion of Section II-8 demonstrates that both gyroscopic slip and ball spin may occur at the inner or outer race of an actual ball bearing. Therefore, to fully evaluate the per-

formance of a ball bearing, the frictional forces between individual ball and race must be calculated, assuming ball motion about all axes.

The commonly used methods (215, 216) assume Coulomb friction at contact. A recent paper (137) employs elastohydrodynamic lubrication theory for line contacts to calculate the frictional torque on a spinning ball in a non-conforming groove. In that paper Crook's simple friction analysis (120) was used to calculate friction but frictional stresses in the direction of the major axis of the contact ellipse, outside a circle of radius of the semi-minor axis of the ellipse, were neglected, and the analytical results were made to match the measurements by bending appropriately the pressure viscosity curve at an arbitrarily chosen high pressure.

In this application the empirical method for determining friction for a lubricated line contact (Appendix IV) is utilized to calculate the frictional forces and torque acting on the ball at a ball-race contact in terms of normal contact load, velocities, ball-race geometry and elastic properties, and lubricant parameters.

#### a. Method of Analysis

Assuming Hertzian contact theory applies, a ball-race contact area is an ellipse in the xy plane perpendicular to the normal contact load, P, as shown in Fig. 107. There, b and a are the semi-minor and semi-major axis of the ellipse respectively, u and v are the rolling and lateral sliding velocity component of the ball at the contact respectively,  $\omega_s$  is the spinning velocity component of the ball about the axis normal to the contact ellipse, and  $u_r$  is the rolling velocity of the contacted race.

The contact ellipse is divided into a number of strips parallel to the x-axis. Each strip is assumed to be a roller rolling in the x-direction. The frictional force in the rolling direction,  $dF_x$ , acting on a strip is determined from Equation IV-3 by first calculating the three friction parameters from Equation IV-2. The appropriate sliding velocity for calculating these parameters is the difference between the rolling speed of the strip,  $u - \omega_s y$ , and the rolling speed of the race,  $u_r$ , namely,

$$u_s = |u - \omega_s y - u_r| \quad (89)$$

According to Hertzian stress distribution, for the strip at y

$$p_{HZ} = \frac{1.5P}{\pi ab} \sqrt{1 - \frac{y^2}{a^2}} \quad (90)$$

The film thickness, h, is calculated by the Dowson and Higginson's formula



$$h = R'_x \left[ 1.6 \frac{(\alpha E')^{0.6} \left( \frac{\mu_o U}{E' R'_x} \right)^{0.7}}{\left( \frac{w}{E' R'_x} \right)^{0.13}} \right] \quad (91)$$

In Equation (91)  $U$  is the average rolling speed, given by:

$$U = \left| u - \omega_s y + u_r \right| / 2, \quad (92)$$

and  $w$  is the load per unit length in  $y$

$$w = \frac{3P}{4b} \left( 1 - \frac{y^2}{a^2} \right) \quad (93)$$

The total frictional force acting on the ball in the  $x$ -direction,  $F_x$ , is simply the sum of all  $dF_x$  over the whole ellipse, i.e.,

$$F_x = \int_{y=-a}^{y=a} dF_x = \int_{-B}^B f w dy \quad (94)$$

The correct sign of  $dF_x$  should be opposite to that of  $u - \omega_s y - u_r$ .

We shall assume that the distribution of shear stress,  $\tau_x$ , is uniform across the strip and that the ratio of the perpendicular shear stress,  $\tau_y$ , to the parallel shear stress,  $\tau_x$ , is equal to the ratio of the shear rates in the respective directions. It follows that

$$\tau_y = - \frac{f w}{2A} \frac{v + \omega_s x}{|u - \omega_s y - u_r|} \quad (95)$$

where  $2A$  is the width of the strip. The lateral frictional force  $F_y$  can then be easily obtained by integration, i.e.,

$$F_y = \int_{-a}^a \int_{-A}^A \tau_y dx dy \quad (96)$$

$$= \int_{-a}^a \frac{-f w v}{|u + \omega_s y - u_r|} dy \quad (97)$$

Finally, the frictional torque  $M_z$  about the normal to the ellipse is calculated as follows:

$$M_z = - \int_{y=-a}^{y=a} y dF_x + \int_{-a}^a \int_{-A}^A \tau_y x dx dy \quad (98)$$

$$= - \int_{-a}^a \left[ f w y + \frac{f w \omega_s b^2 (1 - \frac{y^2}{a^2})}{3 |u - \omega_s y - u_r|} \right] dy \quad (99)$$

#### b. Results

A computer program (Appendix VIII) was written to obtain the frictional coefficient for each strip and to calculate the frictional forces at the contact by numerical integration. The input data include:

Bearing Material Properties:  $E_1, E_2, \nu_1, \nu_2$

Lubricant Parameters:  $\alpha, \beta_1, K_f, \mu_0$

Operating Conditions:  $u, v, \omega_s, u_r, P, T_0$

Ball-Race Geometry:  $R, r, R_G$

In the above,  $R$  is the radius of ball,  $r$  the radius of race, and  $R_G$  the radius of race groove. Other symbols have been previously defined.

A few cases of pure spinning were studied to compare the present method of analysis with the experimental data by Allen, et al (137). The input data are:  $E_1 = E_2 = 3 \times 10^7$  psi,  $\nu_1 = \nu_2 = 0.3$ ,  $\alpha = 0.92 \times 10^{-4}$  psi,  $\beta_1 = 0.028/^\circ\text{F}$ ,  $K_f = 0.1$  BTU/ $^\circ\text{F}$ -hr-ft,  $\mu_0 = 6 \times 10^{-5}$  lb-sec/in<sup>2</sup> at  $30^\circ\text{C}$ ,  $T_0 = 30^\circ\text{C}$ ,  $u = v = u_r = 0$ ,  $R = 0.25$  in.,  $r = \infty$ , and  $R_G = 0.255, 0.275, 0.3$  in. (corresponding to percent conformity = 51, 55, 60 respectively). The calculated spinning torque,  $M_z$ , at spinning velocity  $\omega_s$  of 1050 rpm as a function of maximum Hertz stress together with the experimental data taken from Ref. 137 is shown in Fig. 108. It is seen that the agreement is quite good.

To illustrate the effect of ball spinning on the friction of a ball-race contact, the following case was studied:  $R = 0.25$  in.,  $R_G = 0.275$  in.,  $r = 2.5$  in.,  $u = 300$  in/sec,  $v = 1$  in/sec,  $u_r = 303$  in/sec,  $\omega_s = 0$  to 3000 rpm,  $P = 150$  lbs.,  $T_0 = 86^\circ\text{F}$ , and same lubricant and bearing material as those of the previous cases. The result is shown in Fig. 109. It is seen that, as expected, the frictional torque,  $M_z$ ,



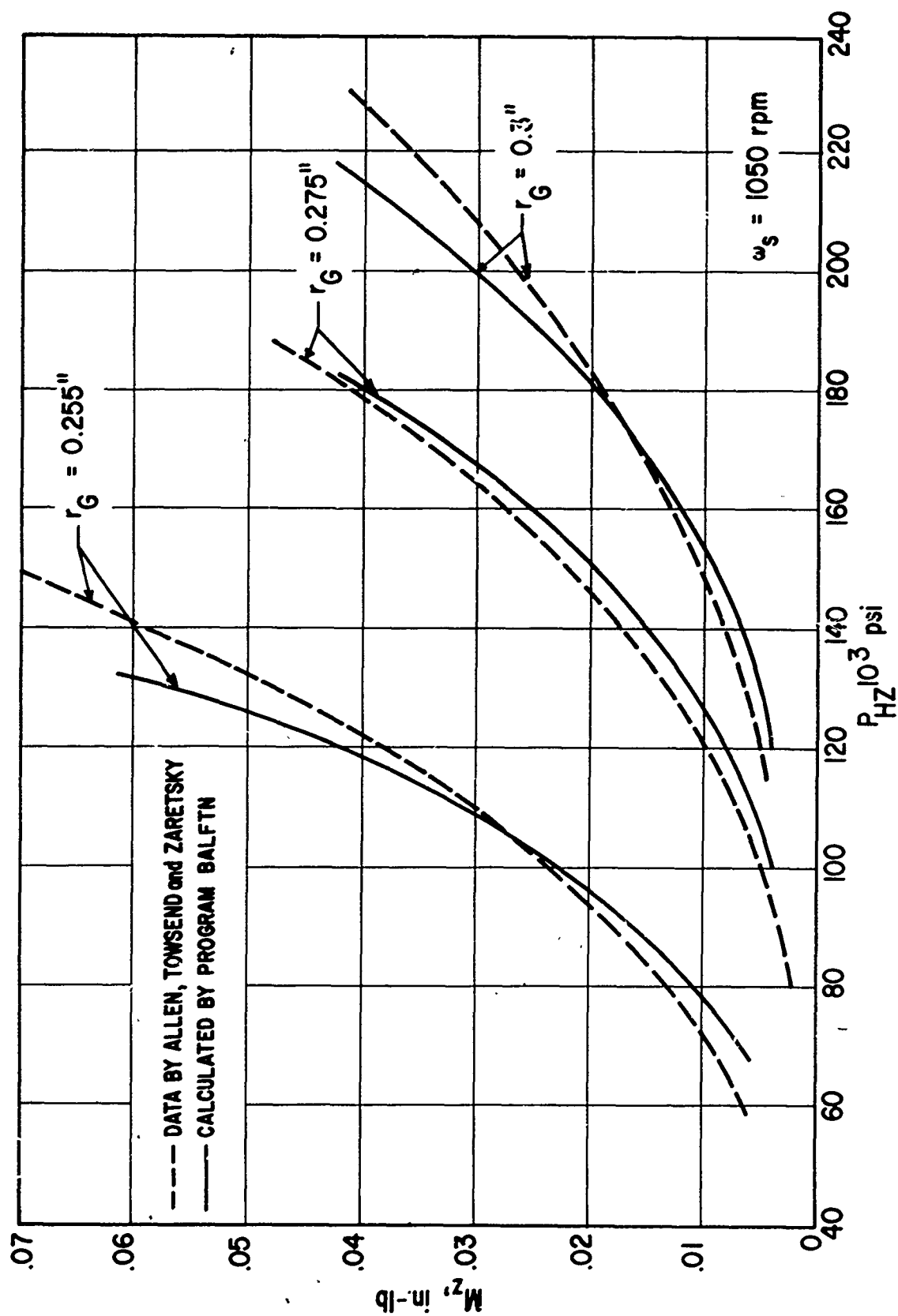


Fig. 108 Frictional Torque as a Function of Spinning Velocity.

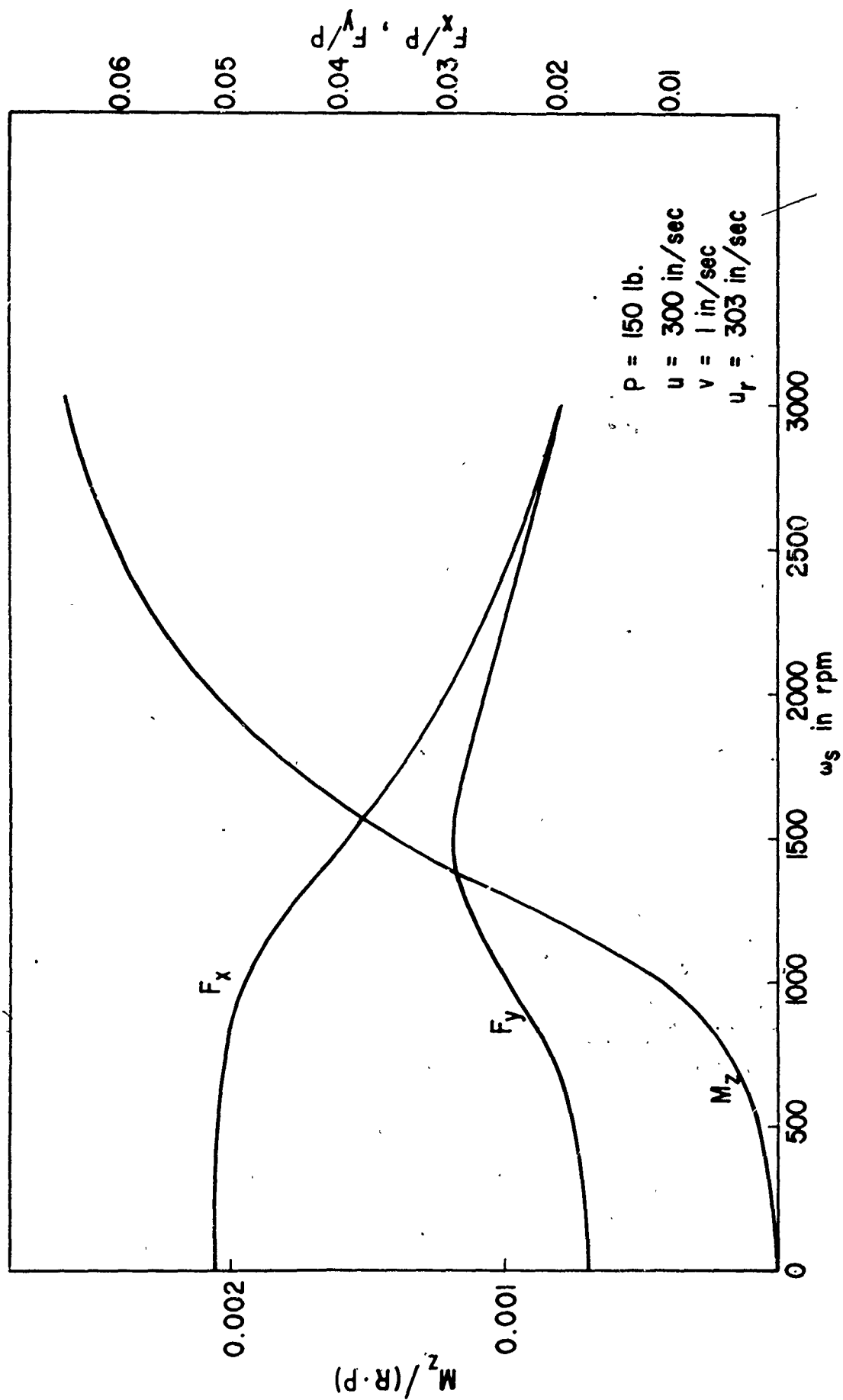


Fig. 109 Effects of Spinning Velocity on Frictional Forces and Torque.

increases with spinning speed, but the rate of increase decreases at high value of spinning speed. The frictional force in the rolling direction,  $F_x$ , decreases with spinning speed. This is because that the effect of sliding speed decreases as spinning speed increases. The existence of a small hump for the later frictional force,  $F_y$ , is due to the fact that at small spinning speed  $F_y$  increases as the result of the slight increase of the frictional coefficients. At very large spinning speed the effect of lateral sliding speed vanishes.

The BALFTN program is intended for use as a subroutine in a larger bearing dynamics program such as that published by Jones (215, 216). It provides a more advanced method for calculating ball frictional forces than used by either Harris (156) or Walters (159). Thermal effects are accounted for and the calculation of friction forces is based on empirical methods.

## SECTION V

### CONCLUSIONS AND RECOMMENDATIONS

Although technical work on elastohydrodynamic lubrication has been going on for some eighteen years both here and abroad, there has been little opportunity to compile and assess the significance and the interrelationships of the diverse research results available today. This report represents such an assessment and, in it, all of the available data on heavily loaded rolling and sliding contact lubrication has been surveyed, compiled and summarized. Out of this assessment, an immediately useful design procedure has been generated and a plan for continued research evolved as outlined below.

#### 1. CONCLUSIONS

Progress in elastohydrodynamic lubrication has advanced to the stage where the development of practical design tools is now possible. Based on an assessment of the literature, a computer program was written which calculates all the major variables in an elastohydrodynamic contact including film thickness, area of contact, friction, pressure distribution, temperature distribution, and stress distribution. The relation of these factors to bearing life and type of ultimate failure has been illustrated by sample calculations.

Conclusions about the accuracy with which the above parameters can be calculated are summarized below.

##### a. Film Thickness

The film separation between steel rolling and sliding contacts can be accurately predicted by film thickness formulae proposed by Dowson and Higginson (91) for rolling speed up to 250 in/sec. For high speed contacts, the reduction of film thickness due to thermal effects may be determined by the data provided by Cheng (93). However, there is still a disagreement between these data and the x-ray data (104) with regard to the effect of load. It is uncertain whether the discrepancy is due to certain factors neglected in the analysis or due to the inherent inaccuracy of the x-ray technique at these small film thicknesses.

##### b. Area of Contact

All available experimental data indicate that the surface roughness distribution of rolling element bearings can be assumed to be Gaussian. If it is further assumed that displaced asperities move vertically down and do not spread horizontally, calculation of the real of area of contact is simple. However, the above model does not allow for relative motion between the surfaces or for the fact that rolling element bearing surface topography is not constant but

changes from one Gaussian distribution to another, as the bearing wears.

#### c. Friction

Presently available elastohydrodynamic theories are far from adequate in predicting the frictional force between two heavily loaded contacts. There are two major reasons for this lack of correlation between the present elastohydrodynamic theories and the measured friction data. First, there is a complete absence of static viscosity data at extremely high pressures. Since the shear stress at a boundary is a product of the viscosity and the shear rate, and since the viscosity is extremely sensitive to both pressure and temperature in the high pressure region, the calculation of friction is inaccurate when using extrapolated viscosity data measured at the moderate pressures or by using an empirical pressure-temperature-viscosity function. A second reason for the lack of correlation is the use of the static viscosity data for conditions where the pressure, temperature, shear stress and shear rate all undergo a tremendous rate of change. Under these circumstances, the flow properties may not have enough time to reach equilibrium and behave in the fashion measured in static experiments. These are the two major reasons which have prevented the development of a satisfactory analytical tool in predicting the traction between elastohydrodynamic contacts.

To overcome this lack of an adequate friction theory, empirical data of Johnson and Cameron (129) was used for determination of friction in the Elastohydrodynamic Performance Calculation. Since Johnson's experimental data covers only a restricted range of rolling and sliding speeds and lubricant parameters, the application of their data at conditions other than those used in their experiment was achieved by expressing their data in terms of pertinent dimensionless parameters.

#### d. Pressure Distribution

Almost all elastohydrodynamic theories thus far have shown that the pressure profile for heavily loaded contacts does not deviate much from the Hertzian elliptical pressure profile. The deviation occurs mainly in the inlet and the exit regions. Due to the elastohydrodynamic action there is a gradual build-up in pressure ahead of the Hertzian region which is absent in the case of a dry contact. In the contact zone the pressure profile is essentially Hertzian. In the exit region, the elastohydrodynamic theories show that there exists a pressure spike right at the point the protrusion begins. After the pressure spike,

the pressure decays extremely rapidly to the ambient pressure.

Unfortunately, the exact details of the pressure profile at the inlet and near the pressure spike can only be obtained by solving numerically the simultaneous elasticity, hydrodynamic and energy equations. Such an iterative numerical solution for the pressure profile required a large amount of computation time and the convergence of the solution is not necessarily guaranteed particularly at high speeds and high loads. For this reason the full elastohydrodynamic solution has not been chosen at this time to obtain the pressure profile for this preliminary design tool. Instead, an approximate pressure profile was computed in this program. It assumes that inlet deformation profile follows the Hertzian elasticity solution and the pressure spike occurs exactly at the point where the protrusion begins except at very low loads.

e. Temperature Distribution

In calculating the surface and film temperature distributions in an elastohydrodynamic contact, the available numerical methods are reasonably complete and accurate. These methods can be divided into two categories. The first category is only applicable to the inlet region and the second category is for the contact region. The inlet thermal methods are for moderate pressure only, and they contain special numerical treatments which avoid the numerical instability associated with the reverse flow in the inlet region. The methods for the contact region are specially designed for high pressure, and are not suitable for calculations at the inlet where there is a negative flow. The descriptions of these methods are given below.

In selecting the tools for calculating the temperature distributions in the Elastohydrodynamic Performance Calculation, a mean viscosity method for the contact region and an integral thermal analysis for the inlet region were used. These methods were chosen mainly because: the analysis is simple, the computation time is short and the results are sufficiently accurate for design purposes.

The limitations of this thermal program have not been fully explored. So far, no convergence difficulties have been experienced for maximum Hertz pressure up to 300,000 psi and speeds up to 2000 in/sec.

f. Stress Distribution

Numerical methods must be used to calculate the stress components in a solid for an arbitrarily distributed surface

traction. A numerical solution based on the elasticity solution for an elastic half-space was used in the calculation procedure to determine the three principal stresses, the maximum shear stress as well as the octahedral stress for any given point in the contact zone.

This calculation procedure is only accurate for larger values of ellipticity, where the stresses at the center can be approximated by line contact theory. This approximation is valid for most rolling element bearing calculations.

In summary, a calculation procedure for predicting all the major variables in an elastohydrodynamic contact has been developed and programmed for computer computation. The procedure is based on the state-of-the-art and best current theories. Although, of necessity containing many approximations, the computed operating parameters are comparable with experimental evidence. The program provides a means for relating these operating parameters to the lubrication regime and type of failure mode.

## 2. RECOMMENDATIONS

An equally important objective of the work conducted in this study is the identification of areas in the elastohydrodynamic field requiring further experimental and analytical exploration. The choice of areas for further investigation is based primarily on the contribution of the proposed work toward the development of practical design procedures and methods of predicting contact failure.

Consequently, more sophisticated or extensive numerical solutions for the thermal-elastohydrodynamic problem in the contact zone than used in this work or available in the general literature is not recommended as such efforts will not materially increase our predictive capability in elastohydrodynamics. Based on our review of the state-of-the-art, four areas of investigation appear to offer the greatest possibility for improving our ability to predict elastohydrodynamic behavior. These are outlined below.

### a. Friction

The most important subject for further work in elastohydrodynamics today from a bearing engineer's point of view is the prediction of contact friction. Accurate values of contact friction are needed for calculation of contact temperatures and prediction of rolling element bearing dynamics. Present elastohydrodynamic theories predict values of friction several times higher than measured values. The most likely reason for this is our imperfect understanding of lubricant rheology under high pressure, temperature, and shear rates. The basic problem is a rheological one and its complete solution must await better understanding of lubricant rheology. While work proceeds on lubricant rheology, however, useful design information can be obtained by adopting an empirical approach such as discussed in Section III

of this report. The empirical correlation described in Section III is based entirely on the limited data published by Johnson and Cameron (129). Further experimental friction measurements are required to verify this correlation over wider ranges of pressure, temperature, shear rate, and lubricant properties. Such empirical friction data is needed to serve as a stop gap design measure until a fuller understanding of lubricant rheology is achieved.

b. Film Thickness

Until recently, methods for the prediction of elastohydrodynamic film thickness have been considered quite accurate. However, recent film thickness measurements obtained by the x-ray technique have cast doubt on the earlier methods based on capacitance measurements by showing an unexpected load dependence both at high and low rolling speeds. It is difficult to account for this discrepancy between the x-ray and capacitance measurements. It is therefore recommended that a direct experimental comparison be made between the two methods under identical test conditions.

c. Contact Zone Topography

The degree of asperity contact is a significant parameter because it is a measure of the effectiveness of the elastohydrodynamic film and a realistic gage of bearing wear and smearing. The model used for the Elastohydrodynamic Calculation Procedure developed in this work is a simple one and does not account for relative motion between the surfaces in contact or the changing surface topography arising from normal bearing operation.

It is proposed to extend the analytical model used in the present analysis to include relative motion of the surfaces and changing surface topography with time. In addition, the model should include a more detailed shape of the exit protrusion because it determines the extent of asperity contact, particularly when the contact zone geometry deviates significantly from the line contact assumption used in the present analysis.

To corroborate this analysis, electrical conductivity measurements should be made with either a ball or roller geometry. In addition, a statistical representation of the test surface microtopography should be recorded with a surface roughness tester, frequency analyses of the roughness signals performed, and the appropriate statistical parameters correlated with asperity contact rate, area of contact, film thickness, and change of surface topography as the surfaces wear.

d. Lubricant Rheology

Many of the unsolved problems in elastohydrodynamics appear related to an imperfect understanding of lubricant rheology at



high temperature, pressure, and shear rates. This then is the basic problem, and unfortunately the most difficult. This lack of knowledge about lubricant rheology under severe conditions cannot simply be overcome by extending the range of measurements using present experimental methods, as these methods are not suitable under such operating conditions.

Therefore, the first task is to develop experimental techniques to determine lubricant rheological properties under high pressure, temperature, and shear rate conditions. Once this is accomplished measurements should be made of the rheological parameters of the candidate lubricants including variation of viscosity with pressure, temperature, and shear rate. In addition, the short-time lubricant behaviors should be determined.

In parallel with the above experimental activity, major analytical effort should be directed toward developing appropriate rheological models capable of predicting friction and film thickness under extreme operating conditions.

In summary, four primary areas in elastohydrodynamic research, contact friction, contact film thickness, contact topography and lubricant rheology have been identified as requiring better understanding before better techniques of predicting elastohydrodynamic behavior can be developed.

## REFERENCES

1. Murphy, C.M. and Zisman, W.A., "Structural Guides for Synthetic Lubricant Development," Ind. and Eng. Chem., Vol. 42, No. 12, Dec. 1950, pp. 2415-2420.
2. Bondi, A., Physical Chemistry of Lubricating Oils, Reinhold Publishing Corp., New York, 1951.
3. Gunderson, R.C. and Hart, A.W., Synthetic Lubricants, Reinhold Publishing Corp., New York, 1962.
4. Lubrication and Lubricants, Edited by E.R. Braithwaite, Elsevier Publishing Company, New York, 1967.
5. Hirschfelder, J.O., Curtiss, C.F., and Bird, R.B., Molecular Theory of Gases and Liquids, Wiley, New York, 1954.
6. Zisman, W.A., Friction and Wear, Edited by R. Davies, Chpt. "Friction, Durability and Wettability Properties of Monomolecular Films on Solids," Elsevier Publishing Company, 1959.
7. Bowden, F.P. and Tabor, D., The Friction and Lubrication of Solids, Vol. 2, Oxford Press, 1964.
8. VanWazer, J.R., et al, Viscosity and Flow Measurement, Interscience Publishers, New York, 1963.
9. Wilcock, D.F. and Booser, E.R., Bearing Design and Application, McGraw-Hill Book Company, Inc., New York, 1957.
10. Georgi, C.W., Motor Oils and Engine Lubrication, Reinhold Publishing Corp., New York, 1950.
11. "Viscosity-I and Viscosity-II," Lubrication, Anon., Vol. 47, Nos. 1 and 2, 1961, Published by Texaco, Inc., New York.
12. ASTM Book of Standards, Vols. 17 and 18, 1969:
  - a) Basic Calibration of Master Viscometers and Viscosity Oil Standards, Test for (D2162), Vol. 17.
  - b) Kinematic Glass Viscometers, Spec. for. (D2512), Vol. 17.
  - c) Viscosity of Transparent and Opaque Liquids (D445), Vol. 18.
  - d) Saybolt Viscosity, Test for (D88), Vol. 18.
  - e) Viscosity and Viscosity Change after Standing at - 65 F of Aircraft Turbine Lubricants, Test for (D2532), Vol. 17.
  - f) Conversion of Kinematic Viscosity to Saybolt Universal Viscosity or to Saybolt Furol Viscosity (D2161), Vol. 17.

13. Ibid. Estimation of Molecular Weight of Petroleum Oils from Viscosity Measurements (D2502), Vol. 17.
14. Symposium on Methods of Measuring Viscosity at High Rates of Shear. ASTM Spec. Tech. Bull. No. 111, 1951.
15. ASME-ASTM-ASLE Symposium on Lubrication and Lubricant Rheology, Trans. ASME J. Lubr. Tech., Vol. 90F, No. 3, pp. 525-613, 1968.
16. ASTM Book of Standards, Vol. 17, 1969:  
Standard Viscosity Temperature Charts (D341), Vol. 17.
17. Ibid. Calculating Viscosity Index from Kinematic Viscosity (D2270), Vol. 17.
18. Gerrard, J.E. and Philippoff, W., "Viscous Heating and Capillary Flow," 4th International Congress of Rheology, 1963, Paper No. 51.
19. Gerrard, J.E., Steidler, F.E., and Appeldoorn, J.K., "Viscous Heating in Capillaries: The Adiabatic Case," ACS Petroleum Division Meeting, Chicago, Illinois, Sept. 1964.
20. Gerrard, J.E., Steidler, F.E., and Appeldoorn, J.K., "Viscous Heating in Capillaries: The Isothermal Wall Case," ACS Petroleum Division Meeting, Atlantic City, N.J., Sept. 1965.
21. Novak, J.D. and Winer, W.O., "Some Measurements of High Pressure Lubricant Rheology," Trans. ASME J. Lubr. Tech., Vol. 90F, pp. 580-591, 1968.
22. Bridgeman, P.W., Collected Works, Harvard University Press.
23. "Viscosity and Density of Over 40 Lubricating Fluids of Known Composition, at Pressures to 150,000 psi and Temperatures to 425 F," ASME, New York, 1966.
24. Cameron, A., Principles of Lubrication, Wiley & Sons, New York, 1966.
25. Ed. by Ling, F.F., Klaus, E.E. and Fein, R.S., Boundary Lubrication - An Appraisal of World Literature, ASME, New York, 1959, Chapter 8 "Physical Properties of Lubricants," by Appeldoorn, J.K.
26. Bridgeman, P.W., "Viscosities to 30,000 kg/cm<sup>2</sup>", Proceedings of the American Academy of Arts and Sciences, Vol. 77, No. 4, pp. 115-128, 1949.
27. Barlow, A.J. and Lamb, J., "The Visco-Elastic Behavior of Lubricating Oils Under Cyclic Shearing Stress," Proc. Royal Society, Vol. 253A, pp. 52-69, 1959.
28. Anderson, W.J. and Carter, T.L., "Effect of Lubricant Viscosity and Type on Ball Fatigue Life," ASLE Trans., Vol. 1, No. 2, 1958, pp. 266-272.
29. Klaus, E.E. and Fenske, M.R., "Some Viscosity-Shear Characteristics of Lubricants," Lubrication Engrg., Vol. 12, No. 2, 1955, pp. 101-108.

30. Selby, T.W., "The Non-Newtonian Characteristics of Lubricating Oils," ASLE Trans., Vol. 1, 1958, pp. 68-81.
31. Philippoff, W., "Viscosity Measurements on Polymer Modified Oils," ASLE Trans., Vol. 1, No. 1, 1958, pp. 82-86.
32. Wright, W.A. and Crouse, W.W., Jr., "A New Concept in Generalizing Non-Newtonian Fluid Flow Data," ASLE Trans., Vol. 8, No. 2, pp. 184-190, 1965.
33. Philippoff, W., "Viscoelasticity of Polymer Solutions at High Pressure and Ultrasonic Frequencies," J. Applied Phys., Vol. 34, No. 5, 1963.
34. Currie, C.C. and Smith, B.F., "Flow Characteristics of Organo Polysiloxane Fluids and Greases," Industrial and Engineering Chemistry, Vol. 42, pp. 2457-2562, 1950.
35. Dow Corning Bulletin No. 05-153.
36. Porter, R.S. and Johnson, J.F., "Viscosity Performance of Lubricating Base Oils at Shears Developed in Machine Elements," Wear, Vol. 4, No. 1, 1961, pp. 32-40.
37. Lewis, P. and Murray, S.F., "Effect of Lubricant Properties on the Coast-down Characteristics of Instrument Bearings," Lubr. Engrg., Vol. 18, No. 1, 1962.
38. Private Communication from W.O. Winér, March 6, 1969.
39. Porter, R.S., Cantow, M.J.R., and Johnson, J.F., "Polymer Degradation VI-Distribution Changes on Polyisobutene Degradation in Laminar Flow," Polymer, Vol. 8, pp. 87-96, 1967.
40. Wright, W.A., Private Communication.
41. ASTM Book of Standards, Vol. 17, 1969.
  - a) Apparent Viscosity of Motor Oils at Low Temperature Using the Cold Cranking Simulator, Test for (D2602), Vol. 17.
  - b) Apparent Viscosity of Motor Oils at Low Temperature Using a Reciprocating Viscometer, Test for (Proposed), Vol. 17.
42. Selby, T.W., "A Low Temperature Study of the Relationship Between Engine Cranking Speed and Lubricant Viscosity," ASLE Trans., Vol. 2, No. 2, 1959, pp. 208-216.
43. Tanner, R.I., "Response of Viscoelastic Fluids in Dynamically Loaded Bearings," Trans. ASME, J. Lubr. Tech., Vol. 90F, pp. 555-560, 1968.
44. Tao, F.F. and Philippoff, W., "Hydrodynamic Behavior of Viscoelastic Liquids in a Simulated Journal Bearing," Trans. ASLE, Vol. 10, pp. 302-315, 1967.
45. Metzner, A.B., "The Significant Rheological Characteristics of Lubricants" Trans. ASME, J. Lubr. Tech., Vol. 90F, pp. 531-540, 1968.

46. Dyson, A. and Wilson, A.R., "Film Thicknesses in Elastohydrodynamic Lubrication by Silicones Fluids," Proc. of I.M.E., Vol. 180, pt. 3K, pp. 97-112, 1965-66.
47. Barlow, A.J., Harrison, G., and Lamb, J., "Visco-elastic Relaxation of Polydimethyl Siloxane Liquids," Proc. Royal Society, Vol. 282A, pp. 228-251, 1964.
48. Forster, E.O., "Relaxation Phenomena in Lubrication," Lubr. Engrg., Vol. 16, No. 11, 1960, pp. 523-528.
49. Borsoff, V.N., "On the Mechanism of Gear Lubrication," Trans. ASME, J. of Basic Engrg., 1959.
50. Smith, F.W., "Some Aspects of Nonlinear Behavior in Lubricants Under Extreme Stress," Trans. ASME, J. Lubr. Tech., Vol. 90F, pp. 549-554, 1968.
51. Bell, J.G., "Lubrication of Rolling Surfaces by a Ree-Eyring Fluid," Trans. ASLE, Vol. 5, No. 1, p. 160, 1962.
52. Lamb, J., "Physical Properties of Fluid Lubricants: Rheological and Viscoelastic Behavior," Proc. I.M.E., Vol. 182, pt. 3A, pp. 293-310.
53. Roelands, C.J.A., "Correlational Aspects of the Viscosity-Temperature-Pressure Relationships of Lubricating Oils," Ph D. Thesis, Delft, 1966.  
  
See also, Roelands, C.J.A., Vlugter, J.E., and Waterman, H.I., "The Viscosity-Temperature-Pressure Relationship of Lubricating Oils and its Correlation with Chemical Constitution," ASME Paper No. 62-WA-178.
54. Appeldoorn, J.K., "A Simplified Viscosity-Pressure-Temperature Equation," SAE Journal, Vol. 71, June 1963, p. 108.
55. Chu, P.S.Y. and Cameron, A., "Pressure Viscosity Characteristics of Lubricating Oils," J. Inst. Petroleum, Vol. 48, pp. 147-155, 1962.
56. Griest, E.M., Webb, W., and Schiessler, R.W., "Effect of Pressure on Viscosity of Higher Hydrocarbons and Their Mixtures," J. Chem. Phys., Vol. 29, No. 4, pp. 711-720, 1958.
57. Hogenboon, D.L., Webb, W., and Dixon, J.A., "Viscosity of Several Liquid Hydrocarbons as a Function of Temperature, Pressure and Free Volume," J. Chem. Phys., Vol. 46, No. 7, pp. 2586-2598, 1967.
58. Cheng, H.S. and Sternlicht, B., "A Numerical Solution for the Pressure-Temperature and Film Thickness Between Two Infinitely Long, Lubricated Rolling and Sliding Cylinders Under High Loads," Trans. ASME, J. Basic Engrg., Vol. 87D, pp. 695-707.
59. Dowson, D. and Whitaker, A.V., "A Numerical Procedure for the Solution of the Elastohydrodynamics Problems of Rolling and Sliding Contacts Lubricated by a Newtonian Fluid," Proc. I.M.E., Vol. 180, pt. 3B, pp. 57-71, 1965-66.

60. Foord, C.A., Hammann, W.C., and Cameron, A., "Evaluation of Lubricants Using Optical Elastohydrodynamics," ASLE Trans., Vol. 11, pp. 31-43, 1968.
61. Criddle, D.W., "Surface Viscosity and Elasticity of Lubricating Oils," Lubr. Engrg., Vol. 13, No. 3, 1957, pp. 131-135.
62. Deryagin, V.V., Abrikosove, I.I., and Lifshitz, E.M., Quarterly Rev., Vol. 10, p. 295, 1956.
63. Cameron, A. and Gohar, R., "Theoretical and Experimental Studies of the Oil Film in Lubricating Point Contact," Proc. Royal Soc., Vol. 291A, pp. 520-536, 1966.
64. Needs, S.J., "Boundary Film Investigation," Trans. ASME, Vol. 62, pp. 331-345, 1940.
65. Fein, R.S., "Possible Role of Compressional Viscoelasticity in Concentrated Contact Lubrication," Trans. ASME, J. Lubr. Tech., Vol. 89F, pp. 127-133, 1967.
66. Fein, R.S. and Kreuz, K.E., "Discussion on 'Boundary Lubrication'", Proceeding of the NASA Symposium on Interdisciplinary Approach to Friction and Wear, 1967, pp. 6.2.1-6.2.25.
67. Wright, W.A., "Prediction of Bulk Moduli and Pressure-Volume-Temperature Data for Petroleum Oils," ASLE Trans., Vol. 10, No. 4, 1967, p. 349.
68. Tichy, J.A. and Winer, W.O., "A Correlation of Bulk Moduli and P-V-T Data for Silicone Fluids at Pressure up to 500,000 psig," ASLE Trans., Vol. 11, No. 4, 1968, pp. 338-344.
69. Hopkins, V., Wilson, D.R., and Bolze, C., "Isothermal Bulk Modulus of Selected Fluids to 700 F and 10,000 psig," Trans. ASME. J. of Basic Engrg. 1964.
70. Beerbower, A. and Green, D.F., "The Behavior of Lubricating Oils in Inert Gas Atmosphere," ASLE Trans., Vol. 4, No. 1, 1966, p. 87.
71. Greeman, P.A., "Gyro Ball Bearings - Technology Today," Presented at 6th AGARD Guidance and Control Meetings, "Inertial Navigation Components," Germany, May 7-9, 1968.
72. Rhoads, W.L. and Sibley, L.B., "Supersonic Transport Lubrication System Investigation," NASA CR-54313, Third Semiannual Report, May 20, 1966.
73. "Cooling Failures," Ed. J. Fisher, Components and Design, Metalworking News, January 27, 1969, p. 19.
74. Murray, S.F. and Lewis, P., "Vacuum Operation of Oil-Lubricated Bearings," MTI 68TR65. October 1968, Work done for NASA Goodard Space Flight Center under Contract NAS5-10433.

75. Fein, R.S. and Krautz, K.L., "Chemistry of Boundary Lubrication of Steel by Hydrocarbons," ASLE Trans., Vol. 8, No. 1, 1965, p. 29.
76. Klaus, E.E. and Hersh, R.E., "Paraffinic Resin - A High Quality Lubricant and Newtonian V.I. Improver for Hydraulic Fluids," SAE Paper 650673, Milwaukee, Wisconsin, September 1965.
77. "Super Refined Hydraulic Oils," Anon. Bulletin from Humble Oil and Refining Company, Houston, Texas.
78. Parker, R.J., Zaretsky, E.V., and Anderson, W.J., "Rolling Contact Lubrication Studied with Polyphenyl Ethers at Reduced Pressures," NASA TN D-3130.
79. Reichard, D.W., Parker, R.J., and Zaretsky, E.V., "Studies of Rolling Element Lubrication and Fatigue Life in a Reduced Pressure Environment," ASLE Trans., Vol. 11, No. 3, 1968, pp. 275-281.
80. Parker, R.J., Bamberger, E.N., and Zaretsky, E.V., "Evaluation of Lubricants for High Temperature Ball Bearing Applications," ASME Paper 67LUB21, Presented at ASLE/ASME Lubr. Conf., Chicago, October 17-19, 1967.
81. Godfrey, D., "Chemical Changes in Steel Surfaces During Extreme Pressure Lubrication," ASLE Trans., Vol. 5, No. 1, 1962, p. 57.
82. Grubin, A.N. and Vinogradova, I.E., Central Scientific Research Institute for Technology and Mechanical Engineering, Book No. 30 (Moscow); D.S.I.R., Trans. No. 337, 1949.
83. Crook, A.W., "The Lubrication of Rollers - I," Phil. Trans. Series A 250, 387, 1958.
84. Crook, A.W., "The Lubrication of Rollers - II. Film Thickness with Relation to Viscosity and Speed," Phil. Trans., Series A 254, 234, 1961.
85. Sibley, L.L. and Orcutt, F.K., "Elastohydrodynamic Lubrication of Rolling Contact Surfaces," Amer. Soc. Lubr. Engrg., Vol. 4, No. 2, p. 234, 1961.
86. Archard, J.F. and Kirk, M.T., "Lubrication at Point Contacts," Proc. R. Soc., Series A 261, p. 532, 1961.
87. Christensen, H. "The Lubrication of Rolling Contacts. Measurement of Film Thickness," Acta Polytech. Scand. Mech. Engrg., Series 15, 1963.
88. Dyson, A., "Flow Properties of Mineral Oils in Elastohydrodynamic Lubrication," Phil. Trans. R. Soc., Series A 258, p. 529, 1965.
89. Cameron, R. and Gregory, R.W., "Measurement of Oil Film Thickness Between Rolling Discs Using a Variable Reluctance Technique," The Institute of Mech. Engrg. Proc. 1967-68, Vol. 182, pt. 3N.
90. Petrusevich, A.I., "Fundamental Conclusions from the Contact-Hydrodynamic Theory of Lubrication," Iz. Akad. Nauk S.S.S.R. (OTN) 2, p. 209, 1951.

91. Dowson, D. and Higginson, G.R., "A Numerical Solution to the Elastohydrodynamic Problem," *F. Mech. Engrg. Sci.* 1 (1), 6, 1959.
92. Archard, G.D., Gair, F.C., and Hirst, W., "The Elastohydrodynamic Lubrication of Rollers," *Proc. R. Soc. Series A* 262, 51, 1961.
93. Cheng, H.S., "A Refined Solution to the Thermal-Elastohydrodynamic Lubrication of Rolling and Sliding Cylinders," *Mechanical Technology Report* 64TR7.
94. Dowson, D. and Higginson, G.R., "New Roller-Bearing Lubrication Formula" *Engineer*, London, 192, 158, 1961.
95. Moes, H., In *Communications, Institute of Mech. Engrg Proc.* 1965-66, Vol. 180, pt. 3B.
96. Koets, O.J., "A Survey of the Isothermal Theory of Elastohydrodynamic Lubrication," *Univ. Tech. Rept.*, Delft, 1962.
97. Martin, H.M., "Lubrication of Gear Teeth," *Engineering*, London, Vol. 102, 199, 1961.
98. Weber, C. and Saalfeld, K., "Schmierfilm bei Walzen mit Verformung," *Zeits. ang. Mech.*, Vol. 34, 64, 1954.
99. Kannel, et al, "A Study of the Influence of Lubricants on High-Speed Rolling-Contact Bearing Performance," *Technical Report No. ASD-TR-61-643, Part III*, 1963.
100. Kannel, et al, "A Study of the Influence of Lubricants on High-Speed Rolling-Contact Bearing Performance," *Technical Report No. ASD-TR-61-643, Part IV*, 1964.
101. Kannel, J.W., "The Measurement of Pressure in Rolling Contacts," *Lubrication and Wear Group Symposium on Elastohydrodynamic Lubrication, Paper II (Instn. Mech. Engrs.)*, London, 1965.
102. Kannel, et al, "A Study of the Influence of Lubricants on High-Speed Rolling-Contact Bearing Performance," *Technical Report No. ASD-TR-61-643, Part VI*, 1966.
103. Kannel, et al, "A Study of the Influence of Lubricants on High-Speed Rolling-Contact Bearing Performance," *Technical Report No. ASD-TR-61-643, Part VII*, 1967.
104. Kannel, et al, "A Study of the Influence of Lubricants on High-Speed Rolling-Contact Bearing Performance," *Technical Report No. ASD-TR-61-643, Part VIII*, 1968.
105. Cheng, H.S., "Calculation of Elastohydrodynamic Film Thickness in High-Speed Rolling and Sliding Contacts," *MTI* 67TR24, 1967.
106. Archard, J.F. and Kirk, M.T., "Film Thickness for a Range of Lubricants Under Severe Stress," *J. Mech. Engrg. Sci.* 6, 101, 1964.



107. Archard, J.F. and Cowking, E.W., "A Simplified Treatment of Elastohydrodynamic Lubrication Theory for a Point Contact," Lubrication and Wear Group Symposium on Elastohydrodynamic Lubrication, Paper 3 (Instn. Mech. Engrs., London), 1965.
108. Gohar, R. and Cameron, A., "The Mapping of Elastohydrodynamic Contacts," ASLE Preprint 66-LC-21.
109. Hingley, C.J., Schmidt, W.E., and Tataiah, K., "A Study of the Geometry of Elastohydrodynamic Films in Point Contact," SKF Report AL66L035.
110. Snidle, R.W. and Archard, J.F., "Lubrication of Elliptical Contacts," Dept. of Engrg., Univ. of Leicester, July 1968 (To be Published.)
111. Door, J., "Schmiermitteldruck und Randverformungen," Ingen. Archiv 22, (3), 171, 1954.
112. Osterle, J.F. and Stephenson, R.R., "A Direct Solution of the Elastohydrodynamic Lubrication Problem," Trans. Amer. Soc. Lubr. Engrs. 5, (2), 365, 1962.
113. Wernick, R.J., "Some Computer Results in the Direct Iteration Solution of the Elastohydrodynamic Equations," MTI Technical Report 62TR38, 1963.
114. Dowson, D. and Whitaker, A.V., "The Isothermal Lubrication of Cylinders" Presented at the ASME-ASLE International Lubrication Conference (Washington, D.C.) Oct. 1964, ASLE Preprint 64-LC-22.
115. Sternlicht, B., Lewis, P., and Flynn, P., "Theory of Lubrication and Failure of Rolling Contact," J. Basic Engrg., Trans. ASLE Vol. 83, Series D, No. 2, p. 213, 1961.
116. Dowson, D. and Longfield, M.S., "Distribution of Pressure and Temperature in a Highly Loaded Lubricated Contact," Proc. Lubr. and Wear Convention (Bournemouth), Paper 3, 27 (Instn. Mech. Engrs., London) 1963.
117. Longfield, M.D., "Pressure Distributions in a Highly Loaded Lubricated Contact," Lubr. and Wear Group Symposium on Elastohydrodynamic Lubr., Paper 9, (Instn. Mech. Engrs., London), 1965.
118. Orcutt, F.K., "Experimental Study of Elastohydrodynamic Lubrication," ASLE Paper No. 65AM423.
119. Kannel, J.W., "The Measurement of Pressure in Rolling Contacts," Lubr. and Wear Group Symposium on Elastohydrodynamic Lubr., Paper 11 (Instn. Mech. Engrs., London) 1965.
120. Crook, A.W., "The Lubrication of Rollers - III. A Theoretical Discussion of Friction and the Temperatures in the Oil Film," Phil. Trans. Series A 254, 237, 1961.

121. Bell, J.C., Kannel, J.W., and Allen, C.M., "The Rheological Behavior of the Lubricant in the Contact Zone of a Rolling Contact System," J. Basic Engrg. Trans. ASME 86, Series D, No. 3, 423, 1964.
122. Orcutt, F.K., "Experimental Study of Elastohydrodynamic Lubrication," MTI Report 64TR6.
123. Cameron, A. and Newman, A.D., Proc. Conference of Steam Turbine Research and Development, London: Institute of Mechanical Engineers.
124. Misharin, J.A., "Influence of the Friction Conditions on the Magnitude of the Friction Coefficient in the Case of Rolling with Sliding," Proceedings of the International Conference on Gearing, the Institute of Mechanical Engineers, London, 1958, pp. 159-164.
125. Benedict, G.H. and Kelley, B.W., "Instantaneous Coefficients of Gear Tooth Friction," Trans. ASLE, Vol. 4, 1959.
126. Crook, A.W., "The Lubrication of Rollers - IV Measurements of Friction and Effective Viscosity," Philosophical Trans. Series A 255, 281.
127. Smith, F.W., "Rolling Contact Lubrication - The Application of Elastohydrodynamic Theory," J. of Basic Engrg, Trans. of ASME, Vol. 87, Series D, No. 1, March 1965, p. 170.
128. Dyson, B., "Frictional Traction and Lubricant Rheology in Elastohydrodynamic Lubrication," To be published.
129. Johnson, K.L. and Cameron, R., "Shear Behavior of Elastohydrodynamic Oil Film at High Rolling Contact Pressures," Proc. of Instn. of Mech. Engrs. 1967-1968, Vol. 182, p. 307.
130. Jefferis, J.A. and Johnson, K.L., "Sliding Friction Between Lubricated Rollers," Proc. of Instn. of Mech. Engrs., 1967-1968, Vol. 182.
131. Plint, M.A., "Traction in Elastohydrodynamic Contacts," Proc. of Instn. of Mech. Engrs., 1967-1968, Vol. 182, p. 300.
132. Dowson, P. and Wholmes, T.L., "Effect of Surface Quality Upon the Traction Characteristics of Lubricated Cylindrical Contacts," Proc. of Instn. Mech. Engrs., Vol. 182.
133. Barlow, A.J. and Lamb, J., "The Visco-elastic Behavior of Lubricating Oils Under Cyclic Shearing Stress," Proc. R. Soc., A, 253, p. 52, 1959.
134. Kannel, J.W. and Walowit, J.A., "Simplified Analyses for Traction Between Rolling-Sliding EHD Contacts," to be published in ASME Trans. J. Lubr. Tech.
135. Dietrich, M.W., Parker, R.J., Zaretsky, E.V., and Anderson, W.J., "Contact Conformity Effects on Spinning Torque and Friction," ASME Paper No. 68-Lub-10.

136. Parker, R.J., Zaretsky, E.V., and Anderson, W.J., "Spinning Friction Coefficients with Three Lubricants," J. of Lubr. Tech. Trans. of ASME, Series F, Vol. 90, No. 1, January 1968, p. 330.
137. Allen, C., Townsend, D., and Zaretsky, E.V., "Elastohydrodynamic Lubrication of a Spinning Ball in a Non-Conforming Groove," ASME Paper No. 69-LubS-11.
138. Hertz, H., "Über die Beruehrung fester elastischer Koerper," 1881; "Ueber die Beruehrung fester elastischer Koerper und ueber die Haerte," 1882: reprinted in "Gesammelte Werke von Heinrich Hertz, Vol. 1, pp. 155-173, 174-196, Leipzig, 1895, English translations in H. Hertz, "Miscellaneous Papers" translated by D.E. Jones and G.A. Schott, pp. 146-162, 163-183, MacMillian, New York, 1896.
139. Smith, J.O. and Liu, C.K., "Stresses Due to Tangential and Normal Loads on an Elastic Solid with Application to Some Contact Stress Problems," Trans. of ASME J. of Applied Mechanics, June, 1953, pp. 157-166.
140. Lubkin, J.L., "Contact Problem," a chapter of Handbook of Engineering Mechanics by W. Flugge. Chapter 42. McGraw Hill.
141. Dowson, D., Higginson, G.R., and Whitaker, A.V., "Elastohydrodynamic Lubrication - A Survey of Isothermal Solutions," J. of Mech. Engrg. Sci. Vol. 2, p. 121, 1962.
142. Thomas, H.R. and Hoersch, V.A., "Stresses Due to the Pressure of One Elastic Solid Upon Another," University of Illinois Bulletin 212, July 15, 1930.
143. Timoshenko, S. and Goodier, J.N., "Theory of Elasticity," McGraw Hill, Second Edition, New York, 1939.
144. Lundberg, G. and Palmgren, A., "Dynamic Capacity of Rolling Bearings," Acta Polytech. Mech. Eng. Ser., Vol. 1, November 3, 1947.
145. Lundberg, G. and Palmgren, A., "Dynamic Capacity of Roller Bearings," Acta Polytech. Mech. Ser. Vol. 2, No. 4.
146. Greenert, W.J., "The Toroid Contact Roller Test as Applied to the Study of Bearing Materials," J. of Basic Engrg., Trans. ASME, March 1962.
147. Poritsky, H., "Stresses and Deflections of Cylindrical Bodies in Contact with Application to Contact of Gears and of Locomotive Wheels," Trans. ASME J. of Applied Mech., Vol. 72, 1950, pp. 191-201.
148. Cheng, H.S. and Wernick, R.J., "Stresses in Lubricated Rollers Considering Arbitrarily Distributed Normal and Tangential Loads," MTI 65TR61, December 1965.
149. Greenwood, J.A., "The Area of Contact Between Rough Surfaces and Flats" J. of Lubr. Tech., Trans. ASME, Vol. 89, Series F, 1967, p. 81.

150. Tallian, T.E. et al, "Lubricant Films in Rolling Contact of Rough Surfaces," ASLE Trans., Vol. 7, 1964.
151. Greenwood, J.A. and Williamson, J.B.P., "The Contact of Nominally Flat Surfaces," Proc. of R. Soc., London, Vol. 295, Series A, 1966, p. 300.
152. Williamson, J.B.P., Pullen, J. ., and Hunt, R.T., 1969 Surface Mechanics New York, ASME.
153. Dowson, D. and Higginson, G.R., "Elastohydrodynamic Lubrication," Pergamon Press, 1966.
154. Harris, T.A., "An Analytical Method to Predict Skidding in High-Speed Roller Bearings," ASLE Trans. Vol. 9, pp. 229-241, 1966.
155. Boness, R.J., "The Effect of Oil Supply on Cage and Roller Motion in a Lubricated Roller Bearing," J. of Lubr. Tech., Trans. ASME, Series F, Vol. 92, No. 1, 1970, pp. 39-53.
156. Harris, T.A., "An Analytical Method to Predict Skidding in Thrust-Loaded Angular-Contact Ball Bearings," to be published.
157. Shevchenko, R. and Bolan, P., "Visual Study of Ball Motion in a High-Speed Thrust Bearing," SAE Paper No. 37, January 14-18, 1957.
158. Poplawski, J.V. and Mauriello, J.A., "Skidding in Lightly Loaded High-Speed Ball Thrust Bearings," ASME Preprint 69-LubS-20.
159. Walters, C.T., "The Dynamics of Ball Bearings," to be published.
160. Kingsbury, E.P., "Ball Motion in Angular Contact Bearings," Vol. II - Ball Bearing Proceedings, Gyro Spin-Axis Hydrodynamic Bearing Symposium, M.I.T., December 12-14, 1966.
161. Allan, R.K., "Rolling Bearings," Sir Isaac Pitman & Sons, Ltd., 1946.
162. Palmgren, A., "Ball and Roller Bearing Engineering," S.H. Burbank & Co., Third Edition, 1959.
163. Kaufman, H.N. and Walp, H.P., "Interpreting Service Damage in Rolling Type Bearings - A Manual on Ball and Roller Bearing Design," Amer. Soc. of Lubr. Eng., 1953.
164. Bisson, E.E. and Anderson, W.J., "Advanced Bearing Technology," Nat'l Aeronautics and Space Admin., Wash., D.C., NASA SP-38, 1964.
165. Simpson, F.F., "Failure of Rolling Contact Bearings," Proc. Instn. Mech. Engrs., 169, pt. 3D, 1964, p. 248.
166. Wren, J.J., and Moyer, C.A., "Modes of Fatigue Failures in Rolling Element Bearings," Proc. Instn. Mech. Engrs., 179, Pt. 3D, 1964, p. 236.

167. Edigaryan, F.S., "Basic Types of Wear in Anti-Friction Bearings," Russian Engr. Jour., XLVI, 4, 1966.
168. Tallian, T.E., "Special Research Report on Rolling Contact Failure Control Through Lubrication, SKF Report AL66Q028, Sep 1966.
169. Cheng, H.S., and Orcutt, F.K., "Summary Report on Elastohydrodynamic Lubrication and Failure of Rolling Contacts," DDC report AD-481 826, Mar 1966.
170. Smalley, A.J. et al, "Review of Failure Mechanisms in Highly loaded Rolling and Sliding Contacts, DDC Report AD-657 337, May 67.
171. O'Connor, J.J. and Boyd, J., "Standard Handbook of Lubrication Engineering," McGraw Hill Book Co., New York, 1968.
172. Moyer, G.J., and Morrow, A.V., "Surface Failure of Bearings and Other Rolling Elements," Univ. of Illinois Engr. Experiment Station, Bulletin 469, 1964.
173. Zaretsky, E.V., "The Changing Technology of Rolling Element Bearings," Machine Design, Oct 66, p 205.
174. Eschmann, Paul, "Rolling Bearing Wear Life," ASME Paper 67-WA/Lub-2, 67.
175. Brothers, B.G., and Halling, J., "Effect of Geometric Conformity Between Rolling Bodies on the Slip and Wear in the Contact Region," Proc. Instn. Mech. Engrs., 3rd Conv. Lub and Wear, 179, Pt. 3, 1964, p. 134.
176. Halling, J., and Brothers, B.G., "Wear Due to the Microslip Between a Rolling Body and its Track," ASME Paper 64-Lub-30, 1964.
177. Tallian, T.E., McCool, J.I., and Sibley, L.B., "Partial Elastohydrodynamic Lubrication in Rolling Contact," Elastohydrodynamic Lubrication Symposium in Leeds, Paper No. 14, Inst. of Mech Engrs, London, 1965.
178. Tallian, T.E., Brady, E.F., McCool, J.I., and Sibley, L.B., "Lubricant Film Thickness and Wear in Rolling Contact, ASLE Trans, 8, 4, 1965, p. 411.
179. Landen, E.W., "Slow Speed Wear of Steel Surfaces Lubricated by Thin Oil Films," ASLE Trans. 11 6-18 (1968).
180. Queener, C.A., Smith, T.C. and Mitchell, W.L., "Transient Wear of Machine Parts," Wear 8, 391 (1965).
181. Devine, M.J., Lamson, E.R., Cerim, J.P., and Carrol, R.J., Session 4, Lubrication and Wear Conference, London, 1967.
182. Cocks, M.F., "The Formation of Wedges of Displace Metal Between Sliding Metal Surfaces," Wear 8, 1965, p. 85.

183. Cocks, M.F., "Shearing of Junctions Between Metal Surfaces," *Wear*, Jul/Aug, 9, 4, 1966, p. 320.
184. Bodensiek, E.J., "Specific Film Thickness - An Index of Gear Tooth Surface Deterioration," *AGMA Aerospace Gear Conference*, Denver Sep 1965.
185. Ibrahim, M., Cameron, A., "Oil Film Thickness and the Mechanism of Scoring in Gear Teeth," Paper 20, *Proc. Conf. Lub. and Wear*, Bournemouth, Inst. Mech Engrs 1963.
186. Peacock, L.A., and Rhoads, W.H., "Extreme Temperature Aerospace Bearing Lubrication Systems," *NASA CR-72446*, 1968.
187. DeGruch, V.J., "Development of an Edge Type Disk Machine and Preliminary Studies of Various Gear Materials Lubricant Combinations," *Proc. Conf. Lubrication and Wear*, Bournemouth, Inst. Mech Engrs, 1964, p. 160.
188. Leach, E.E., Kelley, B.W., "Temperature - The Key to Lubricant Capacity," *ASLE Trans*, 8, 1965, p. 271.
189. Matveesky, R.M., "The Critical Temperature of Oil with Point and Line Contact Machines," *Jour Basic Eng.*, *Trans ASME* 87, 1965, p. 754.
190. Fein, R.S., "Effects of Lubricants on Transition Temperatures," *ASLE Trans* 8, 3, 1965, p. 59.
191. Fein, R.S., Rowe, C.N., Krenz, K.L., "Transition Temperatures in Sliding Systems," *ASLE Trans* 2, 1, 1959, p. 50.
192. Fein, R.S., "Transition Temperatures with the Four Ball Machine," *ASLE Trans* 3, 1, 1960, p. 34.
193. Blok, H., "Surface Temperatures Under Extreme Pressure Conditions," *Congr. Mondiale Petrole Assoc. Franc. des Techniciens du Petrole*, Paris, 1937.
194. Archard, J.F., "The Temperature of Rubbing Surfaces," *Wear*, 2, 1959, p. 438.
195. Tataiah, K. et al, "Summary Report on Project I of a Basic Study of the Sliding Contacts in Rolling Bearings," *U.S. Dept. of Navy, Bureau of Naval Weapons, Contract Now-65-0182f, DDC AD-617 35, SKF Industries Report AL65L045*, 1965.
196. O'Donoghue, J.P., and Cameron, A., "Temperature at Scoring," Paper 6, *Symposium-Elastohydrodynamic Lubrication*, Inst. of Mech Engrs., London, 1965.
197. Smith, F.W., "Lubricant Behavior in Concentrated Contact Systems - The Castor Oil-Steel System," *Wear*, 2, 1959, p. 250.
198. Furey, M.J., "Surface Roughness Effects on Metallic Contact," *ASLE Trans* 6, 1963, p. 49.

199. Courtney-Pratt, J.S., and Eisner, E., "The Effect of Tangential Force on the Contact of Metallic Bodies," Proc. Roy Soc., Ser A, 238, 1957, p. 529.
200. Parker, R.C. and Hatch, D., "The Static Coefficient of Friction and the Area of Contact," Proc. Phy. Soc. 63, 1950, p. 185.
201. Bowden, F.P. and Tabor, D., "The Friction and Lubrication of Solids, Part II, Oxford (London) 1964.
202. Greenwood, J.A. and Tabor, D., "Deformation Properties of Friction Junction," Proc. Phy. Soc. B, 68, pt. 9, 1955, p. 609.
203. Cocks, M., "Role of Displaced Metal in the Sliding of Flat Metal Surfaces," J. Appl. Phy. 35, 6, 1964, p. 1807.
204. Antler, M., "Wear, Friction and Electrical Noise Phenomenon in Severe Sliding Systems," ASLE Trans. 5, 1962, p. 297.
205. Johnson, K.L., "A Review of the Theory of Rolling Contact Stresses," Wear 9, (1966) 4-19.
206. McKelvey, R.D. and Moyer, C.A. "The Relation Between Critical Maximum Compressive Stress and Fatigue Life Under Rolling Contact," Paper No. 1 Proceedings of the Symposium on Fatigue in Rolling Contact, Institution of Mechanical Engineers, London, 1963.
207. Tsukizoe, T. and Hisakdo, T., "On the Mechanism of Contact Between Metal Surfaces - The Penetrating Depth and the Average Clearance," Journal of Basic Engineering, Trans. ASME, Series D, Vol. 87, No. 3, Sept. 1965, pp. 666-674.
208. Dawson, P.H. "Effect of Metallic Contact on the Pitting of Lubricated Rolling Surfaces," J. Mech. Eng. Sci. 4, No. 1 (1962).
209. Dawson, P.H. "The Effect of Metallic Contact and Sliding on the Shape of the S-N Curve for Pitting Fatigue," Paper No. 4 Proc. Symp. Fatigue in Rolling Contact, I. Mech. E. 1962.
210. Dawson, P.H. "Further Experiments on the Effect of Metallic Contact on the Pitting of Lubricated Rolling Surfaces," Elastohydrodynamic Lubrication, Symposium in Leeds, Paper 7, Inst. of Mech. Engrs. London.
211. Christensen, H., "Nature of Metallic Contact in Mixed Lubrication," Proc. Inst. Mech. Engrs. 180, Part 3B, (1965-66).
212. Christensen, H., "Elastohydrodynamic Theory of Spherical Bodies in Normal Approach Motion," MTI Report No. 76TR21 (1967).

213. Cheng, H.S., "A Numerical Solution of the Elastohydrodynamic Film Thickness in an Elliptical Contact," Journal of Lubrication Technology, Trans. ASME, Vol. 92, Series F, No. 1, pp. 155-162.
214. Dowson, D. and Whitaker, A.V., "A Numerical Procedure for the Solution of the Elastohydrodynamic Problem of Rolling and Sliding Contacts Lubricated by a Newtonian Fluid," Lubrication and Wear Group Symposium on Elastohydrodynamic Lubrication, Paper 4, Institution Mech. Engrs., London.
215. Jones, A., "Ball Motion and Sliding Friction in Ball Bearings", ASME Transactions, Journal of Basic Engineering, March 1959.
216. Jones, A., "The Mathematical Theory of Rolling-Element Bearings", Mechanical Design and Systems Handbook, Section 13, McGraw-Hill, 1964.



APPENDIX I  
TYPICAL PROPERTIES OF VARIOUS CLASSES OF LUBRICANTS

I-1. MINERAL OILS

Mineral oils are very complex natural products which are predominantly composed of molecules containing carbon and hydrogen (hydrocarbons). Depending on the origin of the crude oil and refining technique, the basic molecular structure may be largely straight-chain paraffinic type molecules, or it may have a high percentage of aromatic molecules (ring structures). The oils do not consist of one single type of molecule, but rather contain molecules of various chain lengths and molecular weights with a distribution around a mean molecular weight. To complicate matters further, a random sample of mineral oil may also contain hundreds of different types of compounds in trace amounts. These trace compounds can have marked effects on certain properties such as color, surface tension, boundary lubricating characteristics, etc. However, these trace compounds have little or no effect on the bulk properties of the oils such as viscosity and compressibility. The bulk properties are determined by the predominant type of molecular structures in the oil. Thus, if the structure is mostly of the aromatic ring type of structure, rather than paraffinic, the molecules will be more closely packed and the bulk oil will have lower compressibility, higher density, and poorer viscosity-temperature characteristics than the corresponding paraffinic oils.

Mineral oil base lubricants are available in a range of bulk viscosities. Some typical grades are listed below:

TABLE I-I TYPICAL VISCOSITIES OF STANDARD PETROLEUM OILS

Petroleum Oils	Typical Viscosity Centistokes		Density, grams/cc at 60 F.	Flash Point, °F.	Pour Point, °F.
	100 F.	210 F.			
Automotive:					
SAE 10W	41	6.0	0.870	410	-15
30	114	11.3	0.891	460	-5
Industrial gear:					
80	69	7.9	0.934	365	-25
90	287	20.4	0.930	450	-10
140	725	34	0.937	500	0
Turbine:					
Grade 1010	10	2.5	0.864	280	-70
Light	32	5.4	0.872	410	0
Medium	65	8.2	0.877	455	10
Heavy	99	10.8	0.885	470	10
Hydraulic:					
Light	32	4.8	0.887	370	-45
Medium	67	7.3	0.895	405	-15
Heavy	196	14.0	0.901	495	10
Extra low temp.	14	5.2	0.884	230	-80
Wide temp.	56	10.5	0.871	310	-45

Continued

TABLE I-I TYPICAL VISCOSITIES OF STANDARD PETROLEUM OILS - CONTINUED

Petroleum Oils	Typical Viscosity Centistokes		Density grams/cc at 60 F.	Flash Point, °F.	Pour Point, °F.
	100 F.	210 F.			
Steam Cylinder	390	27	0.895	500	55
	810	45	0.910	600	35
	1400	64	0.904	650	60

It is important to note that these are nominal physical property data. Variations from batch to batch are normally on the order of 5 to 10 percent. Pure hydrocarbons with known structure and physical properties are available, but these are too low in viscosity to be used as lubricants.

The super-refined petroleum oils appear to be interesting candidates for this work. Many of these are paraffinic base oils (straight-chain hydrocarbons) which have been carefully deep de-waxed and super-refined to produce lubricants with minimum aromatic content. Many of the trace compounds which are normally present in mineral oils are also removed in this processing. The resulting lubricants are characterized by low pour points, excellent viscosity temperature properties and high thermal and oxidative stability. It is also claimed that they have much better shear stability than the more conventional polymer additives which are used to control the viscosity of mineral oils (Ref. 76). Some typical physical properties of commercially available, super-refined oils are given in Table I-II.

Special oil blends can also be obtained from some of the major oil companies which have the same bulk viscosity at some specified temperature, say 100 F, but widely different viscosity-temperature and viscosity-pressure characteristics. These oils are prepared by blending to obtain predominantly aromatic or paraffinic structures.

Synthetic hydrocarbons are also available from some of the oil companies. These offer the advantages of having known chemical structures and higher purities. Table I-III shows some physical property data on typical oils from one source.

Although the mineral oils are of major importance from a commercial standpoint, the uncertainties regarding purity, chemical structure, etc., make them poor candidates for laboratory studies when the goal is to gain a better understanding of some phenomenon.

To sum up, generalizations about mineral oils are meaningless because it is possible to obtain materials in this class of mineral oils with a very wide range of physical properties. The problem is to decide which properties are important and then base the selection on these criteria.

TABLE I-II TYPICAL PHYSICAL PROPERTIES OF SUPER-REFINED MINERAL  
OIL (FROM REF. 77) CONFORMING TO MLO 7277

Specific Gravity at 60°F	0.887
Density - g/ml	
0 F	0.91
100 F	0.87
300 F	0.80
500 F	0.73
Flash Point CQC, °F	445
Adiabatic Bulk Modulus (100°F)	
0 psig	270,000 psi
1000 psig	280,000
2000 psig	295,000
4000 psig	320,000
5000 psig	330,000
Viscosity - Centistokes	
-65°F	----
0°F	10,289
100°F	78.08
212°F	8.24
550°F	0.96
Viscosity Index	78
ASTM Viscosity/Temp.	0.775
Slope 100°F/210°F	
Pour Point	-30°F
Specific Heat - BTU/lb/°F	
100°F	0.47
200°F	0.517
400°F	0.611
Thermal Conductivity - BTU/hr/ft/°F	
100°F	0.0791
200°F	0.075
400°F	0.0668
Molecular Weight (calculated)	400
Mass Spectrometer Analysis %	
Isoparafins	5.3
1-Ring Naphthenes	23.8
2-Ring Naphthenes	26.2
3+-Ring Naphthenes	44.7

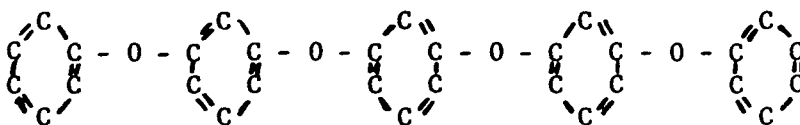
TABLE I-III TYPICAL PROPERTIES FOR MOBIL SYNTHETIC HYDROCARBON FLUIDS\*

PROPERTY	A	B	C
Kinematic Viscosity, Centistokes			
at 400°F	1.1	2.0	6.1
210°F	3.8	9.4	42.6
100°F	16.8	64.7	493.0
0°F			45829.0
-40°F	2159.0	29850.0	>99000.0
-65°F	11011.0		
Pour Point, °F	<-65	<-65	-60
Flash Point, °F	430	495	520
Fire Point, °F	480	560	565
Autogeneous Ignition Temp., °F	700	750	815
Total acid no., mg. KOH/gm Oil	0.07	0.07	0.05
Volatility, Wt. % 400°F, 6-1/2 Hr.	12.6	2.2	1.2
Density at 100°F	0.8056	0.8244	0.8389
200°F			0.8082
300°F	0.7341	0.7582	0.7777
400°F	0.6998	0.7232	0.7428
Specific Heat at 100°F	0.497	0.498	
300°F	0.670	0.612	0.635
400°F	0.691	0.642	0.692

\* Data furnished by Mobil Research and Development Corporation.

## I-2. POLYPHENYL ETHERS

The polyphenyl ethers were the result of extensive efforts by many investigators to develop high temperature, radiation-resistant lubricants. Chemically, the two go hand in hand, i.e., those organic materials with the best resistance to oxidation or thermal degradation are also the most resistant to radiation damage. A typical structure for the polyphenyl ethers is as follows:



This particular compound is made up of alternating phenyl rings connected by oxygen atoms. It is often called 5P4E, which means that there are five phenyl rings and four oxygen atoms joining these rings. (The atomic structure -C-O-C- is called an ether linkage). A 4P3E compound would have four phenyl rings and three oxygen atoms linking the rings.

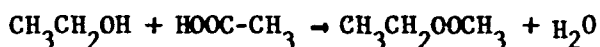
The density and bulk modulus of the polyphenyl ethers is high, indicating close packing and low compressibility for these oils. The 5P4E and the 4P3E have high pour points ( + 10F to +35F) and relatively poor viscosity-temperature behavior. In many respects, the polyphenyl ethers are similar in structure to the aromatic base petroleum oils (except for the ether linkages, and the fact that they are pure compounds). For this reason, the physical behavior of oils in each of these two classes is similar.

The results of several investigations (Refs. 78-80) have indicated that the polyphenyl ethers are poor lubricants in rolling contact bearings. This was ascribed to the fact that these oils do not form elastohydrodynamic films at high unit stresses. However, the reasons for this behavior are not clear at this time.

Typical physical property data on the four ring and five ring polyphenyl ethers are given in Table A-IV. No data on viscosity-shear behavior were found.

## I-3. ESTERS

An ester is the product of the reaction between an alcohol and an organic acid. For example, if ethyl alcohol is reacted with acetic acid, a molecule of water is split off by the following reaction:

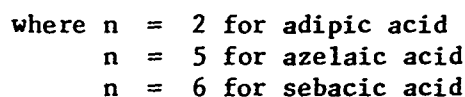


ethyl alcohol + acetic acid  $\rightarrow$  ethyl acetate + water

The resulting compound is a mono-ester, ethyl acetate, with a pleasant, fruity odor, which boils at 77°C.

TABLE I-IV TYPICAL PHYSICAL PROPERTIES OF POLYPHENYL ETHERS

	<u>4-Ring</u>	<u>5-Ring</u>
Viscosity-Centistokes		
28°F	13,000 cs	---
100°F	63.2	355
210°F	6.0	13.1
400°F	1.31	1.25 (500°F)
Density - g/ml		
100°F	1.17	1.18
210°F	1.12	1.14
400°F	1.04	1.06
Pour Point	+ 10°F	+ 35°F
Flash Point	+ 510°F	+ 550°F
Specific Heat-BTU/lb/°F		
100°F	0.36	0.40
200°F	0.40	0.43
500°F	0.50	0.53
Bulk Modulus (3000 psi, 200°F)	--	235,000 psi
Thermal Conductivity		
BTU/hr/ft/°F		
100°F	--	0.078
400°F	--	0.077


$$\begin{array}{ccccccc}
 \text{H} & \text{H} & \text{H} & \text{H} & \text{H} & \text{H} & \\
 | & | & | & | & | & | & \\
 \text{H} - \text{C} - & \text{C} - & \text{C} - & \text{C} - & \text{C} - & \text{C} - & \text{OH} \\
 | & | & | & | & | & | & \\
 \text{H} & \text{H} & \text{H} & \text{H} & \text{H} & \text{C} & \\
 & & & & & | & \\
 & & & & & \text{H} - \text{C} - \text{H} & \\
 & & & & & | & \\
 & & & & & \text{H} - \text{C} - \text{H} & \\
 & & & & & | & \\
 & & & & & \text{H} & 
 \end{array}$$
$$\text{HOOC} - \text{R} - \text{COOH} + 2\text{R}'\text{OH} \rightarrow \text{R}'\text{OOC} - \text{R} - \text{COOR}' + 2\text{H}_2\text{O}$$

dibasic acid                  alcohol                                  diester

In general, the esters have physical properties which are very similar to the petroleum oils. This is not unexpected, since they are predominantly straight chain hydrocarbons with the same atomic make-up. They have lower pour points and better viscosity-temperature properties than conventional mineral oils. Some typical data are given in Table I-V.

TABLE I-V TYPICAL PHYSICAL PROPERTY DATA ON ESTER BASE LUBRICANTS

	<u>MIL-L-7808<sup>(a)</sup></u>	<u>MIL-L-23699<sup>(b)</sup></u>
Viscosity-Centistokes		
- 65°F	10,498 cs	7759 cs (-40°F)
+100°F	13.44	27.5
+210°F	3.23	5.06
Specific Gravity		
+100°F	.936	0.987
+210°F	.892	0.939
+300°F	0.854	0.904
Pour Point	Below - 75°F	Below - 70°F
Flash Point	---	500°F
Specific Heat - Btu/lb/°F		
+100°F	.473	0.447
+300°F	0.55	0.515
Thermal Conductivity		
BTU/hr/ft/°F		
+200°F	0.0867	.0859
+400°F	0.072	.0716

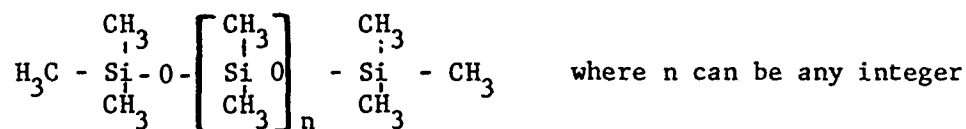
(a) 0-67-22

(b) 0-70-4

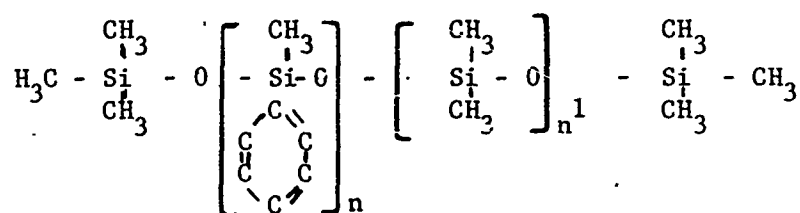


#### I-4. SILICONES

The silicone oils are linear polymers with a structural shape that is similar to the straight chain hydrocarbons. Instead of a chain of - C - C-carbon atoms, the silicones have a chain of repeating -O-Si-O-Si- units for a backbone. Some typical structures are shown below:



Straight chain Dimethyl Silicone



Methyl Phenyl Silicone

These molecules have weaker intermolecular forces than the hydrocarbons, and the molecular chains are much more flexible. Because of their wide molecular spacing, the silicones are easily compressed and have low bulk moduli. A generalized relationship for the bulk modulus of silicones as a function of pressure, temperature and density is presented in Ref. 68. The most outstanding characteristic of the silicones is their small change in viscosity with temperature. The dimethyl silicones are particularly good from this respect. Pour points of most of the dimethyl silicones are on the order of -60 F. By synthesizing molecules with branched chains, the pour point can be reduced to below -100 F.

The viscosity of the silicone oils is markedly dependent on shear rate, especially the more viscous, high molecular weight silicones. This effect is much more pronounced with the silicones than it is with mineral oils and most other synthetic fluids.

The -C-Si bond in the dimethyl silicones is the weak link as far as oxidative or thermal degradation is concerned. To improve the resistance of the molecule to temperature effects, phenyl groups can be substituted for methyl groups. This results in some loss in favorable properties, such as pour point and viscosity-temperature characteristics.

Aside from their relatively high cost, the most outstanding disadvantage of the silicones is their poor boundary lubricating characteristics for steel sliding on steel. Considerable effort has been expended on this problem with little success. The effect is specific since it has been found that steel vs. bronze combinations are effectively lubricated by the silicone oils.

It has been hypothesized (Ref. 81) that the silicone oil decomposes at the metal surface to form inorganic silicides which inhibit conventional anti-wear or extreme-pressure additives from reacting and providing beneficial surface films.

In an attempt to improve the lubricating qualities of these fluids, several types of halogenated silicone oils have been developed. Probably the most commonly known fluid of this type is the chlorinated silicone. Recently, fluids have been developed containing fluorine substitution, and the information which is available on these oils indicates that they are very promising with most of the attributes of the straight silicones and, in addition, they can provide better boundary lubrication.

On the following pages, extracts of the specifications for the MIL-L-9236 B aircraft turbine oil and the new, high temperature MIL-L-27502 ester base lubricant are given for general information on qualification requirements.

I-5 EXTRACTS FROM SPECIFICATION MIL-L-9236B, 4 MARCH 1960

Lubricating Oil, Aircraft Turbine Engine, 400°F

Intended Use: Lubricating oil for specific models of aircraft gas turbine engines.

Requirements

- Viscosity, centistokes: at 400°F, min. 1.0  
at 100°F report
- Viscosity stability at -65°F. The two determinations in the 3 hour test shall not differ by more than 6% of lowest value and both shall be less than 21,000 centistokes. All determinations in the 72 hour test shall be less than 24,000 centistokes.
- Flash point, °F, min. 425
- Pour point, °F, min. -75
- Spontaneous ignition temperature, °F 750
- Evaporation loss: Not more than 15% by weight when tested at 400 F for 6 1/2 hours.
- Gear Tests:
  - Load-carrying ability at 165 F: Average minimum 56% of reference oil "B" rating.
  - Load-carrying ability at 400 F: Report load at which 22.5% of working tooth area is scuffed.
  - Gear fatigue: Determine limit of fatigue pitting under specified conditions.
- Bearing stabilization temperature: The oil shall not cause the bearing temperature to stabilize over 500°F when tested in the ERDCO bearing test rig. Time required to reach stabilization temperature shall be less than 60 minutes. Bulk oil temperature 400°F.
- Bearing shall operate satisfactorily in WADD bearing test rig for at least 50 hours. Oil reservoir, 425°F. Bearing outer race, 525°F.
- 100-Hour engine endurance test. The oil shall perform as well or better than the reference oil qualified under this specification.
- Used Oil control: Increase in oil viscosity at 100°F after the engine test shall not exceed 75%. Must be as good or better than the reference oil.

- Additional requirements include:

- Synthetic rubber swelling test
- Foaming tests
- Deposition test
- Compatibility, turbidity
- Storage stability
- Workmanship

I-6 EXTRACTS FROM PROPOSED SPECIFICATION MIL-L-27502. SUPERSEDING MIL-L-9236B. 4 MARCH 1960

Lubricating Oil, Aircraft Turbine Engine, Ester Base

Intended Use: For specific engines and power equipment requiring an ester base oil with an approximate temperature range capability of -40 to +428°F.

## Requirements

- Viscosity, centistokes:
- |                         |             |
|-------------------------|-------------|
| at 500°F, min.          | 1.0         |
| at 210°F, and 100°F     | report      |
| at -40°F, at 35 minutes | 15,000 max. |
| at 3 hours              | 15,900 max. |
| at 72 hours             | 17,000 max. |
- Flash Point °F 475
  - Pour Point °F, max. -65
  - Autoignition temperature °F, min. 770
  - Evaporation loss: Not more than 5% by weight when tested at 400°F  
for 6 1/2 hours.
  - Specific heat:
- |          |           |
|----------|-----------|
| at 500°F | 0.48 min. |
| at 140°F | 0.40 min. |
- Neutralization number 0.5 max.
  - Specific gravity report
  - Shear stability percent viscosity loss 4.0 max.
  - Gear Tests: Load carrying ability at 165°F. The average of eight relative determinations shall be multiplied by the reference oil specified average value of 2900 ppi and the resulting load-carrying ability shall be equal to or greater than 2400 ppi. Load carrying ability at 428°F.  
The lubricating oil shall be subjected to eight determinations and the average value shall be equal to or greater than 1000 ppi. The reference oil "c" average (8 determinations) shall be reported.
  - 100-Hour engine endurance test. A modified J-57 turbine engine shall be operated using the test oil for 100 hours under test conditions as specified by the qualifying activity.
  - Additional requirements include:
    - Elastomer compatibility
    - Corrosion characteristics
    - Deposition characteristics
    - Compatibility, turbidity

APPENDIX II  
ANALYSIS OF PROTRUSION WIDTH

The pressure in the EHD line contact is governed by the one-dimensional Reynolds Equation,

$$\frac{dq}{dx} = \frac{6\mu_o(U_1 + U_2)}{h^3} (h - h^*) \quad (\text{II-1})$$

where  $q = \frac{1 - e^{-\alpha p}}{\alpha}$

$$\frac{d(1 - e^{-\alpha p})}{d\bar{x}} = \frac{6\alpha\mu_o(U_1 + U_2)b}{h^{*2}} \frac{H - 1}{H^3} \quad (\text{II-2})$$

$$(1 - e^{-\alpha p}) = 6\alpha\mu_o(U_1 + U_2)b \int_{-\infty}^{\bar{x}} \frac{H - 1}{H^3} d\bar{x} \quad (\text{II-3})$$

Referring to the diagram below, the limits in the exit region are from  $\bar{x} = 1 - \bar{e}$  to  $\bar{x} = 1.0$ .

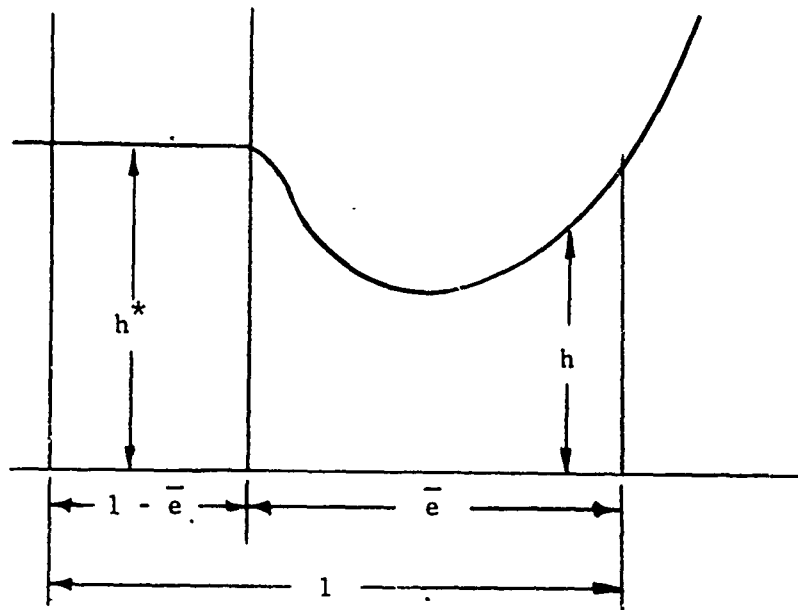


Figure II-1

$$1 - e^{-\alpha p} \Bigg|_{p=\infty}^{p=0} = \frac{6\alpha \mu_0 (U_1 + U_2)b}{h^{*2}} \int_{1-\bar{e}}^{1.0} \left( \frac{H-1}{H^3} \right) d\bar{x} \quad (\text{II-4})$$

$$0 - 1 = \frac{6\alpha \mu_0 (U_1 + U_2)b}{h^{*2}} \int_{1-\bar{e}}^{1.0} \left( \frac{H-1}{H^3} \right) d\bar{x} \quad (\text{II-5})$$

Introducing  $\bar{x}' = \frac{\bar{x} - (1 - \bar{e})}{\bar{e}}$ ;  $\frac{d\bar{x}}{\bar{e}} = d\bar{x}'$  Equation (II-5) becomes

$$\frac{6\alpha \mu_0 (U_1 + U_2)b}{h^{*2}} \bar{e} \int_0^1 \left( \frac{H-1}{H^3} \right) d\bar{x}' = -1 \quad (\text{II-6})$$

$$\text{Let } I_1 = - \int_0^1 \left( \frac{H-1}{H^3} \right) d\bar{x}'$$

It follows that

$$\bar{e} = \frac{h^{*2}}{R_x'^2} R_x'^2 \frac{1}{6\alpha \mu_0 (U_1 + U_2) 2 \sqrt{\frac{WR_x'}{E'}}} \frac{1}{I_1} \quad (\text{II-7})$$

$$\bar{e} = \left( \frac{h^*}{R_x'} \right)^2 \frac{R_x'}{12\alpha \mu_0 (U_1 + U_2) \sqrt{\frac{WR_x'}{E'}}} - \frac{1}{I_1} \quad (\text{II-8})$$

From Dowson Higginson film thickness formula,

$$\left( \frac{h^*}{R_x'} \right)^2 = K (\alpha E')^{1.2} \left( \frac{\mu_0 (U_1 + U_2)}{2 E' R_x'} \right)^{1.4} W^{-.26} \quad (\text{II-9})$$

$$\bar{z} = \frac{1}{24I_1} \left( \frac{H^*}{R'_x} \right) \frac{1}{(\alpha E') \left( \frac{\mu_0 (U_1 + U_2)}{2 E' R'_x} \right) \sqrt{\frac{W}{E' R'_x}}} \quad (\text{II-10})$$

Substituting (II-9) into (II-10), one obtains the final expression for the protrusion width,

$$\bar{e} = \frac{K}{24I_1} (\alpha E')^{.2} \left( \frac{\mu_0 (U_1 + U_2)}{2 E' R'_x} \right)^{.4} W^{-.76} \quad (\text{II-11})$$



## APPENDIX III

### ANALYSIS OF AREA OF CONTACT

#### III-1 ANALYSIS

##### Smooth-Film Profiles

Fig. III-1 shows the assumed smooth-film deformation shape of an elastohydrodynamic line contact. At the entrance, the flat profile forms a uniform film between the surfaces; whereas at the exit the protrusion forms a constricted film. In this figure,

$h_o$  is nominal film thickness

$e$  is the protrusion width

$h_m$  is the exit film thickness

It is convenient to non-dimensionalize the last two quantities to give

$$\bar{e} = e/b$$

$$H_m = h_m/h_o$$

where  $b$  is the half-Hertzian width.

The isothermal film profiles obtained by Dowson and Higginson (153) may be used to estimate the value of  $\bar{e}$  and  $H$  for given load and speed parameter..

#### III-2 SURFACE-ROUGHNESS PROFILES

For a ground surface, Williamson (152) has shown that the height distribution for any arbitrary cross-section of the surface profile is very close to Gaussian distribution. This evidence lends support to the assumption used earlier by Tsukizae and Hisakado (207) to investigate the penetrating depth and the average clearance between two contacting surfaces.

According to Ref. 207, a typical surface roughness profile can be shown as in Fig. III-2a. It is assumed that this profile is made of straight-line segments having equal angle of inclination,  $\theta$ , with a flat surface (see Fig. III-3).

If the height  $2\sigma$  in Fig. III-2a is divided into a number of equal segments  $\Delta u$ , then the number of crosses made by a straight line at a distance  $u$  from the median line within a sample length  $L$  is represented by the distribution histogram Fig. III-2c. The probability density of the surface height distribution can be written as,

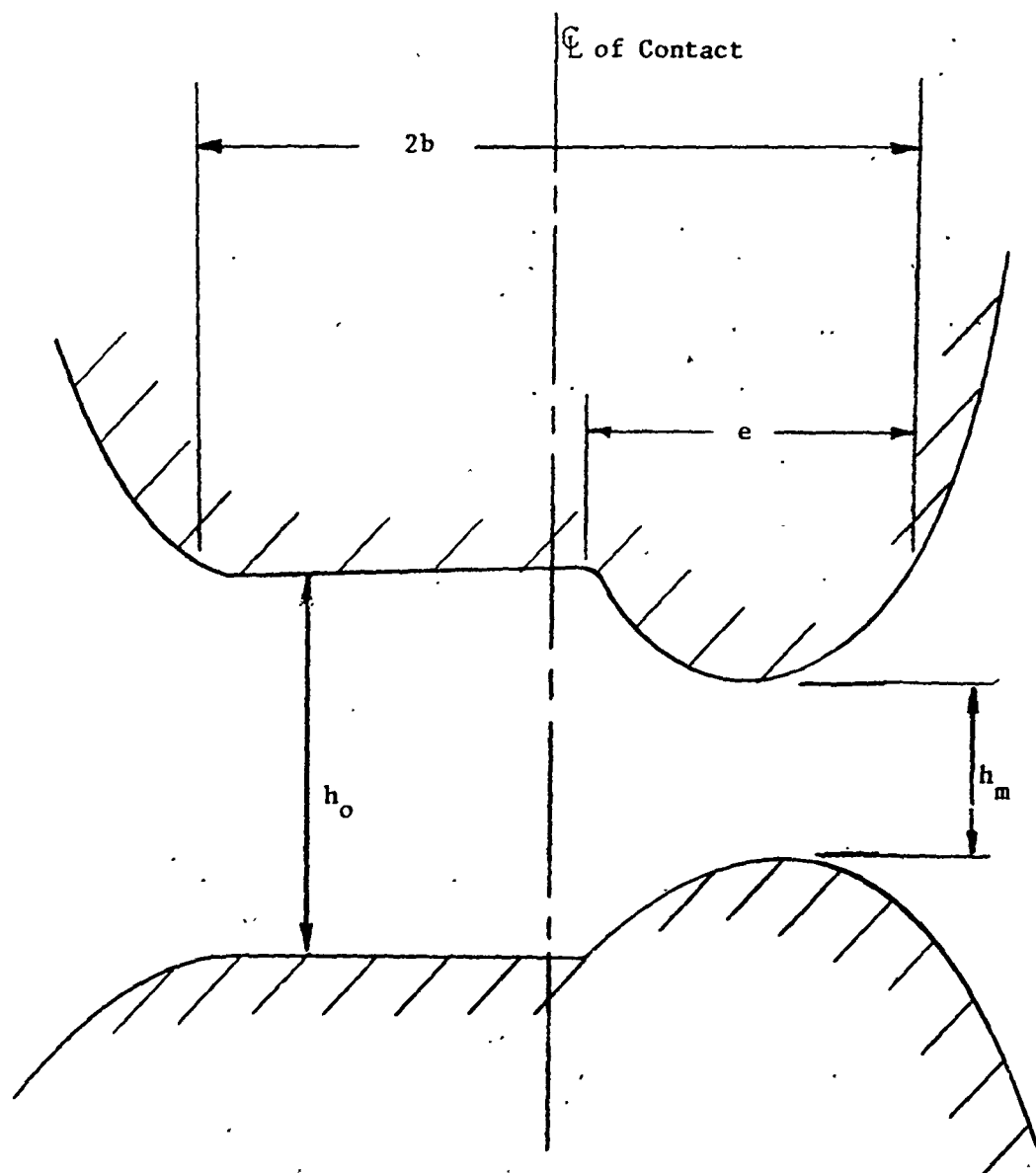


Fig. III-1 Smooth-Film Elastohydrodynamic Deformation Profile.

$$f(u) = \frac{1}{\sqrt{2\pi}\sigma} \exp \left[ -\frac{1}{2} \left( \frac{f}{\sigma} \right)^2 \right] \quad (\text{III-1})$$

where

$f$  = deviation from median line of profile curve

$\sigma$  = standard deviation

From the height distribution, one can readily determine the area of intersection between an ideal, rigid, plane surface and a rough surface at  $f = f$  as follows:

$$A_c = L \frac{\int_u^{+\ell\sigma} f(u) du}{\int_{-\ell\sigma}^{+\ell\sigma} f(u) du} \quad (\text{III-2})$$

where  $A_c$  is the area of intersection per unit width. If one ignores the change of the surface profile due to the plastic deformation, then the area of intersection is simply the contacting area. Fig. III-2b shows the variation of the contacting area curve as a function of  $u$ . This is generally known as the Abbott's bearing area curve.

#### Elastohydrodynamic Contacting Area

In Fig. III-4, the surface roughness profile is now superimposed upon the elastohydrodynamic profile, and the area of surface contact for a differential length  $dx$  becomes,

$$dA_c = F(h) dx \quad (\text{III-3})$$

where

$$F(h) = \frac{\int_h^{+\ell\sigma} f(u) du}{\int_{-\ell\sigma}^{+\ell\sigma} f(u) du}$$

It follows that the total area of contact per unit width becomes

$$A_c = \int_{-a}^{+a} F(h) dx \quad (\text{III-4})$$

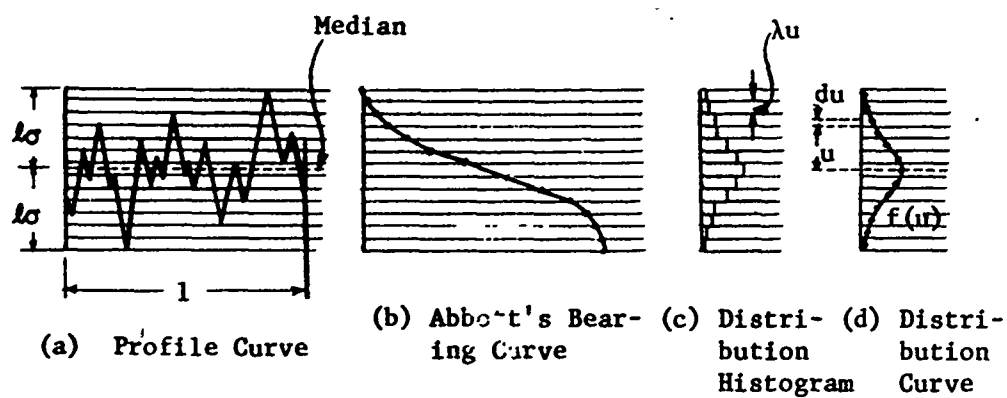


Fig. III-2 Method of Drawing Distribution Curve from Profile Curve

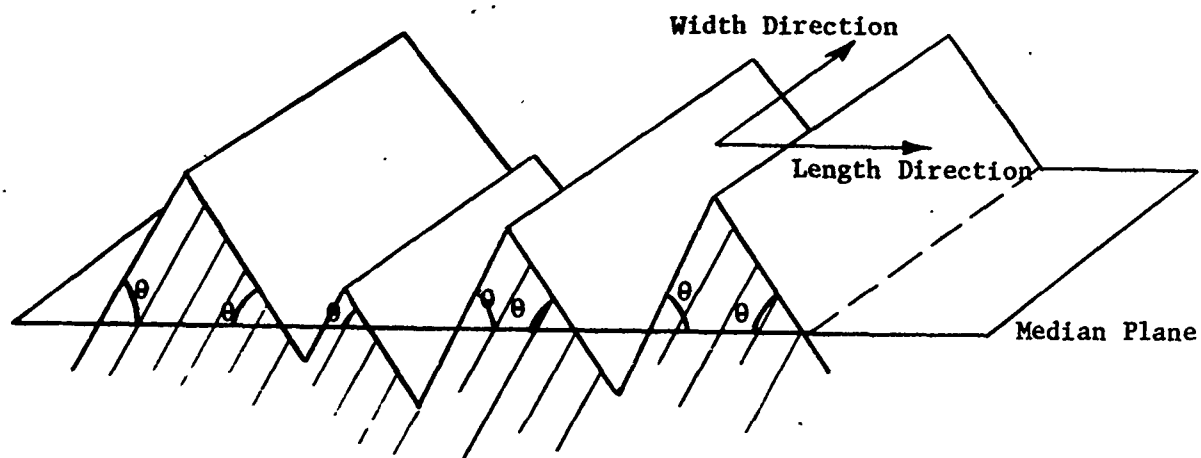


Fig. III-3 Geometry of Two-Dimensional Surface Roughness

Introducing

$$A_c = \frac{A}{2a'}$$

$$\bar{x} = \frac{x}{a'}$$

$$\xi = \frac{h}{\sigma}$$

where  $\sigma$  is the standard deviation of the surface roughness profile, one obtains

$$A_c = \frac{1}{2} \int_{-1}^{+1} F(\bar{h}) d\bar{x} \quad (\text{III-5})$$

For an elastohydrodynamic contact shown in Fig. III-1 the profile may be represented mathematically by the following two curves:

$$\xi = \xi_0 ; \text{ for } -1 < \bar{x} < (1-\bar{e}) \quad (\text{III-6})$$

$$\xi = \xi_0 \left[ 1 - (1-H_m) \sin \left\{ \pi \frac{[\bar{x} - (1-\bar{e})]}{\bar{e}} \right\} \right] \text{ for } (1-\bar{e}) < \bar{x} < 1 \quad (\text{III-7})$$

The total area of contact becomes,

$$A = \frac{1}{2} (2-\bar{e}) F(\xi_0) + \frac{1}{2} \int_{1-\bar{e}}^1 F(\xi) d\bar{x} \quad (\text{III-8})$$

where  $\xi$  in Eq. (III-8) varies according to Eq. (III-7).

Now let  $t = \frac{u}{\sigma}$ ,  $F(\xi)$  becomes,

$$F(\xi) = \frac{\int_{\xi}^{\infty} f(t) dt}{\int_{-\infty}^{\infty} f(t) dt}$$

$$\begin{aligned}
&= \frac{\int_0^l f(t) dt - \int_0^{\xi} f(t) dt}{2 \int_0^l f(t) dt} \\
&= \frac{1}{2} - \frac{\bar{\phi}(\xi)}{2\bar{\phi}(l)} \quad \text{(III-9)}
\end{aligned}$$

where

$$\bar{\phi}(\xi) = \int_0^{\xi} \frac{1}{\sqrt{2\pi}} e^{-\frac{t^2}{2}} dt \quad \text{(III-10)}$$

Equation (III-8) can be readily integrated numerically to obtain the contacting area ratio,  $A_c$ , for a given set of parameters:

$\xi_0$  = specific film thickness,  $\frac{h_0}{\sigma}$

$H_m$  = exit film ratio,  $\frac{h_m}{h_0}$

$\bar{e}$  = dimensionless exit protusion width,  $e/b$

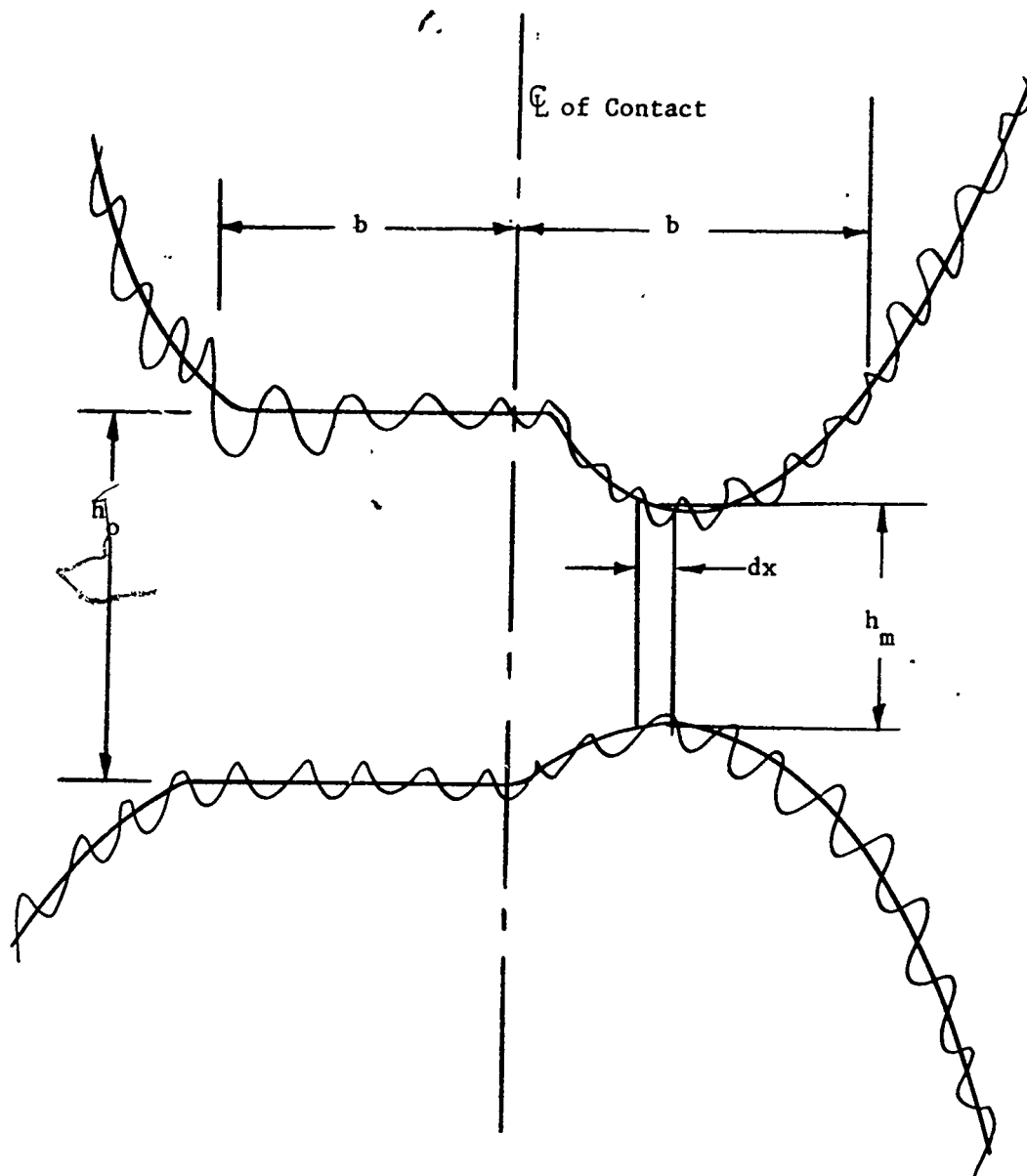


Fig. III-4 Geometry of a Rough-Surface Elastohydrodynamic Contact

# APPENDIX IV SIMPLIFIED ANALYSIS OF FRICTION

Frictional coefficient for a lubricated line contact is to be determined empirically based on the experimental data by Johnson and Cameron (129). In order to cover a broader range of load, speeds and lubricant parameters, the experimental data must be presented in terms of the relevant parameters that govern friction. Following Crook's analysis (120) it can be shown that the coefficient of friction

$$f = \frac{2}{\pi} \left( \frac{\mu_o u_s}{p_{HZ} h_o} \right) \int_{-1}^1 e^{-\alpha p} \frac{\ln \left( \frac{\psi + 1 + \psi}{\psi (\psi + 1)} \right)}{\psi (\psi + 1)} d \left( \frac{x}{b} \right), \quad (IV-1)$$

where  $\psi = \left( \frac{\mu_o \beta_1 u_s^2}{8 K_f} \right) e^{-\alpha p}$

$\mu_o$  = inlet viscosity at inlet temperature  $T_o$

$u_s$  = sliding velocity ( $U_1 - U_2$ )

$p_{HZ}$  = maximum Hertz pressure

$h_o$  = film thickness in the contact zone

$p$  = pressure in the contact zone

$b$  = half width of the contact zone

$\beta_1$  = temperature-viscosity coefficient based on the viscosity function

$$\mu = \mu_o e^{\alpha p - \beta_1 (T - T_o)}$$

$\alpha$  = pressure-viscosity coefficient

$K_f$  = thermal conductivity of lubricant

In the derivation of Eq. (IV-1) the effect of the temperature rise of the contacting surfaces has been neglected. Crook (120) shows the surface temperature rises are not very important to the calculation of frictional coefficient

From Eq. (IV-1) one sees that the coefficient of friction,  $f$ , is governed by the following three parameters:



$$G_1 = \frac{\mu_o u_s}{p_{HZ} h_o},$$

$$G_2 = \frac{\beta_1 \mu_o u_s^2}{8K_f},$$

(IV-2)

$$G_3 = \alpha p_{HZ}$$

Physically  $G_1$  measures the effect of shear rate, whereas  $G_2$  and  $G_3$  represent the thermal heating effect and pressure-viscosity effect respectively.

Graphs of frictional coefficient as a function of  $G_1$  and  $G_3$  for a given  $G_2$  are shown in Figs. 92 through 98. In all the graphs the solid portion of curve is plotted from Johnson and Cameron's experimental data, whereas the dotted curve is extrapolating of the experimental data to cover broader ranges of speed, load, and lubricant parameters. It is seen that at small values of  $G_1$  all curves have a 45 degree slope. This corresponds to the fact that at small sliding speeds frictional coefficient varies linearly with sliding speed. In each graph all curves merge, at large  $G_1$ , to a common value, which is the so-called "ceiling" found by Johnson and Cameron and also by Plint (131). The "ceiling" decreases with increasing  $G_2$ . The existence of a ceiling in friction suggests that there is a limiting shear stress in a lubricant film.

It should be noted that all the frictional coefficient graphs are for a given inlet lubricant temperature 30°C. Change of inlet temperature affects the frictional coefficient due to the dependence of the limiting shear stress upon the inlet temperature effect.

Plint's experiment shows that the variation of frictional coefficient with inlet temperature is approximately linear and the slope does not seem to vary much with either rolling or sliding speed. The slope was found to be -0.001/°F. This will be used to predict frictional coefficients for inlet temperature other than 30°C.

Symbolically the frictional coefficient,  $f$ , is determined as follows:

$$f(T_o) = f(G_1, G_2, G_3, 30^\circ\text{C}) - 0.001 (T_o - 86^\circ\text{F})$$

## APPENDIX V

### CALCULATION OF APPROXIMATE ELASTOHYDRODYNAMIC PRESSURE PROFILE

#### V-1. GRID SPACING

The entire contact region is divided into three regions: the inlet, the central, and the exit region as shown in Fig. V-1. The inlet region is bounded by  $-4.0 < \bar{x} < \bar{x}_a$ , where  $\bar{x}_a$  is the point where the pressure profile begins to match the Hertzian pressure profile. It is assumed that the transition pressure between the inlet and the central region occurs when

$$\frac{\bar{p}_A}{e} = \frac{1}{150} \quad (V-1)$$

or

$$\begin{aligned} \frac{\bar{p}_A}{e} &\approx 5 \\ \bar{p}_A &= \frac{5}{\alpha} = \frac{5b}{w\alpha} \end{aligned} \quad (V-2)$$

It follows that

$$\begin{aligned} \bar{x}_a &= \sqrt{1 - \left(\frac{\pi}{2} \bar{p}_A\right)^2} \\ &= \sqrt{1 - \left(\frac{\pi}{2} \cdot 5 \frac{b}{w\alpha}\right)^2} \end{aligned} \quad (V-3)$$

At the far side of the inlet region ( $-4.0 < \bar{x} < -2.0$ ), form equal divisions are used. It is followed by non-uniform grids as shown in Fig. V-1. The central region is bounded by  $\bar{x}_a < \bar{x} < (1 - 2\bar{e})$  with 12 non-uniform spacings before the center line and 4 uniform spacings after the center line. The exit region is divided into 8 uniform spacings of  $\bar{e}/4$ .

#### V-2. INLET PRESSURE

The pressure at the inlet is obtained directly by integrating the Reynolds equation at the inlet,

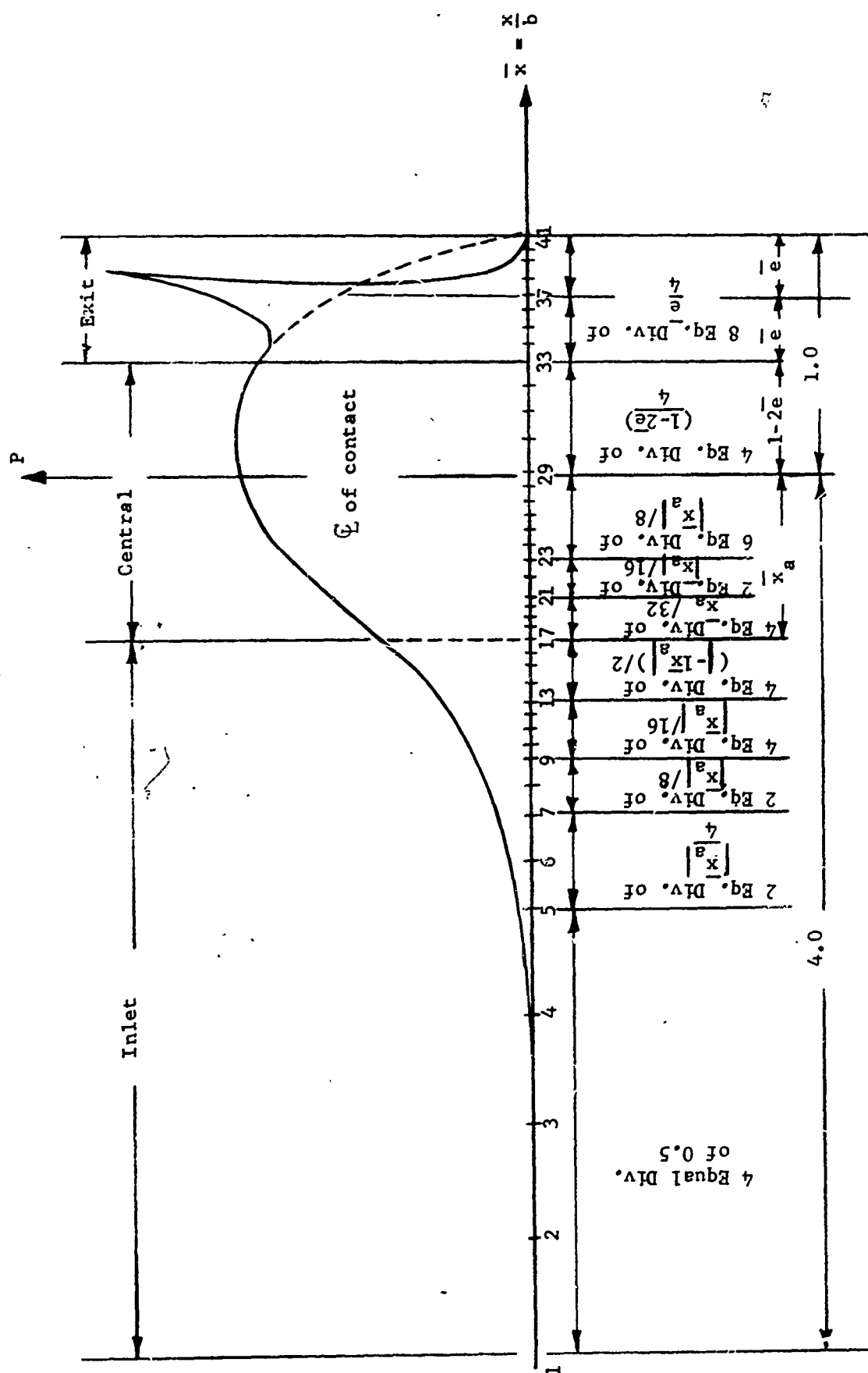


Fig. V-1 Non-Uniform Grid Spacings for Pressure and Temperature Calculations

$$1 - e^{-\alpha p} = \frac{6\mu_o^2 (U_1 + U_2)b}{(h^*)^2} \int_{-4.0}^{\bar{x}} \frac{H-1}{H^3} d\bar{x} \quad (V-4)$$

where  $H(\bar{x})$  is based upon the Hertzian inlet deformation profile.

It follows that the ratio  $\frac{1 - e^{-\alpha p}}{1 - e^{-\alpha p_A}}$  becomes

$$\frac{1 - e^{-\alpha p}}{1 - e^{-\alpha p_A}} = \frac{S}{S_A} \quad (V-5)$$

where

$$S = \int_{-\infty}^{\bar{x}} \frac{H-1}{H^3} d\bar{x} \quad \text{and}$$

$$S_A = \int_{-\infty}^{\bar{x}_a} \frac{H-1}{H^3} d\bar{x} \quad (V-7)$$

From the above relations, the pressure at inlet can be expressed as

$$P = \frac{1}{\alpha} \log_e [1 - (1 - e^{-\alpha p_A}) \frac{S}{S_A}] \quad (V-8)$$

### V-3. CENTRAL PRESSURE

The pressure distribution in the central region is the elliptical Hertzian profile,

$$p = \frac{2}{\pi} \left( \frac{p}{p_{HZ}} \right) = \frac{2}{\pi} \sqrt{1 - \bar{x}^2} \quad (V-9)$$

#### V-4. EXIT PRESSURE

Typically, the exit pressure distribution in a heavily loaded elasto-hydrodynamic contact would be that shown in Fig. V-2. The pressure spike usually occurs at  $\bar{x} = 1 - \bar{e}$ , that is the beginning of the protrusion. In the region  $(1 - 2\bar{e}) < \bar{x} < (1 - \bar{e})$ , the pressure rise rapidly to the maximum pressure  $p_B$ , and it is assumed that the increase of pressure in this region follows a parabolic profile. In the region  $(1 - \bar{e}) < \bar{x} < 1$ , the pressure drops sharply to the ambient pressure. In estimating the pressure here, it assumed that at the spike the pressure takes a finite jump from  $p_B$  to the Hertzian value  $p_{BB}$  and then decays to the ambient pressure parabolically.

To determine the peak pressure  $p_B$ , it is further assumed that the gaining in load represented by the area  $A_5$ . Accordingly, the rising parabolic pressure can be written as

$$p(\bar{x}) = (p_B - p_D) \left( \frac{\bar{x} - \bar{x}_D}{\bar{e}} \right)^2 + p_D \quad (V-10)$$

$$\text{for } (1 - 2\bar{e}) < \bar{x} < (1 - \bar{e})$$

where

$$p_D = \frac{2}{\pi} \sqrt{1 - \bar{x}_D^2} \quad \text{and} \quad \bar{x}_D = 1 - 2\bar{e}$$

Likewise, the decaying parabolic pressure can be expressed

$$p(\bar{x}) = \left( 1 - \frac{\bar{x}}{\bar{e}} \right)^2 p_{BB} \quad (V-11)$$

where

$$p_{BB} = \frac{2}{\pi} \sqrt{1 - (1 - \bar{e})^2}$$

It follows that the gaining in load  $W_G$  before the spike can be written as

$$W_G = \int_{1-2\bar{e}}^{1-\bar{e}} \left[ (p_B - p_D) \left( \frac{\bar{x} - \bar{x}_D}{\bar{e}} \right)^2 + p_D - \frac{2}{\pi} \sqrt{1 - \bar{x}^2} \right] d\bar{x} \quad (V-12)$$

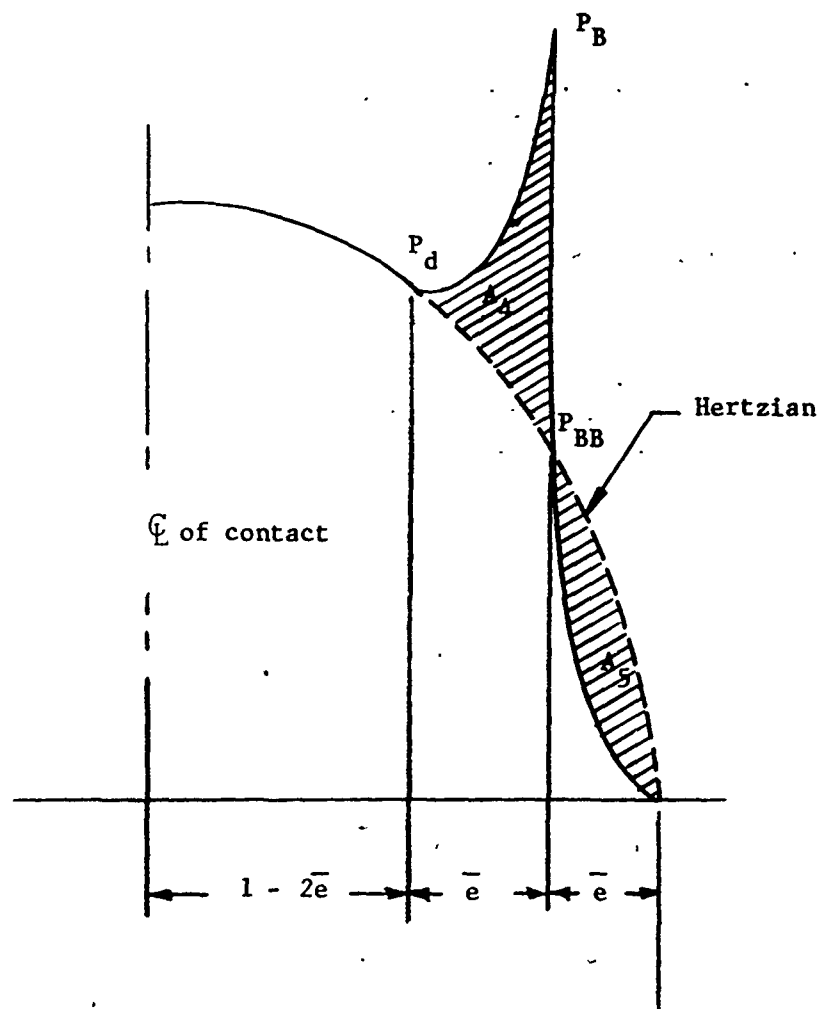


Fig. V-2 Exit Pressure Calculation

and the loss in load  $W_L$  after the spike is

$$W_L = \int_{1-\bar{e}}^1 \left[ \frac{2}{\pi} \sqrt{1-\frac{\bar{x}^2}{\bar{e}}} - \left( \frac{1-\bar{x}}{\bar{e}} \right)^2 p_B \right] d\bar{x} \quad (V-13)$$

Equating  $W_G$  and  $W_L$ , one obtains

$$p_B = \frac{W_L - \int_{1-2\bar{e}}^{1-\bar{e}} \left\{ p_D \left[ 1 - \left( \frac{\bar{x} - \bar{x}_D}{\bar{e}} \right) \right] - \frac{2}{\pi} \sqrt{1-\frac{\bar{x}^2}{\bar{e}}} \right\} d\bar{x}}{\int_{1-2\bar{e}}^{1-\bar{e}} \left( \frac{\bar{x} - \bar{x}_D}{\bar{e}} \right)^2 d\bar{x}} \quad (V-14)$$

For extremely lightly loaded cases,  $\bar{e}$  may exceed 0.5. In which case, the method described here will break down and there will be an error message printed out in computer program and both the pressure, the temperature, and the stress calculations will be bypassed in the program.

# APPENDIX VI INLET TEMPERATURE CALCULATION

An integral method is used to calculate the temperature distribution in the inlet region. The output of this calculation will be employed in the sub-routine TEMPT, which is to calculate the temperature field in the contact zone, as a function of the initial conditions.

In the method the temperature profile of the lubricant in the inlet region is assumed to be a parabolic in terms of surface temperatures and center film temperature, i.e.,

$$T(x, y) = (2T_1 + 2T_2 - 4T_c) \frac{y^2}{h^2} + (-3T_1 - T_2 + 4T_c) \frac{y}{h} + T_1, \quad (\text{VI-1})$$

where  $h$  is the film thickness,  $T_1$  and  $T_2$  are the surface temperatures at  $y = 0$  and  $y = h$  respectively, and  $T_c$  is the center film temperature at  $y = h/2$ . These three temperatures,  $T_1$ ,  $T_c$ , and  $T_2$ , are to be determined by requiring that the assumed temperature profile (VI-1) satisfy the boundary conditions at the two surfaces and the energy equation integrated across the film thickness, which is as follows:

$$c_f \int_0^h (\rho u \frac{\partial T}{\partial x} + \rho v \frac{\partial T}{\partial y}) dy - K_f \int_0^h \frac{\partial^2 T}{\partial y^2} dy = \int_0^h \mu (\frac{\partial u}{\partial y})^2 dy - \frac{dp}{dx} \int_0^h u \frac{T}{\rho} \frac{\partial p}{\partial T} dy \quad (\text{VI-2})$$

In the above equation,  $c$ ,  $\rho$ ,  $K_f$  and  $\mu$  are the specific heat, density, heat conductivity and viscosity of lubricant respectively,  $u$  and  $v$  are the velocity components in the  $x$  and  $y$  direction respectively.

This method of analysis is analogous to the boundary layer integral method in the viscous flow theory. For obtaining numerical solutions this method is simpler than a full finite difference method since the two-dimensional system is reduced to a quasi one-dimensional one.

Since the surface temperatures do not rise appreciably in the inlet region,  $T_1$  and  $T_2$  are assumed equal to the constant inlet temperature  $T_0$ . Lubricant density is set to be constant. The film thickness is given by the Hertzian displacement profile. In non-dimensionalized form the profile is



as follows:

$$\bar{h} = 1 + B \left[ -\bar{x} (\bar{x}^2 - 1) - \ln(-\bar{x} + \sqrt{\bar{x}^2 - 1}) \right], \quad (\text{VI-3})$$

where

$$h = \frac{h}{h_0}$$

$h$  = film thickness

$h_0$  = film thickness in the contact zone

$$B = \frac{b^2}{2R'_x h_0}$$

$b$  = half length of contact zone

$R'_x$  = equivalent radius in the rolling direction

$$\bar{x} = \frac{x}{b}$$

$x$  = coordinate in the rolling direction

The velocity profile in the inlet region is obtained by integrating the Reynolds equation twice:

$$\bar{u} = 3\left(1 - \frac{1}{h}\right) \bar{y}^2 + \left[\frac{U_1 - U_2}{U_1 + U_2} - 3\left(1 - \frac{1}{h}\right)\right] \bar{y} + \frac{U_1}{U_1 + U_2}, \quad (\text{VI-4})$$

where

$$\bar{u} = \frac{u}{U_1 + U_2}$$

$u$  = flow velocity

$U_1, U_2$  = speed of body 1, 2

$$\bar{y} = \frac{y}{h}$$

$y$  = coordinate perpendicular to the rolling direction

Under the assumptions mentioned above and with the temperature profile Eq. VI-1, the non-dimensionalized integrated energy equation takes the following

form:

$$\frac{2 Q_c}{B^2} \frac{d}{d\bar{x}} \bar{h} \int_0^1 \bar{u} [4(1-\theta_c)\bar{y}^2 + 4(\theta_c - 1)\bar{y} + 1] c\bar{y} d\bar{y} =$$

$$Q_m \frac{1}{\bar{h}} \int_0^1 \bar{u} \left( \frac{\partial \bar{u}}{\partial \bar{y}} \right)^2 d\bar{y} - 4 \frac{\theta_c - 1}{\bar{h}} \quad (VI-5)$$

where

$$Q_c = \frac{\rho_o c_f (U_1 + U_2) b^3}{16 K_f R_1^2}$$

$$Q_m = \frac{\mu_o (U_1 + U_2)^2}{2 K_f T_o}$$

$\rho_o$  = density  $\rho$  at inlet temperature  $T_o$

$\mu_o$  = viscosity  $\mu$  at  $T_o$

$$\theta = \frac{T_c}{T_o}$$

$$\bar{u} = \frac{\mu}{\mu_o}$$

This equation is integrated, using Eqs. (VI-3) and (VI-4) for  $\bar{h}$  and  $\bar{u}$  respectively, to obtain the center film temperature  $\theta_c$ . The viscosity function  $\bar{u} = \exp \left[ \beta \left( \frac{1}{T} - \frac{1}{T_o} \right) \right]$  is employed in the integration.

The integration is started where  $\bar{h} = 6$ . The temperature there is assumed equal to the inlet temperature  $T_o$ . The integration stops near the entrance to the contact zone where there is no longer reverse flow. This position is calculated from the velocity profile Eq. (VI-4).

The above calculation is contained in the subroutine THILT in the main elasto-hydrodynamic computer program.

APPENDIX VII  
ELASTOHYDRODYNAMIC PERFORMANCE COMPUTER PROGRAM

VII-1. INPUT ROUTINE

The Fortran statements for the input routine are listed below.

Input Routine

```
120 READ (NR, 3) RX1, RX2, RY1, RMS1, RMS2
    READ (NR, 3) E1, E2, V1, V2
    READ (NR, 3) CONS1, CONS2, CPS1, CPS2, RHOS1, RHOS2
    READ (NR, 3) EPST, EPSRD, DTF
    READ (NR, 2) ITT, ITRDU, NRITE, NPTS, NSTRS
    IF (NSTRS-EQ-1) GO TO 90
    READ (NR, 2) JJFS, NTHE
    READ (NR, 3) (Y(J), J = 1, JJFS)
90  WRITE (NW, 500)
    READ (NR, 1)
    READ (NR, 3) WT, TEMI, U2, U1
    READ (NR, 3) VIS, ALF, BET, GAM, CONF, CPF, RHOF
    READ (NR, 3) PSTAR, NGF
    IF (NEXT-EQ-2) GO TO 120
    CALL EXIT
1  FORMAT (72H
2  FORMAT (17I5)
3  FORMAT (8E10.3)
END
```

Instruction for Input Cards

Card 1 FORMAT (8E10.3)

RX1 = radius of body number 1 in the direction of rolling, in.  
RX2 = radius of body number 2 in the direction of rolling, in.  
RY1 = radius of body number 1 in the direction normal to rolling, in.  
RY2 = radius of body number 2 in the direction normal to rolling, in.  
RMS1 = root mean square surface roughness of body number 1, micro-in.  
RMS2 = root mean square surface roughness of body number 2, micro-in.

Card 2 FORMAT (8E10.3)

E1 = modulus of elasticity of body number 1, psi.  
E2 = modulus of elasticity of body number 2, psi.  
V1 = Poisson's ratio of body number 1  
V2 = Poisson's ratio of body number 2

Card 3 **FORMAT** (8E10.3)

CONS1 = thermal conductivity of body number 1, BTU/°F-hr-ft.  
 CONS2 = thermal conductivity of body number 2, BTU/°F-hr-ft.  
 CPS1 = specific heat of body number 1, BTU/lb-°F.  
 CPS2 = specific heat of body number 2, BTU/lb-°F.  
 RHOS1 = density of body number 1, lb/in<sup>3</sup>.  
 RHOS2 = density of body number 2, lb/in<sup>3</sup>.

Card 4 **FORMAT** (8E10.3)

EPST = calculating the convergence factor for temperature at each grid point, recommended value is 0.0001.  
 EPSRD = this is a convergence factor for the iterations to determine the secondary pressure viscosity coefficient, recommended value is 0.0005.

(In calculating the temperature distribution, the viscosity is assumed to vary with pressure exponentially. Two coefficients are used to represent the pressure-viscosity relations, one in the low pressure region, and one in the high pressure region. The cut-off pressure separating the low and high pressure region is denoted by  $p^*$ . For  $p < p^*$ , the high pressure-viscosity coefficient,  $\alpha_1$ , is used; whereas for  $p > p^*$ , a reduced pressure-viscosity,  $\alpha_2$ , is used.  $\alpha_1$  is considered as given and can be found from the static pressure-viscosity data;  $p^*$  is the cut-off pressure and for most lubricants, the approximate value of  $p^*$  is near 60,000 psi. If the maximum Hertz pressure  $p_{HZ}$  is less than 100,000 psi,  $p^*$  is set in the program equal to  $p_{HZ}/2$ ).

(In this program, the value of  $\alpha_2$  is not given. An iterative procedure is used to determine the ratio of  $\alpha_2/\alpha_1$  such that the friction calculated from the thermal theory with a value of  $\alpha_2/\alpha_1$  matches the friction predicted empirically from Johnson and Cameron's friction data. EPSRD is the maximum error allowed for the difference between the calculated friction and the empirical friction).

DTF = an increment of temperature required to start the iteration at each grid point. The recommended value is 0.1.  
 RDU = initial ratio of  $\alpha_2/\alpha_1$ . For moderate load 0.5 is recommended. For heavy load ( $p_{HZ} \sim 500,000$  psi) 0.1 should be used.

Card 5 **FORMAT** (1715)

ITT = maximum number of iterations allowed for the temperature calculation at each grid point. 20 is recommended.  
 ITRDU = maximum number of iterations allowed for the calculation of  $\alpha_2/\alpha_1$ . ( $RDU = \alpha_2/\alpha_1$ ). 10 is recommended.  
 NRITE = control for diagnostic output data.  
     NRITE = 1, no diagnostics  
     NRITE = 0, print out diagnostics  
 NPIS = 0, calculating pressure, temperature, and stress distributions.  
     = 1, bypass pressure, temperature, and stress calculations.

NSTRS = control for stress calculations  
 NSTRS = 0, calculating stresses  
 NSTRS = 1, bypass stress calculations

Card 6 FORMAT (17I5)

THIS CARD IS ONLY REQUIRED FOR NSTRS = 0.

JJFS = the last grid is an array of y-coordinates where the subsurface stresses are to be calculated. The y-coordinate is measured from the surface into the body.

NTHE = number of plane angle  $\theta$ , between 0 and 90 degrees, to be examined for variation of shearing stresses.

Card 7 FORMAT (8E10.3)

THIS CARD IS ONLY REQUIRED FOR NSTRS = 0.

(Y(J), J = 1, JJFS) = an array of normalized y coordinates at which the subsurface stresses will be calculated. Half Hertzian width  $a$  is used as the normalizing distance. In the x-direction, the stresses will be calculated within the interval  $-a \leq x \leq a$ .

Card 8 FORMAT (72H)

This card reads in a description of the case to be run. A maximum of 72 characters is allowed.

Card 9 FORMAT (8E10.3)

WT = normal load in the contact. In the case of an elliptical contact, WT is the total load of the contact. In the case of a line contact, WT is the load per unit length of the line contact.  
 TEMI = initial temperature of the lubricant,  $^{\circ}\text{F}$ .  
 U2 = surface speed of contacting body number 2 in the rolling direction. (U2 must be greater than U1), in/sec.  
 U1 = surface speed of contacting body number 1 in the rolling direction, in/sec.

Card 10 FORMAT (8E10.3)

VIS =  $\mu_0$ , inlet viscosity of the lubricant, lb-sec/in<sup>2</sup>.  
 ALF =  $\alpha$ , pressure-viscosity coefficient, in<sup>2</sup>/lb. ( $\alpha$  is the pressure-viscosity coefficient in the following viscosity function,

$$\mu = \mu_0 e^{[\alpha p + (\beta + \gamma p)(\frac{1}{T} - \frac{1}{T_0})]}$$

BEI =  $\beta$ , temperature-viscosity coefficient,  $^{\circ}\text{R}$ .  
 GAM =  $\gamma$ , pressure-temperature-viscosity coefficient, in<sup>2</sup>- $^{\circ}\text{R}$ /lb.  
 CONF = thermal conductivity of the lubricant, BTU/ $^{\circ}\text{F}$ -hr-ft.

CPF = specific heat of the lubricant, BTU/lb-°F.  
 RHOF = density of the lubricant, lb/in<sup>3</sup>.

Card 11 FØRMAT (8E10.3)

PSTAR = this is  $p^*$  which separates the two pressure-viscosity coefficients,  $\alpha_1$  and  $\alpha_2$ . For most lubricants, the approximate value of  $p^*$  is near 60,000 psi. However, if the maximum Hertz pressure is less than 100,000 psi,  $p^*$  is set equal to  $p_{HZ}/2$  in the program.

GFC = the frictional coefficient in this program can be either calculated by subroutine FRICT or entered as a given quantity. The variable GFC is used to read in the given frictional coefficient. If the friction is calculated by subroutine FRICT, set GFC = 0.0.

Card 12 FØRMAT (17I5)

LINCON = control for the case of a line contact or an elliptical contact. For a line contact, read LINCON = 1. For an elliptical contact, read LINCON = 0.

NEXT = control for further cases to be run.

NEXT = 1, more cases to come.

NEXT = 0, last case, go to exit.

NGF = control for calculating coefficient of frictional coefficient by FRICT.

NGF = 1, bypassing subroutine FRICT, and frictional coefficient is read in as GFC.

NGF = 0, frictional coefficient is calculated by FRICT.

## VII-2. OUTPUT EXPLANATION

Items of output will be explained below in the order of computation.

a. Write-Out of the Input Data: including geometrical data, material data, operating conditions, and lubricant data.

b. Thermal Parameters:

$$QM = \frac{\mu_o (U_2 + U_1)^2}{2K_f T_o}$$

$$CONV = \frac{\rho C_f (U_2 + U_1)}{16K_f (R'_x)^2} \cdot 3$$

$$D1 = \left( \frac{K_f^2}{\pi \rho_1 C_1 U_1 K_1} \right)^{1/2} \left( \frac{R'_x E'^3}{4w^3} \right)^{1/4}$$

D2 = same as D1 except with subscript 2.

c. Contact Dimensions:

B = b, half Hertzian width in the rolling direction, in.

A = a, half Hertzian width in the direction normal to rolling, in.

A/B = a/b, ratio of semi-major to minor axes of the elliptical contact.

$$M = b \left[ \frac{3\pi}{4} \frac{P}{(\bar{A} + \bar{B})E'} \right]^{-1/3}$$

d. Load, Speed, and Lubricant Parameters:

$$UBAR = \bar{U} = \frac{\mu_o (U_2 + U_1)}{2E'R'_x}$$

$$\bar{G} = \alpha E'$$

$$AFA = \frac{\pi}{2} \alpha P_{HZ}$$

$$BTA = \frac{\beta}{T_o}$$

$$GMA = \gamma \left( \frac{\pi P_{HZ}}{2T_o} \right)$$

Equivalent line contact load =  $\frac{4}{3} \frac{P}{a}$  for the elliptical contact.

For a line contact, this is the load per unit length.

$$WRAR = \frac{w}{E'R'_x}$$

$$PHZ/ED = \frac{P_{HZ}}{E'}$$

$$B = \frac{4w}{\pi E'h_o}$$

$$\text{Slide to Roll Ratio} = \frac{2(U_2 - U_1)}{U_2 + U_1}$$

$$AM = \frac{3\mu_o (U_1 + U_2) E'R'_x}{w^2}$$

e. Reduction Factors:

Self explanatory.

f. Isothermal Minimum FILM and Minimum FILM: in inches.

g. Dimensionless Protrusion Parameters:

$$\text{Protrusion width} = \frac{e}{b}$$

$$\text{Protrusion Depth} = \frac{h_o - h_{\min}}{h_o}$$

$$\text{Percentage of Area Contact} = \frac{\text{real area of contact per unit length}}{2b}$$

$$\text{Specific Film} = \frac{h_o}{\sqrt{\sigma_1^2 + \sigma_2^2}}$$

$$\text{h. Frictional Coefficient} = \frac{\text{frictional force}}{\text{total load}}$$

i. Film Shape and Pressure Distribution:

$$\text{XBAR} = \frac{x}{b}$$

$$\text{Normalized Film} = \frac{h}{h_o}$$

$$\text{Pressure} = \frac{p}{\frac{\pi}{2} \text{ PHZ}}$$

Note: For extremely lightly loaded cases such that the protrusion width  $\bar{e}$  exceeds 0.5, the pressure calculation in the program breaks down (see Appendix V). A message will be printed out for such cases and the pressure, the temperature, and the stress calculations will be bypassed.

j. Temperature Distributions:

First the value of  $\text{RDU} = \alpha_2 / \alpha_1$  is printed out at each iteration, which is to match the determined frictional coefficient. Then the temperatures at various positions (XBAR) are printed out:

T MEAN = mean-film temperature /  $T_o$

T 1 = surface temperature of body number 1 /  $T_o$

T 2 = surface temperature of body number 2 /  $T_o$

SHEAR FORCE = surface shear stress /  $(\frac{\pi}{2} \text{ PHZ})$



#### k. Stress Calculations:

First the arrays of the normalized x and y coordinates, at which stresses are calculated, are printed out. The half Hertzian width, a, is used as the normalizing distance. The y-coordinate is measured from the surface into the body. The normalized stresses at various x at a fixed y are printed out next.  $\frac{\pi}{2}$  PHZ is the normalizing stress:

$$XST = \frac{x}{b}$$

SX = normalized normal stress in x-direction

SY = normalized normal stress in y-direction

SXY = normalized shear stress

PSX = normalized principal stress in x'-direction

PSY = normalized principal stress in y'-direction

PSZ =  $v_1(PSX + PSY)$ , normalized principal stress in z'-direction  
 $v_1$  is the Poisson's ratio of body 1. For body 2 this should be corrected by the ratio of the Poisson's ratios.

PTXY =  $(PSX - PSY)/2$ , normalized maximum shear stress.

OS =  $\frac{1}{3}[(PSX - PSY)^2 + (PSY - PSZ)^2 + (PSZ - PSX)^2]^{1/2}$  normalized maximum octahedral shear stress.

Then, normalized shear stress at every  $(\frac{90}{NTHZ-1})$  degree measured from the x-axis will be printed out. NTHZ is an input integer (see input Card 6).

#### VII-3. NOMENCLATURE FOR INPUT AND OUTPUT

$\mu_o$  = inlet viscosity.

$U_2, U_1$  = surface velocity of body 1 and 2.

$K_f$  = thermal conductivity of the lubricant.

$T_o$  = inlet temperature.

$\rho$  = density of the lubricant.

$c_f$  = specific heat of lubricant.

$R_x^i = \left( \frac{1}{R_{x1}} + \frac{1}{R_{x2}} \right)^{-1}$

b = half Hertzian width.

$\rho_{1,2}$  = density of body 1 and 2.

$C_{1,2}$  = specific heat of body 1 and 2.

$K_{1,2}$  = thermal conductivity of body 1 and 2.

$$E' = \left[ \frac{1}{2} \left( \frac{1-\nu_1^2}{E_1} + \frac{1-\nu_2^2}{E_2} \right) \right]^{-1}$$

$\nu_{1,2}$  = Poisson's ratio of body 1 and 2

$w$  = load per unit length for a line contact.

$P$  = total load of the contact.

$$\bar{A} = \frac{1}{2} \left( \frac{1}{R_{x1}} + \frac{1}{R_{x2}} \right)$$

$$\bar{B} = \frac{1}{2} \left( \frac{1}{R_{y1}} + \frac{1}{R_{y2}} \right)$$

$\alpha, \beta, \gamma$  = see Card 10.

$P_{HZ}$  = maximum Hertz pressure.

$\sigma_1, \sigma_2$  = r.m.s. surface roughness of body 1 and 2.

$e$  = protrusion width

$$\bar{e} = \frac{e}{b}$$

$x$  = rolling direction coordinates

$y$  = coordinates perpendicular to rolling direction

```

C PROGRAM PN458(INPUT,OUTPUT,TAPE5=INPUT,TAPE6=OUTPUT,TAPE22)
C PERFORMANCE CALCULATION OF ELASTOHYDRODYNAMIC
C CONTACT
C
C THIS PROGRAM CALCULATES THE FOLLOWING FOR AN EHD CONTACT
C A) EXIT MINIMUM FILM THICKNESS
C B) EXIT PROTRUSION WIDTH
C C) PERCENT OF AREA OF CONTACT
C D) COEFFICIENT OF FRICTION
C E) SURFACE TEMPERATURES
C F) CENTER FILM TEMPERATURES
C G) SUBSURFACE STRESS DISTRIBUTION
C THE INPUT DATA ARE AS FOLLOWS-
C
C GEOMETRICAL DATA -
C RX1 = RADIUS OF BODY 1 IN THE DIRECTION OF
C ROLLING , IN.
C RX2 = RADIUS OF BODY 2 IN THE DIRECTION OF
C ROLLING , IN.
C RY1 = RADIUS OF BODY 1 NORMAL TO ROLLING , IN.
C RY2 = RADIUS OF BODY 2 NORMAL TO ROLLING , IN.
C RMS1 = R.M.S. SURFACE ROUGHNESS OF BODY 1, MICRO. IN.
C RMS2 = R.M.S. SURFACE ROUGHNESS OF BODY 2, MICRO. IN.
C
C
C MATERIAL DATA -
C
C E1 = MODULUS OF ELASTICITY OF BODY 1,PSI
C E2 = MODULUS OF ELASTICITY OF BODY 2,PSI
C V1 = POISSONS RATIO OF BODY 1
C V2 = POISSONS RATIO OF BODY 2
C CON1
C CON1 = THERMAL CONDUCTIVITY OF BODY 1,BTU/DEG.F-HR-FT
C CON2 = THERMAL CONDUCTIVITY OF BODY 2,BTU/DEG.F-HR-FT
C CPS1 = SPECIFIC HEAT OF BODY 1,BTU/LB-DEG.F
C CPS2 = SPECIFIC HEAT OF BODY 2,BTU/LB-DEG.F
C RHOS1 = DENSITY OF BODY 1,LB/IN**3
C RHOS2 = DENSITY OF BODY 2,LB/IN**3
C
C
C OPERATING CONDITIONS
C
C WT = TOTAL LOAD , LB
C U2 = SURFACE VELOCITY OF BODY 2 , IN/SEC.
C U2 = SURFACE VELOCITY OF BODY 2 , IN/SEC.
C U2 = SURFACE VELOCITY OF BODY 1 , IN/SEC.
C T1 = INLET TEMPERATURE OF THE LUBRICANT , DEG.F.
C
C
C LUBRICANT DATA
C VIS = INLET VISCOSITY LB-SEC/IN**2
C ALF = PRESSURE-VISCOSITY COEF. IN**2/LB
C BET = TEMPERATURE-VISCOSITY COEF. DEG. R
C GAM = PRESSURE-TEMPERATURE-VISCOSITY COEF. IN**2-DEF.R/LB.
C CONF = THERMAL CONDUCTIVITY BTU/DEG.F-HR-FT
C CPF = SPECIFIC HEAT BTU/LB-DEG.F
C RHOF = DENSITY LB/IN**3

```

```

C   READ INPUT DATA
    DIMENSION AMDA(24),FMA(24),AOBA(24)
    DIMENSION SLIPA(9),CCA(9),EEA(9)
    COMMON KI,KC,KG,KA,KO,KD,KB,KE,KF,KR,NR,NW
    COMMON RX1,RX2,RY1,RY2,RMS1,RMS2,E1,E2,V1,V2
    COMMON CONS1,CONS2,CPS1,CPS2,RHOS1,RHOS2,WT,TEMI,U2,U1
    COMMON VIS,ALF,BET,GAM,CONF,CPF,RHOF,PS,PSTAR
    COMMON AFA,BTA,GMA,A,B,AM,SLIP, RXP,RYP,EP,QN,CONV,D(2),COMP,AHZ,
1   PHZ,WBAR,UBAR,PHZE,GG,EDOW,BOA ,WW
    COMMON FCOE,EBAR,FEET,FEES,HMIN,SPFILM,ABAR,SHM
    COMMON EPST,EPSRD,DTF,TWF1,ITRDU,ITT,NRITE
    COMMON XH(50),HE(50),P(50),T(50),TI(2,50),F(2,50),SHS(50)
    COMMON XSTT,XDEX,YSTT,YDEY,XST(31),Y(31) ,JJFS,KKFS,NTHE,NOPL
    NR=5
    NW=6
    DATA(AMDA(I),I=1,24)/ 0.0,0.05,0.1,0.15,0.2,0.25,0.3,0.35,0.4,0.45
1   1.0,0.5,0.55,0.6,0.65,0.7,0.75,0.8,0.85,0.9,0.92,0.94,0.96,0.98,1.0/
    DATA(FMA(I),I=1,24)/1.0,1.035,1.072,1.112,1.155,1.195,1.24,1.29,
1   11.35,1.41,1.485,1.56,1.65,1.77,1.895,2.065,2.29,2.60,3.0956,3.3973
2   2.3,8275,4.5319,5.946,6./
    DATA(AOBA(I),I=1,24)/1.0,0.935,0.875,0.82,0.765,0.710,0.66,0.615,
1   0.57,0.525,0.480,0.44,0.4,0.358,0.32,0.282,0.24,0.195,0.14875,
2   20.12897,0.1075,0.083184,0.055189,0.0/
    DATA(SLIPA(I),I=1,9)/0.0,0.05,0.1,0.15,0.2,0.25,0.3,0.35,0.4/
    DATA(CCA(I),I=1,9)/0.5,0.71,0.92,1.1,1.23,1.3,1.35,1.38,1.4/
    DATA(EEA(I),I=1,9)/0.4,0.41,0.42,0.4255,0.4285,0.43,0.43,0.43,0.43
1 /
120 READ (NR,3) RX1,RX2,RY1,RY2,RMS1,RMS2
    READ (NR,3) E1,E2,V1,V2
    READ (NR,3) CONS1,CONS2,CPS1,CPS2,RHOS1,RHOS2
    READ (NR,3) EPST,EPSRD,DTF,NDU
    READ (NR,2) ITT,ITRDU,NRITE,NPTS,NSTRS
    IF (NSTRS .EQ. 1) GO TO 90
    READ (NR,2) JJFS,NTHE
    NOPL=1
    READ (NR,3) ( Y(J),J=1,JJFS)
90  WRITE (NW,500)
500  FORMAT(1H1)
    WRITE (NW,5)
    WRITE (NW,6)
    WRITE (NW,4)
    READ (NR,1)
    READ (NR,3) WT,TEMI,U2,U1
    READ (NR,3) VIS,ALF,BET,GAM,CONF,CPF,RHOF
    READ (NR,3) PSTAR,GFC
    READ (NR,2) LINCON,NEXT,NGF
    WRITE (NW,1)
    WRITE (NW,4)
    WRITE (NW,10)
    WRITE (NW,11) RX1,RX2
    IF (LINCON.EQ.1) GO TO 600
    WRITE (NW,12) RY1,RY2
600  WRITE (NW,13) RMS1,RMS2
    WRITE (NW,30)
    WRITE (NW,14) E1,E2
    WRITE (NW,15) V1,V2
    WRITE (NW,16) CONS1,CONS2
    WRITE (NW,17) CPS1,CPS2
    WRITE (NW,18) RHOS1,RHOS2
    WRITE (NW,31)

```

```

IF(LINCON.EQ.1) WRITE (NW,57) WT
IF(LINCON.EQ.0) WRITE (NW,19) WT
WRITE (NW,21) TEMI
WRITE (NW,20) U1,U2
WRITE (NW,32)
WRITE (NW,22) VIS
WRITE (NW,23) ALF
WRITE (NW,24) BET
WRITE (NW,25) GAM
WRITE (NW,26) CONF
WRITE (NW,27) CPF
WRITE (NW,28) RHOF
PS=200000.
TWFL=1.
RXP= 1.0/RX1+1.0/RX2
RYP= 1.0/RX1+1.0/RX2
TEMI=TEMI+460.
AA=0.5*RXP
DD=0.5*RYP
RXP = 1.0/RXP
RYP = 1.0/RYP
AMD=(AA-DD)/(AA+DD)
CALL TLU (AMD,FM,AMDA,FMA,24)
CALL TLU (AMD,AOB,AMDA,AOBA,24)
PI=3.1416
EP = PI /((1.0-V1**2)/E1+(1.0-V2**2)/E2)
SB=FM*(0.75*PI*WT/(AA+DD)/EP)**0.333333
WW= 0.75*WT/SB
IF(LINCON.EQ.1) WW=WT
EDOW= EP*2.0/PI
WBAR=WW/EDOW/RXP
UBAR=VIS*(U1+U2)*0.5/EDOW/RXP
IF(LINCON.EQ.1) GO TO 100
IF(AMD-0.9) 101,101,100
100 SA= 2.0*(WW*RXP/EP)**0.5
PHZE= (WW/EP/RXP)**0.5/PI
PHZ=EP*PHZE
GO TO 105
101 SA= SB*A0B
PHZE= 1.5*WT/(PI*SA*SB*EP)
105 CONTINUE
AHZ=SA
A=1.0
SLIP=(U2-U1)/U2
SRRAT=(U2-U1)/(U2+U1)*2.0
AM=6.*VIS*(U1+U2)*EP*RXP/WW**2
PHZ=EP*PHZE
IF(PHZ.LT.1.E5) PSTAR=PHZ/2.
QM=VIS*(U1+U2)**2/(CONF*TEMI)*2.315
F1=(WW/EP)**3/RXP
F2=SQRT(F1)
F1=(F1/4.)**0.25
G1=PI*RHOS1*CPS1*CONS1
G2=PI*RHOS2*CPS2*CONS2
CONV=RHOF*CPF*(U1+U2)*F2/CONF*21600.
D(1)=CONF*0.5*SQRT(1./(G1*U1))/F1/208.
D(2)=CONF*0.5*SQRT(1./(G2*U2))/F1/208.
AFA =ALF*PHZ*PI/2.0
BTA=BET/TEMI
GMA=GAM*PHZ*PI/2.0/TEMI
GG = ALF*EDOW

```

```

BOA=1.0/AOB
IF (LINCON.EQ.1) BOA=10.
CALL FTFS(FEET,FEES)
IF (LINCON.EQ. 1) FEES=1.0
  SHMIT=RXF* GG**0.6*UBAR**0.7/WBAR**0.13 *1.6
  SHM= SHMIT *FEET*FEES
B=2.0*WW/(EP*SHM)
CALL TLU(SLIP,CC,SLIPA,CCA,9)
CALL TLU(SLIP,EE,SLIPA,EEA,9)
EBAR=CC*GG**0.2
EBAR=EBAR*UBAR**EE
EBAR=EBAR*WBAR**(-0.74)
HMIN=0.8
SPFILM=SHM/SQRT(RMS1**2+RMS2**2)*1000000.
PTD=1.-HMIN
C  WRITE OUTPUT DATA
  WRITE (NW,45)
  WRITE (NW,46) OM,CONV
  WRITE (NW,47) D(1),D(2)
  WRITE (NW,35)
  WRITE (NW,36)
  IF (LINCON.EQ.1) GO TO 601
  WRITE (NW,37) SA,SB
  WRITE (NW,38) BOA,FM
  GO TO 602
601 WRITE (NW,60) SA
602 WRITE (NW,39)
  WRITE (NW,42) UBAR
  WRITE (NW,43) GG,AFA
  WRITE (NW,44) BTA,GHA
  WRITE (NW,40) WW,WBAR
  WRITE (NW,41) PHZ,PHZE
  WRITE (NW,55) B,SRRAT
  WRITE (NW,56) AM
  WRITE (NW,49)
  WRITE (NW,48) FEET,FEES
  WRITE (NW,50) SHMIT,SHM
  WRITE (NW,51)
  WRITE (NW,52) EBAR,PTD
  CALL AREA (EBAR,HMIN,SPFILM,ABAR)
  ABAR=100.*ABAR
  WRITE (NW,53) ABAR,SPFILM
  IF (NGF.EQ.1) GO TO 110
  CALL FRIC
110 IF (NGF.EQ.1) FCOE=GFC
  WRITE (NW,54) FCOE
  IF (NPTS.EQ.1) GO TO 200
  IF (EBAR.GE.0.5) GO TO 603
  CALL PRESS
  CALL TEMPT(RDU)
  IF (NSTRS .EQ. 1) GO TO 200
  KKFS=27
  DO 190 K=1, KKFS
  KKK=K+14
190 XST(K)=XH(KKK)
  XSTT=-1.0
  XDEX=0.25
  YSTT=-0.5
  YDEY=0.25
  CALL STRESS
  GO TO 200

```

```

603 WRITE(NW,604)
200 IF(NEXT .EQ. 1) GO TO 120
    CALL EXIT
    1 FORMAT(72H
      1
    2 FORMAT(17I5)
    3 FORMAT(8E10.3)
    4 FORMAT (//)
    5 FORMAT( 40X 45H PERFORMANCE OF AN ELASTOHYDRODYNAMIC CONTACT )
    6 FORMAT( 40X 45H***** )
10 FORMAT(/// 40X 17H GEOMETRIAL DATA ,///)
11 FORMAT(55H RAD. OF BODY 1,2 IN THE DIRECTION OF ROLLING,(IN)
    1, E12.5,2X,E12.5/)
12 FORMAT(55H RAD. OF BODY 1,2 NORMAL TO ROLLING,(IN)
    1, E12.5,2X,E12.5/)
13 FORMAT(55H R.M.S. SURFACE ROUGHNESS OF BODY 1,2,(MICRO IN)
    1, E12.5,2X,E12.5/)
14 FORMAT(55H MODULI OF ELASTICITY OF BODY 1,2,(PSI)
    1, E12.5,2X,E12.5/)
15 FORMAT(55H POISSONS RATIO OF BODY 1,2,
    1, E12.5,2X,E12.5/)
16 FORMAT(55H THERMAL CONDUCTIVITY OF BODY 1,2,(B/DEG.F-HR-FT)
    1, E12.5,2X,E12.5/)
17 FORMAT(55H SPECIFIC HEAT OF BODY 1,2,(B/LB-DEG. F)
    1, E12.5,2X,E12.5/)
18 FORMAT(55H DENSITY OF BODY 1,2,(LB/IN**3)
    1, E12.5,2X,E12.5/)
19 FORMAT(55H TOTAL LOAD,(LB)
    1, E12.5/)
20 FORMAT(55H SURFACE VELOCITY OF BODY 1,2,(IN/SEC)
    1, E12.5,2X,E12.5/)
30 FORMAT(/// 40X 14H MATERIAL DATA ,///)
31 FORMAT(/// 40X 21H OPERATING CONDITIONS ,///)
32 FORMAT(/// 15H LUBRICANT DATA ,/// )
21 FORMAT(55H INLET TEMPERATURE OF THE LUBRICANT,(DEG. F)
    1, E12.5/)
22 FORMAT(55H INLET VISCOSITY,(LB-SEC/IN**2)
    1, E12.5/)
23 FORMAT(55H PRESSURE-VISCOITY COEF.,(IN**2/LB)
    1, E12.5/)
24 FORMAT(55H TEMPERATURE-VISCOSITY COEF.,(DEG. R)
    1, E12.5/)
25 FORMAT(55H PRESSURE-TEMPERATURE-VISCOSITY COEF.(IN**2-DEG.R/LB)
    1, E12.5/)
26 FORMAT(55H THERMAL CONDUCTIVITY OF LUB.,(B/DEG.F-HR-FT)
    1, E12.5/)
27 FORMAT(55H SPECIFIC HEAT OF LUB.,(B/LB-DEG.F)
    1, E12.5/)
28 FORMAT(55H DENSITY OF LUB.,(LB/IN**3)
    1, E12.5/)
35 FORMAT(/// 40X 22H CALCULATED PARAMETERS /// )
36 FORMAT (/// 40X 18H CONTACT DIMENSION ///)
37 FORMAT(35H HALF HERTZ WIDTH(ROLLING DIR.),IN. 9X E12.5,8X
    1 38H HALF HERTZ WIDTH(PERP. TO ROLLING),IN. 2X E12.5)
38 FORMAT(4H A/B 40X E12.5 ,8X 1HM 39X E12.5/)
39 FORMAT( /// 40X 37H LOAD,SPEED,AND LUBRICANT PARAMETERS ///)
40 FORMAT(33H EQUIV. LINE CONTACT LOAD(LB/IN) 11X E12.5 ,8X 4HWBAR
    136X E12.5 /)

```

```

41 FORMAT(20H HERTZ PRESSURE(PSI) 24X E12.5,8X 6MPHZ/ED 34X E12.5/)
42 FORMAT(5H UBAR 39X E12.5 /)
43 FORMAT(3H GG 41X E12.5, 8X 3HAFA 37X E12.5/)
44 FORMAT(4H BTA 40X E12.5, 8X 3HGMA 37X E12.5/)
45 FORMAT(/// 40X 20H THERMAL PARAMETERS ///)
46 FORMAT( 3H QM 41X E12.5, 8X 4HCONV 36X E12.5/)
47 FORMAT( 3H D1 41X E12.5, 8X 2HD2 38X E12.5/)
48 FORMAT(25H THERMAL REDUCTION FACTOR 19X E12.5, 8X 19HSLIDE LEAKAGE
1FACTOR 21X E12.5/)
49 FORMAT(/// 40X 18H REDUCTION FACTORS ///)
50 FORMAT(21H ISOTH. MIN. FILM(IN) 23X E12.5,8X 13HMIN. FILM(IN)
127X E12.5 /)
51 FORMAT(/// 40X 36H DIMENSIONLESS PROTRUSION PARAMETERS /// )
52 FORMAT(17H PROTRUSION WIDTH 27X E12.5, 8X 16HPROTRUSION DEPTH
124X E12.5/)
53 FORMAT(27H PERCENTAGE OF AREA CONTACT 17X E12.5,8X 14HSPECIFIC
1FILM 26X E12.5 /)
54 FORMAT(17H FRICTIONAL COEF. 27X E12.5/)
55 FORMAT(16H  $B=2.0*WW/EP/SHM$  28X E12.5, 8X 36HSLIDE TO ROLL RATI
10= $2(U2-U1)/(U2+U1)$  4X E12.5)
56 FORMAT(31H  $AM=6.*VIS*(U1+U2)*EP*RX/WW**2$  13X E12.5)
57 FORMAT(55H LINE CONTACT LOAD,(LB/IN )
1,E12.5/)
60 FORMAT(35H HALF HERTZ WIDTH(ROLLING DIR.),IN. 9X E12.5)
604 FORMAT(/// 41H THE PROTRUSION WIDTH IS GREATER THAN 0.5 / 58H PR
1ESSURE,TEMPERATURE,AND STRESS CALCULATIONS ARE BYPASSED )
END
SUBROUTINE TEMPT(RDU)
C START
DIMENSION AD(2),ADC(2),SUMT(2),TT(2),AF(2,50),FD(2,50),PP(50),
1 DC(2)
COMMON KI,KC,KG,KA,KU,KD,KB,KE,KF,KR,NR,NW
COMMON RX1,RX2,RY1,RY2,RMS1,RMS2,E1,E2,V1,V2
COMMON CONS1,CONS2,CPS1,CPS2,RHOS1,RHOS2,WT,TEMI,U2,U1
COMMON VIS,ALF,BET,GAM,CONF,CPF,RHOF,PS,PSTAR
COMMON AFA,BTA,GMA,A,B,AM,SLIP, RXP, RYP,EP,QM,CONV,D(2),COMP,AHZ,
1PHZ,UBAR,UBAR,PHZE,GG,EDOW,BOA ,WW
COMMON FCOE,EBAR,FEET,FEES,HMIN,SPFILM,ABAR,SHM
COMMON EPST,EPSRD,DTF,TWF1,ITRDU,ITT,NRITE
COMMON XH(50),HE(50),P(50),T(50),TI(2,50),F(2,50),SHS(50)
FUNA(X,Y)=AFA*X+(BTA+GMA*X)*(1./Y-1.)
FUNB(X,U,Z)=(U*(0.33333*U+0.5*COMP*X)+Z/6.0)
FUNC(X,U,Z)=U*(3.0*(U+COMP*X)+Z)
FUND(X,Y,Z)=RDU*AFA*(X-Z)+(BTA+RDU*GMA*(X-Z))*(1./Y-1.)
RDU=RDUT
WRITE(NW,802)
PSTB=PSTAR*AHZ/WW
U1BAR=U1/(U1+U2)
SLP=(SLIP/(2.0-SLIP))
SLPQ=SLP*SLP
IF(QM-0.5 )775,775,776
775 XINI=-SQRT(3.0/B+1.0)
TINI=1.0
G3=FUNB(P(KI),0.75,SLPQ)
DELTT=EXP(FUNA(P(KI),1.0))*G3*QM
GO TO 777
776 CALL THILT(QM,BTA,CONV,B,U1BAR,XINI,TINI,NRITE)
IF(TINI.EQ.(1.)) GO TO 775
DELTT=TINI-1.0

```



```

777 DO 4 K=KI,KF
    T(K)=1.0
    TI(1,K)=1.0
    4 TI(2,K)=1.0
    DO 755 K=1,KA
    TEMP=XINI-XH(K)
    IF(TEMP)750,755,755
750 KT=K
    TEMP=DELTT / (4.0+XH(KT))
    T(K)=TINI
    T(K+1)=TINI+(XH(KT+1)-XH(KT))*TEMP
    T(K+2)=TINI+(XH(KT+2)-XH(KT))*TEMP
    T(K+3)=TINI+(XH(KT+3)-XH(KT))*TEMP
    GO TO 401
755 CONTINUE
401 FABBA=AM*B*B/SQRTF(A)
500 NKF =KF
    F1 =B/A**0.25
    F11=SQRTF((2.0-SLIP)/(1.0-SLIP))
    F12=SQRTF(2.0-SLIP)
    AD(1)=D(1)*F1
    AD(2)=D(2)*F1
    CABB=CONV*SQRTF(A)/B/B
    FF=EXP(FUNA(P(KT),T(KT)))
    FH=1.0-1.0/HE(KT)
    F10 =FUNC(P(KT),FH,SLPQ)
    F(1,KT)=AD(1)*(F10-2.0*SLIP*FH)*FF/HE(KT)*QM
    F(2,KT)=AD(2)*(F10+2.0*SLIP*FH)*FF/HE(KT)*QM
    KKT=KT+1
    IF(NRITE)88,87,88
87 WRITE(NW,2)
88 CONTINUE
    ITRDU=1
    RDU=RDUT*0.95
    6 DO 40 K=KKT,NKF
    H1=HE(K)
    321 KKK =K-KT+1
C CHECK KKK LESS OR GREATER THAN 3
    IF (KKK-3) 10,10,25
    10 GO TO (11,11,20),KKK
    11 SUMT(1)=T(KI)
    SUMT(2)=T(KI)
    15 IT =1
    FH=1.0-1.0/H1
    G3=FUNB(P(K),FH,SLPQ)
    12 IF (P(K)-PSTB)650,650,651
650 F5=FUNA(P(K),T(K))
    GO TO 652
651 F5=FUND(P(K),T(K),PSTB)+AFA*PSTB
652 IF (ABS(F5)-70.0)70,70,71
    71 NERR=1
    WRITE(NW,72)K,F5
    GO TO 40
    70 FF=EXP(F5)
    G5=FF*G3
    FDET=(T(K)-T(K-1))/(XH(K)-XH(K-1))
    FCDET=CABB*H1*FDET/6.0
    F20=CABB*FDET
    F23=(FH*3.0*(FH+COMP*P(K))+SLPQ)*FF
    F31=F23-2.0*FF*SLP*FH

```

```

F32=F23+2.0*FF*SLP*FH
F(1,K)=AD(1)*(TI(2,K)-TI(1,K)+F31*QM-F20)/H1
F(2,K)=AD(2)*(TI(1,K)-TI(2,K)+F32*QM-F20)/H1
DO 50 J=1,2
50 TT(J)=SUMT(J)+SQRTF(XH(K)-XH(K-1))*(1.3333333*F(J,K)+
1 0.66666666*F(J,K-1))
F7=((-TT(1)+TT(2))*0.5+(QM *G5-FCDET))/T(K)
IF(F7)760,760,190
760 T(K)=(T(K)-1.0)*0.95+1.0
TM2=T(K)
GO TO 763
190 FC2=LOGF(F7)
IF (IT-1) 200,200,205
200 DT=DTF*(T(K)-T(K-1))
TM1 =T(K)
T(K)=T(K)+DT
GO TO 220
205 DFC=(FC2-FC1)/(TM2-TM1)
DTK=FC2/DFC*TWF1
TM1 =T(K)
T(K)=T(K)-DTK
IF (ABSF(DTK)-EPST) 210,210,215
215 IF (IT-ITT) 220,220,85
220 FC1=FC2
TM2=T(K)
TI(1,K)=TT(1)
TI(2,K)=TT(2)
763 IF(NRITE)766,764,766
764 IF(ITRDU-1)766,765,766
765 WRITE(NW,94) FH,FCDET,F(2,K),F(1,K),G5,F7
WRITE(NW,3)XH(K),T(K),IT,TI(1,K),TI(2,K),FC2
766 IF(IT-ITT)770,770,85
770 IT =IT+1
GO TO 12
210 IF(NRITE ) 81,80,81
80 WRITE(NW,3) XH(K),T(K),IT,TI(1,K),TI(2,K)
81 GO TO 40
85 WRITE(NW,86)
NERR=1
GO TO 100
20 F1 =SQRTF(XH(K)-XH(K-1))
F2 =SQRTF(XH(K)-XH(K-2))
DO 21 M=1,2
21 SUMT(M)=T(KI)+0.5*(F(M,K-1) /F1+F(M,K-2) /F2)*
1(XH(K-1)-XH(K-2))
KEO=2
GO TO 15
25 GO TO (35,30),KEO
30 KKF=K-3
KEO=1
GO TO 33
35 KKF=K-4
KEO=2
33 KK=K-1
DO 31 M=1,2
DO 31 J=KI,KK
31 FD(M,J)=F (M,J)/SQRTF(XH(K)-XH(J))
DO 32 M=1,2
SUMT(M)=T(KI)
DO 32 J=KI,KKF,2

```

```

32 SUMT(M)=SUMT(M)+(FD(M,J)          +4.0*FD(M,J+1)          7*FD(M,J+2)
1      )*(XH(J+1)-XH(J)) /3.0
    GO TO (60,150),KE0
150 DO 61 M=1,2
61 SUMT(M)=SUMT(M)+0.5*(FD(M,K-1)          +FD(M,K-2)          )*(XH(
1 K-1)-XH(K-2))
60 T(K)=(T(K-1)-T(K-2))/(XH(K-1)-XH(K-2))*(XH(K)-XH(K-1))+T(K-1)
    DO 160 M=1,2
160 TI(M,K)=TI(M,K-1)
    GO TO 15
40 CONTINUE
    F3=(VIS*(U2+U1)/SHM)/(WW/AHZ)*SLP
    DO 720 K=KI,KF
    IF(P(K)-PSTB) 710,710,711
710 F6=EXP(FUNA(P(K),T(K)))
    GO TO 712
711 F6=EXP(AFA*PSTB+FUND(P(K),T(K),PSTB))
712 SHS(K)=F6/HE(K)*F3
720 CONTINUE
    FRC=0.0
    KKF=KF-2
    DO 725 K=KI,KKF,2
725 FRC=FRC+(SHS(K)+4.*SHS(K+1)+SHS(K+2))*(XH(K+1)-XH(K))/3.0
    FRC2=FRC-FCOE
    IF(ITRDU-1)660,660,661
660 RDU1=RDU
    RDU=RDUT*1.05
    GO TO 730
661 DFRC=(FRC2-FRC1)/(RDU2-RDU1)
    IF(ABSF(FRC2)-EPSKD)100,100,726
726 DRDU=FRC2/DFRC
    RDU1=RDU
    RDU=RDU-DRDU
    IF(ITRDU-ITT)730,730,740
730 FRC1=FRC2
    RDU2=RDU
    ERFR=FRC2
    WRITE(NW,95) ITRDU,RDU,ERFR
    ITRDU=ITRDU+1
    GO TO 6
740 WRITE(NW,96)
    GO TO 100
100 CONTINUE
600 CONTINUE
    WRITE(NW,801)
    DO 800 K=KI,KF
800 WRITE(NW,94) XH(K),P(K),T(K),TI(1,K),TI(2,K),SHS(K)
    RETURN
1 FORMAT (1H0,6E12.5)
2 FORMAT (53H      XH      T      IT      TI      T2      )
3 FORMAT (1H ,F12.7,E12.5,I4,3E12.5)
8 FORMAT (6F 12.7)
72 FORMAT (20H EXP ARG TOO BIG      ,I4,E12.5)
86 FORMAT(20H DIVERGE TEMP      )
90 FORMAT(F12.7,I4)
93 FORMAT (1H ,I7I4)
94 FORMAT (1H ,6F12.7)
95 FORMAT(/7H ITRDU=, 15,6X,5HRDU= ,E12.5,6X, 5HERFR=,E12.5/)
96 FORMAT(20H DIVERGE RDU      )
801 FORMAT(7X 4HXBAR 6X 8HPRESSURE 5X 6HT MEAN 8X 2HT1 10X 2HT2 4X 11H

```

```

1 SHEAR FORCE)
802 FORMAT(///)
END
SUBROUTINE THILT(QM,BETA,QC,B      ,U1,XX,TT,NWRITE)
DIMENSION TC(200),X(200),VT(9),VIST(9),VSQ(9),H(200)
F1(ARG)=-ARG*SQRT(ARG**2-1.)-ALOG(-ARG*SQRT(ARG**2-1.))
SP=1.-2.*U1
DX=0.05
HST=6.
TI=1.
HSP=1./(1.-(1.+2.*SQRT(U1-U1**2))/3.)
XS=-SQRT((HSP-1.)/B+1.0)
IF(XS.GE.(-1.)) XS=-1.-0.001
11 XS=XS-((HSP-1.)/B-F1(XS))/(2.*SQRT(XS**2-1.))
IF(XS.GE.(-1.)) XS=-1.-0.001
HP=1.+B*F1(XS)
IF (ABS(HP-HSP).GT.(0.1)) GO TO 11
XS=AINT(XS*10.)/10.
XSP=XS+0.1
IF(XSP.GE.(-1.)) XSP=-1.05
X0=-SQRT((HST-1.)/B+1.0)
IF(X0.GE.(-1.)) X0=-1.-0.001
10 X0=X0-((HST-1.)/B-F1(X0))/(2.*SQRT(X0**2-1.))
IF(X0.GE.(-1.)) X0=-1.-0.001
HS=1.+B*F1(X0)
IF (ABS(HS-HST).GT.(0.1)) GO TO 10
X0=AINT(X0*10.)/10.
H(1)=1.+B*F1(X0)
IF(NWRITE.EQ.1) GO TO 90
WRITE(6,80) X0,H(1)
90 IF(X0.GE.(-1.1)) GO TO 65
TC(1)=TI
X(1)=X0
M=0
N=0
K=0
J=1
20 IF(X(J).GE.(-1.)) X(J)=-1.-0.00001
H(J)=1.+B*F1(X(J))
PH=1.-1/H(J)
A1=-2.*PH/5.+SP/3.+2.*U1/3.
A2=-PH/10.+SP/6.+U1/3.
IF(M.EQ.1) GO TO 40
IF(K.EQ.1) GO TO 60
AA=(TC(J)*A1+A2)*H(J)
22 AAS=AA
25 Y=0.
SUM=0.
DO 30 K=1,9
VT(K)=1./(-4.*(TC(J)-1.)*(Y**2)+4.*(TC(J)-1.)*Y+1.)-1.
VIST(K)=EXP(BETA*VT(K))
VSQ(K)=36.*(PH*Y)**2+12.*PH*Y*(SP-3.*PH)+(SP-3.*PH)**2
SUM=SUM+VIST(K)*VSQ(K)
30 Y=Y+0.125
TGL=(SUM-VIST(1)*VSQ(1)/2.-VIST(9)*VSQ(9)/2.)*0.125
B1=B**2*QM/QC*TGL/H(J)/2.
B2=2.*B**2/QC*(TC(J)-1.)/H(J)
IF(N.EQ.1) GO TO 50
AA=(B1-B2)*DX/2.+AA
X(J)=X(J)+DX/2.
M=1
GO TO 20

```

```

40 TC(J)=(AA/H(J)-A2)/A1
   M=0
   N=1
   GO TO 25
50 N=N+1
   AA=(B1-B2)*DX+AAS
   L=J
   J=J+1
   X(J)=X(L)+DX/2.
   K=1
   GO TO 20
60 K=0
   TC(J)=(AA/H(J)-A2)/A1
   IF(X(J).LT.XSP) GO TO 22
   XX=X(J)
   TT=TC(J)
   GO TO 70
65 XX=-1.
   TT=1.
70 CONTINUE
   IF(NRITE.EQ.1) GO TO 95
   WRITE(6,80) XX,TT
80 FORMAT(4E14.4)
95 CONTINUE
   RETURN
   END
SUBROUTINE FRIC
  DIMENSION AG1(13),AG2(7),AG3(7),FTN(13,7,7),UZ(7,7),VZ(7)
  COMMON KI,KC,KG,KA,KO,KD,KB,KE,KF,KH,NR,NW
  COMMON RX1,RX2,RY1,RY2,RMS1,RMS2,E1,E2,V1,V2
  COMMON CONS1,CONS2,CPS1,CPS2,RHOS1,RHOS2,WT,TEMI,U2,U1
  COMMON VIS,ALF,BET,GAM,CONF,CPF,RHOF,PS,PSTAR
  COMMON AFA,BTA,GMA,A,B,AM,SLIP, RXP, RYP, EP, QM, CONV, D(2), COMP, AHZ,
  1PHZ, WBAR, UBAR, PHZE, GG, EDOW, BOA, WW
  COMMON FCOE,EBAR,FEET,FEES,HMIN,SPFILM,ABAR,SHM
  COMMON EPST,EPSRD,DTF,TWF1,ITRDU,ITT,NRITE
  COMMON XH(50),HE(50),P(50),T(50),TI(2,50),F(2,50),SHS(50)
  COMMON XSTT,XDEX,YSTT,YDEY,XST(31),Y(31),JJFS,KKFS,NTHE,NOPL
  DATA(FTN(I),I=1,13)/0.00025,0.0007, 0.0014,0.0023,0.0067,
  1 0.0135, 0.021, 0.037, 0.046, 0.052, 0.0615, 0.0685, 0.0775/
  DATA(FTN(I),I=14,26) /0.0007, 0.002, 0.0039, 0.0065, 0.0150,
  1 0.022, 0.029, 0.042, 0.0495, 0.054, 0.0625, 0.069, 0.0775/
  DATA(FTN(I),I=27,39)/ 0.0026, 0.0078, 0.014, 0.018, 0.028,
  1 0.034, 0.0385, 0.0485, 0.054, 0.058, 0.064, 0.0695, 0.0775/
  DATA(FTN(I),I=40,52) / 0.0077, 0.017,0.023, 0.027, 0.035,
  1 0.04, 0.044, 0.051, 0.0565, 0.0605, 0.066, 0.071, 0.0775/
  DATA(FTN(I),I=53,65)/0.019, 0.0285, 0.034, 0.037, 0.044, 0.048,
  1 0.05, 0.056, 0.06, 0.0635, 0.069, 0.0725, 0.0775/
  DATA(FTN(I),I=66,78) / 0.0215, 0.032, 0.037, 0.0415, 0.0475,
  1 0.051, 0.054, 0.06, 0.0635, 0.066, 0.07, 0.073, 0.0775/
  DATA(FTN(I),I=79,91) / 0.0245,0.034, 0.04, 0.0435, 0.05,
  1 0.054, 0.0565, 0.062, 0.0655, 0.0675, 0.071, 0.074, 0.0775/
  DATA(FTN(I),I=92,104)/0.0002,0.0006, 0.0012, 0.002, 0.006, 0.012,
  1 0.019, 0.036, 0.047, 0.054, 0.0645, 0.072, 0.077/
  DATA(FTN(I),I=105,117)/0.0006,0.002, 0.004, 0.0065, 0.015, 0.024,
  1 0.028, 0.043, 0.052, 0.0575, 0.0665, 0.072, 0.077/
  DATA(FTN(I),I=118,130)/ 0.0027, 0.0081, 0.014, 0.019, 0.0285,
  10.035, 0.0395, 0.051, 0.057, 0.061, 0.068, 0.0725, 0.077/
  DATA(FTN(I),I=131,143)/0.0066, 0.015, 0.021, 0.025, 0.034, 0.04,
  1 0.0445, 0.054, 0.06, 0.064, 0.069, 0.073, 0.077/

```

DATA(FTN(I),I=144,156)/ 0.012, 0.0225, 0.029, 0.0345, 0.043,  
 1 0.048, 0.052, 0.059, 0.063, 0.066, 0.070, 0.073, 0.077/  
 DATA(FTN(I),I=157,169)/ 0.019, 0.032, 0.039, 0.0415, 0.05, 0.054,  
 1 0.056, 0.061, 0.064, 0.067, 0.0715, 0.075, 0.077/  
 DATA(FTN(I),I=170,182)/ 0.021, 0.0335, 0.041, 0.0455, 0.053,  
 1 0.056, 0.059, 0.064, 0.068, 0.07, 0.073, 0.076, 0.077/  
 DATA(FTN(I),I=183,195)/.00016,.00055,0.0011,0.0019, 0.0058,0.011,  
 1 0.018, 0.033, 0.042, 0.048, 0.06, 0.068, 0.075/  
 DATA(FTN(I),I=196,208)/.0007,.0021, 0.0043, 0.007, 0.015, 0.023,  
 1 0.027, 0.039, 0.046, 0.052, 0.062, 0.07, 0.075/  
 DATA(FTN(I),I=209,221)/ 0.0018, 0.0053, 0.01, 0.015, 0.0255,  
 1 0.034, 0.037, 0.048, 0.054, 0.058, 0.066, 0.073, 0.075/  
 DATA(FTN(I),I=222,234)/ 0.0046, 0.011, 0.018, 0.024, 0.037,  
 U 0.039, 0.044, 0.0525, 0.057, 0.061, 0.068, 0.074, 0.075/  
 DATA(FTN(I),I=235,247)/ 0.0082, 0.017, 0.025, 0.03, 0.042,  
 10.048, 0.052, 0.06, 0.064, 0.066, 0.070, 0.074, 0.075/  
 DATA(FTN(I),I=248,260)/ 0.015, 0.026, 0.034, 0.04, 0.049,  
 1 0.054, 0.058, 0.063, 0.067, 0.069, 0.073, 0.075, 0.075/  
 DATA(FTN(I),I=261,273)/ 0.018, 0.028, 0.036, 0.043, 0.052,  
 1 0.057, 0.06, 0.065, 0.068, 0.07, 0.074, 0.075, 0.075/  
 DATA(FTN(I),I=274,286)/.00015,.00046,.001, 0.0017, 0.005, 0.01,  
 1 0.016, 0.034, 0.04, 0.046, 0.059, 0.067, 0.073/  
 DATA(FTN(I),I=287,299)/0.00064,0.002, 0.0039, 0.0064, 0.015,  
 1 0.021, 0.026, 0.039, 0.046, 0.052, 0.062, 0.068, 0.073/  
 DATA(FTN(I),I=300,312)/ 0.0017, 0.0048, 0.009, 0.014, 0.025,  
 1 0.031, 0.036, 0.047, 0.053, 0.057, 0.065, 0.0695, 0.073/  
 DATA(FTN(I),I=313,325)/ 0.043, 0.01, 0.017, 0.023, 0.033,  
 1 .039, 0.043, 0.052, 0.058, 0.061, 0.066, 0.07, 0.073/  
 DATA(FTN(I),I=326,338)/ 0.0078, 0.016, 0.024, 0.029, 0.04,  
 1 0.046, 0.051, 0.057, 0.062, 0.064, 0.068, 0.071, 0.073/  
 DATA(FTN(I),I=339,351)/ 0.0145, 0.024, 0.033, 0.039, 0.048,  
 1 0.053, 0.056, 0.062, 0.066, 0.067, 0.07, 0.072, 0.073/  
 DATA(FTN(I),I=352,364)/ 0.016, 0.027, 0.0355, 0.041, 0.052,  
 1 0.056, 0.059, 0.064, 0.067, 0.068, 0.071, 0.073, 0.073/  
 DATA(FTN(I),I=365,377)/.0001,.00027,.00055,0.0009,0.0029,  
 1 0.0059, 0.01, 0.025, 0.036, 0.043, 0.054, 0.062, 0.068/  
 DATA(FTN(I),I=378,390)/.00044,.0013,0.0026, 0.0044, 0.012,  
 1 0.018, 0.024, 0.036, 0.044, 0.048, 0.057, 0.063, 0.068/  
 DATA(FTN(I),I=391,403)/0.001, 0.0029, 0.0056, 0.009, 0.0185,  
 1 0.0255, 0.03, 0.042, 0.0485, 0.053, 0.06, 0.064, 0.068/  
 DATA(FTN(I),I=404,416)/0.0015, 0.0045, 0.0085, 0.013, 0.024,  
 1 0.032, 0.036, 0.047, 0.053, 0.057, 0.063, 0.065, 0.068/  
 DATA(FTN(I),I=417,429)/0.0038, 0.0093, 0.0155, 0.021, 0.032,  
 1 0.038, 0.042, 0.052, 0.056, 0.06, 0.064, 0.066, 0.068/  
 DATA(FTN(I),I=430,442)/0.0088, 0.017, 0.0245, 0.03, 0.04,  
 1 0.0465, 0.051, 0.058, 0.061, 0.063, 0.066, 0.067, 0.068/  
 DATA(FTN(I),I=443,455)/0.012, 0.022, 0.0295, 0.035, 0.0455,  
 1 0.051, 0.055, 0.061, 0.063, 0.065, 0.067, 0.068, 0.068/  
 DATA(FTN(I),I=456,468)/.00005,.00014,.00027,.00045,.0014,  
 1 0.0027, 0.0046, 0.013, 0.023, 0.029, 0.042, 0.052, 0.055/  
 DATA(FTN(I),I=469,481)/.00012,.00042,.00085,.0014,.0044,  
 1 0.0084, 0.013, 0.0245, 0.032, 0.037, 0.0455, 0.053, 0.055/  
 DATA(FTN(I),I=482,494)/.0004,.0012, 0.0024, 0.004, 0.011,  
 1 0.017, 0.023, 0.0345, 0.039, 0.0425, 0.048, 0.0535, 0.055/  
 DATA(FTN(I),I=495,507)/0.0015, 0.0042, 0.008, 0.012, 0.023,  
 1 0.029, 0.033, 0.0395, 0.043, 0.045, 0.050, 0.0535, 0.055/  
 DATA(FTN(I),I=508,520)/0.0034, 0.0084, 0.014, 0.0195, 0.03,  
 1 0.036, 0.04, 0.046, 0.048, 0.049, 0.051, 0.054, 0.055/  
 DATA(FTN(I),I=521,523)/0.0056, 0.013, 0.02, 0.026, 0.0375,  
 1 0.042, 0.045, 0.049, 0.05, 0.052, 0.0525, 0.054, 0.055/

```

DATA(FTN(I),I=534,546)/0.0071, 0.015, 0.023, 0.03, 0.04,
1 0.045, 0.048, 0.051, 0.052, 0.053, 0.054, 0.055, 0.055/
DATA(FTN(I),I=547,559)/.00003,.00009,.00018,.0003,.0009,
1 0.0019, 0.003, 0.009, 0.016, 0.023, 0.037, 0.045, 0.051/
DATA(FTN(I),I=560,572)/.0001,.00026,.00058,.0009,.0029,
1 0.0057, 0.0092, 0.021, 0.029, 0.034, 0.041, 0.047, 0.051/
DATA(FTN(I),I=573,585)/.00025,.00074,0.0015, 0.0024, 0.0072,
1 0.013, 0.018, 0.028, 0.035, 0.039, 0.045, 0.048, 0.051/
DATA(FTN(I),I=586,598)/0.00054, 0.0016, 0.0033, 0.0052, 0.014,
1 0.022, 0.0265, 0.035, 0.04, 0.042, 0.0465, 0.049, 0.051/
DATA(FTN(I),I=599,611)/0.0013, 0.0036, 0.0069, 0.011, 0.023,
1 0.029, 0.0325, 0.0395, 0.044, 0.046, 0.0485, 0.050, 0.051/
DATA(FTN(I),I=612,624)/0.0015, 0.041, 0.008, 0.012, 0.0235,
1 0.0295, 0.033, 0.04, 0.044, 0.0465, 0.049, 0.0505, 0.051/
DATA(FTN(I),I=625,637)/0.0018, 0.0052, 0.0094, 0.014, 0.0255,
1 0.031, 0.035, 0.042, 0.045, 0.047, 0.05, 0.051, 0.051/
DATA(AG1(I),I=1,13)/1.E-8, 3.E-8, 6.E-8, 1.E-7, 3.E-7, 6.E-7,
1 1.E-6, 3.E-6, 6.E-6, 1.E-5, 3.E-5, 1.E-4, 1.E-3/
DATA(AG2(I),I=1,7)/5.E-7, 1.E-6, 5.E-6, 1.E-5, 5.E-5, 5.E-4, 1.E-3
1 /
DATA(AG3(I),I=1,7)/13.32, 15.2, 17.8, 19., 21.19, 27.13, 100./
20 FORMAT(///)
WRITE(NW,20)
TEMP=TEMI/546.-1.
VIS3=VIS*EXP(BTA*TEMP)
THETA=(TEMI-460.-32.)/1.8
ALF3=ALF+GAM*TEMP/TEMI
QM3=QM/VIS*VIS3*TEMI/546.
FEET=FEET
FEEST=FEES
QMT=QM
QM=QM3
BTAT=BTA
BTA=BTA*TEMI/546.
AFAT=AFA
AFA=AFA/ALF*ALF3
CALL FTFS(FEET,FEES)
IF(NRITE.NE.0) GO TO 301
WRITE(NW,300) SHM,ALF3,FEET,FEET,FEES,VIS3,QM3
300 FORMAT(8E12.4)
301 SHM3=SHM*(VIS3/VIS)**0.7*(ALF3 /ALF)**0.6/FEET*FEET
G1=VIS3*(U2-U1)/PHZ/SHM3
G2= VIS3*(U2-U1)**2*BET/(546.*TEMI)/(8.*CONF*778./3600.)
G3=ALF3*PHZ
QM=QMT
FEES=FEEST
FEET=FEET
BTA=BTAT
AFA=AFAT
IF(NRITE) 50,50,51
50 WRITE(NW,1) G1, G2, G3, VIS3
1 FORMAT (4H G1=,E12.5, 4H G2=,E12.5,4H G3=,E12.5,6H VIS3=,E12.5)
51 IF(G1.EQ.0.) GO TO 245
IF(G2.EQ.0.) GO TO 245
DO 100 I=1,7
DO 100 J=1,7
IF(G1-AG1(13)) 40,60,60
40 IF(G1.LT.AG1(1)) GO TO 70
CALL TLUG(G1,UZ(I,J),AG1,FTN(1,I,J),13)
GO TO 100

```

```

60 UZ(1,J)=FTN(13,I,J)
   GO TO 100
70 UZ(1,J)=EXP(ALOG(FTN(1,I,J))+(ALOG(FTN(2,I,J))-ALOG(FTN(1,I,J)))/(
  1ALOG(AG1(2))-ALOG(AG1(1)))*(ALOG(G1)-ALOG(AG1(1))))
100 CONTINUE
   DO 200 K=1,7
   IF(G3-AG3(7)) 140,160,160
140 IF(G3.LT.AG3(1)) GO TO 170
   CALL TLU(G3,VZ(K),AG3,UZ(1,K),7)
   GO TO 200
160 VZ(K)=UZ(7,K)
   GO TO 200
170 VZ(K)=UZ(1,K)-(UZ(2,K)-UZ(1,K))/(AG3(2)-AG3(1))*(AG3(1)-G3)
   IF (VZ(K).LE.0.0) VZ(K)=1.E-5
200 CONTINUE
   IF(G2-AG2(7)) 204,206,206
204 IF(G2.LT.AG2(1)) GO TO 207
   CALL TLUG(G2,FR3,AG2,VZ,7)
   GO TO 210
206 FR3=EXP(ALOG(VZ(6))+(ALOG(VZ(7))-ALOG(VZ(6)))/(ALOG(AG2(7))-ALOG(A
  1G2(6)))*(ALOG(G2)-ALOG(AG2(6))))
   GO TO 210
207 FR3=EXP(ALOG(VZ(2))+(ALOG(VZ(1))-ALOG(VZ(2)))/(ALOG(AG2(1))-ALOG(A
  1G2(2)))*(ALOG(G2)-ALOG(AG2(2))))
210 IF(NWRITE) 205,205,240
205 WRITE(NW,2) FR3
   2 FORMAT(5H FR3=.E12.5)
   5 FORMAT(7F9.4)
   WRITE(NW,5) UZ
   WRITE(NW,5) VZ
240 FCOE=ALOG(FR3)-0.149*(ALOG(THETA)-ALOG(30.))
   FCOE=EXP(FCOE)
   GO TO 250
245 FCOE=0.
250 CONTINUE
   RETURN
   END

```

```

SUBROUTINE TLU(A,B,C,D,N)
C      LINEAR INTERPOLATION ROUTINE
C      A= INDEPENDENT VARIABLE
C      B= DEPENDENT VARIABLE (ANSWER)
C      C= INDEPENDENT TABLE
C      D= DEPENDENT TABLE
C      N= NUMBER OF POINTS IN TABLE
C      INDEPENDENT TABLE MUST BE SORTED, EITHER ASCENDING OR DESCENDING
C      DIMENSION C(1),D(1)
      IF(N-1)1,2,3
1      B=0.
      GO TO 100
2      B=D(1)
      GO TO 100
3      ML=1
      MU=N
      8 IF(MU-ML-1)15,15,9
      9 M=(MU+ML)/2
      IF(C(1)-C(2))11,2,10
10 IF(C(M)-A)13,12,14
11 IF(A-C(M))13,12,14
12 B=D(M)
      GO TO 100
13 MU=M
      GO TO 8

```



```

14 ML=M
GO TO 8
15 B=D(ML)+(D(MU)-D(ML))*((A-C(ML))/(C(MU)-C(ML)))
100 RETURN
END
SUBROUTINE TLUG(A,B,C,D,N)
C      LOGRITHMIC INTERPOLATION
C      A= INDEPENDENT VARIABLE
C      B= DEPENDENT VARIABLE (ANSWER)
C      C= INDEPENDENT TABLE
C      D= DEPENDENT TABLE
C      N= NUMBER OF POINTS IN TABLE
C      INDEPENT TABLE MUST BE SORTED, EITHER ASCENDING OR DESCENDING
      DIMENSION C(1),D(1)
      IF(N-1)1,2,3
1  B=0.
GO TO 100
2  B=D(1)
GO TO 100
3  ML=1
MU=N
8  IF(MU-ML-1) 15,15,9
9  M=(MU+ML)/2
IF(C(1)-C(2))11,2,10
10 IF(C(M)-A)13,12,14
11 IF(A-C(M))13,12,14
12 B=D(M)
GO TO 100
13 MU=M
GO TO 8
14 ML=M
GO TO 8
15 B=EXP(ALOG(D(ML))+(ALOG(D(MU))-ALOG(D(ML)))*((ALOG(A)-ALOG(C(ML)))/
1  /((ALOG(C(MU))-ALOG(C(ML))))))
100 RETURN
END
SUBROUTINE PRESS
COMMON KI,KC,KG,KA,KO,KD,KB,KE,KF,KR,NR,NW
COMMON RX1,RX2,RY1,RY2,RMS1,RMS2,E1,E2,V1,V2
COMMON CONS1,CONS2,CPS1,CPS2,RHOS1,RHOS2,WT,TEMI,U2,U1
COMMON VIS,ALF,BET,GAM,CONF,CPF,RHOF,PS,PSTAR
COMMON AFA,BTA,GMA,A,B,AM,SLIP, RXP,RYP,EP,QM,CONV,D(2),COMP,AHZ,
1PHZ,WBAR,UBAR,PHZE,GG,EDOW,BOA ,WW
COMMON FCOE,EBAR,FEET,FEES,HMIN,SPFILM,ABAR,SHM
COMMON EPST,EPSRD,DTF,TWF1,ITRDU,ITI,NRITE
COMMON XH(50),HE(50),P(50),T(50),TI(2,50),F(2,50),SHS(50)
DIMENSION SUMA(50)
C      ESTABLISH XH(K)
      KI=1
      KC=9
      KG=15
      KA=17
      KO=29
      KD=33
      KB=37
      KF=41
      KR=41
      XH(1)=-4.0
      DX=0.5
      KKI=KI+1
      KK4=KI+4
      DO 50 K=KKI,KK4

```

```

50 XH(K)=XH(K-1)+DX
   P(KA)=5.0/AFA
   XH(KA)=-SQRT(1.0-(3.1416*P(KA)*0.5)**2)
   DX=-XH(KA)/4.0
   XH(6)=XH(5)+DX
   XH(7)=XH(6)+DX
   XH(8)=XH(7)+DX*0.5
   XH(9)=XH(8)+DX*0.5
   DO 55 K=10,13
55 XH(K)=XH(K-1)+DX*0.25
   DX=(1.0+XH(KA))*0.5
   KKA=KA-3
   DO 60 K=KKA,KA
60 XH(K)=XH(K-1)+DX
   DX=-XH(KA)/8.
   KKA=KA+1
   KA4=KA+4
   DO 65 K=KKA,KA4
65 XH(K)=XH(K-1)+DX*0.25
   XH(KA+5)=XH(KA+4)+DX*0.5
   XH(KA+6)=XH(KA+5)+DX*0.5
   KA7=KA+7
   DO 66 K=KA7,KO
66 XH(K)=XH(K-1)+DX
   DX=0.25*(1.0-2.0*EBAR)
   KKO=KO+1
   DO 70 K=KKO,KD
70 XH(K)=XH(K-1)+DX
   DX=0.25*EBAR
   KKD=KD+1
   KKKF=KF-1
   DO 75 K=KKD,KKKF
75 XH(K)=XH(K-1)+DX
   XH(KF)=0.9999999999
   IF(NRITE)77,76,77
76 WRITE(NW,2)(XH(K),K=1,KF)
C   ESTABLISH HE(K)
77 KKA=KA-1
   DEXH=XH(KA-2)-XH(KA)
   DO 80 K=1,KKA
   XHKK=XH(K)+DEXH
   TEMP=SQRT(XHKK **2-1.0)
80 HE(K)=1.0+B*(ABS(XHKK *TEMP)-ALOG(ABS(ABS(XHKK )+TEMP)))
   DO 85 K=KA,KB
85 HE(K)=1.0
   KKB=KB+1
   DO 90 K=KKB,KF
90 HE(K)=1.0-(1.0-HMIN)*SIN(3.1416*(XH(K)-XH(KB))/(1.0-XH(KB)))
   IF(NRITE)92,91,92
91 WRITE(NW,2)(HE(K),K=1,KF)
C   ESTABLISH P(K)
92 SUMA(1)=0.0
   DO 100 K=2,KA
   FK1=(HE(K-1)-1.0)/HE(K-1)**3
   FK2=(HE(K)-1.0)/HE(K)**3
100 SUMA(K)=SUMA(K-1)+(FK1+FK2)*0.5*(XH(K)-XH(K-1))
   P(1)=0.
   DO 105 K=2,K/
   P(K)=ALOG(1.0-SUMA(K)/SUMA(KA)*(1.0-EXP(-AFA*P(KA))))/AFA

```

```

105 P(K)=-P(K)
    PI2=0.63662
    KKA=KA+1
    DO 110 K=KKA,KD
110 P(K)=SQRT(1.0-XH(K)**2)*PI2
    P(KD)=PI2*SQRT(1.0-(1.0-2.0*EBAR)**2)
    PBB=PI2*SQRT(1.0-(1.0-EBAR)**2)
    KKD=KD+1
    KKB=KB+1
    W5=0.0
    DO 115 K=KKB,KF
    F1=-PBB*((1.0-XH(K-1))/EBAR)**2+PI2*SQRT(1.0-XH(K-1)**2)
    F2=-PBB*((1.0-XH(K))/EBAR)**2+PI2*SQRT(1.0-XH(K)**2)
115 W5=W5+(F1+F2)*0.5*(XH(K)-XH(K-1))
    SUM4=0.0
    SUM5=0.0
    DO 120 K=KKD,KB
    F1=((XH(K-1)-XH(KD))/EBAR)**2
    F2=((XH(K)-XH(KD))/EBAR)**2
    F3=P(KD)*(1.0-F1)-PI2*SQRT(1.0-XH(K-1)**2)
    F4=P(KD)*(1.0-F2)-PI2*SQRT(1.0-XH(K)**2)
    SUM4=SUM4+(F1+F2)*0.5*(XH(K)-XH(K-1))
120 SUM5=SUM5+(F3+F4)*0.5*(XH(K)-XH(K-1))
    W(KB)=(W5-SUM5)/SUM4
    DO 125 K=KKD,KB
125 P(K)=(P(KB)-P(KD))*((XH(K)-XH(KD))/EBAR)**2+P(KD)
    DO 126 K=KKB,KF
126 P(K)=PBB*((1.0-XH(K))/EBAR)**2
    WRITE (NW,1)
    1 FORMAT(10X 4HXBAR 6X 12HNORMALZD FILM 5X 8HPRESSURE
    DO 130 K=KI,KF
130 WRITE(NW,2)XH(K),HE(K),P(K)
    2 FORMAT(3X 6(3X E12.5))
    RETURN
    END
    SUBROUTINE STRESS
C      STRESS CALCULATION FOR EHD (MODIFIED AND COMPILED ON SCI-TEK)
C      REVISED FOR TIME DEPENDENT RESULTS, 2-14-69 ,PN452 , REEL NO.//13
C      BASED ON ORIGINAL VERSION OF 4-9-64
C      NSW DIAGNOSTIC OUTPUT CONTROL, NSW= 1 DIAGNOSTIC OUTPUT
    DIMENSION SX(31),SY(31),TXY(31),PSX(31),PSY(31),PTXY(31)
    DIMENSION AP(31),AQ(31),BP(31),BQ(31),CP(31),CQ(31)
    DIMENSION ZU2(31),ZU0(31),OS(31),PSZ(31), RTXY(50,31)
    DIMENSION IPUF(1000),XARRY(31),YARRY(31),Q(50)
    COMMON KI,KC,KG,KA,KO,KD,KB,KE,KF,KR,NR,NW
    COMMON RX1,RX2,RY1,RY2,RMS1,RMS2,E1,E2,V1,V2
    COMMON CONS1,CONS2,CPS1,CPS2,RHOS1,RHOS2,WT,TEMI,U2,U1
    COMMON VIS,ALF,BET,GAM,CONF,CPF,RHOF,PS,PSTAR
    COMMON AFA,BTA,GMA,A,B,AM,SLIP, RXP,RYP,EP,QM,CONV,D(2),COMP,AHZ,
    1PHZ,WBAR,UBAR,PHZE,GG,EDOW,BOA ,WW
    COMMON FCOE,EBAR,FEET,FEES,HMIN,SPFILM,ABAR,SHM
    COMMON EPST,EPSRD,DTF,TWF1,ITRDY,ITT,NRITE
    COMMON XH(50),HE(50),P(50),T(50),TI(2,50),F(2,50),SHS(50)
    COMMON XSTT,XDEX,YSTT,YDEY,XST(31),Y(31) ,JJFS,KKFS,NTHE,NOPL
    WRITE(6,700)
    JJF=JJFS
    KKF=KKFS
    ANU=V1
    DO 20 K=KI,KF
    20 Q(K)=SHS(K)
    NSW=2
    520 FORMAT (75H STARTING VALUE OF X INTERVAL OF X STARTING VALUE 0
    1F Y INTERVAL OF Y )

```

```

522 FORMAT (4XE12.5,7XE12.5,8XE12.5,7XE12.5)
152 ANT=NTHE-1
   DELA=3.14159265/ANT
   DEG=90./ANT
   KFP1=KKF+1
   KFP2=KFP1+1
   WRITE (6,512)
   WRITE(6,2) (XST(K),K=1,KKF)
   WRITE(6,701)
   WRITE (6,514)
   WRITE (6,2) (Y(J), J=1, JJF)
   WRITE(6,701)
   DO 300 L=1,JJF
   YJ=Y(L)
   Y2=YJ**2
   WRITE (6,8) YJ
   DO 400 J=1,KKF
   XH7=XST(J)
   UKI=XH7 -XH(KI)
   UKF=XH7 -XH(KF)
   YKI2=Y2+UKI**2
   YKF2=Y2+UKF**2
   Y2KI=Y2/YKI2
   Y2KF=Y2/YKF2
   YUKI=YJ*UKI/YKI2
   YUKF=YJ*UKF/YKF2
   SSX=P(KI)*YUKI-P(KF)*YUKF-Q(KI)*Y2KI+Q(KF)*Y2KF
   SXY=P(KI)*Y2KI-P(KF)*Y2KF+Q(KI)*YUKI-Q(KF)*YUKF
   SSY=-SSX
   GO TO (58,59),NSW
58 WRITE(6,2) SSX,SXY,SSY
59 N2=KF-2
   DO 350 I=KA,N2,2
   II=(I+1)/2
   IF(L-1) 356,355,356
355 ZU2(II)=XH7 -XH(I+2)
   ZU0(II)=XH7 -XH(I)
   HSQ=1.0/(2.0*(XH(I+1)-XH(I))**2)
   Z2=ZU2(II)
   Z0=ZU0(II)
   Z1=XH7 -XH(I+1)
   P0=P(I)
   P1=P(I+1)
   P2=P(I+2)
   GO TO (50,51),NSW
50 WRITE(6,2) Z0,Z1,Z2,P0,P1,P2,HSQ
51 NPQ=1
357 QQA=(Z2*(P0*Z1-2.0*P1*Z0)+P2*Z0*Z1)*HSQ
   QQB=-(P0*(Z1+Z2)-4.0*P1*Z1+P2*(Z0+Z1))*HSQ
   QQC=(P0-2.0*P1+P2)*HSQ
   GO TO (52,53),NSW
52 WRITE(6,2) QQA,QQB,QQC
53 GO TO (358,359), NPQ
358 AP(II)=QQA
   BP(II)=QQB
   CP(II)=QQC
   P0=Q(I)
   P1=Q(I+1)
   P2=Q(I+2)
   NPQ=2
   GO TO 357

```

0064  
0065  
0066  
0067  
0068  
0069  
0070  
0071  
0072

0075  
0076  
0077

0081  
0082  
0083

0085  
0086  
0087

0090  
0091  
0092  
0093

0096  
0097  
0098  
0099

0100  
0101  
0102  
0103  
0104

359	AQ(II)=QQA	0105
	BQ(II)=QQB	0106
	CQ(II)=QQC	0107
356	AI=AP(II)	0108
	CI=CP(II)	0109
	CY2=CI*Y2	0110
	AP3Y=AI-3.0*CY2	0111
	AP2Y=AI-2.0*CY2	0112
	APY=AI+CY2	0113
	AI=AQ(II)	0114
	CI=CQ(II)	0115
	CQY2=CI*Y2	0116
	AQ3Y=AI-3.0*CQY2	0117
	AQ2Y=AI-2.0*CQY2	0118
	AQY=AI+CQY2	0119
	Z2=ZU2(II)	0120
	Z0=ZU0(II)	0121
	FLOG=ALOG((Y2+Z2**2)/(Y2+Z0**2))	
	FTAN=ATAN(Z2/YJ)-ATAN(Z0/YJ)	
	CPI=CP(II)	0124
	CQI=CQ(II)	0125
	BPI=BP(II)	0126
	BQI=BQ(II)	0127
	UY=(Z2-Z0)*YJ	0128
	U3Y=3.0*UY	0129
	UU2=2.0*(Z2-Z0)	0130
	U2Y2=Z2**2-Z0**2	0131
	YTAN=YJ*FTAN	0132
	YLOG=YJ*FLOG	0133
	Y2LOG=YJ*YLOG	0134
	GO TO (55,56),NSW	
55	WRITE(6,2)AP3Y,AP2Y,APY,AQ3Y,AQ2Y,AQY,U3Y,UU2,U2Y2,YTAN,YLOG,Y2LOG	01
56	SSX=SSX-CPI*U3Y-AP3Y*FTAN-BPI*YLOG-(BQI*UU2+CQI*U2Y2-3.0*BQI*YTAN	0137
	1+AQ2Y*FLOG)	0138
	SXY=SXY-BPI*YTAN-CPI*Y2LOG-CQI*U3Y-AQ3Y*FTAN-BQI*YLOG	0139
350	SSY=SSY+CPI*UY-APY*FTAN-BQI*YTAN-CQI*Y2LOG	0140
	SX(J)=-SSX*0.3175	0141
	SY(J)=-SSY*0.3175	0142
	TXY(J)=-SXY*0.3175	0143
	SHEA=(0.5*(SX(J)-SY(J)))*2+TXY(J)*2	0144

```

1111 PTXY(J)=SQRT (SHEA)
      S3=(SX(J)+SY(J))*0.5
      PSX(J)=PTXY(J)+S3
      PSY(J)=S3-PTXY(J)
      PSZ(J)=(PSX(J)+PSY(J))*ANU
      OS(J)=SQRT ((PSX(J)-PSY(J)) **2+(PSX(J)-PSZ(J))**2+(PSY(J)-PSZ(J))
1**2)/3.0
      WRITE (6,10)
      WRITE(6,12) XST(J),SX(J),SY(J),TX(J),PSX(J),PSY(J),PSZ(J),PTXY(J),
10S(J)
      ANG2=0.
      DO 410 MM=1,NTHE
      SI9=SIN(ANG2)
      CO9=COS(ANG2)
      RTXY(J,MM)=0.5*(SX(J)-SY(J))*SI9+TX(J)*CO9
410 ANG2=ANG2+DELA
      WRITE(6,518)DEG
      WRITE (6,12) (RTXY(J,MM),MM=1,NTHE)
      WRITE (6,14)
400 CONTINUE
      ANGL=0.
      GO TO (300,602),NOPL
602 NKT=1
603 DO 600 I=1,KKF
      IF(NKT-1) 604,604,600
604 XARRY(I)=XST(I)
600 YARRY(I)=RTXY(I,NKT)
      XARRY(KFP1)=XSTI
      XARRY(KFP2)=XDEX
      YARRY(KFP1)=YSTI
      YARRY(KFP2)=YDEY
      IF(NKT.NE.1) GO TO 530
      CALL PLOTS(1BUF,1000,22)
      CALL PLOT(0.0,0.5,-3)
      CALL AXIS(0.0,0.0,10H)DISTANCE-X,-10,5.0,0.0,XARRY(KFP1),XARRY(KFP2
1))
      CALL AXIS(0.0,0.0,21H)SHEAR STRESS SIGMA-XY,21,6.0,90.0,XARRY(KFP1)
1,YARRY(KFP2))
      CALL SYMBOL(0.5,9.0,0.14,29H) VARIATION OF SHEARING STRESS,0.0,29)
      AP=8.0
530 CALL LINE(XARRY,YARRY, KKF,1,1,NKT)
      AP=AP-.4
      CALL SYMBOL(0.5,AP,0.14,NKT,0.0,-1)
      CALL SYMBOL(999.,AP,0.14,2H= ,0.0,2)
      CALL NUMBER (999.,999.,0.14,ANGL,0.0,2)
      CALL PLOT(0.,0.,-3)
      IF(NKT-NTHE) 610,560,560
610 NKT=NKT+1
      ANGL=ANGL+DEG
      GO TO 603
560 CALL PLOT(12.0,0.0,999)
      GO TO 300
300 CONTINUE
      RETURN
      1 FORMAT(72H
1
2 FORMAT( 6E14.5)
4 FORMAT(15I5)
8 FORMAT (5X2HY=.1XE12.5//)
10 FORMAT(5X3HXST,8X2HSX,8X2HSY,9X3HSXY,7X3HPSX,7X3HPSY,7X3HPSZ,6X4HP
1TX,7X2HOS)

```

0146  
0147  
0148  
0150  
0151

0155

```

12 FORMAT(12(1XF9.5))
14 FORMAT (1H//)
500 FORMAT(14H POISSON RATIO)
502 FORMAT (35H  KF  JJF  NC  KKF  NTHE  NCPL  )
504 FORMAT(34H DIMENSIONLESS NORMAL LOADING Q(K))
506 FORMAT(38H DIMENSIONLESS TANGENTIAL LOADING P(K))
508 FORMAT(37H  DIMENSIONLESS WIDTH  XH(K))
512 FORMAT(37H  ARRAY OF X-COORD. FOR STRESS CALCU.
514 FORMAT(37H  ARRAY OF Y-COORD. FOR STRESS CALCU.
518 FORMAT(23H  SHEAR STRESS AT EVERY.F10.5,8H DEGREES)
700 FORMAT(///)
701 FORMAT(/)
END
SUBROUTINE AREA(EBAR,HMIN,SPFILM,ABAR)
DIMENSION HH(51),FH(51)
KS=9
C1=1./SQRT(2.)
IF (SPFILM)10,11,11
10 FH0=0.5+0.5*ERROR(ABS(SPFILM)*C1)
GO TO 12
11 FH0=0.5-0.5*ERROR(ABS(SPFILM)*C1)
12 ABAR=0.5*(2.-EHAR)*FH0
FKS=KS
DO 20 K=1,KS
FK=K
HH(K)=SPFILM*(1.-(1.-HMIN)*SIN(3.1416*(FK-1.)/(FKS-1.)))
TEMP=0.5*ERROR(ABS(HH(K))*C1)
IF (HH(K))14,15,15
14 FH(K)=0.5+TEMP
GO TO 20
15 FH(K)=0.5-TEMP
20 CONTINUE
DX3=(EBAR/(FKS-1.))/3.0
KKS=KS-2
DO 30 K=1,KKS,2
30 ABAR=ABAR+DX3*0.5*(FH(K)+4.0*FH(K+1)+FH(K+2))
RETURN
END
FUNCTION ERROR (X)
E=1.0/(1.0+0.3275911*X)
S=(((((0.940646070*E)-1.287822453)*E+1.25969513)*E-0.252128668)
1*E+0.225836846)*E
F=X**2
S=S*EXP (-F ) *1.128379167
ERROR=1.0-S
RETURN
END
SUBROUTINE FTFS (PHIT,PHIS)
REAL N1,N2
DIMENSION AQM(11),ALPHA(3),BETA(3),FAB(11,3,3),U(3,3),V(3),
1B2(5,3,3),GAA(4),C(4),N1(4),N2(4),W(3,3),XX(3),QMB(5)
COMMON KI,KC,KG,KA,KD,KD,KB,KE,KF,KR,NR,NW
COMMON RX1,RX2,RY1,RY2,RMS1,RMS2,E1,E2,V1,V2
COMMON CONS1,CONS2,CPS1,CPS2,RHOS1,RHOS2,WT,TEM1,U2,U1
COMMON VIS,ALF,BET,GAM,CONF,CPF,RHOF,PS,PSTAR
COMMON AFA,BTA,GMA,A,B,AM,SLIP, RXP, RYP,EP,QM,CONV,D(2),COMP,AHZ,
1PHZ,WBAR,UBAR,PHZE,GG,EDOW,BOA ,WW
COMMON FCOE,EBAR,FEET,FEES,HMIN,SPFILM,ABAR,SHM
COMMON EPST,EPSRD,QTF,TWF1,ITRDU,ITT,NRITE
COMMON XH(50),HE(50),P(50),T(50),TI(2,50),F(2,50),SHS(50)
DATA (BETA(I),I=1,3)/0.35,0.5,0.75/

```

```

DATA (AQM(I),I=1,11)/0.,.01,.02,.05,.1,.2,.5,1.0,2.0,5.0,10.0/
DATA (ALPHA(I),I=1,3)/15.71,23.564,31.419/
DATA (FAB(I),I=1,11) /1.0,.99,.98,.96,.93,.89,.8,.72,.62,.47,
1 .36/
DATA (FAB(I),I=12,22) /1.0,.98,.96,.94,.9,.86,.78,.65,.53,.37,
2 .27/
DATA (FAB(I),I=23,33) /1.,.99,.98,.93,.89,.81,.66,.56,.44,.3,
3 .22/
DATA (FAB(I),I=34,44) /1.,.99,.98,.95,.9,.86,.77,.67,.57,.44,
4 .34/
DATA (FAB(I),I=45,55) /1.,.97,.95,.92,.87,.81,.7,.6,.47,.32,.22/
DATA (FAB(I),I=56,66) /1.,.97,.94,.9,.84,.76,.62,.5,.36,.24,.17/
DATA (FAB(I),I=67,77) /1.,.98,.96,.93,.9,.84,.75,.66,.56,.43,
5 .34/
DATA (FAB(I),I=78,88) /1.,.98,.95,.9,.85,.78,.66,.56,.45,.31,
6 .21/
DATA (FAB(I),I=89,99) /1.,.98,.94,.89,.82,.74,.59,.46,.35,.23,
7 .15/
DATA(B2(I),I=1,5) /0.,.0.,.0.,.47.5,107.2/
DATA(B2(I),I=6,10) /0.,.3.6,12.8,48.8,75.6/
DATA(B2(I),I=11,15) /0.,.3.95,12.4,40.7,51.4/
DATA(B2(I),I=16,20) /0.,.0.,.0.,.26.5,52.9/
DATA(B2(I),I=21,25) /0.,.3.78,11.4,17.6,26.5/
DATA(B2(I),I=26,30) /0.,.4.34,8.2,30.1,25.6/
DATA(B2(I),I=31,35) /0.,.0.,.4.1,12.9,25.6/
DATA(B2(I),I=36,40) /0.,.8.3,12.4,13.75,20.9/
DATA(B2(I),I=41,45) /0.,.4.6,12.0,19.4,19.5/
DATA(GAA(I),I=1,4)/5.,2.,1.,.5/
DATA(C(I),I=1,4)/1.625,1.56,1.415,1.132/
DATA(N1(I),I=1,4)/.74,.736,.725,.688/
DATA(N2(I),I=1,4)/-.22,-.209,-.174,-.066/
DATA(QMB(I),I=1,5)/0.0,0.5,1.0,5.0,10.0/
DO 100 I=1,3
DO 100 J=1,3
IF(QM.LE.AQM(11)) GO TO 20
U(I,J)=EXP(ALOG(FAB(11,I,J))-(ALOG(FAB(10,I,J))-ALOG(FAB(11,I,J))))
1/(ALOG(AQM(11))-ALOG(AQM(10)))*(ALOG(QM)-ALOG(AQM(11))))
GO TO 100
20 CALL TLU(QM,U(I,J),AQM,FAB(1,I,J),11)
100 CONTINUE
AFM=AFA*100000./PHZ
ALBT=BTA/AFM
IF(NWRITE.NE.0) GO TO 101
50 FORMAT(8E12.4)
WRITE(NW,50) QM,AFM,ALBT
101 DO 200 K=1,3
CALL TLU(ALBT,V(K),BETA,U(1,K),3)
200 CONTINUE
CALL TLU(AFM,XFAB,ALPHA,V,3)
DO 300 II=1,3
DO 300 JJ=1,3
IF(QM.LE.QMB(5)) GO TO 30
W(II,JJ)=EXP(ALOG(B2(5,II,JJ))+(ALOG(B2(5,II,JJ))-ALOG(B2(4,II,J
1J)))/(ALOG(QMB(5))-ALOG(QMB(4)))*(ALOG(QM)-ALOG(QMB(5)))))
GO TO 300
30 CALL TLU(QM,W(II,JJ),QMB,B2(1,II,JJ),5)
300 CONTINUE
DO 400 KK=1,3
CALL TLU(ALBT,XX(KK),BETA,W(1,KK),3)

```



```

400 CONTINUE
    CALL TLU(AFM,XB2,ALPHA,XA,3)
    CALL TLU(BOA,XC,GAA,C,4)
    CALL TLU(BOA,XN1,GAA,N1,4)
    CALL TLU(BOA,XN2,GAA,N2,4)
    IF(BOA.GT.5.) PHIS=1.
    IF(BOA.GT.5.) GO TO 450
    PHIS=(XC/C(1))*((UBAR*GG)**(XN1-N1(1)))*((PHZE*(3.14159/2.))**
    1XN2-N2(1)))
    450 PHIT=XFAB*(1.+(-.1*SLIP))*(1.-XB2*PHZE)
1010 FORMAT(/,1X,3HF =,E12.5)
1011 FORMAT(1X,4HB2 =,E12.5)
1012 FORMAT(1X,3HC =,E12.5)
1013 FORMAT(1X,4HN1 =,E12.5)
1014 FORMAT(1X,4HN2 =,E12.5)
    RETURN
    END

```

APPENDIX VIII  
CALCULATION OF FRICTIONAL FORCES  
AT A BALL-RACE CONTACT COMPUTER PROGRAM

All the calculations mentioned in Section IV-B are included in the computer program BALFTN. In addition to calculating the frictional forces and torque at a ball-race contact, it provides the option to compute the derivatives of forces and torque with respect to speeds and load. With the aid of Fig. VIII-1, where a ball-race contact is shown, the instruction for input cards and the description of output data are given below.

VIII-1. INPUT INSTRUCTION

Card 1 Read NGLG, IDY, NDV  
FORMAT (10I5)

- NGLG = 1 Speed input will be linear velocities.  
       = 2 Speed input will be in terms of angular velocities of ball and race.  
 IDY = Number of strips across the major axis of the contact ellipse. 40 is recommended.  
 NDV = 1 Only frictional forces and torque will be calculated. Forces acting on each strip will be printed out.  
       = 2 Derivations of forces with respect to speeds and load will also be calculated. Forces on each strip will not be printed out.

Card 2 Read R, RG, RR, W2, WR, WL, WS  
FORMAT (8E10.3)

- If NGLG = 1, this card should be omitted.  
 R = radius of ball in inches.  
 RG = radius of race groove in inches. It should always be negative.  
 RR = radius of race in inches, positive for inner race and negative for outer race.  
 W2 = angular velocity of race in rpm, used to calculate rolling velocity of race;  $u_r = |RR| \cdot W2 \cdot \frac{2\pi}{60}$ .  
 WR = rolling angular velocity of ball in rpm, used to calculate rolling velocity of ball,  $u = R \cdot WR \cdot \frac{2\pi}{60}$ .  
 WL = sliding angular velocity of ball in rpm, used to calculate lateral sliding velocity of ball,  $v = R \cdot WL \cdot \frac{2\pi}{60}$ .  
 WS =  $\omega_s$  in Fig. VIII-1, spinning velocity of ball about z-axis in rpm.

Card 3 Read R, RG, RR, U1, U2, V1, WS

FORMAT (8E10.3)

If NGLG = 2, this card should be omitted.

R, RG, RR = have been explained in the instruction for Card 2.

U1 =  $u$  in Fig. VIII-1, velocity of ball in the rolling direction  $x$ , in in/sec.

U2 =  $u_r$  in Fig. VIII-1, velocity of race in  $x$ -direction, in in/sec.

V1 =  $v$  in Fig. VIII-1, lateral sliding velocity of ball, in in/sec.

WS =  $\omega_s$  in Fig. VIII-1, spinning velocity of ball about  $z$ -axis, in rpm.

Card 4 Read ALPHA, BETA, VIS, FK, WT, TI

FORMAT (8E10.3)

ALPHA =  $\alpha$ , pressure-viscosity coefficient of lubricant in the viscosity function  $\mu = \mu_0 e^{\alpha P} + \beta_1 (T - T_0)$  in  $\text{in}^2/\text{lb}$ .

BETA =  $\beta_1$ , temperature-viscosity coefficient of lubricant in the above viscosity function, in  $^\circ\text{F}$ .

VIS =  $\mu_0$ , viscosity of lubricant at inlet temperature  $T_0$ , in  $\text{lb-sec/in}^2$ .

FK = thermal conductivity of lubricant, in  $\text{BTU}/^\circ\text{F-hr-ft}$ .

WT =  $P$  in Fig. VIII-1, normal contact load, in lb.

TI = inlet temperature, in  $^\circ\text{F}$ .

Card 5 Read EB, ER, SB, SR

FORMAT (8E10.3)

EB = Young's modulus of elasticity of ball, in  $\text{lb/in}^2$ .

ER = Young's modulus of elasticity of race, in  $\text{lb/in}^2$ .

SB = Poisson's ratio of ball.

SR = Poisson's ratio of race.

Card 6 Read DU, DV, DWS, DWT

FORMAT (8E10.3)

If NDV = 1, this card should be omitted.

DU =  $1/2 \Delta u$ , where  $\Delta u$  is the increment in  $u$  (rolling velocity of ball) to calculate derivatives with

respect to  $u$ , e.g.,  $\frac{\delta F}{\delta u} = \frac{\Delta F}{\Delta u}$ , in in/sec.

DV =  $1/2 \Delta v$ , where  $\Delta v$  is the increment  $v$  (lateral sliding velocity of ball) to calculate derivatives with respect to  $v$ , in in/sec.

DWS =  $1/2 \Delta \omega_s$ , where  $\Delta \omega_s$  is the increment in  $\omega_s$  (spinning velocity of ball) to calculate derivatives with respect to  $\omega_s$ , in rpm.

DWT =  $1/2 \Delta P$ , where  $\Delta P$  is the increment in  $P$  (normal contact load) to calculate derivatives with respect to  $P$ , in lb.

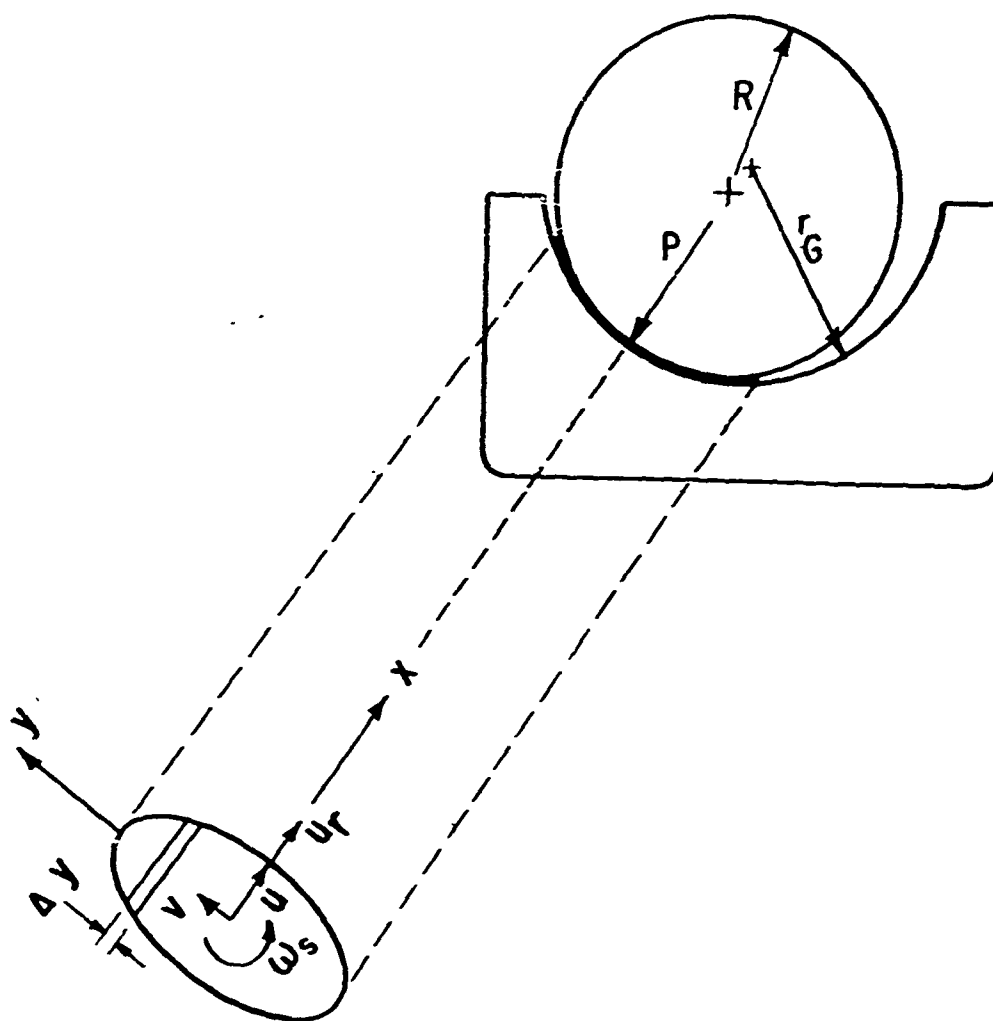


Fig. VIII-1 A Ball-Race Contact.

## VIII-2. OUTPUT EXPLANATION

The first section contains the write-out of the input data. Symbols and units used have been explained in the instructions for input.

The second section includes the calculated area of contact ellipse and maximum Hertz stress:

B = b, semi-minor axis of contact ellipse, in in.  
A = a, semi-major axis of contact ellipse, in in.  
PHZ = PHZ, maximum Hertz stress, in lb/in<sup>2</sup>.

If NDV = 1, the next section contains details of all forces and moments acting on each strip. If NDV = 2, this section is omitted.

The still next section represents the calculated forces and moments acting on the ball. In each line the second number is a normalized quantity. Contact load, P is used as the normalizing force and the product of the load and ball radius, PR is employed as the normalizing moment.

The last section (if NDV = 1, this section is omitted) contains the derivatives of forces and moment with respect to speeds and load. Let  $F_x$  be the force in the x-direction acting on the ball,  $F_y$  the force in the y-direction, and  $M_z$  the moment acting on the ball about the z-axis:

$$DFX/DU = \frac{\delta F_x}{\delta u}, \text{ in lb-sec/in.}$$

$$DFX/DV = \frac{\delta F_x}{\delta v}, \text{ in lb-sec/in.}$$

$$DFX/D\omega_s = \frac{\delta F_x}{\delta \omega_s}, \text{ in lb/rpm.}$$

$$DFX/DW = \frac{\delta F_x}{\delta P}, \text{ in lb/lb.}$$

$$DFY/DU = \frac{\delta F_y}{\delta u}, \text{ in lb-sec/in.}$$

$$DFY/DV = \frac{\delta F_y}{\delta v}, \text{ in lb-sec/in.}$$

$$DFY/D\omega_s = \frac{\delta F_y}{\delta \omega_s}, \text{ in lb/rpm.}$$

$$DFY/DW = \frac{\delta F_y}{\delta P}, \text{ in lb/lb.}$$

$$DMZ/DU = \frac{\delta M_z}{\delta u}, \text{ in lb-sec.}$$

$$DMZ/DV = \frac{\delta M_z}{\delta v}, \text{ in lb-sec.}$$

$$DMZ/D\omega_s = \frac{\delta M_z}{\delta \omega_s}, \text{ in in-lb/rpm.}$$

$$DMZ/DW = \frac{\delta M_z}{\delta P}, \text{ in in.}$$

```

C      PROGRAM BALFTN(INPUT,OUTPUT,TAPES=INPUT,TAPE6=OUTPUT)
C      FRICTION CALCULATION OF ANGULAR CONTACT BALL BEARING
C      INPUT DESCRIPTION---
C      R=RADIUS OF BALL,IN.
C      RG=Groove RADIUS Of RACE,IN.
C      RR=RADIUS OF RACE,IN.
C      TJ=INLET TEMPERATURE, DEG.F.
C      WR=ROLLING ANG. VEL. OF BALL, RPM.
C      WL=LATERAL ROLLING VEL. OF BALL, RPM.
C      WS=SPINNING VEL. OF BALL, RPM.
C      W2=ROLLING VEL. OF RACE, RPM.
C      U1,V1=ROLLING AND LATERAL VEL. OF BALL, IN/SEC.
C      W=TOTAL LOAD, LBF.
C      U2=ROLLING VEL. OF RACE, IN/SEC.
C      VIS=INLET VISCOSITY, Lbf-SEC/IN**2
C      ALPHA=PRESSURE-VISCOSITY COEF., IN**2/LBF.
C      BETA=TEMPERATURE-VISCOSITY COEF., /DEG.F.
C      FK=THERMAL CONDUCTIVITY OF LUBRICANT, BTU/DEG.F-IN-FT
C      DIMENSION AMDA(24),FMA(24),AORA(24)
C      DIMENSION U(3),V(3),WSS(3),WTT(3),SW(3),SA(3),SB(3),PHZ(3),Y(60),
C      IRATIO(60),FFXX(3,3,6),FFYY(3,3,6),TMM(3,3,6)
C      COMMON G1,G2,G3,FCOE,THETA
C      DATA(AMDA(I),I=1,24)/ 0.0,0.05,0.1,0.15,0.2,0.25,0.3,0.35,0.4,0.45
C      1.0,5.0,55.0,6.0,65.0,7.0,75.0,8.0,85.0,9.0,92.0,94.0,96.0,98.1,0./
C      DATA(FMA(I),I=1,24)/1.0,1.035,1.072,1.112,1.155,1.195,1.24,1.29,
C      11.35,1.41,1.485,1.56,1.65,1.77,1.895,2.065,2.29,2.60,3.095,3.3973
C      2.3,8275,4.5319,5.946,6./
C      DATA(AORA(I),I=1,24)/1.0,0.935,0.875,0.82,0.765,0.710,0.66,0.615,
C      1 0.57,0.525,0.480,0.44,0.4,0.358,0.32,0.282,0.24,0.195,0.14875,
C      20.12897,0.1075,0.083184,0.055189,0.0/
C      READ(5,1) NNLG,IOY,NDV
C      1 FORMAT(10I5)
C      IF(NNLG.EQ.1) GO TO 20
C      READ(5,2) R,RG,RR,W2,WL,WS
C      U1=R*W2*2.*3.1416/60.
C      U2=ABS(W2)*W2*2.*3.1416/60.
C      V1=R*WL*2.*3.1416/60.
C      GO TO 30
C      20 READ(5,2) R,RG,RR,U1,U2,V1,WS
C      30 READ(5,2) ALPHA,BETA,VIS,FK,W1,T1
C      READ(5,2) EN,ER,GB,GN
C      IF(NOV.EQ.1) GO TO 31
C      READ(5,2) DU,DV,DWS,DWT
C      U(2)=U1+DU
C      U(3)=U1-DU
C      V(2)=V1+DV
C      V(3)=V1-DV
C      WSS(2)=WS+DWS
C      WSS(3)=WS-DWS
C      WTT(2)=W1+DWT
C      WTT(3)=W1-DWT
C      2 FORMAT(HE10.3)
C      3 FORMAT(/// 3H R= E12.4,5X 4H RG= E12.4,5X 4H RR= E12.4)
C      31 WRITE(6,3) R,RG,RR
C      4 FORMAT(/ 4H U1= E12.4,5X 4H U2= E12.4,5X 4H V1= E12.4,5X 4H WS= E1
C      12.4)
C      WRITE(6,4) U1,U2,V1,WS
C      WRITE(6,5) ALPHA,BETA,VIS
C      5 FORMAT(/ 7H ALPHA= E12.4,5X 6H BETA= E12.4,5X 11H VISCOSITY= E12.4
C      )

```

```

6 FORMAT(/ 6H LOAU= E12.4 SX 3H T= E12.4)
WRITE(6,6) T,11
THETA=(T1-32.)/1.6
RXP=1./R*1./R2
RYP=1./R*1./R2
AA=0.5*RXP
DD=0.5*RYP
RXP=1./RXP
RYP=1./RYP
AMD=(AA-DD)/(AA+DD)
CALL TLU(AMD,FM,AMDA,FMA,24)
CALL TLU(AMD,A0B,AMDA,A0BA,24)
EP=3.1416/((1.-GB**2)/EB*(1.-GR**2)/ER)
U(1)=U1
V(1)=V1
WSS(1)=WS
WT(1)=WT
DY=2./IDY
DO 45 I=1,3
SB(I)=FM*(0.75*3.1416*WT(I)/(AA+DD)/EP)**0.33333
SA(I)=SH(I)*AOM
PHZ(I)=1.5*WT(I)/(3.1416*SA(I)*SB(I))
SW(I)=0.75*WT(I)/SB(I)
IF (NDV.EU.1) GO TO 46
45 CONTINUE
46 WRITE(6,7) SA(1),SH(1)
7 FORMAT(/ 14H ELLIPTIC AXES A= E12.4 SX 3H B= E12.4)
WRITE(6,8) PHZ(1)
8 FORMAT(/ 5H P= E12.4)
IF(NDV.EU.2) GO TO 35
WRITE(6,9)
9 FORMAT(/ 5X 14H 1X FMW(LB/IN) 3X 8PHZ(PSI) 4X 5HH(IN) 7X 2HG1 9
1X 2HG2 9X 2HG3 9X 1HF 7X 6HF(LB) 5X 6HFY(LB) 9X 2HMX 9X 2HMY /
2 )
35 VIS3=VIS*EXP(THETA*(T1-86.))
AL3=ALPHA*930.*ALPHA*(T1-86.)/(546.*(T1+460.))
MM=1.58*ALPHA**0.6*VIS**0.7*EP**0.03*RXP**0.43
GIT=VIS3*(ALPHA/AL3)**0.6*(VIS/VIS3)**0.7
G2T=VIS3*THETA/(8.*FK*0.216)
I=1
J=1
K=1
L=1
N=1
48 FFY=0.
FFX=0.
TM2=0.
TM1=0.
SS=WSS(K)*2.*3.1416/60.*SB(L)
IF((K.EQ.1).AND.(L.EU.1).AND.((I.NE.1).OR.(J.NE.1))) GO TO 49
IF(SS.EQ.0.) GO TO 43
YS=(U(I)-U2)/SS
IF((YS.GE.1.).OR.(YS.LE.(-1.))) GO TO 43
GO TO 44
43 Y(1)=1.*DY/2.
MM=1
GO TO 42
44 NN=1
Y(1)=YS

```



```

41 Y(MN+1)=Y(MN)+DY
   RATIO(MN+1)=1.-Y(MN+1)**2
   MN=MN+1
   IF(Y(MN).LT.(1.-DY/2.)) GO TO 41
   IF(Y(MN).GT.1.) NV=MN-1
   MN=MN+1
   Y(MN)=Y5-DY
   RATIO(MN)=1.-Y(MN)**2
42 Y(MN+1)=Y(MN)-DY
   RATIO(MN+1)=1.-Y(MN+1)**2
   MN=MN+1
   IF(Y(MN).GT.(-1.+DY/2.)) GO TO 42
   IF(Y(MN).LT.(-1.)) MN=MN-1
   IF(NDV.EQ.2) GO TO 49
   WRITE(6,10) Y(1)
49 DO 50 M=2,MN
   UBAR=ABS((U(1)+U2-SS*Y(M))/2.)
   W=SW(L)*RATIO(M)
   H=M*UBAR**0.7/W**0.13
   PPHZ=PHZ(L)*SGRT(RATIO(M))
   US=ABS(U2-U(1)+SS*Y(M))
   G1=G1T*US/H/PPHZ
   G2=G2T*US**2
   G3=AL3*PPHZ
   CALL FRCTN
   FX=-FCOE*W*DY*SB(L)
   IF((U(1)-SS*Y(M)).LT.U2) FX=-FX
   FY=-FCOE*W*Y(J)/US*DY*SB(L)
   FFX=FFX+FX
   FFY=FFY+FY
   TFX=-FX*Y(M)*SB(L)
   TM1=TM1+TFX
   TFY=-FCOE*W*SS*SA(L)**2*RATIO(M)/3./US*DY
   TM2=TM2+TFY
   IF (NDV.EQ.2) GO TO 50
   WRITE(6,10) Y(M),W,PPHZ,H,G1,(2,G3,FCOE,FX,FY,TFX,TFY)
10 FORMAT(12E11.3)
50 CONTINUE
   TM=TM1+TM2
   FFXX(I,J,N)=FFX
   FFYY(I,J,N)=FFY
   TMM(I,J,N)=TM
   IF(NDV.EQ.1) GO TO 80
   IF((I.GE.3).OR.(J.GT.1).OR.(K.GT.1).OR.(L.GT.1)) GO TO 55
   I=I+1
   GO TO 48
55 I=1
   IF((J.GE.3).OR.(K.GT.1).OR.(L.GT.1)) GO TO 56
   J=J+1
   GO TO 48
56 J=1
   IF((K.GE.3).OR.(L.GT.1)) GO TO 57
   K=K+1
   N=N+1
   GO TO 48
57 K=1
   IF(L.GE.3) GO TO 58
   L=L+1
   N=N+1

```

```

80 FFFX=FFXX(1.1.1)/WT
   FFY=FFYY(1.1.1)/WT
   FTM=TMM(1.1.1)/(WT*P)
   WRITE(6.11) FFX(1.1.1),FFF
11 FORMAT(/ / 44M FRICTION IN THE DIRECTION OF ROLLING (LB.)= E12.4.5X
   , F10.5)
12 FORMAT(/ / 44M FRICTION IN THE LATERAL DIRECTION (LB.)= E12.4.5X F10
   1.5)
   WRITE(6.12) FFY(1.1.1),FF
13 FORMAT(/ / 26M SPINNING TORQUE (IN-LB.)= E12.4.5X F10.5)
   WRITE(6.13) TMM(1.1.1),FTM
   IF(NDV.EQ.1) GO TO 120
   WRITE(6.81) FXDU
81 FORMAT(/ / 20M DFX/DU (LB/IN/SEC)= E12.4)
   WRITE(6.82) FXDV
82 FORMAT(/ / 20M DFX/DV (LB/IN/SEC)= E12.4)
   WRITE(6.83) FXDWS
83 FORMAT(/ / 16M DFX/DWS (LB/RPM)= E12.4)
   WRITE(6.84) FXDW
84 FORMAT(/ / 16M DFX/DW (LB/LB)= E12.4)
   WRITE(6.85) FYDU
85 FORMAT(/ / 20M DFY/DU (LB/IN/SEC)= E12.4)
   WRITE(6.86) FYDV
86 FORMAT(/ / 20M DFY/DV (LB/IN/SEC)= E12.4)
   WRITE(6.87) FYDWS
87 FORMAT(/ / 16M DFY/DWS (LB/RPM)= E12.4)
   WRITE(6.88) FYDW
88 FORMAT(/ / 16M DFY/DW (LB/LB)= E12.4)
   WRITE(6.89) TMDU
89 FORMAT(/ / 23M DMZ/UD (IN-LB/IN/SEC)=E12.4)
   WRITE(6.90) TMDV
90 FORMAT(/ / 23M DMZ/DV (IN-LB/IN/SEC)= E12.4)
   WRITE(6.91) TMDWS
91 FORMAT(/ / 21M DMZ/DWS (IN-LB/RPM)= E12.4)
   WRITE(6.92) TMDW
92 FORMAT(/ / 19M DMZ/DW (IN-LB/LB)= E12.4)
120 STOP
END
SUBROUTINE FRCTN
  DIMENSION AG1(13),AG2(7),AG3(7),FTN(13,7,7),UZ(7,7),VZ(7)
  COMMON G1,G2,G3,FCOE,THETA
  DATA(FTN(I),I=1,13)/0.00025,0.0007, 0.0014, 0.0023, 0.0067,
1 0.0135, 0.021, 0.037, 0.046, 0.052, 0.0615, 0.0685, 0.0775/
  DATA(FTN(I),I=14,26) /0.0007, 0.002, 0.0039, 0.0065, 0.0150,
1 0.022, 0.029, 0.042, 0.0495, 0.054, 0.0625, 0.069, 0.0775/
  DATA(FTN(I),I=27,39)/ 0.0026, 0.0078, 0.014, 0.018, 0.028,
1 0.034, 0.0385, 0.0485, 0.054, 0.058, 0.064, 0.0695, 0.0775/
  DATA(FTN(I),I=40,52) / 0.0077, 0.017,0.023, 0.027, 0.035,

```

DATA(FIN(I),I=53,65)/0.019, 0.0285, 0.034, 0.037, 0.044, 0.048,  
 1 0.05, 0.056, 0.06, 0.0635, 0.069, 0.0725, 0.0775/  
 DATA(FIN(I),I=66,78) / 0.0215, 0.032, 0.037, 0.0415, 0.0475,  
 1 0.051, 0.054, 0.06, 0.0635, 0.066, 0.07, 0.073, 0.0775/  
 DATA(FIN(I),I=79,91) / 0.0245, 0.034, 0.04, 0.0435, 0.05,  
 1 0.054, 0.0565, 0.062, 0.0655, 0.0675, 0.071, 0.074, 0.0775/  
 DATA(FIN(I),I=92,104)/0.0002, 0.0006, 0.0012, 0.002, 0.006, 0.012,  
 1 0.019, 0.036, 0.047, 0.054, 0.0645, 0.072, 0.077/  
 DATA(FIN(I),I=105,117)/0.0006, 0.002, 0.004, 0.0065, 0.015, 0.024,  
 1 0.028, 0.043, 0.052, 0.0575, 0.0665, 0.072, 0.077/  
 DATA(FIN(I),I=118,130)/ 0.0027, 0.0081, 0.014, 0.019, 0.0285,  
 10.035, 0.0395, 0.051, 0.057, 0.061, 0.068, 0.0725, 0.077/  
 DATA(FIN(I),I=131,143)/0.0066, 0.015, 0.021, 0.025, 0.034, 0.04,  
 1 0.0445, 0.054, 0.06, 0.064, 0.069, 0.073, 0.077/  
 DATA(FIN(I),I=144,156)/ 0.012, 0.0225, 0.029, 0.0345, 0.043,  
 1 0.048, 0.052, 0.059, 0.063, 0.066, 0.070, 0.073, 0.077/  
 DATA(FIN(I),I=157,169)/ 0.019, 0.032, 0.039, 0.0415, 0.05, 0.054,  
 1 0.056, 0.061, 0.064, 0.067, 0.0715, 0.075, 0.077/  
 DATA(FIN(I),I=170,182)/ 0.021, 0.0335, 0.041, 0.0455, 0.053,  
 1 0.056, 0.059, 0.064, 0.068, 0.07, 0.073, 0.076, 0.077/  
 DATA(FIN(I),I=183,195)/.00016, .00055, 0.0011, 0.0019, .00058, 0.011,  
 1 0.018, 0.033, 0.042, 0.048, 0.06, 0.068, 0.075/  
 DATA(FIN(I),I=196,208)/.0007, .0021, 0.0043, 0.007, 0.015, 0.023,  
 1 0.027, 0.039, 0.046, 0.052, 0.062, 0.07, 0.075/  
 DATA(FIN(I),I=209,221)/ 0.0018, 0.0053, 0.01, 0.015, 0.0255,  
 1 0.034, 0.037, 0.048, 0.054, 0.058, 0.066, 0.073, 0.075/  
 DATA(FIN(I),I=222,234)/ 0.0046, 0.011, 0.018, 0.024, 0.037,  
 1 0.039, 0.044, 0.0525, 0.057, 0.061, 0.068, 0.074, 0.075/  
 DATA(FIN(I),I=235,247)/ 0.0082, 0.017, 0.025, 0.03, 0.042,  
 10.048, 0.052, 0.06, 0.064, 0.066, 0.070, 0.074, 0.075/  
 DATA(FIN(I),I=248,260)/ 0.015, 0.026, 0.034, 0.04, 0.049,  
 1 0.054, 0.058, 0.063, 0.067, 0.069, 0.073, 0.075, 0.075/  
 DATA(FIN(I),I=261,273)/ 0.018, 0.028, 0.036, 0.043, 0.052,  
 1 0.057, 0.06, 0.065, 0.068, 0.07, 0.074, 0.075, 0.075/  
 DATA(FIN(I),I=274,286)/.00015, .00046, .001, 0.0017, 0.005, 0.01,  
 1 0.016, 0.034, 0.04, 0.046, 0.059, 0.067, 0.073/  
 DATA(FIN(I),I=287,299)/0.0006, 0.002, 0.0039, 0.0064, 0.015,  
 1 0.021, 0.026, 0.039, 0.046, 0.052, 0.062, 0.068, 0.073/  
 DATA(FIN(I),I=300,312)/ 0.0017, 0.0048, 0.009, 0.014, 0.025,  
 1 0.031, 0.036, 0.047, 0.053, 0.057, 0.065, 0.0695, 0.073/  
 DATA(FIN(I),I=313,325)/ 0.043, 0.01, 0.017, 0.023, 0.033,  
 1 0.039, 0.043, 0.052, 0.058, 0.061, 0.066, 0.07, 0.073/  
 DATA(FIN(I),I=326,338)/ 0.0078, 0.016, 0.024, 0.029, 0.04,  
 1 0.046, 0.051, 0.057, 0.062, 0.064, 0.068, 0.071, 0.073/  
 DATA(FIN(I),I=339,351)/ 0.0145, 0.024, 0.033, 0.039, 0.048,  
 1 0.053, 0.056, 0.062, 0.066, 0.067, 0.07, 0.072, 0.073/  
 DATA(FIN(I),I=352,364)/ 0.016, 0.027, 0.0355, 0.041, 0.052,  
 1 0.056, 0.059, 0.064, 0.067, 0.068, 0.071, 0.073, 0.073/  
 DATA(FIN(I),I=365,377)/.0001, .00027, .00055, 0.0009, 0.0029,  
 1 0.0059, 0.01, 0.025, 0.036, 0.043, 0.054, 0.062, 0.068/  
 DATA(FIN(I),I=378,390)/.00044, .0013, 0.0026, 0.0044, 0.012,  
 1 0.018, 0.024, 0.036, 0.044, 0.048, 0.057, 0.063, 0.068/  
 DATA(FIN(I),I=391,403)/0.001, 0.0029, 0.0056, 0.009, 0.0185,  
 1 0.0255, 0.03, 0.042, 0.0485, 0.053, 0.06, 0.064, 0.068/  
 DATA(FIN(I),I=404,416)/0.0015, 0.0045, 0.0085, 0.013, 0.024,  
 1 0.032, 0.036, 0.047, 0.053, 0.057, 0.063, 0.065, 0.068/  
 DATA(FIN(I),I=417,429)/0.0038, 0.0093, 0.0155, 0.021, 0.032,  
 1 0.038, 0.042, 0.052, 0.056, 0.06, 0.064, 0.066, 0.068/  
 DATA(FIN(I),I=430,442)/0.0088, 0.017, 0.0245, 0.03, 0.04,  
 1 0.0465, 0.051, 0.058, 0.061, 0.063, 0.066, 0.067, 0.068/

```

DATA(FIN(I),I=443,455)/0.012, 0.022, 0.0295, 0.035, 0.0455,
1 0.051, 0.055, 0.061, 0.063, 0.065, 0.067, 0.068, 0.068/
DATA(FIN(I),I=456,468)/.00005,.00014,.00027,.00045,.0014,
1 0.0027, 0.0046, 0.013, 0.023, 0.029, 0.042, 0.052, 0.055/
DATA(FIN(I),I=469,481)/.00012,.00042,.00085,.0014,.0044,
1 0.0084, 0.013, 0.0245, 0.032, 0.037, 0.0455, 0.053, 0.055/
DATA(FIN(I),I=482,494)/.0004,.0012, 0.0024, 0.004, 0.011,
1 0.017, 0.023, 0.0345, 0.039, 0.0425, 0.048, 0.0535, 0.055/
DATA(FIN(I),I=495,507)/0.0015, 0.0042, 0.008, 0.012, 0.023,
1 0.029, 0.033, 0.0395, 0.043, 0.045, 0.050, 0.0535, 0.055/
DATA(FIN(I),I=508,520)/0.0034, 0.0084, 0.014, 0.0195, 0.03,
1 0.036, 0.04, 0.046, 0.048, 0.049, 0.051, 0.054, 0.055/
DATA(FIN(I),I=521,533)/0.0056, 0.013, 0.02, 0.026, 0.0375,
1 0.042, 0.045, 0.049, 0.05, 0.052, 0.0525, 0.054, 0.055/
DATA(FIN(I),I=534,546)/0.0071, 0.015, 0.023, 0.03, 0.04,
1 0.045, 0.048, 0.051, 0.052, 0.053, 0.054, 0.055, 0.055/
DATA(FIN(I),I=547,559)/.00003,.00009,.00018,.0003,.0009,
1 0.0019, 0.003, 0.009, 0.016, 0.023, 0.037, 0.045, 0.051/
DATA(FIN(I),I=560,572)/.0001,.00026,.00058,.0009,.0029,
1 0.0057, 0.0092, 0.021, 0.029, 0.034, 0.041, 0.047, 0.051/
DATA(FIN(I),I=573,585)/.00025,.00074,0.0015, 0.0024, 0.0072,
1 0.013, 0.018, 0.028, 0.035, 0.039, 0.045, 0.048, 0.051/
DATA(FIN(I),I=586,598)/0.00054, 0.0016, 0.0033, 0.0052, 0.014,
1 0.022, 0.0265, 0.035, 0.04, 0.042, 0.0465, 0.049, 0.051/
DATA(FIN(I),I=599,611)/0.0013, 0.0036, 0.0069, 0.011, 0.023,
1 0.029, 0.0325, 0.0395, 0.044, 0.046, 0.0485, 0.050, 0.051/
DATA(FIN(I),I=612,624)/0.0015, 0.041, 0.008, 0.012, 0.0235,
1 0.0295, 0.033, 0.04, 0.044, 0.0465, 0.049, 0.0505, 0.051/
DATA(FIN(I),I=625,637)/0.0018, 0.0052, 0.0094, 0.014, 0.0255,
1 0.031, 0.035, 0.042, 0.045, 0.047, 0.05, 0.051, 0.051/
DATA(AG1(I),I=1,13)/1.E-4, 3.E-8, 6.E-8, 1.E-7, 3.E-7, 6.E-7,
1 1.E-6, 3.E-6, 6.E-6, 1.E-5, 3.E-5, 1.E-4, 1.E-3/
DATA(AG2(I),I=1,7)/5.E-7, 1.E-6, 5.E-6, 1.E-5, 5.E-5, 5.E-4, 1.E-3
1 /
DATA(AG3(I),I=1,7)/13.32, 15.2, 17.8, 19., 21.19, 27.13, 100./
IF(G1.EQ.0.) GO TO 240
IF(G2.EQ.0.) GO TO 240
DO 100 I=1,7
DO 100 J=1,7
IF(G1-AG1(I)) 40,60,60
40 IF(G1.LT. AG1(I)) GO TO 70
CALL TLUG(G1,UZ(I,J),AG1,FIN(I,I,J),13)
GO TO 100
60 UZ(I,J)=FIN(I,J,1,J)
GO TO 100
70 UZ(I,J)=EXP(ALOG(FIN(I,I,J))+(ALOG(FIN(2,I,J))-ALOG(FIN(1,I,J)))/
1ALOG(AG1(2))-ALOG(AG1(1)))*(ALOG(G1)-ALOG(AG1(I))))
100 CONTINUE
DO 200 K=1,7
IF(G3-AG3(7)) 140,160,160
140 IF(G3.LT. AG3(1)) GO TO 170
CALL TLUG(G3,VZ(K),AG3,UZ(1,K),7)
GO TO 200
160 VZ(K)=UZ(7,K)
GO TO 200
170 VZ(K)=UZ(1,K)-(UZ(2,K)-UZ(1,K))/(AG3(2)-AG3(1))*(AG3(1)-G3)
IF (VZ(K).LE.0.0) VZ(K)=1.E-5
200 CONTINUE

```

```

      CALL TLUG(G2,FR3,AG2,VZ,7)
      GO TO 210
206 FR3=EXP(ALOG(VZ(6))+(ALOG(VZ(7))-ALOG(VZ(6)))/(ALOG(AG2(7))-ALOG(AG2(6))))*(ALOG(G2)-ALOG(AG2(6))))
      GO TO 210
207 FR3=EXP(ALOG(VZ(2))+(ALOG(VZ(1))-ALOG(VZ(2)))/(ALOG(AG2(1))-ALOG(AG2(2))))*(ALOG(G2)-ALOG(AG2(2))))
210 FCOE=ALOG(FR3)-0.149*(ALOG(THETA)-ALOG(30.))
      FCOE=EXP(FCOE)
      GO TO 250
240 FCOE=0.
250 CONTINUE
      RETURN
      END
      SUBROUTINE TLU(A,B,C,D,N)
      DIMENSION C(1),D(1)
      IF(N-1)1,2,3
1      B=0.
      GO TO 100
2      B=D(1)
      GO TO 100
3      ML=1
      MU=N
8      IF(MU-ML-1) 15,15,9
9      M=(MU+ML)/2
      IF(C(1)-C(2))11,2,10
10     IF(C(M)-A)13,12,14
11     IF(A-C(M))13,12,14
12     B=D(M)
      GO TO 100
13     MU=M
      GO TO 8
14     ML=M
      GO TO 8
15     B=D(ML)+(D(MU)-D(ML))*((A-C(ML))/(C(MU)-C(ML)))
100 RETURN
      END
      SUBROUTINE TLUG(A,B,C,D,N)
      DIMENSION C(1),D(1)
      IF(N-1)1,2,3
1      B=0.
      GO TO 100
2      B=D(1)
      GO TO 100
3      ML=1
      MU=N
8      IF(MU-ML-1) 15,15,9
9      M=(MU+ML)/2
      IF(C(1)-C(2))11,2,10
10     IF(C(M)-A)13,12,14
11     IF(A-C(M))13,12,14
12     B=D(M)
      GO TO 100
13     MU=M
      GO TO 8
14     ML=M
      GO TO 8
15     B=EXP(ALOG(D(ML))+(ALOG(D(MU))-ALOG(D(ML)))*((ALOG(A)-ALOG(C(ML)))/(ALOG(C(MU))-ALOG(C(ML)))))
100 RETURN
      END

```

UNCLASSIFIED

Security Classification

## DOCUMENT CONTROL DATA - R &amp; D

(Security classification of title, body of abstract and indexing annotation must be entered when the overall report is classified)

1. ORIGINATING ACTIVITY (Corporate author) Mechanical Technology Incorporated		12a. REPORT SECURITY CLASSIFICATION UNCLASSIFIED	
		2b. GROUP N/A	
3. REPORT TITLE  ELASTOHYDRODYNAMIC LUBRICATION PRELIMINARY DESIGN MANUAL			
4. DESCRIPTIVE NOTES (Type of report and inclusive dates) First Annual Report Feb 1969 - Feb 1970			
5. AUTHOR(S) (First name, middle initial, last name) John M. McGrew      S. F. Murray A. Gu H. S. Cheng			
6. REPORT DATE August 1970	7a. TOTAL NO. OF PAGES 333	7b. NO. OF REFS 216	
8a. CONTRACT OR GRANT NO Contract F33615-69-C-1305	9a. ORIGINATOR'S REPORT NUMBER(S) None		
b. PROJECT NO. 3048	9b. OTHER REPORT NO(S) (Any other numbers that may be assigned this report) None		
c. Task 304806			
d.			
10. DISTRIBUTION STATEMENT This document is subject to special export controls and each transmittal to foreign governments or foreign nationals may be made only with prior approval of the Air Force, Aero Propulsion Laboratory, Wright-Patterson Air Force Base, Ohio 45433			
11. SUPPLEMENTARY NOTES None		12. SPONSORING MILITARY ACTIVITY Air Force Aero Propulsion Laboratory Fuel, Lubrication, & Hazards Division Wright-Patterson AFB, Ohio 45433	
13. ABSTRACT  The available data on elastohydrodynamic lubrication are summarized. Based on an assessment of these data, a design procedure is developed for evaluating the performance of an elastohydrodynamic contact. The procedure includes the calculation of minimum film thickness, real area of contact, traction, pressure distribution, temperature profile, and subsurface stress distribution in the contact, based on either available theory or on experimental data. A computer program listing plus illustrative examples are included. Determination of film thickness and traction are identified as areas in elastohydrodynamic lubrication requiring further investigation.			

DD FORM 1 NOV 65 1473

UNCLASSIFIED

Security Classification

14. KEY WORDS	LINK A		LINK B		LINK C	
	ROLE	WT	ROLE	WT	ROLE	WT